

PDF hosted at the Radboud Repository of the Radboud University Nijmegen

The following full text is a publisher's version.

For additional information about this publication click this link.

<http://hdl.handle.net/2066/115721>

Please be advised that this information was generated on 2017-12-05 and may be subject to change.

Quantum Einstein Gravity

the Metric and the Foliated Formulation

Proefschrift

ter verkrijging van de graad van doctor
aan de Radboud Universiteit Nijmegen
op gezag van de rector magnificus, prof. mr. S.C.J.J. Kortmann,
volgens besluit van het college van decanen
in het openbaar te verdedigen op donderdag 21 november 2013
om 12.30 uur
door
Stefan Rechenberger
geboren op 1 september 1983
te Dresden, Duitsland

Promotor: prof. dr. Renate Loll
Copromotor: dr. Frank Saueressig

De manuscriptcommissie: prof. dr. Ronald Kleiss
prof. dr. Jan Ambjørn (Universiteit Kopenhagen)
prof. dr. Martin Reuter (Universiteit Mainz)
prof. dr. Holger Gies (Universiteit Jena)
prof. dr. Jens Braun (Universiteit Darmstadt)

Quantum Einstein Gravity

the Metric and the Foliated Formulation

Doctoral thesis

to obtain the degree of doctor
from Radboud University Nijmegen
on the authority of the Rector Magnificus, prof. dr. S.C.J.J. Kortmann,
according to the decision of the Council of Deans
to be defended in public on Thursday 21 November 2013
at 12.30 hours
by
Stefan Rechenberger
born in Dresden, Germany
on 1 September 1983

Supervisor: prof. dr. Renate Loll
Co-supervisor: dr. Frank Saueressig

Doctoral thesis committee: prof. dr. Ronald Kleiss
prof. dr. Jan Ambjørn (University Copenhagen)
prof. dr. Martin Reuter (University Mainz)
prof. dr. Holger Gies (University Jena)
prof. dr. Jens Braun (University Darmstadt)

To Jacky and Ben

Samenvatting

De klassieke Algemene Relativiteitstheorie biedt een onbetwiste beschrijving van de zwaartekracht, tussen sub-millimeter en de cosmologische schalen. Echter, tot op heden blijft het verenigen van de zwaartekracht en de kwantummechanica een open probleem in de theoretische natuurkunde. Dit proefschrift levert een bijdrage aan de constructie van een consistente en voorspellende theorie van de kwantumzwaartekracht in de context van kwantumveldentheorie. Hierin behandelen we op expliciete wijze de niet-perturbatieve aspecten van de stroom van de renormalisatiegroep (RG) van Kwantum Einstein zwaartekracht (QEG) en projecteerbare Hořava-Lifschitz zwaartekracht (HLG), samen met een aantal fenomenologische toepassingen ervan.

QEG vorm een implementatie van Weinbergs scenario van ‘Asymptotische Veiligheid’, welke stelt dat de UV-afwerking van zwaartekracht gebaseerd moet zijn op een niet-Gaussisch vast punt van de RG-stroom. Om in overeenstemming te zijn met experimentele waarnemingen, moet het RG-pad dat de Natuur beschrijft over een zogenoemd klassiek regime beschikken, waar de Algemene Relativiteitstheorie een goede benadering vormt. We classificeren de RG-stroom van de Einstein-Hilbert actie en een veralgemenisering daarvan, waarin er een hogere-afgeleide operator R^2 aan toegevoegd is. De resulterende fasegrammen worden in detail bestudeerd, waarbij de nadruk wordt gelegd op de trajecten die beginnen bij een niet-Gaussisch vast punt in het UV-regime en bij lage energieën de overgang maken naar een klassiek regime. Deze classificaties vormen de basis voor elke fenomenologische toepassing.

Als een eerste voorbeeld wordt de spectrale dimensie van de effectieve QEG-ruimtetijd bepaald. De ruimtetijd beschikt over een multi-fractale structuur, in de zin dat de spectrale dimensie afhangt van de RG-schaal, en verschillende plateaus vormt. Het bestaan van deze plateaus wordt herleid tot de universele eigenschappen van de onderliggende RG-stroom, welke gedirigeerd wordt door een vast punt of singuliere punten. Aangetoond wordt dat dit beeld overeind blijft na toevoeging van hogere-afgeleide operatoren.

Dit werk voert tevens voor het eerst een studie uit naar RG-stromen in projecteerbare HLG. Deze theorie verschilt van QEG in de zin dat zijn gereduceerde symmetriegroep een asymmetrie toestaat tussen tijd en ruimte. Voor deze context is een nieuwe, anisotropische, functionale RG-vergelijking van het Wetterich-type ontwikkeld. Op basis van deze vergelijking worden de bèta-functies geconstrueerd die op lage energieën de schaal-afhankelijkheid van HLG vatten. Deze bèta-functies bevatten het volgende:

- a) de overgang van een Euclidische signatuur naar een Lorentz-signatuur heeft slechts een klein effect op de Asymptotische Vrijheid,
- b) de RG-stroom van projecteerbare HLG beschikt over een niet-Gaussisch vast punt, waarvan de eigenschappen vergelijkbaar zijn met die van QEG,
- c) sommige van de trajecten die voortvloeien uit dit niet-Gaussisch vast punt van HLG maken de overgang naar een klassiek regime.

Hiermee toont dit proefschrift aan dat QEG en projecteerbare HLG over trajecten beschikken die in overeenstemming zijn met experimentele waarnemingen, zodat beide theorieën consistente kandidaten zijn voor een theorie van de kwantumzwaartekracht.

Summary

Classical General Relativity provides a well established description of the gravitational force from sub-millimeter up to cosmological scales. Unifying gravity and Quantum Mechanics however is still an outstanding problem in theoretical physics today. This thesis contributes to the construction of a consistent and predictive quantum theory of gravity within the framework of Quantum Field Theory. Explicitly we discuss non-perturbative aspects of the Renormalisation Group (RG) flows of Quantum Einstein Gravity (QEG) and projectable Hořava-Lifshitz gravity (HLG) together with some phenomenological applications.

QEG implements Weinberg's Asymptotic Safety scenario, which states that the UV completion of gravity is based on a non-Gaussian fixed point of the RG flow. In order to be compatible with experimental observations the RG trajectory, describing Nature, must possess a classical regime where General Relativity provides a good approximation. We classify the RG flow of the Einstein-Hilbert action and its generalisation including a higher-derivative R^2 operator. The resulting phase diagrams are analysed in detail with the main focus on those trajectories which start from a non-Gaussian fixed point in the UV and cross over to a classical regime at low energies. These classifications provide the foundation for any phenomenological application.

As a first example the spectral dimension of the effective QEG spacetime is constructed. The spacetime possesses a multi-fractal structure in the sense that the spectral dimension varies with the RG scale and develops various plateaus. The existence of these plateaus is traced back to universal features of underlying RG flow, controlled by fixed point or singular loci. This picture is shown to be robust against the inclusion of the higher-derivative operator.

This work also performs the first study of RG flows in projectable HLG. This theory differs from QEG in the sense that its reduced symmetry group admits an asymmetry between space and time. For this framework a novel, anisotropic, Wetterich type, functional RG equation is constructed. Based on this equation the beta functions capturing the scale-dependence of HLG at low energies are constructed explicitly. These entail that

- a) the change from Euclidean to Lorentzian signature has only a marginal effect on Asymptotic Safety,
- b) the RG flow of projectable HLG possesses a non-Gaussian fixed point whose properties are similar to the one observed in QEG,
- c) some trajectories emanating from this non-Gaussian HLG fixed point cross over to a classical regime.

Thus, this thesis establishes that QEG and projectable HLG possess trajectories which are compatible with experimental observations so that both theories are consistent candidates for a quantum theory of gravity.

Contents

Introduction	1
I The Method and the Scenario	7
1 The Wilsonian Approach to Renormalisation	9
2 The Functional Renormalisation Group Equation	15
2.1 The Wetterich Equation for Scalars	15
2.2 The Wetterich Equation for Gauge Fields	18
3 The Asymptotic Safety Scenario	21
II Metric Gravity	25
4 Motivation	27
5 Flow Equations for Metric Gravity	31
5.1 The Einstein-Hilbert Truncation	31
5.2 The R^2 Truncation	39
6 The Phase Diagram of Metric Gravity	43
6.1 Phase Diagram of the Einstein-Hilbert Truncation	43
6.2 Phase Diagram of the R^2 Truncation	49
7 The Spectral Dimension	63
7.1 The Notion of Dimension	63
7.2 Spectral Dimension within the Einstein-Hilbert Truncation	66
7.3 Spectral Dimension within the R^2 Truncation	70

III	Foliated Gravity	75
8	Motivation	77
8.1	Field Content and Symmetry	77
8.2	An Excursion to Hořava-Lifshitz Gravity	79
9	The Wetterich Equation for Foliated Spacetimes	83
10	Flow Equations for Foliated Gravity	87
10.1	A Versatile Truncation	87
10.2	Evaluating the Functional Traces	92
11	RG Flows of Foliated Gravity	99
11.1	Phase Diagram of the Foliated Einstein-Hilbert Truncation	99
11.2	Phase Diagram of Hořava-Lifshitz Gravity	107
	Conclusion and Outlook	115
A	Notation and Conventions	121
B	Gauge Symmetry and Quantisation	123
B.1	The Faddeev-Popov Method	123
B.2	The Background Field Method	124
C	The Heat-Kernel Technique	127
C.1	The Early-Time Expansion	127
C.2	The York Decomposition and Spherical Backgrounds	128
C.3	Heat-Kernel Coefficients for Fields with Constraints	130
C.4	The Threshold Functions	134
D	The Coefficient Functions for the R^2 Truncation	137
E	The Arnowitt-Deser-Misner Decomposition	143
F	The Right Hand Side of the Foliated Flow Equation	147
F.1	The Second Variations of the Anisotropic Gravitational Action	147
F.2	The Scalar Trace	150
F.3	Summing the Matsubara Modes	154

List of Figures

1.1	Operator generated while UV modes are integrated out.	13
2.1	An exemplary regulator.	17
6.1	The phase diagram of the Einstein-Hilbert truncation.	45
6.2	Slices of the phase diagram of the R^2 truncation.	51
6.3	$\bar{G}_k = 0$ slices of the phase diagram of the R^2 truncation.	53
6.4	$\bar{b}_k = 0$ slice of the phase diagram of the R^2 truncation.	55
6.5	Slices of the phase diagram of the R^2 truncation using b_k instead of β_k	56
6.6	Three-dimensional plot of a sample of Type Ia and Type IIIa trajectories.	57
6.7	Slices of the phase diagram of the R^2 truncation in $D = 4$	59
6.8	Three-dimensional plot of a sample of Type Ia and Type IIIa trajectories.	62
7.1	Scale-dependent spectral dimension for a Type IIIa trajectory of the Einstein-Hilbert truncation.	68
7.2	Scale-dependent spectral dimension for three different Type IIIa trajectories of the Einstein-Hilbert truncation.	69
7.3	Scale-dependent spectral dimension for the separatrix and a Type Ia trajectory of the Einstein-Hilbert truncation.	70
7.4	Scale-dependent spectral dimension of the R^2 truncation in $D = 4$	73
7.5	Scale-dependent spectral dimension of the R^2 truncation in $D = 3$	73
11.1	The phase diagram of the foliated Einstein-Hilbert truncation in the compactification limit for $d = 4$	103
11.2	The phase diagram of the foliated Einstein-Hilbert truncation for $m = 2\pi$	105
11.3	Fixed-point values and critical exponents depending on the Kaluza-Klein mass m in $d = 3$	106

11.4	Analytic Structure of the beta function for the low-energy limit of Hořava-Lifshitz gravity.	108
11.5	Fixed-point values and critical exponents depending on the Kaluza-Klein mass m in $d = 3$ for the asymmetric truncation.	110
11.6	Line of vanishing $\beta_{\bar{\lambda}}$ for $\bar{\lambda}_k = 1$, $m = 2\pi$ and $\varepsilon = 1$	111
11.7	A sample of trajectories developing a classical regime in the IR.	113
11.8	Scale dependence of the dimensionful couplings for a trajectory exhibiting a classical regime.	113
E.1	The foliation of spacetime.	144

List of Tables

4.1	Diffeomorphism invariant terms.	28
6.1	Classification of trajectories in the Einstein-Hilbert truncation. . . .	47
6.2	Classification of trajectories in the three-dimensional R^2 truncation. . . .	54
6.3	Classification of trajectories in the $(4 - \epsilon)$ -dimensional R^2 truncation. . . .	61
8.1	Comparison of gravitational theory spaces.	81
11.1	Analytic Structure of the beta function for the foliated Einstein-Hilbert truncation.	100
11.2	Fixed points in the Compactification limit of the foliated Einstein-Hilbert truncation.	102
11.3	Fixed points in the foliated Einstein-Hilbert truncation for $m = 2\pi$ in $d = 3$	104
11.4	Analytic Structure of the beta function for the low-energy limit of Hořava-Lifshitz gravity.	108
11.5	Fixed points in the low-energy limit of HLG for $m = 2\pi$ in $d = 3$	109
A.1	List of frequently used constants.	122
C.1	Eigenvalues and degeneracies of the background Laplacian.	130
C.2	List of heat-kernel coefficients a_0 and a_2	133
C.3	List of heat-kernel coefficients a_4	134

Abbreviations

ADM	Arnowitt-Deser-Misner
BEA	Background Effective Action
BEAA	Background Effective Average Action
BFM	Background Field Method
EA	Effective Action
EAA	Effective Average Action
EDT	Euclidean Dynamical Triangulation
FRG	Functional Renormalisation Group
FRGE	Functional Renormalisation Group Equation
GFP	Gaussian Fixed Point
GR	General Relativity
HLG	Hořava-Lifshitz Gravity
IR	Infrared
NGFP	Non-Gaussian Fixed Point
QCD	Quantum Chromodynamics
QED	Quantum Electrodynamics
QEG	Quantum Einstein Gravity
QFT	Quantum Field Theory
QG	Quantum Gravity
RG	Renormalisation Group
TT	Transverse Traceless
UV	Ultraviolet

Introduction

Today's theoretical physicists are facing many problems in a wide range of topics ranging from High Energy Physics over Solid State Physics to General Relativity (GR). The complexity of all areas is increasing in time and thus one is tempted to go back "to the roots" and review the great advances in physics of the 20th century. The development of quantum physics on the one hand and GR on the other hand mark two major breakthroughs in the understanding of Nature. Both theoretical frameworks are confirmed experimentally with outstanding precision. The success of these theories raises hope that availing oneself of the underlying concepts may shed some light on current problems as well. Therefore it seems reasonable to start with a brief retrospect, see [1] for an extensive overview.

In 1901 the century started with the quantum hypothesis of Max Planck. He suggested that energy might be exchanged between radiation and matter in discrete portions, called quanta. This is the birth of quantum physics. After the particle-wave-duality proposal of de Broglie in 1924, Heisenberg, Born and Jordan developed the matrix formulation of Quantum Mechanics in 1925. Afterwards Schrödinger found his wave equation and explained the connection to the matrix formulation in 1926. One year later Dirac quantised the electromagnetic field, unifying the quantum-mechanical ideas with the theory of Special Relativity invented by Einstein in 1905. This leads to the theory of Quantum Electrodynamics (QED) and marks the advent of Quantum Field Theory (QFT). At the end of the 60s Salam, Glashow and Weinberg combined QED with the weak interaction to the electroweak theory. The advances of experimental physics in the 50s and 60s revealed a growing amount of new particles. For the understanding of this particle zoo the proton and neutron as elementary particles were insufficient. Therefore Gell-Mann and Zweig independently proposed quarks as fundamental particles in 1964. These interact with each other and with the gluons via the strong force, described by Quantum Chromodynamics (QCD). The combination of the electroweak theory and QCD is called the standard model of particle physics and is experimentally verified to very high precision. Notably, recent experiments at the Large Hadron

Collider (LHC) observed a new bosonic particle which is very likely to be the Higgs particle, the last particle of the standard model which has not been observed before [2, 3]. This collection of theories forms the basis of today's understanding of matter and its interaction via the electromagnetic, weak and strong force.

The fourth known force in Nature, the gravitational interaction, is not included in the standard model of particle physics. Gravity is described by the theory of GR, invented by Einstein in 1915. Many predictions of this theory have been verified since then. Its breakthrough was the verification that light is deflected by the sun in 1919 by Eddington. Other predictions, as the perihelion shift of planets or the gravitational redshift, are observed too.

These passed tests of GR have been performed at scales comparable to the size of the solar system. However, going to larger scales GR faces some experimental results it can not explain. Examples are the flattening of galaxy rotation curves or the accelerated expansion of the universe. One possibility to explain these phenomena is to introduce dark matter and dark energy. At very small scales on the other hand, the situation is even worse. Here we know that the quantum-mechanical effects have to be considered. The standard model of particle physics teaches us that matter is quantised and thus one might wonder if spacetime should be considered as a classical object, or also follows the rules of Quantum Mechanics.

However, a quantisation similar to the procedure in the standard model of particle physics does not work for GR. A crucial difference between the interactions of the standard model and gravity is that the coupling constants, determining the strength of interactions, are dimensionless in the standard model, while the Newton constant has negative mass dimension. Therefore gravity is perturbatively non-renormalisable [4–6]. Nevertheless, quantum effects of GR can be treated in an effective-field-theory approach (see [7–9] for an introduction). As the name suggests, effective field theories are effective theories, valid up to some energy scale. Beyond this scale such a treatment would be insufficient. However the conflicts between GR and QFT arise at very high energies (at the Planck scale if we exclude theories with extra dimensions) and therefore it would be of interest to have a complete quantised theory of GR which is valid at arbitrary high energy scales. Such a theory very often is called Quantum Gravity (QG), but following the author of [10] one should say "Quantum Gravity denotes a problem, not a theory". In fact there are several approaches towards a consistent theory of QG, and each approach has its own strengths and weaknesses.

The failure of a perturbative quantisation of GR together with the lack of experimental guidance has spawned many ideas how a quantum theory of gravity could look like. One possible suggestion would be the introduction of new physics, as it is done in String Theory [11, 12]. Another possibility would be to adjust the rules of quantisation, which is done in Loop Quantum Gravity [13]. A more conservative point of view would be the assumption that the failure of perturbative renormalisa-

tion is an artefact of perturbation theory. According to a proposal of Weinberg [14] a theory might be non-perturbatively renormalisable despite being perturbatively non-renormalisable. The corresponding scenario is called Asymptotic Safety and the analysis of some of its aspects is the aim of this thesis. Yet another possible solution would be the relaxation of the symmetry principles underlying the theory. This is done in Hořava-Lifshitz gravity (HLG), which was introduced by Hořava in 2009 [15, 16].

As this thesis does not discuss all these approaches, we will sketch only those ideas, which will be relevant in the following. Starting with the Asymptotic Safety scenario, we notice that non-perturbative tools are necessary to reveal the quantum nature of gravity within this scenario. One non-perturbative tool is the lattice. However, the lattice calculations known from QFT on flat backgrounds are not applicable for gravitational theories, as the metric itself is a dynamical variable. A possible solution is based on the work by Regge in 1961 [17], called Regge calculus. Here the discretised version of spacetime is constructed by gluing together four-simplices. A modification of this was introduced by Ambjørn, Jurkiewicz and Loll, [18–20], and is called Causal Dynamical Triangulation (CDT). The main difference is that CDT uses a causal structure of spacetime. Therefore it is possible to restrict the geometries considered in the path integral to those, which are causally well behaved. For a review of discrete approaches see [21] and for a more recent introduction to CDT see [22]. Furthermore Euclidean Dynamical Triangulations (EDT) seems to reproduce many results known from CDT by introducing a non-trivial measure term within the gravitational path integral [23–25].

In contrast to these discrete methods, this thesis employs continuum Functional Renormalisation Group (FRG) techniques introduced and reviewed in [26–28]. As in the discrete approaches we suppose that the failure of the perturbative renormalisation of gravity is a shortcoming of perturbation theory. The non-perturbative renormalisability can then be established by finding a suitable non-trivial fixed point in the Renormalisation Group (RG) running of the couplings. If in addition the theory is invariant under diffeomorphisms it is called Quantum Einstein Gravity (QEG).

The second proposal considered within this thesis is HLG. Within this approach the perturbative renormalisability is restored by assuming that the diffeomorphism invariance, as the symmetry underlying GR, is broken at high energies and replaced by the so-called foliation-preserving diffeomorphism invariance. The latter allows the introduction of an asymmetry between space and time. The full diffeomorphism invariance, which is experimentally very well verified, has to be restored dynamically at low energies.

At the first sight it might be surprising that, for decades, an incredible amount of approaches try to explain the same thing, while it has not been possible so far to exclude some of them. The reason for this becomes obvious if we compare

the development of the field of QG to the development of the standard model. The latter was mainly driven by new experimental results, especially the collider experiments in the 50s and 60s, which could not be explained by the established theories of that time. In contrast to this, experiments of quantum-gravitational effects are not yet available. Furthermore the complexity of the different approaches makes it hard to do solid predictions. Therefore an exclusion of candidate theories is possible only by internal inconsistencies or a conflict with GR. This might be interpreted pessimistically as a drawback. An optimistic viewpoint would consider it a feature, as it enables us to compare the various approaches and in this way possibly discover predictions shared by different theories. This might open the door towards a deeper understanding of spacetime and its quantisation.

Following this line, we compare the FRG analysis of the Asymptotic Safety scenario with HLG. Therefore we start to discuss first the metric formulation of QEG on the spacetime manifold \mathcal{M} . Here the degrees of freedom are carried by the spacetime metric $\tilde{g}_{\mu\nu}$ and, motivated by GR, we assume the theory to be invariant under spacetime diffeomorphisms $\text{Diff}(\mathcal{M})$. One possible bridge between QEG and other QG candidates is the spectral dimension of the resulting spacetimes. The interest in this topic actually is twofold. First, the spectral dimension and dynamical dimensional reduction give us information about the spacetime itself. Secondly and probably more rewarding is the possibility to compare the results to other approaches to QG. Besides the FRG approach [29–31], the spectral dimension was investigated in many other approaches. This topic was discussed first within CDT [32–34]. Further research was done e.g. in EDT [23], HLG [35], Loop Quantum Gravity and spin foam models [36–38] and in spacetimes with a minimal length [39]. For a better understanding toy models of spacetime, as e.g. quantum spheres, κ -Minkowski space and others [40] or multigraph ensembles [41, 42], have been discussed. The author in [43, 44] used the strong coupling limit of the Wheeler-DeWitt equation to work on this subject, the dispersion relation corresponding to the scale-dependent spectral dimension was discussed in [45, 46] and a fractional differential calculus [47] was used to equip spacetime with spectral features seen by many approaches to quantum gravity (see e.g. [48] and references therein).

For the analysis of the spectral dimension within the FRG framework we utilise RG-improved diffusion processes. Such RG improvements were already used to study consequences of running coupling constants in various settings. Examples are black holes [49–55], galaxy rotation curves [56, 57], various scattering processes in gravitational theories with large extra dimensions [54, 58–63] and cosmology [64–80]. A general discussion of the RG improvement can be found in [81]. Among the various applications of RG improvement we will concentrate on the spectral dimension as a very interesting one. The analysis of the latter requires a sufficient knowledge about the space of all action functionals under consideration. Therefore we extensively discuss the corresponding space underlying QEG. This analysis is

interesting in its own right as it is necessary for finding a suitable low-energy limit of the quantum theory. By suitable we mean that at low energies the theory of GR has to be reproduced in order to meet the experimentally verified effects.

Besides the comparison of predictions, as the spectral dimension, a treatment of HLG within the FRG setting is an interesting way of discussing its quantisation. Therefore we investigate anisotropic effects between space and time by introducing a foliation structure of the manifold \mathcal{M} , causing a split of the spacetime metric $\tilde{g}_{\mu\nu}$ into the lapse function \tilde{N} , the shift vector \tilde{N}_i and the spatial metric $\tilde{\sigma}_{ij}$. Sticking to the diffeomorphism invariance $\text{Diff}(\mathcal{M})$ we arrive at the foliated formulation of QEG. This setting can be used to switch the signature of the metric and for the first time investigate Asymptotic Safety in a Lorentzian setting. Besides the switch of signature, the foliation structure enables us to introduce an asymmetry between space and time as proposed by Hořava. In this thesis we discuss the low-energy limit of HLG where one expects to find the limit of GR. In terms of symmetries this means the restoration of invariance under $\text{Diff}(\mathcal{M})$ is expected. This requirement is used to identify those RG trajectories which are most likely compatible with the experimental data.

The thesis is organised as follows. In Appendix A we fix the notation and conventions used here. During the main text we do not comment on conventions and the interested reader can find the details in this appendix. Apart from the appendix the thesis is divided into three parts. The first discusses the FRG techniques and introduces the notion of Asymptotic Safety in a general context. After this general introductory part we specify, within the following considerations, to gravitational theories. Explicitly we are discussing gravity in two different formulations. Starting with Part II we discuss the metric formulation, where the degrees of freedom are encoded in the spacetime metric. Part III covers the foliated formulation, where the metric is split into lapse function, shift vector and spatial metric. Part II and Part III are written such that they can be read independently.

Part II starts with a short motivation in Chapter 4. Afterwards, the flow equation of the Einstein-Hilbert truncation and the R^2 truncation are discussed in Chapter 5. Here we concentrate on the former, for simplicity, and reduce the discussion of the latter to the main conceptual issues. Technical details are provided in the Appendices B, C and D. In Chapter 6 the phase diagrams corresponding to the flow equations of Chapter 5 are analysed. The discussion of the phase diagram corresponding to the R^2 truncation constitutes one of the main results of this thesis. The last chapter of Part II uses the results of Chapter 6 to analyse the spectral dimension. We start with a brief introduction to the notion of dimension before discussing the spectral dimension emerging in the Einstein-Hilbert and the R^2 truncation.

The structure of Part III is similar to the one of Part II. Again we start with a short motivation, where we discuss the field content and symmetry of HLG on

foliated spacetimes. A short overview of HLG is included as well. Chapter 9 gives a detailed derivation of the Wetterich equation in the foliated formulation while Chapter 10 discusses its simplest truncation. Again the technical details have been moved to Appendices E and F. Within the last chapter the phase diagram of the low-energy limit of HLG is discussed and a comparison of foliated QEG with Lorentzian and Euclidean metric is given. The conclusion finally summarises the results of the main text and gives an outlook for possible future developments based on these findings.

Part I

The Method and the Scenario

The Wilsonian Approach to Renormalisation

Different types of theories will be discussed within this thesis. Some of them are introduced just for pedagogical reasons as e.g. the scalar theory. The metric and the foliated formulation of QEG on the other hand are the topic of this thesis and are discussed extensively.

Throughout this work we will adopt a Wilsonian viewpoint on renormalisation. In this framework, a theory is defined by the field content and its symmetry. As an example let us discuss the scalar theory. Its field contents is the scalar field $\tilde{\varphi}$ and it satisfies the Z_2 symmetry. The corresponding Euclidean, microscopic action¹ $S[\tilde{\varphi}]$ satisfies this symmetry and all physical information of such a theory, as e.g. amplitudes of scattering processes, are stored in the correlation functions. If we consider exemplarily a scattering process with two incoming and $(n - 2)$ outgoing particles we have to discuss the n -point correlation function. Using the Euclidean path integral, this is defined as

$$\langle \tilde{\varphi}(x_1) \dots \tilde{\varphi}(x_n) \rangle = \mathcal{N} \int_{\Lambda} \mathcal{D}\tilde{\varphi} \tilde{\varphi}(x_1) \dots \tilde{\varphi}(x_n) e^{-S[\tilde{\varphi}]} \quad (1.1)$$

with a suitable normalisation \mathcal{N} and the microscopic action $S[\tilde{\varphi}]$ in the exponent. The index Λ at the integral denotes a UV cutoff, required for a well-defined path integral. Here we consider a simple sharp cutoff in the sense that we do not integrate over fields $\tilde{\varphi}(p)$ with $|p| > \Lambda$. The generating functional for all n -point correlation functions is the partition function $Z[J]$, which is defined as

$$Z[J] = \int_{\Lambda} \mathcal{D}\tilde{\varphi} e^{-S[\tilde{\varphi}] + \int d^D x J(x)\tilde{\varphi}(x)}. \quad (1.2)$$

¹We are working with the Euclidean setting and the Minkowski analog can be found by analytical continuation.

The n -point correlators (1.1) contain contributions from connected and disconnected physical processes. The latter can be factored out by considering only the connected Green functions. The generating functional for them is the Schwinger functional $W[J] = \ln Z[J]$. An even more efficient way to store the information are the one-particle irreducible (1PI) vertex functions. Their generating functional is the Effective Action (EA) $\Gamma[\varphi]$ which is the Legendre transformation of the Schwinger functional

$$\Gamma[\varphi] = \sup_J \left(\int d^D x J(x) \varphi(x) - W[J] \right). \quad (1.3)$$

Here $\varphi(x) = \frac{\delta W[J]}{\delta J(x)} = \langle \tilde{\varphi} \rangle_J$ is the classical or averaged field. In the following we will abbreviate the n th derivative with respect to the field with an upper index (n). Thus the n th derivative of the EA action reads

$$\Gamma^{(n)}(p_1, \dots, p_n) = \frac{\delta^n \Gamma[\varphi]}{\delta \varphi(p_1) \dots \delta \varphi(p_n)}. \quad (1.4)$$

Here $\varphi(p)$ denotes the Fourier transform of $\varphi(x)$ and the $\Gamma^{(n)}$ constitute the 1PI n -point function of the theory, containing all quantum effects.

After having introduced these basics of QFT for fixing the notation, we can proceed and discuss the renormalisation of our exemplary scalar theory. We start with the perturbative setting before contrasting it with the Wilsonian setting. More details can be found in any standard text book as [82].

To start with, we introduce the classical action of the scalar $\tilde{\varphi}^4$ theory. It reads

$$S[\tilde{\varphi}] = \int d^D x \left(\frac{1}{2} (\partial_\mu \tilde{\varphi})^2 + \frac{m_0^2}{2} \tilde{\varphi}^2 + \frac{\lambda_0}{4!} \tilde{\varphi}^4 \right) \quad (1.5)$$

with the spacetime dimension D . Here we find the kinetic and the mass term corresponding to a free theory and the last terms, including the coupling λ_0 , introduces an interaction into the system. Note that we used a lower index 0 on m_0^2 and λ_0 in order to show that these are the constants corresponding to the classical action. The perturbative expansion of the EA corresponding to the classical action (1.5), up to 1-loop, reads

$$\Gamma[\varphi] = S[\varphi] + \Gamma^{1\text{-loop}}[\varphi], \quad \Gamma^{1\text{-loop}}[\varphi] = \frac{1}{2} \text{Tr} \ln S^{(2)}. \quad (1.6)$$

Evaluating the Feynman diagrams at 1-loop order in $D = 4$ we find that $\Gamma^{(2)1\text{-loop}}$ has a divergence proportional to Λ^2 where Λ denotes the UV cutoff. Additionally we find a divergence proportional to $\ln \Lambda$ in $\Gamma^{(4)1\text{-loop}}$. However, this does not mean that the QFT is ill defined. The source of these divergences are fluctuations at all

scales and thus the right question to ask is: Is it useful to determine a quantity to be measured with correlation functions depending on parameters of the microscopic action, although the measurement might take place at a macroscopic scale? The answer is: No. Indeed the parameters m_0^2 and λ_0 of our microscopic action do not correspond to the measured quantities. In contrast, the latter ones are related to the renormalised couplings, which we will denote by m_r^2 and λ_r . Furthermore we introduce the renormalised field φ_r via $\varphi = Z^{1/2}\varphi_r$ with the wave-function renormalisation Z . These renormalised quantities can be used to eliminate the bare couplings m_0^2 and λ_0 . Therefore we define δ_Z, δ_m and δ_λ , in order to fix the relation between the bare quantities and the renormalised ones, via

$$\delta_Z = Z - 1, \quad \delta_m = m_0^2 Z - m_r^2, \quad \delta_\lambda = \lambda_0 Z^2 - \lambda. \quad (1.7)$$

The insertion of these expressions into the classical action (1.5) leads to

$$\begin{aligned} S[\varphi] = & \int d^D x \left(\frac{1}{2} (\partial_\mu \varphi_r)^2 + \frac{m_r^2}{2} \varphi_r^2 + \frac{\lambda_r}{4!} \varphi_r^4 \right) \\ & + \int d^D x \left(\frac{\delta_Z}{2} (\partial_\mu \varphi_r)^2 + \frac{\delta_m}{2} \varphi_r^2 + \frac{\delta_\lambda}{4!} \varphi_r^4 \right). \end{aligned} \quad (1.8)$$

The first integral is exactly the classical action, but with the renormalised quantities. In the second integral we find the so-called counter terms which can be adjusted such that they contain the divergences identified before.

To make sense out of the relation between the bare and the renormalised quantities (1.7) we have to specify the definition of the renormalised ones. As discussed above m_r^2 and λ_r are determined via an experiment. This experiment takes place at a typical scale μ . Let us consider e.g. $\mu = 0$. At this scale we find $m_r^2 = \Gamma^{(2)}(0, 0)$ and $\lambda_r = \Gamma^{(4)}(0, 0, 0, 0)$, with the second and fourth derivative of Γ defined in (1.4). These are the so-called renormalisation conditions. The important point to notice here is that the identification at a different scale μ would lead to different renormalised couplings. Of course, the choice of the renormalisation scale should not affect physics. Moving from one scale to another, we can adapt the renormalised couplings without changing physics. This is called the renormalisation group (RG) and the relation between the renormalised couplings at different scales is described by renormalisation group equations as e.g. the Callan-Symanzik equation.

In contrast to this perturbative discussion, this thesis is based on the Wilsonian idea of renormalisation. Although the ansatz is very different from the perturbative viewpoint above, we will find the same scale dependent couplings as in the perturbative setting. Starting with the partition function (1.2) we can split the field modes into modes within a momentum shell of large momenta and soft modes

with small momenta according to $\tilde{\varphi}(p) = \tilde{\varphi}'(p) + \tilde{\varphi}''(p)$ with

$$\begin{aligned}\tilde{\varphi}'(p) &= \tilde{\varphi}(p) \theta \left(\left(\frac{\Lambda}{b} \right)^2 - p^2 \right), \\ \tilde{\varphi}''(p) &= \tilde{\varphi}(p) \left[\theta \left(\Lambda^2 - p^2 \right) - \theta \left(\left(\frac{\Lambda}{b} \right)^2 - p^2 \right) \right].\end{aligned}\quad (1.9)$$

Here θ denotes the Heaviside step function and the $\tilde{\varphi}'$ are soft modes with momenta $|p| < \frac{\Lambda}{b}$ where b is a constant parameter. The modes marked with two primes on the other hand are the modes of the momentum shell $\frac{\Lambda}{b} < |p| < \Lambda$. Inserting this decomposition into the partition function we find

$$\begin{aligned}Z[J] &= \int_{\Lambda/b} \mathcal{D}\tilde{\varphi}' \int_{\Lambda/b < |p| < \Lambda} \mathcal{D}\tilde{\varphi}'' e^{-S[\tilde{\varphi}', \tilde{\varphi}''] + \int \frac{d^D p}{(2\pi)^D} (J'(p)\tilde{\varphi}'(p) + J''(p)\tilde{\varphi}''(p))} \\ &= \int_{\Lambda/b} \mathcal{D}\tilde{\varphi}' e^{-S_W[\tilde{\varphi}'] + \int \frac{d^D p}{(2\pi)^D} J'(p)\tilde{\varphi}'(p)}\end{aligned}\quad (1.10)$$

where the modes of the momentum shell have been integrated out in the second line. The resulting action, S_W , in the exponent determines the dynamics of the soft modes and is called the Wilsonian effective action. As the high momentum modes have been integrated out, S_W contains their quantum effects. Note that therefore it can contain terms different from those of the microscopic action. Within our exemplary scalar theory its general form is

$$\begin{aligned}S_W[\tilde{\varphi}'] &= \int d^D x \left[\frac{1}{2}(1 + \Delta Z)(\partial_\mu \tilde{\varphi}')^2 + \frac{1}{2}(m^2 + \Delta m^2)\tilde{\varphi}'^2 + \frac{1}{4!}(\lambda + \Delta\lambda)\tilde{\varphi}'^4 \right. \\ &\quad \left. + \frac{1}{6!}\Delta\lambda_6 \tilde{\varphi}'^6 + \Delta Z_2(\partial_\mu \tilde{\varphi}')^4 + \dots \right].\end{aligned}\quad (1.11)$$

Here the dots denote all further terms which might be produced. In Figure 1.1 an example for the generation of higher-order operators is depicted. Explicitly it shows, how a $\tilde{\varphi}'^6$ operator is generated by the $\tilde{\varphi}'^4$ operator, while the modes of the momentum shell are integrated out. Note that also higher-order derivative terms are induced as indicated by the last term in (1.11).

For a concrete comparison of S and S_W we perform a rescaling. Explicitly the rescaling reads

$$p' = bp, \quad x' = \frac{x}{b}, \quad \Rightarrow \quad \int d^D x = \int d^D x' b^D, \quad \int_{|p| < \Lambda/b} \mathcal{D}\tilde{\varphi}' = \int_{|p'| < \Lambda} \mathcal{D}\tilde{\varphi}'. \quad (1.12)$$

An additional redefinition of the scalar field according to $\tilde{\varphi} = [b^{D-2}(1+\Delta Z)^{-1}]^{1/2}\tilde{\varphi}'$ leads us to the following rescaled Wilsonian action

$$S_W[\tilde{\varphi}] = \int d^D x' \left[\frac{1}{2}(\partial'_\mu \tilde{\varphi})^2 + \frac{m'^2}{2}\tilde{\varphi}^2 + \frac{\lambda'}{4!}\tilde{\varphi}^4 + \frac{\lambda'_6}{6!}\tilde{\varphi}^6 + Z'_2(\partial'_\mu \tilde{\varphi})^4 + \dots \right]. \quad (1.13)$$

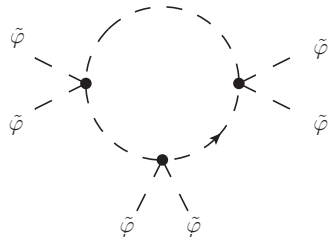


Figure 1.1: Depicted is a graph illustrating the dynamical generation of a $\tilde{\varphi}^6$ interaction from the classical $\tilde{\varphi}^4$ operator. Within the loop, modes of the momentum shell are circulating.

Besides the redefinition of the field, we also introduced rescaled couplings. The new couplings, marked with a prime, in terms of the old couplings read

$$\begin{aligned}
 (m')^2 &= (m^2 + \Delta m^2)(1 + \Delta Z)^{-1} b^2, \\
 \lambda' &= (\lambda + \Delta\lambda)(1 + \Delta Z)^{-2} b^{4-D}, \\
 \lambda'_6 &= (\lambda_6 + \Delta\lambda_6)(1 + \Delta Z)^{-3} b^{6-2D}, \\
 Z'_2 &= (Z_2 + \Delta Z_2)(1 + \Delta Z)^{-2} b^{-D}, \\
 &\vdots
 \end{aligned} \tag{1.14}$$

To summarise, we started with the microscopic action and separated the modes with momenta in a thin momentum shell, from the soft modes with low momenta. We integrated out the former and rescaled the latter. Furthermore we rescaled the couplings to find an expression of the Wilsonian action which can be compared to the microscopic action. This can be interpreted as a transformation on the space of actions and thus constitutes a RG transformation. Repeating this procedure iteratively one can integrate out all quantum fluctuations step by step. Choosing the parameter b infinitesimal close to 1 this transformation becomes continuous and we can find a continuous RG flow for the couplings.

This momentum-shell-wise integration shows very well that the divergences which appeared in the perturbative analysis above are caused by the fact that modes at all scales are contributing to a potentially diverging expression. This makes the Wilsonian approach to renormalisation very well suited to address the issue of these divergences. Therefore we will use this viewpoint in the rest of this thesis, starting with the derivation of an equation describing the aforementioned RG flow.

The Functional Renormalisation Group Equation

2.1 The Wetterich Equation for Scalars

Within this section we derive and discuss the functional renormalisation group equation (FRGE) for the so-called effective average action (EAA) within a scalar theory. This equation was first derived in [83] and thus is also called the Wetterich equation. It is used as a tool to implement a suitable version of the Wilsonian approach to renormalisation, see Chapter 1, which we discuss in the following from a more technical perspective.

Starting point for our considerations is the k -dependent partition function

$$Z_k[J] = \int \mathcal{D}\tilde{\varphi} \exp \left[-S[\tilde{\varphi}] - \Delta S_k[\tilde{\varphi}] + \int d^D x J(x)\tilde{\varphi}(x) \right]. \quad (2.1)$$

Here $S[\tilde{\varphi}]$ denotes the microscopic action of the theory and J is the source corresponding to the scalar field $\tilde{\varphi}$. Note that this expression is similar but not exactly the same as (1.2). The crucial ingredient, making the difference, is the regulator term $\Delta S_k[\tilde{\varphi}]$. The index k denotes the RG scale in the sense that ΔS_k modifies the path integral such that the field modes $\tilde{\varphi}$ with momenta $p^2 > k^2$ are integrated out. In contrast, the integration over field modes with $p^2 < k^2$ are suppressed. Therefore it is solely this term which implements the Wilsonian idea and passes the k dependence to the partition function.

In order to find a modification of the path integral as described above, we choose the regulator term to be quadratic in the field $\tilde{\varphi}$. This can be interpreted as a k -dependent mass term, suppressing the low energy modes with $p^2 < k^2$. Thus

the regulator term reads

$$\Delta S_k[\tilde{\varphi}] = \frac{1}{2} \int \frac{d^D p}{(2\pi)^D} \tilde{\varphi}(-p) \mathcal{R}_k(p) \tilde{\varphi}(p). \quad (2.2)$$

In order to meet the Wilsonian idea, the regulator $\mathcal{R}_k(p)$ has to satisfy three conditions.

$$\begin{aligned} (1) \quad & \lim_{k^2/p^2 \rightarrow 0} \mathcal{R}_k = 0 \\ (2) \quad & \lim_{k^2 \rightarrow \Lambda^2 \rightarrow \infty} \mathcal{R}_k \rightarrow \infty \\ (3) \quad & \lim_{p^2/k^2 \rightarrow 0} \mathcal{R}_k > 0. \end{aligned} \quad (2.3)$$

Condition (1) tells us that for $k \rightarrow 0$ the regulator term vanishes and we regain our standard partition function $Z = \lim_{k \rightarrow 0} Z_k$. This implies that Z computed from Z_k will be independent of the explicit form of \mathcal{R}_k . The other extreme $k \rightarrow \infty$ is given by condition (2). It tells us that the regulator term gives rise to a divergent mass term which suppresses all fluctuations in the path integral. Therefore no quantum fluctuations are integrated out. Between these two extrema, parts of the quantum fluctuations are integrated out and we can treat the resulting generating functional, described by Z_k , as an effective one at the scale k . Condition (3) causes the regulator to be non vanishing in the limit $p^2/k^2 \rightarrow 0$ which thus serves as an IR regularisation. Note that typically $\mathcal{R}_k \sim k^2$ for $p^2 \ll k^2$, which gives a k -dependent mass $\sim k$. This motivates the introduction of the so-called profile function $R^{(0)}$ depending on p^2/k^2 via

$$\mathcal{R}_k(p) = k^2 R^{(0)}\left(\frac{p^2}{k^2}\right). \quad (2.4)$$

Apart from the three conditions (2.3) the regulator can be chosen freely. An example is depicted in Figure 2.1. It uses a smeared Heaviside function, which is useful to demonstrate the properties of the regulator. The conditions (1) and (2) are very well visible. Furthermore one realises that the logarithmic scale derivative $k \frac{d}{dk}$ of the regulator is peaked around $p^2 = k^2$. However during the calculation we will use the so-called Litim cutoff [84, 85] which is related to the Heaviside function itself and reads

$$\mathcal{R}_k^{\text{Litim}} = (k^2 - p^2) \theta\left(1 - \frac{p^2}{k^2}\right). \quad (2.5)$$

Instead of the scale-dependent partition function Z_k we would like to examine the EAA which is the k -dependent version of the EA. Thus we first introduce the k -dependent Schwinger functional W_k via $e^{W_k} = Z_k$. Next we take the logarithmic derivative with respect to the scale k . For brevity we introduce the (RG) time t as

$$t = \ln(k/k_0) \quad \Rightarrow \quad \partial_t = k \frac{d}{dk} \quad (2.6)$$

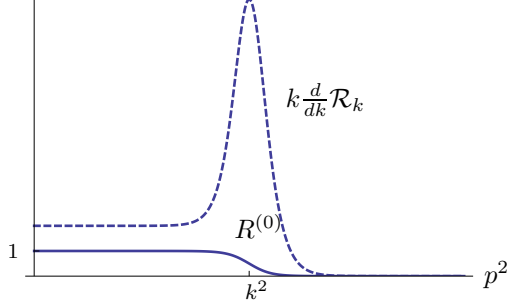


Figure 2.1: Illustration of the profile function $R^{(0)}$ (full line) and the logarithmic derivative of the regulator with respect to the scale k (dashed line). The depicted example is a smeared Heaviside function $R^{(0)} = 1 - \frac{1}{1 + \exp[-c(\frac{p^2}{k^2} - 1)]}$ with a constant c .

with a reference scale k_0 . The logarithmic derivative of W_k thus reads

$$\begin{aligned} \partial_t W_k[J] &= -\frac{1}{2Z_k} \int \mathcal{D}\hat{\phi} \int \frac{d^D p}{(2\pi)^D} \tilde{\varphi}(-p) \partial_t \mathcal{R}_k(p) \tilde{\varphi}(p) e^{-S - \Delta S_k + \int d^D x J(x) \tilde{\varphi}(x)} \\ &= -\frac{1}{2} \int \frac{d^D p}{(2\pi)^D} W_k^{(2)}(p) \partial_t \mathcal{R}_k(p) + \partial_t \Delta S_k[\varphi]. \end{aligned} \quad (2.7)$$

Here $W_k^{(2)}$ denotes the second functional derivative of W_k with respect to the sources and $\varphi = \langle \tilde{\varphi} \rangle$ denotes the expectation value of the fluctuation field. The EAA is then defined as the modified Legendre transformation of W_k .

$$\Gamma_k[\varphi] = \sup_J \left(\int d^D x J(x) \varphi(x) - W_k[J] \right) - \Delta S_k[\varphi]. \quad (2.8)$$

At the supremum the expectation value satisfies the relation $\varphi = \delta W_k / \delta J$ and thus we get $\delta\varphi / \delta J = W_k^{(2)}$. The quantum equations of motion read $J = \delta\Gamma_k / \delta\varphi + \mathcal{R}_k \varphi$. Taking another derivative with respect to the expectation value reveals

$$\frac{\delta J}{\delta\varphi} = \Gamma_k^{(2)} + \mathcal{R}_k \quad (2.9)$$

with $\Gamma_k^{(2)}$ being the second functional derivative of the EAA with respect to φ . Combining (2.9) with $\delta\varphi / \delta J = W_k^{(2)}$ gives us

$$\mathbb{1} = \left(\Gamma_k^{(2)} + \mathcal{R}_k \right) W_k^{(2)}. \quad (2.10)$$

Thus $\Gamma_k^{(2)} + \mathcal{R}_k$ is the inverse of $W_k^{(2)}$. At this point we have all ingredients to derive the flow equation for the EAA by using the Legendre transformation (2.8) for fixed φ at the supremum of the source J , inserting (2.7) and simplifying the result by using (2.10). We find

$$\begin{aligned} \partial_t \Gamma_k[\varphi] &= -\partial_t W_k[J]|_{\varphi} + \int (\partial_t J)\varphi - \partial_t \Delta S_k[\varphi] \\ &= -\partial_t W_k[J]|_J - \partial_t \Delta S_k[\varphi] \\ &= \frac{1}{2} \int \frac{d^D p}{(2\pi)^D} W_k^{(2)}(p) \partial_t \mathcal{R}_k(p). \end{aligned} \quad (2.11)$$

Substituting $W_k^{(2)}(p)$ by (2.10), the final form of the flow equation reads

$$\partial_t \Gamma_k[\varphi] = \frac{1}{2} \text{Tr} \left[(\Gamma_k^{(2)} + \mathcal{R}_k)^{-1} \partial_t \mathcal{R}_k \right]. \quad (2.12)$$

The important result (2.12) is the FRGE or Wetterich equation which will be the main technical tool of this thesis. It is an exact equation capturing the scale dependence of the EAA Γ_k . Note that in (2.12) the regulator appears twice. Therefore, in comparison with Figure 2.1, we find that it simultaneously serves as a UV regulator (numerator) and as an IR regulator (denominator). The contribution of the trace is peaked, as depicted in Figure 2.1, and thus the flow is driven by fluctuations at $k^2 \sim p^2$.

The Wetterich equation can be interpreted in a QFT context. One can use a microscopic theory S as a starting point Γ_Λ at some high UV scale Λ . Integrating down towards $k \rightarrow 0$, the EAA flows to the EA thus defining the quantum theory. This limit is independent of the regulator although the trajectory from the UV to the IR is not. Note however that it is not clear a priori which interaction terms are created during the renormalisation group running, as discussed in (1.11). Thus one has to consider all terms satisfying the symmetry constraints. These are infinitely many and therefore we have to stick to truncations. Examples are the derivative expansion or the vertex expansion. Since these approximations are non-perturbative, in the sense that they do not rely on an expansion in a small coupling, we will use this technique of truncating Γ_k when performing explicit computations. Unfortunately such an approximation spoils the fact that the IR limit is independent of the regulator. To come as close as possible to the true result one can use optimised regulators, see [86] for a detailed discussion.

2.2 The Wetterich Equation for Gauge Fields

After having derived the Wetterich equation for a scalar theory in Section 2.1 we generalise the construction to gauge symmetries, see [87–90] for the original work

and [91] for an introduction. As the derivation is analogous to the preceding section we stay brief here and concentrate on the main differences.

These differences are caused by the presence of gauge freedom, which leads to an ill-defined path integral due to the integration over physically equivalent field configurations. To get a well-defined path integral one can use the gauge-fixing procedure. The Jacobians produced by it can be dealt with by introducing ghost fields. More details can be found in Appendix B.1. This appendix shows that the microscopic action has to be complemented by a gauge-fixing and a ghost action. All three of them shall be summarised and denoted by S in the rest of this section.

In the following, the field content of our theory is denoted by $\tilde{\Phi}$ and collects the quantum fields of the theory as well as the ghost fields. To handle the symmetry during the RG flow we use the Background Field Method (BFM), explained in Appendix B.2. Therefore we split the field $\tilde{\Phi}$ linearly into the sum of a background field $\bar{\Phi}$ and the fluctuations $\hat{\Phi}$ via $\tilde{\Phi} = \bar{\Phi} + \hat{\Phi}$. Here the fluctuations $\hat{\Phi}$ are not assumed to be small in any sense. Furthermore, the background $\bar{\Phi}$ is merely a technical tool and no physical meaning should be attributed to it. Within this notation the k -dependent partition function reads

$$Z_k[J, \bar{\Phi}] = \int \mathcal{D}\hat{\Phi} \exp \left[-S[\hat{\Phi}, \bar{\Phi}] - \Delta S_k[\hat{\Phi}, \bar{\Phi}] + \int d^D x J(x) \hat{\Phi}(x) \right]. \quad (2.13)$$

Here J collects the sources corresponding to the field content of the theory. Besides these sources Z_k depends parametrically on the background $\bar{\Phi}$. To get a momentum-shell-wise integration we introduced a regulator term ΔS_k into the exponent which passes a k dependence to the partition function and is quadratic in the fluctuation fields. Again the regulator has to satisfy the three conditions (2.3), but will depend on the background field. It can be constructed such that it is compatible with the background transformation.

The transition from the k -dependent partition function to the Background Effective Average Action (BEAA), which is the background dependent version of the EAA, can be performed analogously to Section 2.1. The main difference is that all quantities receive a background-field dependence. Therefore the Legendre transformation reads

$$\Gamma_k[\Phi; \bar{\Phi}] = \sup_J \left(\int J\Phi - W_k[J; \bar{\Phi}] \right) - \Delta S_k[\Phi; \bar{\Phi}] \quad (2.14)$$

with $\Phi = \bar{\Phi} + \langle \hat{\Phi} \rangle$ being the expectation value of the fluctuation. Following further the derivation of the Wetterich equation in Section 2.1 and keeping track of the background-field dependence we find the exact FRGE for a gauge theory

$$\partial_t \Gamma_k[\Phi; \bar{\Phi}] = \frac{1}{2} \text{STr} \left[\left(\Gamma_k^{(2)} + \mathcal{R}_k \right)^{-1} \partial_t \mathcal{R}_k \right]. \quad (2.15)$$

An important point which should be stressed is that the supertrace STr includes a trace over field space and all further internal indices as well as a momentum integration. Furthermore it encodes a minus sign for fermionic field contributions as, e.g., the ghost fields.

Integrating the Wetterich equation (2.15) from a microscopic scale $k = \Lambda$ down to $k = 0$ we find the background effective action (BEA) $\Gamma[\Phi, \bar{\Phi}]$. It is invariant under background gauge transformations, as the BEAA is. The ordinary EA can be found if we set $\Phi = \bar{\Phi}$ as discussed in Appendix B.2. With this choice the EA regains the invariance under the initial gauge symmetry and describes the quantised theory.

The Asymptotic Safety Scenario

This chapter introduces the Asymptotic Safety scenario, first formulated by S. Weinberg [14,92] to handle the cumbersome UV divergences appearing in the quantisation of gravitational theories. This scenario proposes a way of constructing a well-defined QFT without resorting to perturbative renormalisability. Therefore it constitutes a possible UV completion in the sense that it gives a consistent and predictive quantum theory of gravity valid on all length scales.

In order to motivate the scenario, we start with a brief discussion of QCD, the theory of quarks, gluons and the strong interaction. This theory is perturbatively renormalisable and the beta function of the coupling constant g , to lowest order in the perturbative expansion, depends on the number of flavours N_f

$$\beta(g) = \frac{g^3}{16\pi^2} \left(-11 + \frac{2N_f}{3} \right). \quad (3.1)$$

Here we work in four dimensions and thus g is dimensionless. According to the standard model of particle physics we assume $N_f = 3$ in (3.1) and find $\beta(g) < 0$. This corresponds to a decreasing coupling constant for increasing energy scale. Therefore, in the high-energy limit, we find $g \rightarrow 0$. As the beta function vanishes in this limit, the point $g_* = 0$ is a fixed point. Furthermore, the coupling constant vanishes at the fixed point, which is referred to as the Gaussian Fixed Point (GFP). This behaviour is called asymptotic freedom and renders the theory well defined at arbitrarily high energy scales, in the sense that the coupling constant stays finite. This is in contrast to, e.g., the gauge coupling of QED which diverges at the Landau pole. It is crucial that the finiteness holds for the dimensionless couplings, as these are the ones appearing in observables. The corresponding dimensionful counterparts might still diverge, but do so in a controlled way.

The Asymptotic Safety scenario can be considered a generalisation of asymptotic freedom. Instead of decreasing continuously and asymptotically running to-

wards the GFP $g_* = 0$, the dimensionless coupling constant might run towards a non-Gaussian fixed (NGFP) point $g = g_* \neq 0$. Therefore the scenario requires a non-perturbative tool as the FRGE, discussed in Chapter 2. In the following, we discuss the Asymptotic Safety scenario within the Wilsonian approach in terms of the EAA and the Wetterich equation.

In Chapter 1 we have seen that the momentum-shell-wise integration of modes potentially produces an infinite amount of field monomials. The set of all action functionals, build from the field content Φ and compatible with the symmetry constraints, is called theory space. Assuming a basis $\mathcal{O}_n[\Phi]$, any theory might be described by an EAA given as an expansion in this basis

$$\Gamma_k[\Phi] = \sum_n \bar{g}_{n,k} \mathcal{O}_n[\Phi], \quad (3.2)$$

with an infinite sum and dimensionful coupling constants $\bar{g}_{n,k}$ corresponding to the field monomials $\mathcal{O}_n[\Phi]$. The dimensionless counterparts of the coupling constants, denoted by $g_{n,k}$, vary with the scale and the dependence on the latter is described by the beta functions

$$\beta_n(g_{1,k}, g_{2,k}, \dots) = \partial_t g_{n,k}. \quad (3.3)$$

Here t denotes the RG time defined in (2.6). Within this notation a GFP would be given for a suitable definition of the couplings if we find $\beta_n(g_1^*, g_2^*, \dots) = 0$ for all n and $g_1^* = g_2^* = \dots = 0$. On the other hand, a fixed point is called non-Gaussian, if at least one coupling does not vanish.

Note that a GFP is not sufficient for asymptotic freedom, as we have seen in the example of QCD. To clarify this, consider a beta function depending on one coupling constant given by

$$\beta(g_k) = c g_k, \quad (3.4)$$

where c is a constant. Obviously the point $g^* = 0$ is a GFP. Nevertheless, if the constant c is positive, the coupling constant increases for increasing energy and thus the corresponding theory would not be asymptotically free. To arrive at the GFP at high energies one would have to start already at $g = 0$ in the IR. This simple example demonstrates that the fixed point alone does not suffice to get an asymptotically free or asymptotically safe theory. Besides the fixed point itself, one has to investigate the critical behaviour close to it.

Considering again a general theory described by the EAA (3.2), the running close to a proposed fixed point (g_1^*, g_2^*, \dots) is described by a linearisation of the beta functions around the fixed point. This linearisation reads

$$\partial_t g_{i,k} \approx \sum_j B_i^j (g_{j,k} - g_j^*), \quad B_i^j = \left. \frac{\partial \beta_i}{\partial g_{j,k}} \right|_{g^*} \quad (3.5)$$

with the so-called stability matrix B_i^j . Diagonalising this system of linearised flow equations gives us the critical exponents θ_i as the negative of the eigenvalues of the stability matrix. The solution of the linearised system reads

$$g_{i,k} = g_i^* + \sum_j c_j v_i^j \left(\frac{k_0}{k}\right)^{\theta_j} \quad (3.6)$$

with v_i^j as the right eigenvectors of B_i^j . Furthermore k_0 is a reference scale and the c_j denote some constants of integration. For a positive critical exponent the corresponding eigendirection is UV-attractive, in the sense that the behaviour close to the fixed point would be similar to the behaviour of (3.4) with negative c . The flow is attracted towards the fixed point for increasing RG scale, independent of the starting value at low energies. This is called a UV-relevant direction. In contrast to this, the eigendirections corresponding to a negative critical exponents are UV-repulsive, similar to (3.4) with positive c . These directions are called UV-irrelevant. For vanishing critical exponents one has to consider higher orders in (3.5) to decide whether the corresponding direction is marginal-relevant or marginal-irrelevant. Note that the behaviour is mirrored if we turn the flow and consider decreasing energy. Therefore UV-relevant directions are IR-irrelevant and vice versa.

Performing a stability analysis as explained above, gives us very important information about a theory connected to a fixed point. The IR value of a coupling constant that corresponds to a UV-repulsive direction is a prediction of the theory itself. The requirement of this coupling to approach the fixed point in the UV fixes its IR value. Coupling constants corresponding to a UV-attractive direction on the other hand can have any value in the IR. Therefore these couplings have to be determined by experiment. The space which is spanned by all UV-relevant directions is called UV-critical surface S_{UV} . It is a hypersurface in the infinite-dimensional theory space spanned by all couplings.

The predictions that arise from requiring a finite dimensionality of the UV-critical surface provide the opportunity to test Asymptotic Safety. Consider a theory with at least one UV-repulsive direction. The IR-value of the corresponding coupling constant is determined by the requirement of reaching the fixed point in the UV. Clearly, this prediction has to match the experimental results.

Let us summarise the conditions for an asymptotically safe theory in the context of gravity. To define a theory of Quantum Gravity from the Wilsonian viewpoint we have to find a QFT of the gravitational degrees of freedom, well defined at arbitrary high energy scales. Such an asymptotically safe theory has to meet three requirements. Most importantly, a NGFP is needed capable of controlling the theory at high energies. Secondly, the predictivity of the theory requires that the UV-critical hypersurface of the NGFP is finite dimensional. Finally this NGFP has to be connected to a classical regime, where GR constitutes a good approximation. If the theory, beyond that, is invariant under diffeomorphisms it is called QEG.

Since the introduction of Asymptotic Safety several theories have been found, whose UV completion can be implemented by means of this scenario. Besides gravity, this includes scalar field theory at the Wilson-Fisher fixed point [93], four-fermion models [94–97], Yukawa systems [98–102], non-linear sigma models [103–108] and gauge theories in extra dimensions [109]. Notably the influence of asymptotically safe gravity on the standard model predicts a Higgs mass [110, 111] compatible with the recent measurements at the Large Hadron Collider (LHC) [112].

Part II

Metric Gravity

*This part of the thesis is based on the publication
"The R^2 phase-diagram of QEG and its spectral dimension",
by Stefan Rechenberger and Frank Saueressig,
Phys.Rev., D86:024018, 2012.*

Motivation

This part of the thesis covers the metric formulation of QEG, the first Asymptotic Safety related investigation in the context of gravity. This theory, described by a spacetime metric carrying the degrees of freedom, is invariant under spacetime diffeomorphisms. Finding a suitable NGFP as described in Chapter 3 would render such a theory asymptotically safe and thus it would be a viable candidate for a quantum theory of gravity.

The Wetterich equation, derived in Chapter 2, using the FRG techniques, constitutes an exact equation. It describes the scale dependence of the EAA and thus the scale dependence of the coupling constants of the theory. The EAA is constructed from the interaction monomials respecting the symmetry of the theory which span the theory space, coordinatised by the corresponding coupling constants. In general this theory space is infinite dimensional and it is not known how to deal with all coupling constants. Therefore, from a technical point of view we have to restrict ourselves to a finite set of interaction monomials and truncate the infinite-dimensional theory space.

For the metric formulation of gravity the simplest truncation uses the diffeomorphism invariant Einstein-Hilbert action which reads

$$S^{\text{EH}}[g_{\mu\nu}] = \frac{1}{16\pi G_{\text{N}}} \int d^D x \sqrt{g} (R - 2\Lambda) \quad (4.1)$$

with the D -dimensional spacetime metric $g_{\mu\nu}$ and the corresponding determinant g , the Newton constant G_{N} , the cosmological constant Λ and the Ricci scalar R . Here we used two distinguished terms which are invariant under spacetime diffeomorphisms, the constant term -2Λ and the curvature term R . Note that the Ricci scalar depends on the spacetime metric $g_{\mu\nu}$ and contains two derivatives. Besides these two terms there are infinitely many further terms respecting the symmetry. These further terms can be ordered depending on the number of derivatives contained, as it was done in [113] and is shown in Table 4.1. The Einstein-Hilbert truncation, corresponding to the two lowest lines, was investigated in the pioneering

∂^{10}	R^5	\vdots	\vdots	\vdots	
∂^8	R^4				
∂^6	R^3	$C_{\mu\nu}{}^{\rho\sigma}C_{\rho\sigma}{}^{\kappa\lambda}C_{\kappa\lambda}{}^{\mu\nu}$	$R\Delta R$	7	more terms
∂^4	R^2	$C_{\mu\nu\rho\sigma}C^{\mu\nu\rho\sigma}$	$R_{\mu\nu}R^{\mu\nu}$		
∂^2	R				
∂^0	$\mathbf{1}$				

Table 4.1: Diffeomorphism invariant terms ordered depending on the number of derivatives appearing in them. Here Δ denotes the contracted second covariant derivative, R is the Ricci scalar, $R_{\mu\nu}$ the Ricci tensor and $C_{\mu\nu\rho\sigma}$ the Weyl tensor.

work of Martin Reuter in 1996 [114]. Since these days a lot of extended truncations have been considered. Higher derivative gravity, corresponding to the ∂^4 line in Table 4.1, was discussed in [115] and [116] with and without a one-loop approximation respectively. The first truncation beyond the Einstein-Hilbert analysis was an inclusion of the R^2 term in [117–119]. The first column in Table 4.1 was studied further in [120,121] up to R^8 , in [74] up to R^{10} and in [122] up to R^{35} . A more general truncation of the form $f(R)$ was used to investigate logarithms and negative powers of the Ricci scalar in [123]. The function $f(R)$ itself was studied in [124] and [125,126]. Since the calculation for improved truncations become harder the authors of [127] proposed an automatisation, which they call the universal renormalisation group machine. The techniques necessary for such an automatisation was studied in [128,129]. A check of the automatisation was performed within the Einstein-Hilbert truncation [127] and the machine was used for investigations of higher derivative gravity [130].

Besides the purely gravitational improvement of the truncation some other aspects have been studied as well. Examples are boundary terms [131,132], the ghost sector [133–135], coupling to matter [102,136–144] and coupling to gauge fields [145–147]. All these extensions of the truncation support the Asymptotic Safety scenario for the metric version of QEG. Although there is no rigorous proof found yet, these works form a serious evidence that gravity might be non-perturbatively renormalisable.

The search for a possible non-Gaussian fixed point, although very important, is not the only task within the Asymptotic Safety approach to QG. There are other interesting aspects which partly have been investigated. As explained in Chapter 3 it is important to study the behaviour of the flow equations close to the fixed point for the analysis of the UV critical hypersurface. Furthermore the Asymptotic

Safety scenario requires a suitable classical regime. To find such a regime, the flow equations given by the beta functions for the coupling constants can be solved with suitable starting values. The resulting trajectories can be depicted in phase diagrams and classified according to their behaviour. This was done so far only for the Einstein-Hilbert truncation. An extensive analysis can be found in [148]. The trajectory compatible with observations was singled out in [149], again using the simplest truncation.

However, all theoretical investigations of QG candidates share one main problem. Unfortunately all observations available for the gravitational interaction are restricted to the classical level. The predictions of quantum-gravitational effects, so far, can not be checked with experiments. Here we do not consider scenarios with extra dimensions where observations of a fixed-point behaviour might be possible as explained in [61–63]. Thus we do not have any observation at hand to discriminate any QG approach. This is one reason for the variety of candidate theories as e.g. string theory, loop quantum gravity, HLG, CDT and many others. Although a discrimination of candidate theories is not possible one can at least compare the different approaches to see, whether or not, some of them lead to the same predictions. This might lead to further insights and developments in the different approaches.

Within this part of the thesis we will recapitulate the derivation of the beta functions for the simplest truncation of the metric formulation of QEG along the lines of [114, 150]. This introduces some basic technical aspects of the FRG technique on the level of a rather simple example. Afterwards, the phase diagram corresponding to these flow equations is analysed, by following [148]. This picture is extended to the R^2 truncation, where we omit most of the technical details and concentrate on the analysis of the three-dimensional phase diagram [31]. In the last chapter of this part we introduce and analyse the spectral dimension. This is a prediction incorporating quantum-gravitational effects and can be compared to other approaches to a quantum theory of gravity. We summarise the findings within the Einstein-Hilbert truncation [30] and extend the results to the R^2 truncation [31].

Flow Equations for Metric Gravity

5.1 The Einstein-Hilbert Truncation

In this section we derive the beta functions for the Newton constant and the cosmological constant with the FRG techniques along the lines of [114, 150]. A metric formulation of a quantum theory of gravity within the path-integral framework is described by the functional integral

$$\int \mathcal{D}\tilde{g}_{\mu\nu} \exp \left[-S^{\text{grav}}[\tilde{g}_{\mu\nu}] + \int d^D x \sqrt{\tilde{g}} t^{\mu\nu} \tilde{g}_{\mu\nu} \right] \quad (5.1)$$

with the quantum spacetime metric $\tilde{g}_{\mu\nu}$, the corresponding source $t^{\mu\nu}$ and a gravitational action S^{grav} . This serves as a starting point for the following considerations.

The first important fact to notice is that GR, as the desired classical limit of our quantum theory, is invariant under D -dimensional diffeomorphisms, where D denotes the spacetime dimension. Thus the microscopic action S is supposed to be invariant under the corresponding transformation, which reads

$$\tilde{g}_{\mu\nu} \rightarrow \tilde{g}_{\mu\nu} + \delta\tilde{g}_{\mu\nu}, \quad \delta\tilde{g}_{\mu\nu} = \mathcal{L}_v \tilde{g}_{\mu\nu}. \quad (5.2)$$

Here \mathcal{L}_v denotes the Lie derivative with respect to the D -dimensional vector v . As the diffeomorphism invariance is a gauge symmetry, the path integral in (5.1) is ill-defined due to the integration over gauge-equivalent field configurations. As explained in Appendix B.1 this problem can be circumvented by introducing a gauge-fixing and a ghost term. Thus our partition function, defining the quantum theory, reads

$$Z = \int \mathcal{D}\tilde{g}_{\mu\nu} \mathcal{D}\bar{\omega}^\mu \mathcal{D}\omega^\mu \exp \left[-S^{\text{grav}} - S^{\text{gf}} - S^{\text{gh}} + S^{\text{source}} \right]. \quad (5.3)$$

Here the source term S^{source} contains sources for the metric as well as for the ghost fields.

The next step, within the FRG approach, consists of introducing a regulator insertion ΔS_k in the exponent. It depends on the RG scale k that discriminates between modes of high and low momenta. As described in Chapter 2 this regulator insertion is chosen quadratic in the fields and contains a regulator \mathcal{R}_k which has to satisfy the three conditions (2.3). The full quantum theory is found in the limit $k \rightarrow 0$ since the regulator vanishes due to the first condition and thus we find the partition function (5.3). In this limit we would like to find invariance under gauge transformations. As described in Appendix B.2 this is true if the classical action as well as the regulator insertion is invariant. However, the regulator term ΔS_k in general is not invariant, which leaves us with the two options discussed in Appendix B.2. The first is a clever choice of the initial condition at large scales k . The second is the one we will follow here, the BFM. Following the appendix we split the quantum metric into a fixed but arbitrary background $\bar{g}_{\mu\nu}$ and fluctuations $\hat{g}_{\mu\nu}$ around it via

$$\tilde{g}_{\mu\nu} = \bar{g}_{\mu\nu} + \hat{g}_{\mu\nu}. \quad (5.4)$$

Note that the fluctuations are not assumed to be small in any sense. With this split we can distinguish two versions of the original gauge transformation $\tilde{g}_{\mu\nu} \rightarrow \tilde{g}_{\mu\nu} + \delta\tilde{g}_{\mu\nu}$. The first is called the quantum gauge transformation and the second is called the background gauge transformation. They read

$$\begin{aligned} \text{Quantum:} & \quad \hat{g}_{\mu\nu} \rightarrow \hat{g}_{\mu\nu} + \delta\hat{g}_{\mu\nu} & \bar{g}_{\mu\nu} & \rightarrow \bar{g}_{\mu\nu}, \\ \text{Background:} & \quad \hat{g}_{\mu\nu} \rightarrow \hat{g}_{\mu\nu} + \bar{\delta}\hat{g}_{\mu\nu} & \bar{g}_{\mu\nu} & \rightarrow \bar{g}_{\mu\nu} + \bar{\delta}\bar{g}_{\mu\nu}. \end{aligned} \quad (5.5)$$

As explained in Appendix B.2 we find a theory invariant under the gauge transformation, independent of the initial condition at large scales in the following way. First, we ask the gravitational action, the ghost action, the gauge fixing term and the regulator insertion to be invariant under background gauge transformations and derive the beta functions. Afterwards, we integrate them from large scales down to small scales and finally set $\hat{g}_{\mu\nu} = 0$. This last step turns the invariance under background gauge transformations into an invariance under the initial gauge transformation.

Summarising the previous considerations we start with a scale-dependent partition function Z_k , given in terms of a path integral, which reads

$$Z_k = \int \mathcal{D}\hat{g}_{\mu\nu} \mathcal{D}\bar{\omega}^\mu \mathcal{D}\omega^\mu e^{-S^{\text{grav}}[\hat{g};\bar{g}] - S^{\text{gf}}[\hat{g};\bar{g}] - S^{\text{gh}}[\hat{g},\bar{\omega},\omega;\bar{g}] - \Delta S_k[\hat{g},\bar{\omega},\omega;\bar{g}] + S^{\text{source}}}. \quad (5.6)$$

For convenience we would like to analyse the BEAA Γ_k instead of the scale dependent partition function Z_k . Thus we introduce the scale dependent Schwinger

functional W_k via $Z_k = e^{W_k}$ and take its modified Legendre transform, as in (2.8), to find

$$\Gamma_k[h_{\mu\nu}, \bar{c}_\mu, c^\mu; \bar{g}_{\mu\nu}] \quad \text{with} \quad h_{\mu\nu} = \langle \hat{g}_{\mu\nu} \rangle, \bar{c}_\mu = \langle \bar{\omega}_\mu \rangle, c^\mu = \langle \omega^\mu \rangle. \quad (5.7)$$

As discussed above we have to stick to a truncation. Following [114] we use the simplest ansatz, the Einstein-Hilbert truncation, that includes the invariants of GR. It is given in terms of the classical metric $g_{\mu\nu} = \bar{g}_{\mu\nu} + h_{\mu\nu}$, contains the scale dependent Newton constant G_k and the scale dependent cosmological constant Λ_k and reads

$$\Gamma_k^{\text{EH}} = \frac{1}{16\pi G_k} \int d^D x \sqrt{\bar{g}} [-R + 2\Lambda_k] + S^{\text{gf}} + S^{\text{gh}}. \quad (5.8)$$

Here we follow [114] and use the classical gauge-fixing and ghost terms S^{gf} and S^{gh} . For the gauge fixing we use the background harmonic gauge condition, containing the covariant derivative with respect to the background metric denoted by $\bar{\nabla}_\mu$. This gauge condition reads

$$F_\mu = \frac{\sqrt{2}}{\sqrt{32\pi G_k}} (\delta_\mu^\beta \bar{g}^{\alpha\gamma} \bar{\nabla}_\gamma - \frac{1}{2} \bar{g}^{\alpha\beta} \bar{\nabla}_\mu) h_{\alpha\beta} = 0 \quad (5.9)$$

and leads us to the following gauge-fixing action

$$S^{\text{gf}} = \frac{1}{2\alpha} \int d^D x \sqrt{\bar{g}} \bar{g}^{\mu\nu} F_\mu F_\nu \quad (5.10)$$

with the gauge parameter α . Along the lines of [114] we stick to the Feynman-'t Hooft gauge $\alpha = 1$. Note that there are arguments for $\alpha = 0$ being an IR-attractive fixed point [151] and thus our choice is an approximation of the physical gauge. The corresponding ghost action can be derived as explained in Appendix B.1 and reads

$$S^{\text{gh}} = -\sqrt{2} \int d^D x \sqrt{\bar{g}} \bar{c}_\mu \left(\bar{g}^{\mu\rho} \bar{g}^{\sigma\lambda} \bar{\nabla}_\lambda (g_{\rho\nu} \nabla_\sigma + g_{\sigma\nu} \nabla_\rho) - \bar{g}^{\rho\sigma} \bar{g}^{\mu\lambda} \bar{\nabla}_\lambda g_{\sigma\nu} \nabla_\rho \right) c^\nu \quad (5.11)$$

with the covariant derivative with respect to the classical metric $g_{\mu\nu} = \bar{g}_{\mu\nu} + h_{\mu\nu}$ denoted by ∇_μ .

Following the derivation in Section 2.2 we finally find the Wetterich equation for the metric formulation of QEG which reads

$$\partial_t \Gamma_k = \frac{1}{2} \text{Tr} \left[\frac{\partial_t \mathcal{R}_k^{\text{grav}}}{\frac{\delta^2 \Gamma_k}{\delta h^2} + \mathcal{R}_k^{\text{grav}}} \right] - \text{Tr} \left[\frac{\partial_t \mathcal{R}_k^{\text{gh}}}{\frac{\delta^2 \Gamma_k}{\delta \bar{c} \delta c} + \mathcal{R}_k^{\text{gh}}} \right]. \quad (5.12)$$

Here $\frac{\delta^2 \Gamma_k}{\delta h^2}$ denotes the second variation of Γ_k with respect to the metric fluctuation $h_{\mu\nu}$ and $\frac{\delta^2 \Gamma_k}{\delta \bar{c} \delta c}$ the variation of Γ_k with respect to the ghost and anti-ghost fields.

The regulator function \mathcal{R}_k has been separated into $\mathcal{R}_k^{\text{grav}}$ and $\mathcal{R}_k^{\text{gh}}$ such that off diagonal terms, mixing gravitational and ghost contributions, do not contribute in (5.12). The specification of $\mathcal{R}_k^{\text{grav}}$ and $\mathcal{R}_k^{\text{gh}}$ shall be postponed for the moment.

For the evaluation of the second variations in (5.12) we use two simplifications, explained in Appendix C.2. The first one is a special choice of the background. As discussed in Appendix B.2 this background is arbitrary and can be chosen freely. For convenience we choose the spherical one which uses a constant background curvature scalar \bar{R} and simplifies the background Riemann tensor $\bar{R}_{\mu\nu\rho\sigma}$ and the background Ricci tensor $\bar{R}_{\mu\nu}$ according to

$$\bar{R}_{\mu\nu} = \frac{1}{D}\bar{g}_{\mu\nu}\bar{R}, \quad \bar{R}_{\mu\nu\rho\sigma} = \frac{1}{D(D-1)}(\bar{g}_{\mu\rho}\bar{g}_{\nu\sigma} - \bar{g}_{\mu\sigma}\bar{g}_{\nu\rho})\bar{R}. \quad (5.13)$$

Using this background, the second variation with respect to the ghost fields is obvious from (5.11). At $g_{\mu\nu} = \bar{g}_{\mu\nu}$ we find

$$S^{\text{gh}}|_{g=\bar{g}} = \sqrt{2} \int d^D x \sqrt{\bar{g}} \bar{c}_\mu \left(\Delta - \frac{\bar{R}}{D} \right) c^\mu \quad (5.14)$$

with the Laplace operator given as $\Delta = -\nabla^\mu \nabla_\mu$. As the ghost action (5.11) does not depend on the fluctuation metric $h_{\mu\nu}$, it can be separated from the evaluation of the second variation with respect to the metric. Therefore, we split the truncated BEAA (5.8) into the ghost action and the rest. The latter contains the Einstein-Hilbert action as well as the gauge-fixing part and we denote it with Γ_k^{grav} . Using the spherical background we write the gravitational part of our truncation as $\Gamma_k^{\text{grav}}[h_{\mu\nu}; \bar{g}_{\mu\nu}] = \Gamma_k^{\text{grav}}[0; \bar{g}_{\mu\nu}] + \frac{1}{2}\delta^2\Gamma_k^{\text{grav}}[h_{\mu\nu}; \bar{g}_{\mu\nu}]$ where we omit terms linear in the fluctuation $h_{\mu\nu}$ as well as higher terms. The quadratic term reads

$$\begin{aligned} \delta^2\Gamma_k^{\text{grav}} &= \frac{1}{16\pi G_k} \int d^D x \sqrt{\bar{g}} \frac{1}{2} h_{\mu\nu} \left(\Delta - 2\Lambda_k + \frac{D^2-3D+4}{D(D-1)}\bar{R} \right) h^{\mu\nu} \\ &\quad - \frac{1}{16\pi G_k} \int d^D x \sqrt{\bar{g}} \frac{1}{4} h_{\mu\nu} \bar{g}^{\mu\nu} \left(\Delta - 2\Lambda_k + \frac{D^2-5D+8}{D(D-1)}\bar{R} \right) \bar{g}_{\rho\sigma} h^{\rho\sigma} \end{aligned} \quad (5.15)$$

and shows in the second line that it is not diagonal in the metric fluctuation.

In order to invert $\frac{\delta^2\Gamma_k}{\delta h^2} + \mathcal{R}_k^{\text{grav}}$ in (5.12) we diagonalise the second variation in a second step. Therefore we use the transverse traceless (TT) decomposition of $h_{\mu\nu}$, explained in Appendix C.2. It consists in the split

$$h_{\mu\nu} = h_{\mu\nu}^{\text{TT}} + \bar{\nabla}_\mu \xi_\nu + \bar{\nabla}_\nu \xi_\mu + \bar{\nabla}_\mu \bar{\nabla}_\nu \zeta - \frac{1}{D}\bar{g}_{\mu\nu}\bar{\nabla}^2\zeta + \frac{1}{D}\bar{g}_{\mu\nu}\phi \quad (5.16)$$

where $h_{\mu\nu}^{\text{TT}}$ is transverse and traceless, ϕ is the trace of $h_{\mu\nu}$ and ξ_μ is a transverse vector. Thus we find

$$\bar{g}^{\mu\nu} h_{\mu\nu}^{\text{TT}} = 0, \quad \bar{\nabla}^\mu h_{\mu\nu}^{\text{TT}} = 0, \quad \bar{\nabla}^\mu \xi_\mu = 0, \quad \bar{g}^{\mu\nu} h_{\mu\nu} = \phi. \quad (5.17)$$

This split seems a bit like taking a sledgehammer to crack a nut. Indeed the simpler split into traceless and trace part as $h_{\mu\nu} = h_{\mu\nu}^T + D^{-1}\bar{g}_{\mu\nu}\phi$ would be sufficient, as shown in [114]. However, we will use the TT decomposition to show some technical details at the level of the rather simple Einstein-Hilbert truncation. Using this split, the quadratic term (5.15) in terms of the fluctuation field $h_{\mu\nu}^{\text{TT}}, \xi_\mu, \varsigma$ and ϕ reads

$$\begin{aligned} \delta^2\Gamma_k^{\text{grav}} &= \frac{Z_{Nk}}{16\pi G_0} \int d^D x \sqrt{\bar{g}} \frac{1}{2} h_{\mu\nu}^{\text{TT}} \left(\Delta - 2\Lambda_k + \frac{D^2-3D+4}{D(D-1)} \bar{R} \right) h^{\text{TT}\mu\nu} \\ &+ \frac{Z_{Nk}}{16\pi G_0} \int d^D x \sqrt{\bar{g}} \xi_\mu \left(\Delta - 2\Lambda_k + \frac{D-3}{D} \bar{R} \right) \left(\Delta - \frac{\bar{R}}{D} \right) \xi^\mu \\ &+ \frac{Z_{Nk}}{16\pi G_0} \int d^D x \sqrt{\bar{g}} \frac{D-1}{2D} \varsigma \left(\Delta - 2\Lambda_k + \frac{D-4}{D} \bar{R} \right) \left(\Delta^2 - \frac{\bar{R}}{D-1} \Delta \right) \varsigma \\ &- \frac{Z_{Nk}}{16\pi G_0} \int d^D x \sqrt{\bar{g}} \frac{D-2}{4D} \phi \left(\Delta - 2\Lambda_k + \frac{D-4}{D} \bar{R} \right) \phi. \end{aligned} \quad (5.18)$$

Here we traded the k -dependent Newton constant for the wave function renormalisation Z_{Nk} by $G_k = G_0/Z_{Nk}$. This expression for the second variation makes obvious that a further simplification can be achieved by performing a momentum-dependent field redefinition. Explicitly, we use

$$\xi_\mu \rightarrow \frac{1}{\sqrt{\Delta - \frac{\bar{R}}{D}}} \xi_\mu, \quad \varsigma \rightarrow \frac{1}{\sqrt{\Delta^2 - \frac{\bar{R}}{D-1} \Delta}} \varsigma. \quad (5.19)$$

Besides the simplifications in (5.18) these field redefinitions have a second advantage. So far we did not mention the fact that a change of integration variable under the path integral from $h_{\mu\nu}$ to $h_{\mu\nu}^{\text{TT}}, \phi, \varsigma, \xi_\mu$ produces a Jacobian. However, this Jacobian is identically cancelled by the Jacobian corresponding to the momentum-dependent field redefinition as shown in [119]. Thus we do not consider these Jacobians any further. Note that this cancellation is true only for spherical backgrounds. If one uses non-spherical backgrounds the Jacobians can be exponentiated by introducing auxiliary fields. This, of course, makes the calculation much more complicated. Summarising our findings for the second variations we write

$$\begin{aligned} \left. \frac{\delta^2\Gamma_k}{\delta h^2} \right|_{\text{TT}} &= \frac{Z_{Nk}}{32\pi G_0} \left(\Delta - 2\Lambda_k + \frac{D^2-3D+4}{D(D-1)} \bar{R} \right), \\ \left. \frac{\delta^2\Gamma_k}{\delta h^2} \right|_{\xi\xi} &= \frac{Z_{Nk}}{16\pi G_0} \left(\Delta - 2\Lambda_k + \frac{D-3}{D} \bar{R} \right), \\ \left. \frac{\delta^2\Gamma_k}{\delta h^2} \right|_{\varsigma\varsigma} &= \frac{Z_{Nk}}{32\pi G_0} \frac{D-1}{D} \left(\Delta - 2\Lambda_k + \frac{D-4}{D} \bar{R} \right), \\ \left. \frac{\delta^2\Gamma_k}{\delta h^2} \right|_{\phi\phi} &= -\frac{Z_{Nk}}{64\pi G_0} \frac{D-2}{D} \left(\Delta - 2\Lambda_k + \frac{D-4}{D} \bar{R} \right), \end{aligned}$$

$$\frac{\delta^2 \Gamma_k}{\delta \bar{c} \delta c} = \sqrt{2} \left(\Delta - \frac{1}{D} \bar{R} \right). \quad (5.20)$$

Now we can discuss the last missing ingredient on the right hand side of the Wetterich equation (5.12), the regulator. As we have seen in Chapter 2 the regulator can be chosen freely as long as the conditions (2.3) are fulfilled. We utilise this freedom and choose the regulators $\mathcal{R}_k^{\text{grav}}$ and $\mathcal{R}_k^{\text{gh}}$ such that the Laplace operators appearing in $\frac{\delta^2 \Gamma_k}{\delta \phi^2}$, $\frac{\delta^2 \Gamma_k}{\delta \varsigma^2}$, ... and $\frac{\delta^2 \Gamma_k}{\delta \bar{c} \delta c}$, in (5.20), combine with the regulator to become

$$P_k = \Delta + R_k, \quad R_k = k^2 R^0 \left(\frac{\Delta}{k^2} \right) \quad (5.21)$$

in $\frac{\delta^2 \Gamma_k}{\delta \phi^2} + \mathcal{R}_k$, ... Still there is the freedom to choose the shape function R^0 . Here we will stick to the Litim cutoff $R^0(z) = (1-z)\theta(1-z)$ with the Heaviside step function θ [84, 85], see also Appendix C.4. Thus, we use

$$\begin{aligned} \mathcal{R}_k|_{\text{TT}} &= \frac{Z_{\text{N}k} k^2 R^0 \left(\frac{\Delta}{k^2} \right)}{32\pi G_0}, & \mathcal{R}_k|_{\xi\xi} &= \frac{Z_{\text{N}k} k^2 R^0 \left(\frac{\Delta}{k^2} \right)}{16\pi G_0}, & \mathcal{R}_k|_{\bar{c}c} &= \sqrt{2} k^2 R^0 \left(\frac{\Delta}{k^2} \right), \\ \mathcal{R}_k|_{\varsigma\varsigma} &= \frac{Z_{\text{N}k} k^2 R^0 \left(\frac{\Delta}{k^2} \right) D - 1}{32\pi G_0 D}, & \mathcal{R}_k|_{\phi\phi} &= -\frac{Z_{\text{N}k} k^2 R^0 \left(\frac{\Delta}{k^2} \right) D - 2}{64\pi G_0 D}. \end{aligned} \quad (5.22)$$

In summary the right hand side of the truncated flow equation (5.12) consists of five different parts. These are the TT trace, the $\xi\xi$ trace, the two scalar traces with respect to $\phi\phi$ and $\varsigma\varsigma$ and finally the ghost trace. These are now purely diagonal terms and read

$$\begin{aligned} \mathcal{T}_{\text{TT}} &= \frac{1}{2} \text{Tr}_{(2\text{T})} \left[\frac{\partial_t (Z_{\text{N}k} k^2 R^0 \left(\frac{\Delta}{k^2} \right))}{Z_{\text{N}k}} \frac{1}{\Delta - 2\Lambda_k + \frac{D^2 - 3D + 4}{D} \bar{R}} \right], \\ \mathcal{T}_{\xi\xi} &= \frac{1}{2} \text{Tr}'_{(1\text{T})} \left[\frac{\partial_t (Z_{\text{N}k} k^2 R^0 \left(\frac{\Delta}{k^2} \right))}{Z_{\text{N}k}} \frac{1}{\Delta - 2\Lambda_k + \frac{D-3}{D} \bar{R}} \right], \\ \mathcal{T}_{\varsigma\varsigma} &= \frac{1}{2} \text{Tr}''_{(0)} \left[\frac{\partial_t (Z_{\text{N}k} k^2 R^0 \left(\frac{\Delta}{k^2} \right))}{Z_{\text{N}k}} \frac{1}{\Delta - 2\Lambda_k + \frac{D-4}{D} \bar{R}} \right], \\ \mathcal{T}_{\phi\phi} &= \frac{1}{2} \text{Tr}_{(0)} \left[\frac{\partial_t (Z_{\text{N}k} k^2 R^0 \left(\frac{\Delta}{k^2} \right))}{Z_{\text{N}k}} \frac{1}{\Delta - 2\Lambda_k + \frac{D-4}{D} \bar{R}} \right], \\ \mathcal{T}_{\bar{c}c} &= - \text{Tr}_{(1)} \left[\frac{\partial_t (k^2 R^0 \left(\frac{\Delta}{k^2} \right))}{\Delta - \frac{1}{D} \bar{R}} \right]. \end{aligned} \quad (5.23)$$

The notation has to be understood in the following way. The index (2T) at the trace marks that the trace is taken with respect to transverse traceless tensors. Accordingly (1T) denotes transverse vectors, (1) marks unconstrained vectors and (0)

is placed for scalar traces. Furthermore the primes denote that the lowest eigenvalues are excluded from the trace. One prime means the very lowest eigenvalue has to be excluded and two primes mean that the two lowest eigenvalues are excluded. This is necessary since not all modes of ξ_μ and ς of the TT decomposition contribute to the full metric, as discussed in detail in Appendix C.2. The constrained traces are analysed in Appendix C.3.

Before evaluating these functional traces let us investigate the left hand side of the truncated flow equation (5.12). The t derivative acts on the scale dependent cosmological constant Λ_k and the wave function renormalisation, Z_{Nk} , carrying the running of the inverse Newton constant. As the next step we have to identify the background with the full metric. Note that this identification is the single-metric approximation. Treating the background metric dynamically leads to bimetric truncations discussed in [152–154]. However, here we stick to the single-metric approximation which corresponds to vanishing fluctuations. Thus, the left hand side of the truncated flow equation (5.12) with the fluctuations set to zero reads

$$\partial_t \Gamma_k = \frac{1}{16\pi G_0} \int d^D x \sqrt{\bar{g}} \left[-\bar{R} \partial_t Z_{Nk} + 2\partial_t (Z_{Nk} \Lambda_k) \right]. \quad (5.24)$$

This shows that we can derive the beta function for the Newton constant by comparison of the terms proportional to \bar{R} on the left and the right hand side of the Wetterich equation. The running of the cosmological constant is determined by the terms proportional to the volume. All higher terms in the curvature scalar \bar{R} can be neglected.

Since we are only interested in the two lowest orders of the expansion in the Ricci scalar we can perform such an expansion on the right hand side. This simplifies the evaluation of the traces. Thus (5.23) gets

$$\begin{aligned} \mathcal{T}_{\text{TT}} &= \frac{1}{2} \text{Tr}_{(2\text{T})} \left[\frac{\partial_t (Z_{Nk} k^2 R^0(\frac{\Delta}{k^2}))}{Z_{Nk}} \left(\frac{1}{\Delta - 2\Lambda_k} - \frac{D^2 - 3D + 4}{D(D-1)} \frac{\bar{R}}{(\Delta - 2\Lambda_k)^2} \right) \right], \\ \mathcal{T}_{\xi\xi} &= \frac{1}{2} \text{Tr}'_{(1\text{T})} \left[\frac{\partial_t (Z_{Nk} k^2 R^0(\frac{\Delta}{k^2}))}{Z_{Nk}} \left(\frac{1}{\Delta - 2\Lambda_k} - \frac{D-3}{D} \frac{\bar{R}}{(\Delta - 2\Lambda_k)^2} \right) \right], \\ \mathcal{T}_{\varsigma\varsigma} &= \frac{1}{2} \text{Tr}''_{(0)} \left[\frac{\partial_t (Z_{Nk} k^2 R^0(\frac{\Delta}{k^2}))}{Z_{Nk}} \left(\frac{1}{\Delta - 2\Lambda_k} - \frac{D-4}{D} \frac{\bar{R}}{(\Delta - 2\Lambda_k)^2} \right) \right], \\ \mathcal{T}_{\phi\phi} &= \frac{1}{2} \text{Tr}_{(0)} \left[\frac{\partial_t (Z_{Nk} k^2 R^0(\frac{\Delta}{k^2}))}{Z_{Nk}} \left(\frac{1}{\Delta - 2\Lambda_k} - \frac{D-4}{D} \frac{\bar{R}}{(\Delta - 2\Lambda_k)^2} \right) \right], \\ \mathcal{T}_{\bar{c}c} &= - \text{Tr}_{(1)} \left[\partial_t (k^2 R^0(\frac{\Delta}{k^2})) \left(\frac{1}{\Delta} + \frac{1}{D} \frac{\bar{R}}{\Delta^2} \right) \right] \end{aligned} \quad (5.25)$$

where we omitted terms of higher order in the scalar curvature \bar{R} . Now all traces are of the form discussed in Appendix C.4. Instead of writing the result in terms of the threshold functions $\phi_l^{p,q}(w)$ defined in (C.31), we use $q_l^{p,q}(w) = \phi_l^{p,q}(w) - \frac{1}{2}\eta_N \tilde{\phi}_l^{p,q}$ with the anomalous dimension $\eta_N = -\partial_t \ln Z_{Nk}$. We finally find the right hand side to be

$$\begin{aligned} \mathcal{T}_{\text{TT}} + \dots + \mathcal{T}_{cc} &= \frac{1}{(4\pi)^{D/2}} \int d^D x \sqrt{\bar{g}} k^D \left[\frac{D}{2}(D+1)q_{D/2}^{1,0}(-2\bar{\Lambda}_k) - 2D\phi_{D/2}^{1,0}(0) \right. \\ &+ \left. \frac{\bar{R}}{k^2} \left(C_1 q_{D/2-1}^{1,0}(-2\bar{\Lambda}_k) - C_2 q_{D/2}^{2,0}(-2\bar{\Lambda}_k) - \frac{D}{3}\phi_{D/2-1}^{1,0}(0) - 2\phi_{D/2}^{2,0}(0) \right) \right] \end{aligned} \quad (5.26)$$

where we switched, for convenience, to dimensionless quantities

$$\bar{\Lambda}_k = k^{-2}\Lambda_k, \quad \bar{G}_k = k^{D-2}G_k. \quad (5.27)$$

Furthermore we introduced

$$C_1 = \frac{D^4 - 13D^2 - 24D + 12}{12D(D-1)}, \quad C_2 = \frac{D^4 - 2D^3 - D^2 - 4D + 2}{2D(D-1)}. \quad (5.28)$$

Note that in general terms proportional to the Kronecker delta $\delta_{D,2}$ appear for traces over constrained fields. However, here all these terms cancel each other. Explicitly the terms appearing as corrections to the traces, denoted by the prime, are minus the terms appearing as $\delta_{D,2}$ corrections in the heat-kernel coefficient. For details see Appendix C.

After evaluating the different parts, the comparison of the left (5.24) and the right hand side (5.26), to order \bar{R} , yields an expression for the anomalous dimension $\eta_N = -\partial_t \ln Z_{Nk}$

$$\begin{aligned} \eta_N &= \frac{16\pi\bar{G}_k}{(4\pi)^{D/2}} \left(C_1 q_{D/2-1}^{1,0}(-2\bar{\Lambda}_k) - C_2 q_{D/2}^{2,0}(-2\bar{\Lambda}_k) \right. \\ &\quad \left. - \frac{D}{3}\phi_{D/2-1}^{1,0}(0) - 2\phi_{D/2}^{2,0}(0) \right). \end{aligned} \quad (5.29)$$

For the other terms we find

$$\frac{1}{k^2} \frac{\partial_t(Z_{Nk} k^2 \bar{\Lambda}_k)}{Z_{Nk}} = \frac{8\pi\bar{G}_k}{(4\pi)^{D/2}} \left[\frac{D}{2}(D+1)q_{D/2}^{1,0}(-2\bar{\Lambda}_k) - 2D\phi_{D/2}^{1,0}(0) \right]. \quad (5.30)$$

This last equation gives us the beta function for the dimensionless cosmological constant in terms of the dimensionless couplings $\bar{\Lambda}_k, \bar{G}_k$ and the anomalous dimension η_N

$$\partial_t \bar{\Lambda}_k = (\eta_N - 2)\bar{\Lambda}_k + \frac{\bar{G}_k}{(4\pi)^{D/2-1}} \left[D(D+1)q_{D/2}^{1,0}(-2\bar{\Lambda}_k) - 4D\phi_{D/2}^{1,0}(0) \right]. \quad (5.31)$$

For the beta function of the dimensionless Newton constant, in terms of $\bar{\Lambda}_k, \bar{G}_k$ and the anomalous dimension, we find

$$\partial_t \bar{G}_k = \partial_t \left(k^{D-2} \frac{G_0}{Z_{Nk}} \right) = (D - 2 + \eta_N) \bar{G}_k. \quad (5.32)$$

At the end we still need an expression for the anomalous dimension. This can be derived by solving (5.29) for η_N (recall that the q functions contain the anomalous dimension by definition). The final result reads

$$\eta_N = \frac{\bar{G}_k B_1(\bar{\Lambda}_k)}{1 - \bar{G}_k B_2(\bar{\Lambda}_k)} \quad (5.33)$$

with

$$\begin{aligned} B_1 &= \frac{16\pi}{(4\pi)^{D/2}} \left(C_1 \phi_{D/2-1}^{1,0}(-2\bar{\Lambda}_k) - C_2 \phi_{D/2}^{2,0}(-2\bar{\Lambda}_k) - \frac{D}{3} \phi_{D/2-1}^{1,0}(0) - 2\phi_{D/2}^{2,0}(0) \right) \\ B_2 &= \frac{8\pi}{(4\pi)^{D/2}} \left(C_1 \tilde{\phi}_{D/2-1}^{1,0}(-2\bar{\Lambda}_k) - C_2 \tilde{\phi}_{D/2}^{2,0}(-2\bar{\Lambda}_k) \right). \end{aligned} \quad (5.34)$$

Summarising, we find a system of coupled flow equations for the dimensionless Newton constant \bar{G}_k and the dimensionless cosmological constant $\bar{\Lambda}_k$ by inserting the anomalous dimension (5.33) into (5.32) and (5.31). This system is given by

$$\begin{aligned} \beta_{\bar{\Lambda}}(\bar{G}_k, \bar{\Lambda}_k) &= (\eta_N - 2)\bar{\Lambda}_k + \frac{\bar{G}_k}{(4\pi)^{D/2-1}} \left[D(D+1)q_{D/2}^{1,0}(-2\bar{\Lambda}_k) - 4D\phi_{D/2}^{1,0}(0) \right], \\ \beta_{\bar{G}}(\bar{G}_k, \bar{\Lambda}_k) &= (D - 2 + \eta_N)\bar{G}_k \end{aligned} \quad (5.35)$$

with η_N given in (5.33). The flow corresponding to these beta functions will be analysed in Section 6.1.

5.2 The R^2 Truncation

This section is devoted to the beta functions of QEG within the R^2 truncation. After the very explicit derivation of the beta functions within the Einstein-Hilbert truncation we will be brief here. The main techniques have been explained in Section 5.1 and we just go through the important steps and mention the differences between the Einstein-Hilbert and the R^2 truncation. The final result will be given and the interested reader might be referred to [117–119] for the technical details and all intermediate steps.

The truncation involves the field monomials associated to the Newton constant and the cosmological constant as in the Einstein-Hilbert truncation of Section 5.1.

Furthermore, it includes an R^2 term with a coupling β_k in front. So, in total, the ansatz reads

$$\Gamma_k^{R^2} = \int d^D x \sqrt{g} \left[\frac{1}{16\pi G_k} (-R + 2\Lambda_k) + \beta_k R^2 \right] + S^{\text{gf}} + S^{\text{gh}} \quad (5.36)$$

with the gauge fixing and ghost term as they are given in the Einstein-Hilbert analysis (5.10), (5.11).

Next we proceed to the evaluation of the right hand side of the flow equation (5.12). As in Section 5.1 the first task is to find the second variation of the ansatz with respect to the fields. This is very lengthy, but mainly analogous to the previous section. Again we use the TT decomposition

$$h_{\mu\nu} = h_{\mu\nu}^{\text{TT}} + \bar{\nabla}_\mu \xi_\nu + \bar{\nabla}_\nu \xi_\mu + \bar{\nabla}_\mu \bar{\nabla}_\nu \varsigma - \frac{1}{D} \bar{g}_{\mu\nu} \bar{\nabla}^2 \varsigma + \frac{1}{D} \bar{g}_{\mu\nu} \phi \quad (5.37)$$

and the spherical background described in Appendix C.2. In contrast to the Einstein-Hilbert calculation here the simple split into the traceless and trace part is not sufficient to diagonalise the second variation, which would simplify the inversion of $\Gamma_k^{(2)} + \mathcal{R}_k$ considerably. Within this truncation, even the TT decomposition is not able to diagonalise the second variation. This is prevented by the R^2 term. The best one can get is a block diagonal form where the fields ϕ and ς mix. However, such a block-diagonal matrix can be inverted anyway, one just has to take into account that the two fields have different expansions in eigenfunctions of the Laplace operator as discussed in Appendix C.2. Again, we stick to the Feynman-'t Hooft gauge $\alpha = 1$.

Before inverting the matrix we have to specify the cutoff \mathcal{R}_k . In the last section we chose the cutoff such that any Laplace operator that appeared in the second derivative was replaced by P_k .

$$\Delta \rightarrow P_k = \Delta + R_k, \quad R_k = k^2 R^{(0)} \left(\frac{\Delta}{k^2} \right). \quad (5.38)$$

Note that there are other choices given in [121], where the authors classify several possibilities. Within this notation our choice is called Type I. Again we use the Litim cutoff for the shape function $R^{(0)}(z) = (1-z)\theta(1-z)$. Next we can explicitly invert $\Gamma_k^{(2)} + \mathcal{R}_k$.

Due to the TT decomposition the trace on the right hand side of the flow equation (5.12) splits into a trace over transverse-traceless tensors, another trace over transverse vectors and finally the scalar trace where one should pay attention to the different expansions of ϕ and ς . Note that the block-diagonal form leads to a 2×2 operator matrix in the scalar sector. Nevertheless, these traces can be evaluated with the help of the heat-kernel techniques explained in Appendix C. Again, we have to deal with constrained fields and thus the heat-kernel coefficients contain

terms proportional to $\delta_{D,2}$. Since we have to take into account one higher order in the heat-kernel expansion, in comparison to the Einstein-Hilbert truncation, terms proportional to $\delta_{D,4}$ appear as well. Furthermore we have to exclude the lowest eigenvalues from the constrained traces and consider the different expansions of ϕ and ς in terms of the eigenfunctions. This again leads to terms proportional to $\delta_{D,2}$ and $\delta_{D,4}$.

The evaluation of the left hand side of the flow equation (5.12) is straightforward and leads to

$$\partial_t \Gamma_k[\bar{g}; \bar{g}] = \int d^D x \sqrt{\bar{g}} \left[\frac{1}{16\pi G_0} (2\partial_t(Z_{Nk}\Lambda_k) - \bar{R}\partial_t Z_{Nk}) + \bar{R}^2 \partial_t \beta_k \right]. \quad (5.39)$$

Here we identified the full metric with the background metric as we did in Section 5.1. Now we can compare the different orders in \bar{R} on the left and the right hand side of the Wetterich equation. The terms proportional to \bar{R} finally lead to an expression for the anomalous dimension η_N , which governs the running of Newton's constant G_k . The terms proportional to the volume can be used to derive the beta function for the cosmological constant Λ_k . Finally the terms proportional to \bar{R}^2 are responsible for the running of the coupling β_k .

The flow equations can be expressed in terms of the dimensionless quantities

$$\bar{G}_k = k^{D-2} G_k, \quad \bar{\Lambda}_k = k^{-2} \Lambda_k, \quad \bar{\beta}_k = k^{4-D} \beta_k \quad (5.40)$$

and the anomalous dimensions

$$\eta_N = -\partial_t \ln Z_{Nk}, \quad \eta_\beta = -\partial_t \ln \beta_k. \quad (5.41)$$

The final result for the beta functions reads

$$\begin{aligned} \beta_{\bar{G}}(\bar{G}_k, \bar{\Lambda}_k, \bar{\beta}_k) &= \partial_t \bar{G}_k = (D-2 + \eta_N) \bar{G}_k, \\ \beta_{\bar{\beta}}(\bar{G}_k, \bar{\Lambda}_k, \bar{\beta}_k) &= \partial_t \bar{\beta}_k = (4-D - \eta_\beta) \bar{\beta}_k, \\ \beta_{\bar{\Lambda}}(\bar{G}_k, \bar{\Lambda}_k, \bar{\beta}_k) &= \partial_t \bar{\Lambda}_k = A_1 + A_2 \eta_N + A_3 \eta_\beta \end{aligned} \quad (5.42)$$

with η_N and η_β given as

$$\begin{aligned} \eta_N &= \bar{G}_k \frac{B_1(\bar{\beta}_k + C_3) - C_1 B_3}{(1 - \bar{G}_k B_2)(\bar{\beta}_k + C_3) + \bar{G}_k C_2 B_3}, \\ \eta_\beta &= -\frac{C_1(1 - \bar{G}_k B_2) + \bar{G}_k B_1 C_2}{(1 - \bar{G}_k B_2)(\bar{\beta}_k + C_3) + \bar{G}_k C_2 B_3}. \end{aligned} \quad (5.43)$$

Here all functions A_i , B_i and C_i depend on \bar{G}_k , $\bar{\Lambda}_k$ and $\bar{\beta}_k$. Their explicit form can be found in Appendix D and the interested reader might be referred to the original work [117–119] for more technical details. The flow corresponding to this system of beta functions is analysed in Section 6.2.

The Phase Diagram of Metric Gravity

6.1 Phase Diagram of the Einstein-Hilbert Truncation

After deriving the flow equations in Chapter 5 we proceed to analyse them in detail. This section is devoted to the analysis of the beta functions of the Einstein-Hilbert truncation. They have been derived in Section 5.1 and the final result is given in (5.35).

As discussed in Chapter 3 we need a non-Gaussian fixed point (NGFP) for a possible Asymptotic Safety scenario. Inspecting the flow equations, the first point of vanishing beta functions $\partial_t \bar{G}_k = 0$ and $\partial_t \bar{\Lambda}_k = 0$, is the GFP at the origin $(\bar{G}_{\text{GFP}}^*, \bar{\Lambda}_{\text{GFP}}^*) = (0, 0)$. Besides this trivial fixed point the system of flow equations gives rise to a non-trivial fixed point, which in four spacetime dimensions is situated at

$$(\bar{G}^*, \bar{\Lambda}^*) = (0.698, 0.166). \quad (6.1)$$

This result is in accordance with previous calculations [114, 150]. Numerical differences appear due to differences in the choice of the regulator and the gauge fixing.

Besides the existence of a non-trivial fixed point the Asymptotic Safety scenario asks for a finite-dimensional UV-critical hypersurface. Since we are using a truncation with only two distinguished coupling constants the hypersurface can have at most two dimensions.¹ However it is interesting to evaluate the critical exponents, since they do not just give us the number of relevant and irrelevant directions, but also give us information about the behaviour close to the fixed point. Therefore

¹The dimension of the critical surface within the infinite dimensional $f(R)$ truncation was discussed in [155].

we evaluate the linearisation of the beta functions

$$\begin{pmatrix} \partial_t \bar{\Lambda}_k \\ \partial_t \bar{G}_k \end{pmatrix} \approx \begin{pmatrix} \partial_{\bar{\Lambda}_k} \beta_{\bar{\Lambda}} & \partial_{\bar{G}_k} \beta_{\bar{\Lambda}} \\ \partial_{\bar{\Lambda}_k} \beta_{\bar{G}} & \partial_{\bar{G}_k} \beta_{\bar{G}} \end{pmatrix} \Big|_{\bar{\Lambda}^*, \bar{G}^*} \begin{pmatrix} \bar{\Lambda}_k - \bar{\Lambda}^* \\ \bar{G}_k - \bar{G}^* \end{pmatrix} \quad (6.2)$$

and the matrix is called stability matrix. The negative of their eigenvalues are the critical exponents $\theta_{1/2}$ and read in four dimensions

$$\theta_{1/2} = 1.72 \pm 2.39 i. \quad (6.3)$$

Both real parts are positive and thus correspond to UV-attractive directions. This means that the IR value has to be measured by an experiment and is not a prediction of the theory, as discussed in Chapter 3. The fact that the critical exponents build a complex pair tells us that the RG flow close to the fixed point is a spiral in the two dimensional theory space spanned by $\bar{\Lambda}_k$ and \bar{G}_k . A similar analysis at the GFP leads to critical exponents $+2$ and -2 in four dimensions. As expected these are the canonical dimensions of the coupling constants. Therefore the GFP has one UV-relevant and one UV-irrelevant direction which can be interpreted as IR-irrelevant and IR-relevant respectively.

The last missing ingredient of the Asymptotic Safety scenario is a classical limit at low energies in order to reproduce GR. Explicitly we have to find a region within the theory space where the dimensionful couplings stay constant over a large range of scales. In terms of the dimensionless couplings we are looking for a region where \bar{G}_k and $\bar{\Lambda}_k$ are equipped with a pure dimensional running. Indeed such a region exists close to $\bar{G}_k = 0$. To show this we expand the beta functions in powers of the dimensionless Newton coupling. To lowest order we find

$$\partial_t \bar{G}_k = 2\bar{G}_k, \quad \partial_t \bar{\Lambda}_k = -2\bar{\Lambda}_k \quad (6.4)$$

which is exactly the sought-after dimensional running. Thus at low energies we have to end up with $\bar{G}_k \ll 1$ in order to find a classical regime.

However, such a classical regime is useless as long as we do not connect it to the NGFP. Thus we have to find trajectories running from the NGFP at high energies towards small values of \bar{G}_k at low energies. Before searching for explicit flows it is useful to discuss the range of validity of the beta functions. It is obvious from (5.33) that the anomalous dimension η_N , and thus the flow equations itself, diverge for $1 - \bar{G}_k B_2(\bar{\Lambda}_k) = 0$. This equation can be solved for \bar{G}_k to give in four dimensions

$$\bar{G}_k^{\text{pole}} = \frac{72\pi(1 - 2\bar{\Lambda}_k)^2}{29 - 9\bar{\Lambda}_k}. \quad (6.5)$$

At this line the validity of the beta functions breaks down and we should not trust them any more. However, away from this line and within our approximation, the

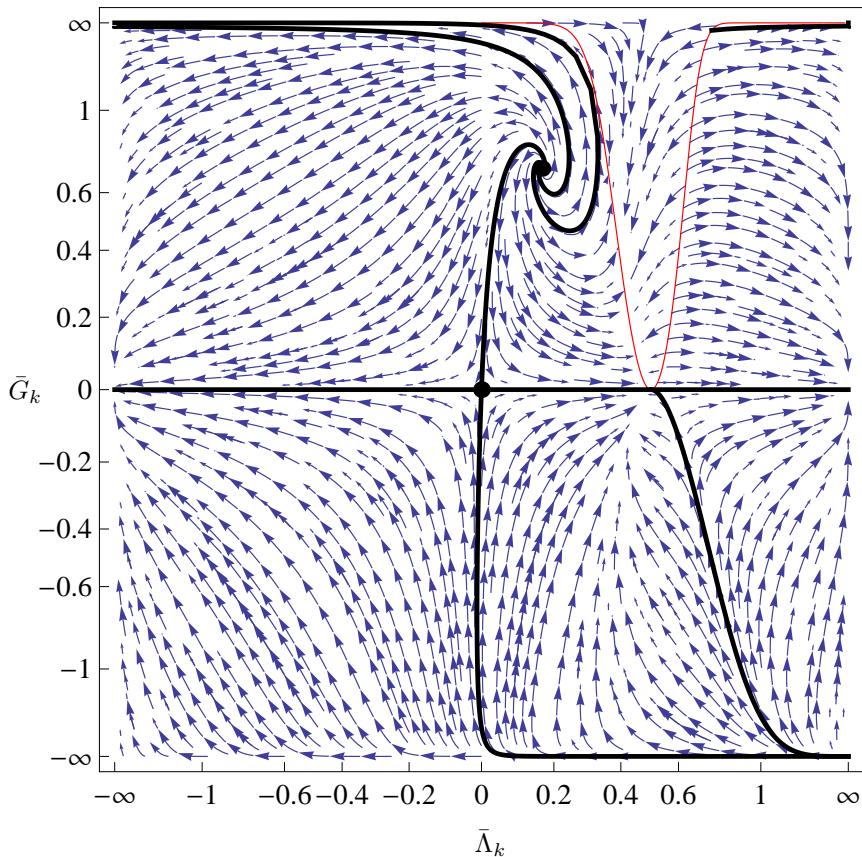


Figure 6.1: The phase diagram of the Einstein-Hilbert truncation, including the GFP, the NGFP and some specific trajectories. The pole of diverging anomalous dimension η_N is depicted in red and the arrows point from UV to IR.

flow equations are valid and we can look for trajectories possibly connecting the fixed point with a classical regime and thus serving an Asymptotic Safety scenario.

Integrating the full beta functions with some suitable starting values of the coupling constants gives rise to trajectories in the truncated theory space, being the \tilde{G}_k - $\tilde{\Lambda}_k$ plane in the Einstein-Hilbert truncation. These can be depicted in a two-dimensional plot as shown in Figure 6.1. This plot illustrates the vector field of the beta functions on the two-dimensional theory space. The arrows point from

the UV to the IR and the axes are rescaled in order to display the behaviour also for large values of the couplings.

This phase space was analysed extensively for the first time in [148] and a comparison to the phase space of a minisuperspace approximation can be found in [156]. In the following discussion we mainly follow the former work but point out the differences. These appear since the authors of [148] used the beta functions derived without the TT decomposition and furthermore used a different regulator.

In Figure 6.1 one can see various things. Highlighted in red is the pole of the anomalous dimension η_N given in (6.5). There the beta functions diverge and are not valid. The GFP at the origin and the non-Gaussian one, given in (6.1), are depicted as black dots. Close to the NGFP one can see the spiral form of the vector field caused by the complex pair of critical exponents (6.3). Close to the GFP the two eigendirections are visible. Since the trajectories on the $\bar{\Lambda}_k$ axis are pulled into the GFP, the $\bar{\Lambda}_k$ direction is the UV-attractive one. The UV-repulsive eigendirection is in the direction of the second highlighted trajectory attached to the GFP.

These specific, thick trajectories serve another purpose. They separate the different types of trajectories. Their classification and the corresponding nomenclature shall be done along the lines of [148] and will be extended. The whole classification is summarised in Table 6.1. As a useful starting point we choose the trajectory which connects the GFP with the NGFP, given as a thick black line in Figure 6.1. It is called separatrix and shall appear in our classification as the single trajectory of Type IIa.

There is another specific trajectory which we will call Type IVa. It is the trajectory connecting the NGFP at high energies with the point $(\bar{G}_k, \bar{\Lambda}_k) = (6\pi/7, -\infty)$. This trajectory is marked as a thick black line in Figure 6.1 as well. Note that, due to the rescaling of the axes, this trajectory looks as if it was going towards $\bar{G}_k = \infty$. That the trajectory reaches exactly this point follows from

$$\lim_{\bar{\Lambda}_k \rightarrow -\infty} \partial_t \bar{G}_k = \frac{1}{3} \bar{G}_k \left(6 - \frac{7\bar{G}_k}{\pi} \right). \quad (6.6)$$

The trajectories to the left of the Type IIa and Type IVa trajectories in Figure 6.1 are called Type Ia. They start at the NGFP at high energies and spiral out due to the complex critical exponents. Afterwards they cross the line $\bar{\Lambda}_k = 0$ and turn to negative values of the cosmological constant. At very low energies they tend towards the point $(\bar{G}_k, \bar{\Lambda}_k) = (0, -\infty)$.

The next class of trajectories is called Type IIIa. This class collects those flows which are on the right of the Type IIa and Type IVa trajectories and are connected to the NGFP, where all of them start in the UV. In the IR they run into the pole where the beta functions are ill defined. However it is a Type IIIa trajectory which would describe Nature the best. Explicitly it is a trajectory which passes by the

Type	IR limit	UV limit
Ia	$(\bar{G}_k, \bar{\Lambda}_k) = (0, -\infty)$	NGFP
IIa	GFP	NGFP
IIIa	pole	NGFP
IVa	$(\bar{G}_k, \bar{\Lambda}_k) = (6\pi/7, -\infty)$	NGFP
Va	pole	pole
VIa	pole	pole
VIIa	$(\bar{G}_k, \bar{\Lambda}_k) = (0, \infty)$	pole
VIIIa	$(\bar{G}_k, \bar{\Lambda}_k) = (6\pi/7, \infty)$	pole
IXa	pole	pole
Ib	$(\bar{G}_k, \bar{\Lambda}_k) = (0, -\infty)$	$(\bar{G}_k, \bar{\Lambda}_k) = (-\infty, \infty)$
IIb	GFP	$(\bar{G}_k, \bar{\Lambda}_k) = (-\infty, \infty)$
IIIb	$(\bar{G}_k, \bar{\Lambda}_k) = (0, \infty)$ via $(\bar{G}_k, \bar{\Lambda}_k) = (0, 1/2)$	$(\bar{G}_k, \bar{\Lambda}_k) = (-\infty, \infty)$
IVb	$(\bar{G}_k, \bar{\Lambda}_k) = (0, \infty)$	$(\bar{G}_k, \bar{\Lambda}_k) = (-\infty, \infty)$
Ic	$(\bar{G}_k, \bar{\Lambda}_k) = (0, -\infty)$	GFP
IIIc	$(\bar{G}_k, \bar{\Lambda}_k) = (0, \infty)$	GFP

Table 6.1: The various types of trajectories are classified according to their IR and UV values.

GFP very closely. There we find the classical regime as discussed above including a positive cosmological constant. The trajectory compatible with measurements in the IR was discussed in detail in [149].

One of the Type IIIa trajectories is marked as a thick black line in Figure 6.1. This separates the Type IIIa trajectories from the trajectories we will call Type Va. On the right side they are bordered by the pole. This pole is reached by them at high energies and at low energies.

The last four classes on the upper half plane have not been classified in [148]. The first of them shall be called Type VIa and contains those trajectories which run from pole to pole and are bordered by the pole from below. These trajectories can be found in the middle region of the first quadrant in Figure 6.1. Next, those trajectories on the upper half plane which run between $(\bar{G}_k, \bar{\Lambda}_k) = (0, \infty)$ and the pole are called Type VIIa. As for negative cosmological constant we find a special trajectory which we depicted as a thick black line. It connects the pole with the point $(\bar{G}_k, \bar{\Lambda}_k) = (6\pi/7, \infty)$ and shall be called Type VIIIa. Finally all other trajectories of the upper half plane are called Type IXa and run from pole to pole and are bordered by the Type VIIIa trajectory from below and the pole itself from above.

In the lower half plane our classification will differ much from the one given in [148]. Within their calculations the authors found another pole at $\bar{G}_k = -6\pi/5$. Since we do not find such a pole our flow behaves differently for negative \bar{G}_k . However we will follow their notation as close as possible.

Again we can start with a single trajectory. It is highlighted as a thick black line in Figure 6.1 and connects the GFP at the origin with $(\bar{G}_k, \bar{\Lambda}_k) = (-\infty, \infty)$. This shall be called Type IIb.

To the left of it one finds the Type Ib trajectories. At low energies they reach the point $(\bar{G}_k, \bar{\Lambda}_k) = (0, -\infty)$. For increasing scale they change the sign of the cosmological constant and finally turn towards $(\bar{G}_k, \bar{\Lambda}_k) = (-\infty, \infty)$.

On the very right side of the lower half plane one finds the flows classified as Type IVb. Their IR value is $(\bar{G}_k, \bar{\Lambda}_k) = (0, \infty)$ and the corresponding UV limit reaches $(\bar{G}_k, \bar{\Lambda}_k) = (-\infty, \infty)$. Note that this class was not considered in [148].

The left-over trajectories of the lower half plane are called Type IIIb and have to be discussed carefully. The reason is the point $(\bar{G}_k, \bar{\Lambda}_k) = (0, 1/2)$. This point recently is under debate and might serve as an IR fixed point. We will not go too much into detail here and the interested reader might be referred to [157–159]. To clarify the occurring problem note that the discussed point is part of the pole (6.5) depicted in red in Figure 6.1. Therefore the flow at this point depends on the direction from which it is approached. An approach from above or from below gives $\partial_t \bar{\Lambda}_k = 2$. In contrast to this, an approach along the $\bar{\Lambda}_k$ axis gives $\partial_t \bar{\Lambda}_k = -1$. As $\partial_t \bar{G}_k = 0$ for $\bar{G}_k = 0$, we will leave this cumbersome point in $\bar{\Lambda}_k$ direction, independent of the direction we approached it. Therefore we stick to $\partial_t \bar{\Lambda}_k = -1$.

Assuming this behaviour at the cumbersome point, the Type IIIb trajectories find $(\bar{G}_k, \bar{\Lambda}_k) = (-\infty, \infty)$ at high energies and tend towards $(\bar{G}_k, \bar{\Lambda}_k) = (0, 1/2)$ while lowering the scale. From this point they run along the $\bar{\Lambda}_k$ axis towards $(\bar{G}_k, \bar{\Lambda}_k) = (0, \infty)$ in the deep IR.

The very last two classes shall be called Type Ic and Type IIIc. They correspond to the trajectory trapped on the $\bar{\Lambda}_k$ axis and running from $(\bar{G}_k, \bar{\Lambda}_k) = (0, -\infty)$ in the IR to the GFP in the UV and from $(\bar{G}_k, \bar{\Lambda}_k) = (0, \infty)$ in the IR to the GFP. Here we assumed the behaviour discussed above for the cumbersome point $(\bar{G}_k, \bar{\Lambda}_k) = (0, 1/2)$. These two classes have not been discussed in [148].

6.2 Phase Diagram of the R^2 Truncation

In the last section we analysed the beta functions of the Einstein-Hilbert truncation. We found a NGFP suitable for the Asymptotic Safety scenario with the corresponding critical exponents. Furthermore we investigated in detail the phase diagram of the two-dimensional theory space. In this section we will follow the same procedure and analyse the beta functions of the R^2 truncation. The discussion significantly extends earlier investigations by Rechenberger and Saueressig [31] and constitutes one of the main results of this thesis.

The beta functions under consideration in this section have been derived in [117–119] for the first time and the main aspects of their derivation can be found in Chapter 5. Their final form is given in (5.42). For simplicity we start to analyse the beta functions in $D = 3$ spacetime dimensions. The case of $D = 4$ and its complications will be discussed below. The first task is the search for fixed points suitable for an Asymptotic Safety scenario. One might expect that the point $(\bar{G}_k, \bar{\Lambda}_k, \bar{\beta}_k) = (0, 0, 0)$ serves as a GFP. However, the beta function for the coupling constant $\bar{\beta}_k$ does not vanish at this point but reads $\partial_t \bar{\beta}_k(0, 0, 0) = \frac{79}{864\pi^2}$. Therefore the proposed point is not a fixed point which was already stated in [119]. Nevertheless, the GFP did not vanish. It can be found by trading the coupling $\bar{\beta}_k$ in front of the R^2 term in our truncation for its inverse

$$\bar{b}_k = \frac{1}{\bar{\beta}_k}, \quad \partial_t \bar{b}_k = -\bar{b}_k^2 \partial_t \bar{\beta}_k. \quad (6.7)$$

Since the action is in the exponent of our path integral, with a minus sign in front, $\bar{\beta}_k = 0$ as well as $\bar{b}_k = 0$ removes the R^2 term. Thus, one is as good as the other and indeed, the point $(\bar{G}_k, \bar{\Lambda}_k, \bar{b}_k) = (0, 0, 0)$ serves as a GFP.

Besides this GFP a numerical analysis shows that the R^2 truncation in three

spacetime dimensions gives rise to four NGFPs situated at

$$\begin{aligned}
\text{NGFP}_1^{3D} &: (\bar{G}_k, \bar{\Lambda}_k, \bar{b}_k) = (0.19, 0.02, 126.41), \\
\text{NGFP}_2^{3D} &: (\bar{G}_k, \bar{\Lambda}_k, \bar{b}_k) = (0.15, 0.36, 18.17), \\
\text{NGFP}_3^{3D} &: (\bar{G}_k, \bar{\Lambda}_k, \bar{b}_k) = (0.22, 0.10, 18.84), \\
\text{NGFP}_4^{3D} &: (\bar{G}_k, \bar{\Lambda}_k, \bar{b}_k) = (0, 0, -\frac{864\pi^2}{79}).
\end{aligned} \tag{6.8}$$

The analysis of the stability properties at these fixed points reveals that the critical exponents corresponding to the NGFPs read

$$\begin{aligned}
\text{NGFP}_1^{3D} &: (\theta_1, \theta_2, \theta_3) = (8.39, 1.86, 1.35), \\
\text{NGFP}_2^{3D} &: (\theta_1, \theta_2, \theta_3) = (-9.85, 1.56 + 4.84\iota, 1.56 - 4.84\iota), \\
\text{NGFP}_3^{3D} &: (\theta_1, \theta_2, \theta_3) = (1.68, 0.19 + 0.97\iota, 0.19 - 0.97\iota), \\
\text{NGFP}_4^{3D} &: (\theta_1, \theta_2, \theta_3) = (2, -1, -1).
\end{aligned} \tag{6.9}$$

Therefore the first and the third NGFP are UV-attractive in all three directions, where the third will show a spiraling behaviour close to the fixed point due to the complex pair of critical exponents. The second fixed point as well has a complex pair of critical exponents, but is UV-repulsive in one and UV-attractive in two directions. The opposite is true for the fourth NGFP which does not show a complex pair. Please note that the critical exponents corresponding to the latter are the canonical mass dimensions. This behaviour is usually found at the GFP.

As we did in Section 6.1 we next determine the singular loci of the beta functions before we analyse possible trajectories. Again we find poles where some or all of the flow equations diverge. At these poles the system of flow equations loses its validity. Of course, the beta functions here are much more complicated compared to those of the Einstein-Hilbert truncation and therefore it is not surprising that the pole structure is also more complicated. As an extension of [31], we elucidate the complete pole structure within some two-dimensional subspaces of the three-dimensional theory space. Due to the complicated structure, a complete three-dimensional plot of the singular loci is too elusive and thus we stick to the two-dimensional projections given in Figure 6.2. In these plots we show slices of constant \bar{G}_k and slices of constant $\bar{\Lambda}_k$, where we rescaled the axes in order to show the full range on a finite interval. Furthermore we added a relative rescaling of a factor 100 for the $\bar{\beta}_k$ axis for better readability of the plots. The values of the constant \bar{G}_k and $\bar{\Lambda}_k$ increase from top to bottom and correspond to the NGFP values. Explicitly the middle left and the upper right plot correspond to NGFP_1^{3D} , the upper left and the bottom right plot correspond to the NGFP_2^{3D} and finally the bottom left and the middle right plot correspond to NGFP_3^{3D} . The poles appear as red lines in the projections and become two-dimensional hypersurfaces of the three-dimensional

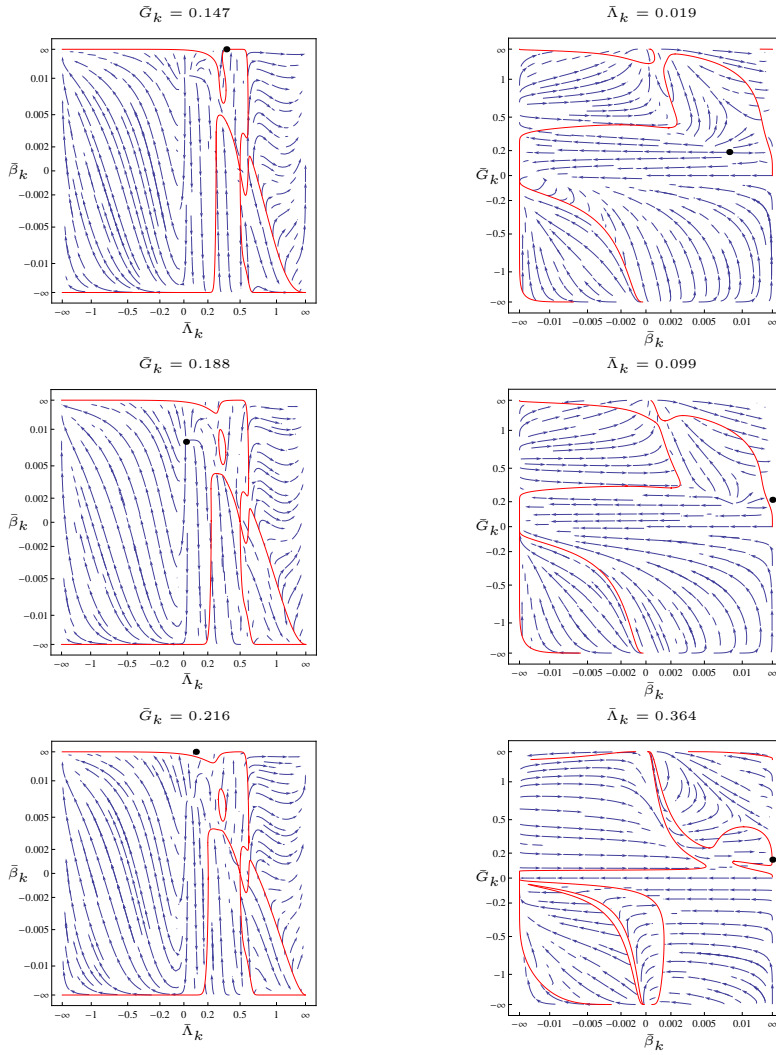


Figure 6.2: Phase-diagram slices of the R^2 truncation in $D = 3$ for constant \bar{G}_k (left) and $\bar{\Lambda}_k$ (right). Depicted are the poles (red lines) and the NGFPs (black dots). The arrows of the vector field point towards low energies.

theory space if we leave the projection. The form of these hypersurfaces follows from the two orthogonal projections given in Figure 6.2. Please note that the NGFP_1^{3D} and the $\text{NGFP}_{2,3}^{3D}$ are situated on different sides of the singular locus.

We proceed as we did in the Einstein-Hilbert truncation and discuss possible trajectories in theory space. We start in three dimensions with the limit $\bar{G}_k = 0$. In this limit the beta functions simplify considerably and we find

$$\begin{aligned}\partial_t \bar{G}_k \Big|_{\bar{G}_k=0} &= 0, \\ \partial_t \bar{\Lambda}_k \Big|_{\bar{G}_k=0} &= -2\bar{\Lambda}_k, \\ \partial_t \bar{\beta}_k \Big|_{\bar{G}_k=0} &= -\frac{-79 - 1290\bar{\Lambda}_k + 3132\bar{\Lambda}_k^2 - 1752\bar{\Lambda}_k^3 - 864\pi^2\bar{\beta}_k(1 - 2\bar{\Lambda}_k)^3}{864\pi^2(1 - 2\bar{\Lambda}_k)^3}, \\ \partial_t \bar{b}_k \Big|_{\bar{G}_k=0} &= -\frac{\bar{b}_k(864\pi^2(1 - 2\bar{\Lambda}_k)^3 + \bar{b}_k(79 + 1290\bar{\Lambda}_k - 3132\bar{\Lambda}_k^2 + 1752\bar{\Lambda}_k^3))}{864\pi^2(1 - 2\bar{\Lambda}_k)^3}.\end{aligned}\tag{6.10}$$

Note that the complicated pole structure shown in Figure 6.2 simplifies according to the limits of the flow equations (6.10) and becomes a straight line at $\bar{\Lambda}_k = 1/2$. This simplified pole and the corresponding slices of the phase diagram, using $\bar{\beta}_k$ and \bar{b}_k respectively, are depicted in Figure 6.3. The limit of the flow equation for the dimensionless Newton constant becomes zero and thus the trajectories are trapped on the slice $\bar{G}_k = 0$. In other words, the solution $\bar{G}_k = 0$ is self-consistent. In Section 6.1 we used the name "Type c" and we will stick to this notation here as well. A list of the types of trajectories discussed in the following can be found in Table 6.2. Similar to the Einstein-Hilbert truncation we find a Type Ic and a Type IIIc trajectory connecting the GFP with $(\bar{G}_k, \bar{\Lambda}_k, \bar{b}_k) = (0, -\infty, 0)$ and $(\bar{G}_k, \bar{\Lambda}_k, \bar{b}_k) = (0, \infty, 0)$ respectively. The R^2 truncation gives us a third direction in theory space and thus we can define a Type IIc trajectory running from the GFP at high energies towards the NGFP_4^{3D} at low energies. Furthermore we find Type IVc and Type VIc trajectories connecting the point $(\bar{G}_k, \bar{\Lambda}_k, \bar{b}_k) = (0, -\infty, 288\pi^2/73)$ in the IR with the GFP and the NGFP_4^{3D} in the UV respectively. The Type Vc and Type VIIc trajectories find this pole as an IR limit while the UV limit is the GFP and the NGFP_4^{3D} respectively. At very large values of $\bar{\Lambda}_k$ we find the Type VIIIc trajectories with the pole as a UV limit and the point $(\bar{G}_k, \bar{\Lambda}_k, \bar{b}_k) = (0, \infty, 288\pi^2/73)$ as the IR limit.

Besides the limit $\bar{G}_k = 0$ there is another interesting limit, which is $\bar{b}_k = 0$. At this limit the beta functions as well as the pole structure simplifies considerably.

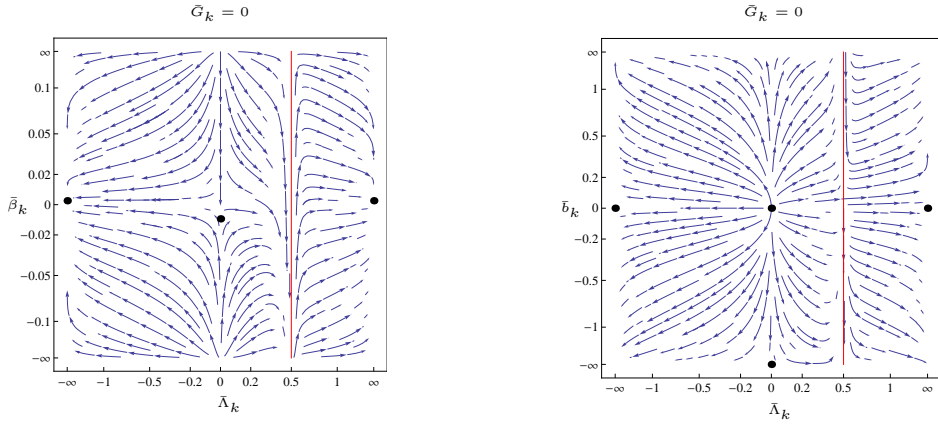


Figure 6.3: Two-dimensional slices of the phase diagram for the R^2 truncation in $D = 3$. The plots show slices of constant $\bar{G}_k = 0$, using $\bar{\beta}_k$ (left plot) and \bar{b}_k (right plot) respectively. The singular locus of the beta functions and the fixed points correspond to the red line and the black dots respectively. The arrows of the vector field point towards low energies.

Most importantly we find

$$\partial_t \bar{b}_k \Big|_{\bar{b}_k=0} = 0. \quad (6.11)$$

Therefore, similar to $\bar{G}_k = 0$ we find the self-consistent solution $\bar{b}_k = 0$. The slice of the phase diagram, corresponding to this limit, can be found in Figure 6.4. Depicted is the GFP as a black dot and the pole as a red line. Note that none of the NGFPs are visible, as they are not situated in the $\bar{b}_k = 0$ plane. Concentrating on the line $\bar{G}_k = 0$ in this plot reveals a fixed point at $\bar{\Lambda}_k = 3/5$. Note that we did not see any fixed point at the line $\bar{b}_k = 0$ in the right plot of Figure 6.3 depicting the slice $\bar{G}_k = 0$. The reason is that the $\bar{\Lambda}_k$ axis lies on the pole depicted in Figure 6.2. The situation thus is similar to the point $(\bar{G}_k, \bar{\Lambda}_k) = (0, 1/2)$ in the Einstein-Hilbert truncation. The beta function on the $\bar{\Lambda}_k$ axis of the R^2 truncation depends on the way we approach this line. The two limits discussed above correspond to

$$\lim_{\bar{b}_k \rightarrow 0} \lim_{\bar{G}_k \rightarrow 0} \partial_t \bar{\Lambda}_k = -2\bar{\Lambda}_k, \quad \lim_{\bar{G}_k \rightarrow 0} \lim_{\bar{b}_k \rightarrow 0} \partial_t \bar{\Lambda}_k = \frac{2}{3}\bar{\Lambda}_k (-3 + 5\bar{\Lambda}_k). \quad (6.12)$$

This explains the difference and tells us that we have to be careful with the beta functions on the $\bar{\Lambda}_k$ axis. There is even another issue addressed by these two limits,

Type	IR limit	UV limit
Ia	$(\bar{G}_k, \bar{\Lambda}_k, \bar{b}_k) = (0, -\infty, 288\pi^2/73)$	NGFP ₁ ^{3D}
IIIa	pole	NGFP ₁ ^{3D}
IVa	$(\bar{G}_k, \bar{\Lambda}_k, \bar{b}_k) = (9\pi/76, -\infty, 288\pi^2/73)$	NGFP ₁ ^{3D}
Ic	$(\bar{G}_k, \bar{\Lambda}_k, \bar{b}_k) = (0, -\infty, 0)$	GFP
IIc	NGFP ₄ ^{3D}	GFP
IIIc	$(\bar{G}_k, \bar{\Lambda}_k, \bar{b}_k) = (0, \infty, 0)$	GFP
IVc	$(\bar{G}_k, \bar{\Lambda}_k, \bar{b}_k) = (0, -\infty, 288\pi^2/73)$	GFP
Vc	pole	GFP
VIc	$(\bar{G}_k, \bar{\Lambda}_k, \bar{b}_k) = (0, -\infty, 288\pi^2/73)$	NGFP ₄ ^{3D}
VIIc	pole	NGFP ₄ ^{3D}
VIIIc	$(\bar{G}_k, \bar{\Lambda}_k, \bar{b}_k) = (0, \infty, 288\pi^2/73)$	pole

Table 6.2: Some types of trajectories in three dimensions are classified according to their IR and UV values.

the classical regime. Recall that within the Einstein-Hilbert truncation the classical limit was found close to $\bar{G}_k = 0$. Now we can see that within the R^2 truncation it is important how we are approaching the regime of $\bar{G}_k \ll 1$. The first limiting process in (6.12) gives us the dimensional running and thus is the correct side of the pole.

If we leave the specific slice of $\bar{G}_k = 0$ it is helpful, for a better understanding of the behaviour at small \bar{b}_k or large $\bar{\beta}_k$, to have the plots of Figure 6.2 depending on \bar{b}_k rather than on $\bar{\beta}_k$. These plots can be found in Figure 6.5. We start with those trajectories which are connected to the NGFP₁^{3D} at high energies. This fixed point is depicted in the middle plot on the left hand side and the upper plot on the right hand side of Figures 6.2 and 6.5. First we realise that there is no Type IIa trajectory which would connect the NGFP₁^{3D} with the GFP. Such a trajectory is prevented by the pole structure. Note that, although a separatrix does not exist, we can find trajectories passing by the GFP very close with negative as well as positive values for the coupling constant \bar{b}_k .

In comparison to the Einstein-Hilbert truncation we find trajectories similar to those of Type Ia and of Type IVa in Section 6.1. Recall that they reached $\bar{\Lambda}_k \rightarrow -\infty$ at low energies. To find the corresponding classification in our R^2 truncation we

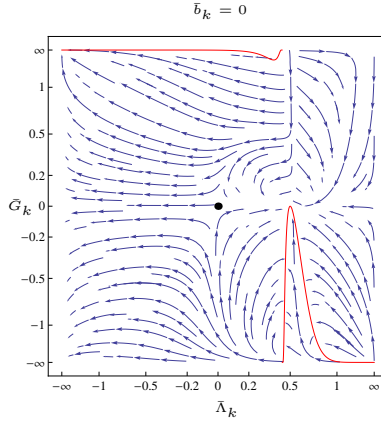


Figure 6.4: Two-dimensional slice of the phase diagram for the R^2 truncation in $D = 3$. The plot shows the slice of constant $\bar{b}_k = 0$. Depicted is the pole of the beta functions (red line) and the GFP (black dot). The arrows of the vector field point towards low energies.

have to investigate the limits $\bar{\Lambda}_k \rightarrow -\infty$ of our beta functions. These read

$$\lim_{\bar{\Lambda}_k \rightarrow -\infty} \partial_t \bar{G}_k = \bar{G}_k - \frac{76\bar{G}_k^2}{9\pi}, \quad \lim_{\bar{\Lambda}_k \rightarrow -\infty} \partial_t \bar{b}_k = -\bar{b}_k + \frac{73\bar{b}_k^2}{288\pi^2}. \quad (6.13)$$

The two possible IR limits with $\bar{b}_k = 0$ are not reachable from the NGFP_1^{3D} since the \bar{b}_k direction is IR repulsive in both cases and thus the pole structure prevents us from running into these points. Besides these two points we find two other possible IR limits with $\bar{b}_k = 288\pi^2/73$. There are trajectories which connect the NGFP_1^{3D} with the point $(\bar{G}_k, \bar{\Lambda}_k, \bar{b}_k) = (9\pi/76, -\infty, 288\pi^2/73)$ and we will call these trajectories Type IVa. Furthermore we find trajectories flowing from the NGFP_1^{3D} at high energies towards the point $(\bar{G}_k, \bar{\Lambda}_k, \bar{b}_k) = (0, -\infty, 288\pi^2/73)$ at low energies. These trajectories shall be called Type Ia. However, the trajectory describing our universe should have a positive cosmological constant at low energies. Therefore, it will not belong to the described classes. We will classify all trajectories running from the NGFP_1^{3D} at high energies to one of the poles at low energies as Type IIIa. Therefore the most interesting one, describing our universe, would belong to this class.

For a better visualisation we give a three-dimensional plot of a sample of Type Ia and Type IIIa trajectories in Figure 6.6. Here we used the coupling constant

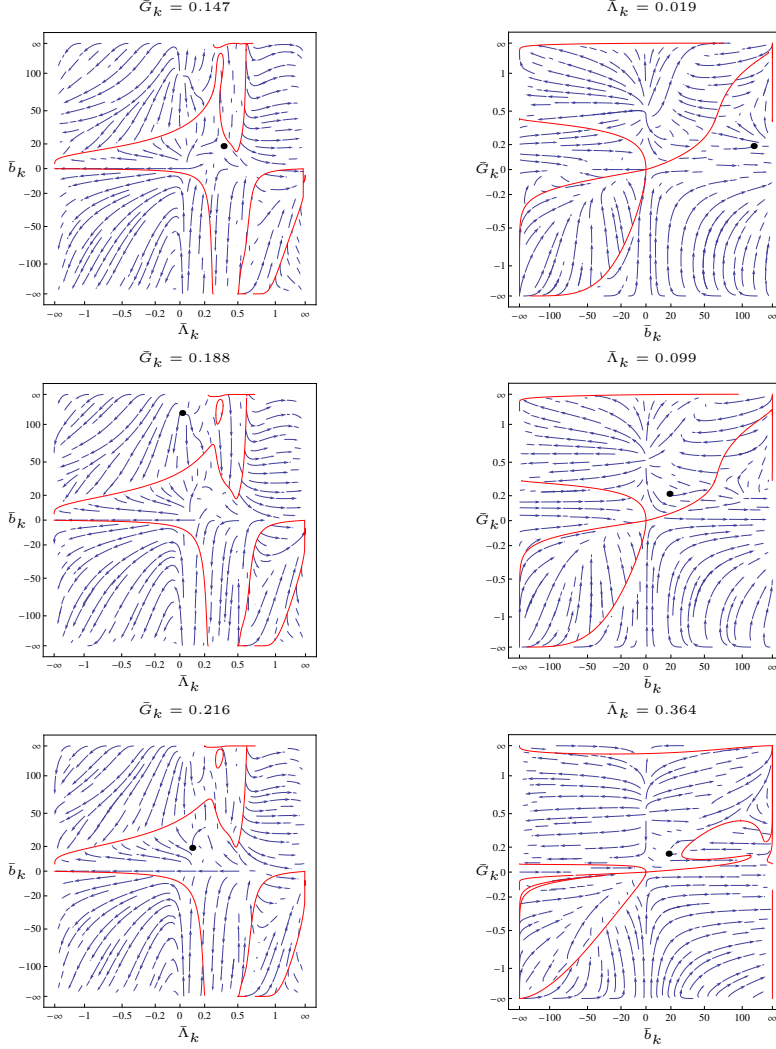


Figure 6.5: Phase-diagram slices of the R^2 truncation in $D = 3$ for constant \bar{G}_k (left) and $\bar{\Lambda}_k$ (right), using \bar{b}_k . Depicted are the poles (red lines) and the NGFPs (black dots). The arrows of the vector field point towards the IR.

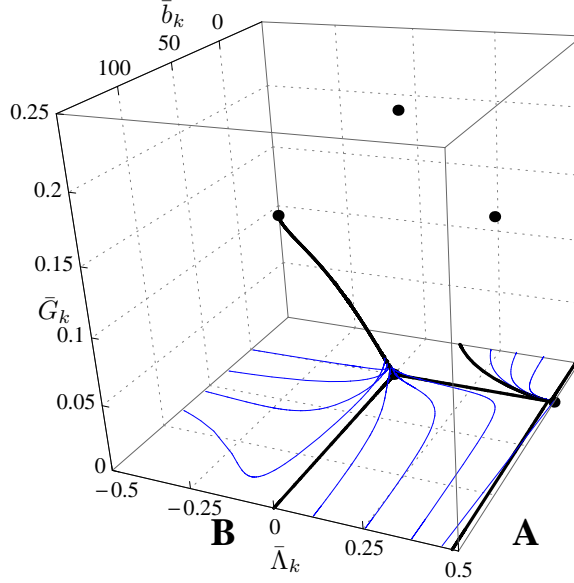


Figure 6.6: Three-dimensional plot of a sample of Type Ia and Type IIIa trajectories of the R^2 truncation in three spacetime dimensions. Depicted are the fixed points as black dots and a sample of trajectories as blue lines. Two trajectories are labeled as A and B for later purpose.

\bar{b}_k to show the behaviour close to the GFP as well. Depicted are the fixed points as black dots and a sample of trajectories as blue and black lines. All trajectories start at high energies at the NGFP_1^{3D} and run towards the GFP for positive \bar{b}_k . However, before reaching the latter the pole redirects the trajectories. Sooner or later all those who stay at positive cosmological constant receive a strong running in \bar{b}_k direction. If we would have used $\bar{\beta}_k$ instead of \bar{b}_k it would be obvious that the R^2 coupling changes sign. Here this behaviour causes a disappearance of the trajectories at $\bar{b}_k \rightarrow \infty$ and a reappearance at $\bar{b}_k \rightarrow -\infty$. Afterwards the depicted Type IIIa trajectories come close to the point $(\bar{G}_k, \bar{\Lambda}_k, \bar{b}_k) = (0, 1/2, 0)$ where they hit the pole. Those trajectories which run towards negative cosmological constant after leaving the GFP are of Type Ia. They finally reach the point $(\bar{G}_k, \bar{\Lambda}_k, \bar{b}_k) = (0, -\infty, 288\pi^2/73)$.

While inspecting Figure 6.5 we see that the trajectories connected to NGFP_1^{3D}

and NGFP_2^{3D} are not compatible with a classical limit at low energies, as they are on the wrong side of the pole. Therefore we refrain from classifying them here. Furthermore there are many trajectories which are not connected to any fixed point. These are not interesting for an Asymptotic Safety scenario and thus we skip the classification of these trajectories as well.

The situation in $D = 4$ spacetime dimensions is similar, but worse. Nevertheless, we start to analyse possible fixed points of the beta functions. First of all we find again the GFP at $(\bar{G}_k, \bar{\Lambda}_k, \bar{b}_k) = (0, 0, 0)$. Besides this trivial solution of the flow equations we find two NGFPs, which read

$$\begin{aligned} \text{NGFP}_1^{4D} &: (\bar{G}_k, \bar{\Lambda}_k, \bar{b}_k) = (0.74, 0.16, 341.81), \\ \text{NGFP}_2^{4D} &: (\bar{G}_k, \bar{\Lambda}_k, \bar{b}_k) = (0.70, 0.17, 437.53). \end{aligned} \quad (6.14)$$

Following the analysis in three spacetime dimensions we evaluate the critical exponents as the next step and start with the GFP. Unfortunately the GFP is situated on top of the pole, similar to the point $(\bar{G}_k, \bar{\Lambda}_k) = (0, 1/2)$ in the Einstein-Hilbert truncation. Therefore the linearisation depends on the limiting process with which we approach this fixed point. However, since the GFP is not suitable for an Asymptotic Safety scenario, we are not interested in its critical exponents and move on to the NGFPs. Their critical exponents read

$$\begin{aligned} \text{NGFP}_1^{4D} &: (\theta_1, \theta_2, \theta_3) = (3.49, 1.65 + 3.10 \iota, 1.65 - 3.10 \iota), \\ \text{NGFP}_2^{4D} &: (\theta_1, \theta_2, \theta_3) = (25.56, 1.40 + 2.78 \iota, 1.40 - 2.78 \iota). \end{aligned} \quad (6.15)$$

Both fixed points are UV-attractive in all three directions and show a complex pair of critical exponents. These will cause a spiralled behaviour as we have seen already within the Einstein-Hilbert truncation.

Before we search for trajectories connected to the NGFPs we analyse the structure of the flow equations to find the limits of their validity. Again we find singular loci similar to those given in Figure 6.2. However, the main difference between $D = 3$ and $D = 4$ appears due to the terms proportional to the Kronecker delta $\delta_{D,4}$ in the beta functions. Recall that these zero-mode contributions arise due to the York decomposition discussed in Appendix C.2 and can be found as part of the functions C_1, C_2 and C_3 given in Appendix D. Unfortunately these terms induce an additional pole in the beta functions. In Figure 6.7 we show a slice of the phase space of the four-dimensional R^2 truncation similar to those of Figure 6.2. The situation in four dimensions is similar to the one in three dimensions and thus we refrain from giving further plots here. The left plot in Figure 6.7 shows the phase diagram resulting from beta functions without the terms proportional to $\delta_{D,4}$. The flow shown in the second plot includes the zero-mode contributions. The poles appearing in both cases correspond to the red lines, while the new pole, present only if we include the zero-mode contributions, appears as a black line. As this

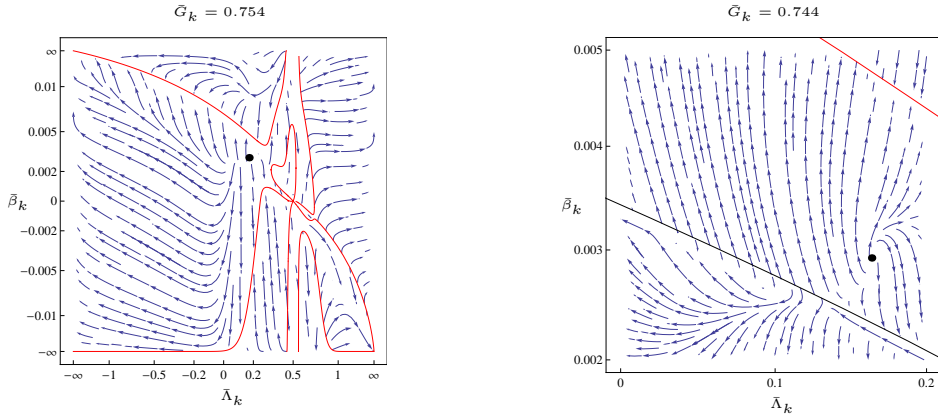


Figure 6.7: Two-dimensional slice of the phase diagram obtained from the R^2 truncation. The first plot shows the slice of constant $\bar{G}_k = 0.754$ in $D = 4 - \epsilon$. Depicted are the poles of the beta functions (red lines) and the NGFP (black dot). The arrows of the vector field point towards low energies. The flow in the right plot corresponds to $D = 4$ and zooms onto the NGFP.

new pole appears close to the NGFP, we magnify this region in the second plot. Furthermore we depict the NGFP_1^{4D} as a black dot situated between the two poles. This makes the numerical analysis of trajectories connected to this NGFP almost impossible and we will circumvent this problem by analysing the beta functions without the zero-mode contributions.² To simplify our discussion we will discuss in the following the R^2 truncation in $D = 4 - \epsilon$ dimensions instead of $D = 4$ to circumvent the tedious new pole.

In $D = 4 - \epsilon$ spacetime dimensions we find again the GFP on top of the pole at $(\bar{G}_k, \bar{\Lambda}_k, \bar{b}_k) = (0, 0, 0)$. Furthermore we find a unique NGFP at

$$\text{NGFP}^{4D\epsilon} : (\bar{G}_k, \bar{\Lambda}_k, \bar{b}_k) = (0.75, 0.17, 336.25) \quad (6.16)$$

which is depicted in the left plot of Figure 6.7. The corresponding critical exponents are

$$\text{NGFP}^{4D\epsilon} : (\theta_1, \theta_2, \theta_3) = (3.95, 1.57 + 3.31\iota, 1.57 - 3.31\iota) \quad (6.17)$$

²Note that, in principle, one could rederive the beta functions without the decomposition. This would lead to the absence of the tedious second pole.

and therefore the fixed point is UV-attractive in all three directions. Furthermore it shows a complex pair which causes a spiralled behaviour close to the fixed point. Notably the value of the first critical exponent differs considerably from the one evaluated in [119] with an exponential cutoff. There the authors found $\theta_1 = 28.8$. This discrepancy is caused by the fact that we are working in $D = 4 - \epsilon$ dimensions.

Let us elaborate on this non-trivial issue a bit more. The NGFP_1^{4D} is depicted in the right plot of Figure 6.7 and turns into $\text{NGFP}^{4D\epsilon}$ when removing the zero-mode contributions. Comparing the critical exponents, the second fixed point, NGFP_2^{4D} , seems to be related to the one found in [119]. However, removing the zero-mode contributions this fixed point vanishes. Following our argument that the zero-mode contributions are a technical artefact, this NGFP might be unphysical.

There are two further arguments supporting this reasoning. First, we can use a strength of the functional renormalisation group technique, the ability to change the dimension continuously. This was already used in [160] where the author finds the appearance of new fixed points while lowering the dimension in a \mathbb{Z}_2 -effective potential. Starting in three spacetime dimensions in the R^2 truncation and continuously changing the dimension towards $D = 4$, we find that NGFP_2^{3D} and NGFP_3^{3D} annihilate each other at $D = 3.84$. Furthermore we find that the NGFP_1^{3D} is continuously connected with $\text{NGFP}^{4D\epsilon}$. This continuity serves as one argument that the zero-mode contributions are unphysical. The second argument considers higher orders in the polynomial expansion of the scalar curvature in the truncation (see first row in Table 4.1). The new critical exponent $\theta_1 = 3.949$ fits much better to the critical exponents in higher truncations given e.g. in [121]. There the authors find $\theta_1 = 2.068$ for the R^3 truncation, $\theta_1 = 1.546$ for the R^4 truncation, and so on. Of course these two arguments are no proof and one should resort to beta functions without the York decomposition to resolve the fate of NGFP_2^{4D} .

However it would be interesting to have a glance at $D = 4 - \epsilon$ spacetime dimensions, where we are able to find trajectories connected to the $\text{NGFP}^{4D\epsilon}$. The situation is at least similar to the one in three dimensions. The most important difference is that, although we have an analog of NGFP_1^{3D} , which is $\text{NGFP}^{4D\epsilon}$, we do not have an analogue of the other NGFPs in three dimensions, neither $\text{NGFP}_{2/3}^{3D}$, nor NGFP_4^{3D} . The resulting classification of trajectories restricted to $\bar{G}_k = 0$ and trajectories connected to the $\text{NGFP}^{4D\epsilon}$ will not be discussed in detail but are summarised in Table 6.3. Again we give a three-dimensional plot for a better visualisation of some Type Ia and Type IIIa trajectories in $4 - \epsilon$ spacetime dimensions in Figure 6.8. The most peculiar difference between Figure 6.6 and Figure 6.8 is the characteristic spiralled approach towards the NGFP in $4 - \epsilon$ spacetime dimensions due to the complex pair of critical exponents (6.17). Besides this obvious feature there is another difference which is not directly visible in the plot. Between the $\text{NGFP}^{4D\epsilon}$ and the GFP the trajectories switch the sign of the cosmological constant for a finite interval. This feature does not appear in

Type	IR limit	UV limit
Ia	$(\bar{G}_k, \bar{\Lambda}_k, \bar{b}_k) = (0, -\infty, 288\pi^2/73)$	NGFP $^{4D\epsilon}$
IIIa	pole	NGFP $^{4D\epsilon}$
IVa	$(\bar{G}_k, \bar{\Lambda}_k, \bar{b}_k) = (9\pi/76, -\infty, 288\pi^2/73)$	NGFP $^{4D\epsilon}$
Ic	$(\bar{G}_k, \bar{\Lambda}_k, \bar{b}_k) = (0, -\infty, 0)$	GFP
IIc	GFP	GFP
IIIc	$(\bar{G}_k, \bar{\Lambda}_k, \bar{b}_k) = (0, \infty, 0)$	GFP
Vc	pole	GFP

Table 6.3: Some types of trajectories in $(4 - \epsilon)$ dimensions are classified according to their IR and UV values.

three spacetime dimensions. Note that a similar effect has been seen in [161] in a completely different context. Again two of the Type IIIa trajectories are marked as A and B. These two and the two of Figure 6.6 are singled out in order to use them as exemplary trajectories to evaluate the spectral dimension in the following section.

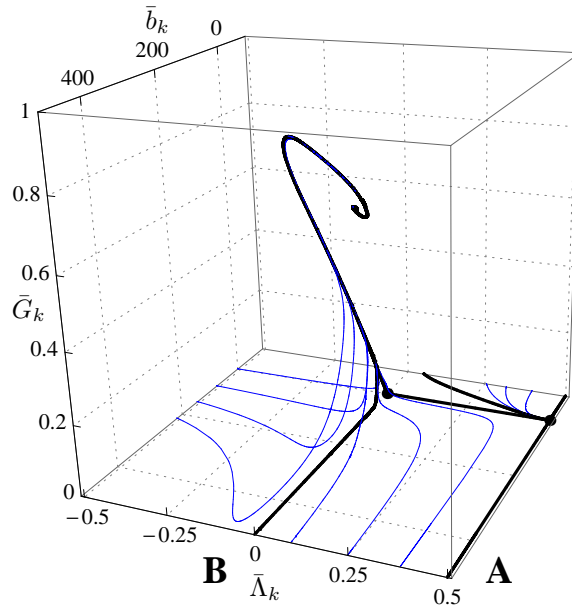


Figure 6.8: Three-dimensional plot of a sample of Type Ia and Type IIIa trajectories of the R^2 truncation in $4 - \epsilon$ spacetime dimensions. Depicted are the fixed points as black dots and a sample of trajectories as blue lines. Two trajectories are labeled as A and B for later purpose.

The Spectral Dimension

7.1 The Notion of Dimension

The last two chapters have been devoted to the flow equations itself and the analysis of the corresponding phase space. Based on this, the present chapter discusses structural properties of the effective quantum spacetime implied by scale dependent coupling constants.

In [119, 150] it was shown that, for QEG, the spacetime becomes self-similar at high energies and the graviton propagator is effectively two dimensional. These are fingerprints that the spacetime at small scales is effectively a fractal. For this reason it is useful to generalise the notion of dimension in order to capture the dynamical dimensional reduction of spacetime. In particular we will discuss the spectral dimension. However, before we analyse the latter with the FRG tools we will start with some general remarks. For the details the interested reader might be referred to [162]. For brevity we will follow [30] for the introduction of the most important terms of the following considerations.

We start with the so-called Hausdorff dimension. For the sake of simplicity we do not give a mathematically rigorous definition, but discuss a simple example in order to get an intuition of the Hausdorff dimension. Thinking of a set of points embedded into a metric space, this dimension is given with the help of balls of radius R . The number of such balls $N(R)$, necessary to cover the set of points, definitely depends on their radius and in the limit of vanishing radius the relation can be given as

$$N(R) \sim R^{-d_{\text{H}}} \quad \text{for } R \rightarrow 0. \quad (7.1)$$

The number d_{H} in the exponent defines the Hausdorff dimension of the set of points. If we consider a smooth line and cover it with circles of radius R , we find the Hausdorff dimension to be 1 as one expects from a line. However, the situation is different if we consider fractals instead of a smooth line.

The name fractals has been introduced by Mandelbrot and probably the most

famous example is the coast line of Britain [163]. Typical properties of a fractal are self-similarity and scale invariance. These properties have been found in QEG at short scales [119, 150] and thus, spacetime has at least fractal features at high energies. Therefore raising the question about dimensionality of spacetime forces us to discuss the notion of dimension on less-regular sets.

Let us consider the coast line of Britain as an example. If we ask for its length the paradox arises that the result of a measurement depends on the length of the yardstick used to measure it [164]. This paradox is related to the fact that the Hausdorff dimension is not equal to one. Again we use circles of radius R and decrease this radius while counting the number of balls necessary to cover the coast line. While decreasing the radius we have to zoom in and find a more and more refined structure. This causes a Hausdorff dimension between 1 and 2. Although being a line, due to its non-smoothness the coast line of Britain is not one-dimensional. Note that the same statement is true for any other coast line.

The definition of the Hausdorff dimension is a static one. In contrast to this we can define a dimension in a dynamical way by using diffusion processes. On a Riemannian manifold a Brownian motion and thus the diffusion process is described by the heat equation

$$\partial_T K(x, x', T) = -\Delta K(x, x', T) \quad (7.2)$$

and the corresponding heat kernel $K(x, x', T)$. Here Δ denotes the Laplace operator of the metric $g_{\mu\nu}$ with which the manifold is equipped. In the special case of flat space the well known solution reads

$$K(x, x', T) = \int \frac{d^D p}{(2\pi)^D} e^{ik(x-x')} e^{-p^2 T}. \quad (7.3)$$

In curved manifolds, of course, the solution is not that easy. However, assuming the knowledge about the heat kernel we can define the return probability of our random walker $P(T)$ depending on the time of the walk as the trace per unit volume

$$P(T) = \frac{\int d^D x \sqrt{g(x)} K(x, x, T)}{\int d^D x \sqrt{g(x)}}. \quad (7.4)$$

In the limit of short random walks the spectral dimension D_s is defined by the T dependence of the return probability as

$$P(T) \sim T^{-D_s/2} \quad \text{for } T \rightarrow 0 \quad \Rightarrow \quad D_s = -2 \frac{d}{d \ln T} \ln P(T) \Big|_{T=0}. \quad (7.5)$$

For a D -dimensional, smooth manifolds the return probability satisfies an early time expansion which reads

$$P(T) = \frac{1}{(4\pi T)^{D/2}} \sum_{n=0}^{\infty} A_n T^n \quad (7.6)$$

where D is the dimension of the manifold and A_n are the Seeley-DeWitt coefficients or heat-kernel coefficients [165, 166] (see also Appendix C.1). In this case the spectral dimension D_s equals the dimension D of the manifold. In the context of QG one needs different effective dimensions on different length scales. Therefore it is useful to generalise the definition of the spectral dimension (7.5) into a T -dependent version which we will use in the following. It reads

$$D_s(T) = -2 \frac{d}{d \ln T} \ln P(T). \quad (7.7)$$

This definition used a random walk and thus is a dynamical definition, in contrast to the Hausdorff dimension. Using the Brownian motion a further notion of dimension can be introduced, the so-called walk dimension D_w . It is defined through the average square distance of the random walker and given by $\langle r^2 \rangle \sim T^{2/D_w}$. All these notions of dimension discussed above show that the concept of dimension has to be taken with care, but can be handled on smooth manifold as well as on less-regular sets. Thus we have everything at hand to discuss the dimension of effective spacetime in the context of QG.

In the following we will concentrate on the spectral dimension. We start to equip the definition with a scale dependence in order to discuss the spacetime at different energy scales. For this purpose we use an RG improvement of the heat equation (7.2) as it was proposed in [30]

$$\partial_T K(x, x', T) = -\Delta(k) K(x, x', T). \quad (7.8)$$

Here we replaced the Laplace operator in (7.2) by a scale-dependent version in order to take into account that at each scale we have a different metric. Note that we assumed here that the scale k is the only relevant scale for the diffusion process. For the solution of the heat equation (7.8) we introduce a reference scale k_0 which we choose to be at low energies. Denoting the Laplace operator at this scale by $\Delta(k_0)$ we can relate it to the Laplace operator at scale k via a function $F(k^2)$ by

$$\Delta(k) = F(k^2) \Delta(k_0). \quad (7.9)$$

In order to be physical, our theory has to become classical at low energies and thus we can approximate the spacetime metric at the scale k_0 with the flat metric. In this case we know that the eigenvalues of the Laplace operator are p^2 and the eigenfunctions are plane waves. After substituting $\Delta(k)$ by (7.9) we use them to find

$$P(T) = \int \frac{d^D p}{(2\pi)^D} e^{-p^2 F(p^2) T} = \frac{1}{(4\pi)^{D/2} \Gamma(\frac{D}{2})} \int_0^\infty dz z^{D/2-1} e^{-z F(z) T}. \quad (7.10)$$

Note that we identified p with k here. This can be motivated by the fact that the plane waves probe length scales of order $1/|p|$ and thus p is the relevant scale.

Without considering the RG improvement we find the classical $F(z) = 1$. Inserting this into (7.10) leads to $P(T) = (4\pi T)^{-D/2}$ and (7.7) finally leads us to the expected classical result $D_s = D$.

However, we are interested in non-trivial functions $F(z)$ incorporating the information about the scale dependence of the spectral dimension. Since a general treatment is very hard we concentrate here on the special case that $F(k^2)$ follows a power law on a long range of scales. Based on this assumption we find

$$F(k^2) \sim k^\delta \quad \Rightarrow \quad D_s = \frac{2D}{2 + \delta} \quad (7.11)$$

which relates a constant spectral dimension to the spacetime for this range of scales. Note that $\delta = 0$ corresponds to the classical case. In the following we will discuss the form of the function $F(k^2)$ in detail and use it to find numerical results for the spectral dimension.

7.2 Spectral Dimension within the Einstein-Hilbert Truncation

At the end of the last section we showed that we can find the scale-dependent spectral dimension if we know the function $F(k^2)$ relating the Laplace operator at the scale k with the one at a reference scale k_0 chosen in the IR. In the following we will derive an expression for this function $F(k^2)$ within the Einstein-Hilbert truncation along the lines of [30]. The ansatz for the EAA is given in (5.8) and at vanishing fluctuations and ghost it reads

$$\Gamma_k^{\text{EH}}|_{g=\bar{g}, c=0} = \frac{1}{16\pi G_k} \int d^D x \sqrt{g} [-R + 2\Lambda_k]. \quad (7.12)$$

This ansatz includes the scale-dependent cosmological constant Λ_k and the scale-dependent Newton constant G_k . It gives us a single-metric expression working as the analog of the EA at the scale k . The corresponding field equation is given by

$$R_{\mu\nu}(\langle g \rangle_k) = \frac{2}{2 - D} \Lambda_k \langle g_{\mu\nu} \rangle_k \quad (7.13)$$

with $\langle g_{\mu\nu} \rangle_k$ denoting the effective metric at the scale k and $R_{\mu\nu}(\langle g \rangle_k)$ as the Ricci tensor corresponding to it. Note that, apart from the k dependencies, these are Einstein's field equations.

In order to finally find the function $F(k^2)$ we are interested in the solution of (7.13) for the effective metric $\langle g_{\mu\nu} \rangle_k$ to find its k dependence. For this goal we introduce the reference scale k_0 mentioned above to rewrite (7.13) as

$$\frac{\Lambda_{k_0}}{\Lambda_k} R_{\nu}^{\mu}(\langle g \rangle_k) = \frac{2}{2 - D} \Lambda_{k_0} \delta^{\mu}_{\nu}. \quad (7.14)$$

Utilising the fact that $R_\nu^\mu(cg) = c^{-1}R_\nu^\mu(g)$ for an arbitrary constant $c > 0$ and comparing the result to (7.13) at the scale k_0 gives us $R_\nu^\mu(\langle g \rangle_{k_0}) = \frac{2}{2-D}\Lambda_{k_0}\delta_\nu^\mu = R_\nu^\mu(\frac{\Lambda_k}{\Lambda_{k_0}}\langle g \rangle_k)$. At the end we find the relation between $\langle g_{\mu\nu} \rangle_k$ and $\langle g_{\mu\nu} \rangle_{k_0}$ reading

$$\langle g_{\mu\nu} \rangle_k = \frac{\Lambda_{k_0}}{\Lambda_k} \langle g_{\mu\nu} \rangle_{k_0}, \quad \langle g^{\mu\nu} \rangle_k = \frac{\Lambda_k}{\Lambda_{k_0}} \langle g^{\mu\nu} \rangle_{k_0}. \quad (7.15)$$

This can be translated into a relation between the Laplace operator at k and the one at k_0 reading

$$\Delta(k) = \frac{\Lambda_k}{\Lambda_{k_0}} \Delta(k_0) \quad \Rightarrow \quad F(k^2) = \frac{\Lambda_k}{\Lambda_{k_0}}. \quad (7.16)$$

Now that we know the explicit form of the function $F(k^2)$ we see that its k dependence is governed by the running of the cosmological constant Λ_k . This of course depends on the RG trajectory we choose to describe the theory. For different RG trajectories we will find different k dependencies of the spectral dimension. Furthermore we learn from (7.16) that the power-law behaviour of $F(k^2)$, which we asked for in (7.11), is not true in general. However, we will stick to this approximation, since it captures the most important information, as we will see below.

Based on the assumption that δ , defined in (7.11) depends on k only weakly, we can solve $F(k^2) = \Lambda_k/\Lambda_{k_0} = k^\delta$ for δ to find

$$\delta(k) = k\partial_k \ln \Lambda_k. \quad (7.17)$$

Inserting this into (7.11), gives us the correct spectral dimension as long as Λ_k and therefore $F(k^2)$ undergoes the supposed power-law scaling. If this is not the case the result for the spectral dimension has to be taken with care. For convenience we introduce the dimensionless cosmological constant $\bar{\Lambda}_k = k^{-2}\Lambda_k$ in order to analyse the trajectories discussed in Section 6.1. Therefore we find

$$\delta(k) = k\partial_k \ln(k^2\bar{\Lambda}_k) = 2 + \frac{1}{\bar{\Lambda}_k} \partial_t \bar{\Lambda}_k \quad (7.18)$$

which gives us the scale-dependent spectral dimension $D_s(k)$ depending on the cosmological constant and the corresponding beta function, via (7.11). If we express the beta function as a function of the coupling constants (see (5.31)) we finally get the spectral dimensions depending on the dimensionless Newton constant and the dimensionless cosmological constant

$$D_s(\bar{G}_k, \bar{\Lambda}_k) = \frac{2D}{4 + \bar{\Lambda}_k^{-1} \partial_t \bar{\Lambda}_k(\bar{G}_k, \bar{\Lambda}_k)}. \quad (7.19)$$

Integrating the beta functions with suitable starting points we find the scale dependence of the coupling constants along the corresponding trajectory. Inserting this into (7.19) we find $D_s(t)$, where t denotes the RG time. As mentioned

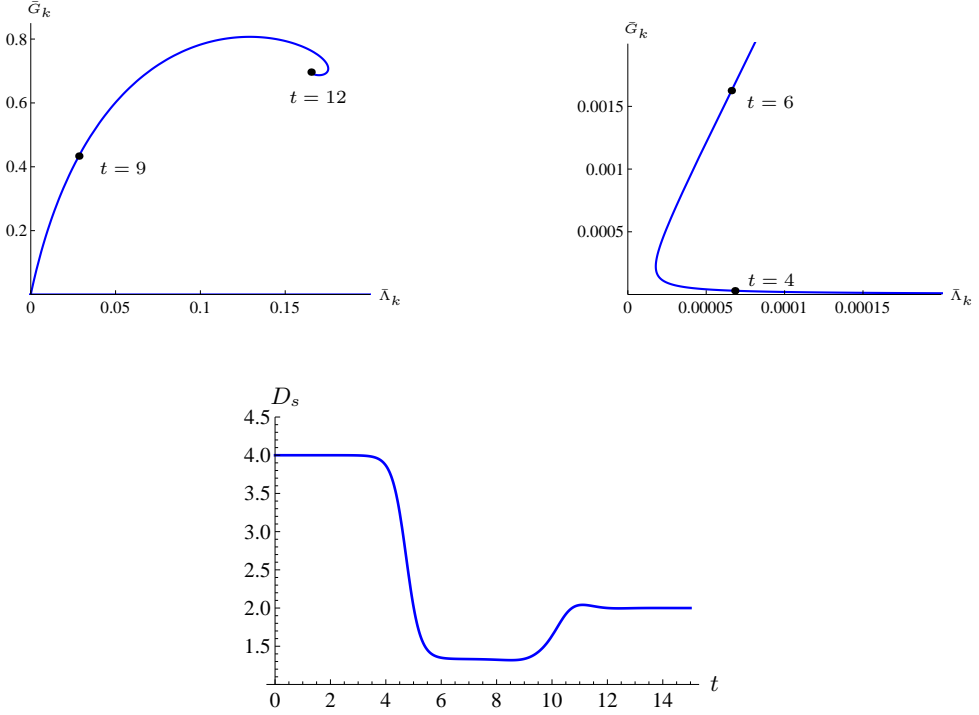


Figure 7.1: A typical Type IIIa trajectory (upper left plot), a zoom into the region close to the GFP (upper right plot) and the spectral dimension corresponding to this trajectory (lower plot).

before, the trajectory describing our world would be of Type IIIa (see Section 6.1) and pass by the Gaussian fixed point very close. Such a trajectory and the corresponding spectral dimension is depicted in Figure 7.1. Explicitly, the trajectory was evaluated with the starting point $(\bar{G}_k, \bar{\Lambda}_k) = (10^{-8}, 0.2)$ at $t = 0$. The latter one was chosen in the IR for technical simplicity. We find three plateaus where D_s is approximately scale-independent. This corresponds to a constant $\delta(k)$ and according to our discussion above these regions are reliable. In contrast to this, the regions of strongly varying D_s should be taken with care. However, we concentrate on the plateaus and ignore the other regions.

Starting in the IR (small t) we see that the spectral dimension agrees with the dimension of the manifold. This regime extends up to $t \approx 4$, which is marked in the upper right plot of Figure 7.1 with a black dot. Thus the trajectory is close to the $\bar{\Lambda}_k$ axis and therefore we are in the classical regime discussed in Section

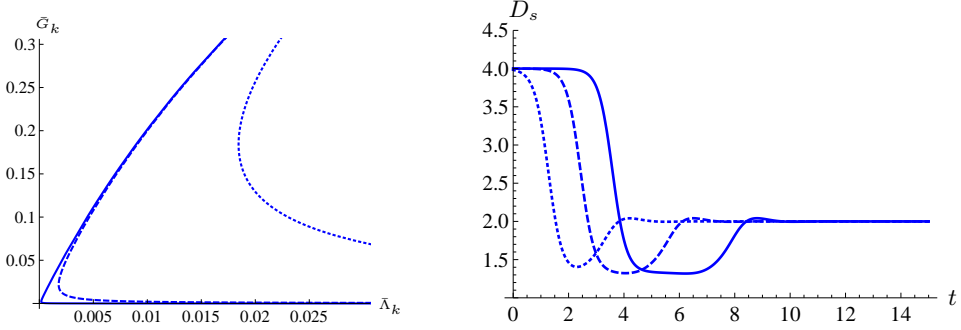


Figure 7.2: Three Type IIIa trajectories (left plot) with different distance to the GFP and the spectral dimension corresponding to them (right plot).

6.1. The result $D_s = 4$ can be understood by inspecting the beta function in this region. We have seen that the dimensionless cosmological constant has a purely dimensional running $\partial_t \bar{\Lambda}_k = -2\bar{\Lambda}_k$. Inserting this into (7.19) results in $D_s = 4$. From a more physical perspective we can argue in the following way. We know that in the classical regime the dimensionful cosmological constant is independent of the scale. Therefore we find $F(k^2) \sim k^0$ in (7.11), which gives us $\delta = 0$ and $D_s = D$. Thus, the result $D_s = D$ is a consequence of the classical behaviour within the Einstein-Hilbert truncation.

In contrast to this classical regime we find $D_s = 2$ in the UV ($t \gtrsim 12$). The point $t = 12$ is marked in the upper left plot of Figure 7.1 with a black dot close to the NGFP. Thus the right plateau corresponds to the NGFP regime, where the dimensionful coupling constants run with their canonical dimension. Therefore $\delta = 2$ holds exactly in (7.11) and is a consequence of the existence of the NGFP, without using any approximations.

The last plateau in the middle extends from $t \gtrsim 6$ up to $t \lesssim 9$, depicted as black dots in the upper left plot of Figure 7.1. This regime shall be called semi-classical and corresponds to the range of the trajectory where it runs along the UV-repulsive eigendirection of the GFP, where $\Lambda_k \sim k^D$. Therefore we find $\delta = D = 4$ and thus $D_s = 4/3$.

To demonstrate that the classical and the semi-classical plateau are related to the GFP and the $\bar{\Lambda}_k$ axis, we can choose other trajectories with the starting value of $\bar{\Lambda}_k = 0.2$ and the starting value for $\bar{G}_k = 10^{-6}, 10^{-4}, 10^{-2}$. The corresponding trajectories close to the GFP are depicted in the left plot of Figure 7.2 as solid, dashed and dotted lines respectively. One can see that the trajectory passing by the GFP very closely produces three very well established plateaus. The dashed trajectory,

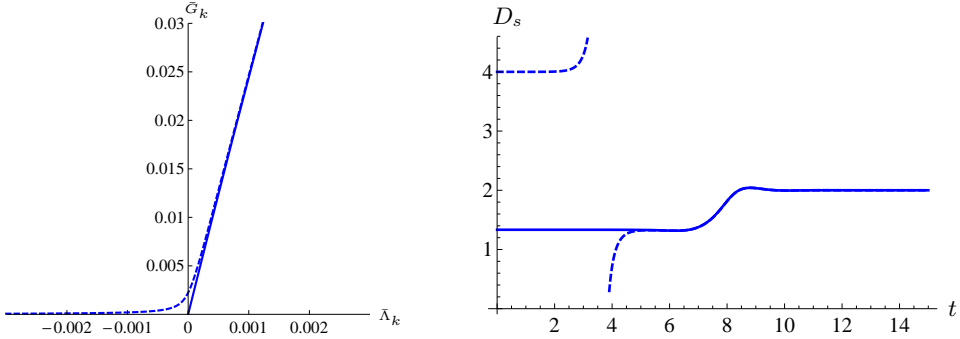


Figure 7.3: The left plot shows the separatrix (solid line) and a Type Ia trajectory (dashed line) passing by close to the GFP. The right plot depicts the spectral dimension corresponding to them.

although showing three distinguished plateaus, has less pronounced classical and semi-classical plateaus. Finally the trajectory passing by the GFP with quite some distance neither shows a classical nor a semi-classical plateau. Note that going to smaller scales, not depicted in the plot, we run into the pole discussed in Section 6.1 before a classical plateau is established.

As a last interesting feature we would like to leave the Type IIIa trajectories and investigate the Type IIa and a Type Ia trajectory. These are depicted in the left plot of Figure 7.3 and the corresponding spectral dimension is given in the right plot. The separatrix connects the NGFP with the GFP and thus it is not surprising that we do not find any classical plateau. Here $\Lambda_k \simeq \Lambda_0 + ak^\delta$ with $\Lambda_0 = 0$ and a constant a . Thus the semi-classical plateau extends to arbitrary small scale t or k , respectively. The Type Ia trajectory shows a NGFP plateau at high energies, since the trajectory runs towards the NGFP. Going to smaller scales, the trajectory passes by the GFP very close and thus develops a semi-classical plateau. However, the trajectory leaves the GFP regime in direction of negative cosmological constant. Therefore, we find a pole in (7.19) and the spectral dimension diverges. However, as we discussed above, the regime of strongly varying D_s is not trustworthy and thus no physical properties should be attributed to this feature. Finally at very small scales the trajectory runs close to the $\bar{\Lambda}_k$ axis and we find $D_s = 4$ again.

7.3 Spectral Dimension within the R^2 Truncation

After discussing the scale-dependent spectral dimension within the simplest truncation in Section 7.2 we now proceed to discuss the influence of higher derivative

terms. Explicitly we will discuss the scale dependence of the spectral dimension within the R^2 truncation. For this purpose we will use the trajectories of Type IIIa discussed in Section 6.2. However, before analysing the spectral dimension along these trajectories we have to find an expression analogous to (7.19), defining the spectral dimension depending on the coupling constants.

Therefore, we start to rewrite the ansatz of the R^2 truncation given in (5.36) at vanishing fluctuations and ghost fields. It reads

$$\Gamma_k^{R^2} \Big|_{g=\bar{g}, c=0} = \int d^D x \sqrt{g} \left[\frac{1}{16\pi G_k} (-R + 2\Lambda_k) + \beta_k R^2 \right]. \quad (7.20)$$

The equations of motion corresponding to this ansatz read

$$\begin{aligned} \left(-R + 2\Lambda_k + \frac{16\pi G_k R^2}{b_k} \right) g^{\mu\nu} + \left(2 - \frac{64\pi G_k R}{b_k} \right) R^{\mu\nu} \\ + \frac{64\pi G_k}{b_k} (\nabla^\mu \nabla^\nu R + (\Delta R) g^{\mu\nu}) = 0 \end{aligned} \quad (7.21)$$

where we integrated by part and dropped appearing surface terms. In order to find the scale dependence of the metric $g_{\mu\nu}$, we solve these equations of motion, for fixed scale k . For this purpose we substitute the ansatz

$$R_{\mu\nu}(\langle g \rangle_k) = \frac{c_k}{D} \langle g_{\mu\nu} \rangle_k, \quad (7.22)$$

implying $R(\langle g \rangle_k) = c_k$, into the equations of motion and find that the second line vanishes. The first line simplifies to

$$2\Lambda_k - \frac{1}{D}(D-2)c_k + \frac{1}{D}(D-4)\frac{16\pi G_k}{b_k}c_k^2 = 0 \quad (7.23)$$

which can be solved for c_k . Note that the ansatz (7.22) is similar to (7.13), so that we can do the same manipulations as in Section 7.2 to find

$$\begin{aligned} \langle g_{\mu\nu} \rangle_k &= \frac{c_{k_0}}{c_k} \langle g_{\mu\nu} \rangle_{k_0}, & \langle g^{\mu\nu} \rangle_k &= \frac{c_k}{c_{k_0}} \langle g^{\mu\nu} \rangle_{k_0} \\ \Rightarrow \Delta(k) &= \frac{c_k}{c_{k_0}} \Delta_{k_0} & \Rightarrow F(k^2) &= \frac{c_k}{c_{k_0}}. \end{aligned} \quad (7.24)$$

This result for $F(k^2)$ is equivalent to (7.16), apart from Λ_k being replaced by c_k , which depends on the coupling constants.

At this point it becomes useful to distinguish the cases $D = 4$ and $D \neq 4$ to discuss them separately. We start with $D = 4$ and find the solution of (7.23) to be

$$c_k|_{D=4} = 4\Lambda_k \quad \Rightarrow \quad F(k^2)|_{D=4} = \frac{\Lambda_k}{\Lambda_{k_0}}. \quad (7.25)$$

Formally, this result seems identical to the one of the Einstein-Hilbert truncation and thus we get the same expression for the scale-dependent spectral dimension

$$D_s(\bar{G}_k, \bar{\Lambda}_k, \bar{b}_k)|_{D=4} = \frac{2D}{4 + \bar{\Lambda}_k^{-1} \partial_t \bar{\Lambda}_k(\bar{G}_k, \bar{\Lambda}_k, \bar{b}_k)}. \quad (7.26)$$

Note that, although we find the same expression for D_s , the final result differs, since the beta function is different.

In $D \neq 4$ the situation is a bit more complicated. Here the quadratic equation (7.23) has the two solutions

$$c_k^\pm = \frac{(D-2)b_k}{32\pi(D-4)G-k} \left(1 \pm \sqrt{1 - \frac{h_D G_k \Lambda_k}{b_k}} \right) \quad (7.27)$$

with

$$h_D = \frac{128\pi D(D-4)}{(D-2)^2}. \quad (7.28)$$

In the following we discard the solution c_k^+ and concentrate on c_k^- . The reason is that the solution c_k^- has a well defined limit $D \rightarrow 4$ where it reduces to (7.25). Therefore, selecting the c_k^- branch leads to a definition of the spectral dimension continuous in D . The latter one can be derived by inserting (7.27) into (7.24) to find

$$F(k^2) = \frac{G_{k_0} b_k}{G_k b_{k_0}} \frac{1 - \sqrt{1 - h_D G_k \Lambda_k / b_k}}{1 - \sqrt{1 - h_D G_{k_0} \Lambda_{k_0} / b_{k_0}}}. \quad (7.29)$$

Using $\delta(k) = \partial_t \ln(F(k^2))$ we find

$$\delta = 2 - \frac{\partial_t \bar{G}_k}{\bar{G}_k} + \frac{\partial_t \bar{b}_k}{\bar{b}_k} + \frac{\frac{h_D}{2} \left(\frac{\bar{G}_k}{\bar{b}_k} \partial_t \bar{\Lambda}_k - \frac{\bar{G}_k \bar{\Lambda}_k}{\bar{b}_k^2} \partial_t \bar{b}_k + \frac{\bar{\Lambda}_k}{\bar{b}_k} \partial_t \bar{G}_k \right)}{\left(1 - \sqrt{1 - h_D \bar{G}_k \bar{\Lambda}_k / \bar{b}_k} \right) \sqrt{1 - h_D \bar{G}_k \bar{\Lambda}_k / \bar{b}_k}}. \quad (7.30)$$

This is the final expression for δ and depends on the dimensionless coupling constants. Thus the former attributes a value for the spectral dimension, via (7.11), to any point in theory space.

Now we can use the expressions for the spectral dimension depending on the coupling constants in $D = 4$ and $D = 3$ to evaluate the scale dependent spectral dimension along specific trajectories. Starting with $D = 4$ we will use the trajectories A and B depicted as thick black lines in Figure 6.8. The spectral dimension depending on the logarithmic RG scale t and corresponding to these Type IIIa trajectories are depicted in Figure 7.4. The left plot depicts the spectral dimension of trajectory A in Figure 6.6. At high energies the trajectory starts at the NGFP $^{4D\epsilon}$ where we find $D_s = 2$. This is exactly the result of the Einstein-Hilbert truncation. The same statement is true for low energies, where we find a classical regime with $D_s = D = 4$. The spectral dimension associated with the semi-classical plateau differs from the one in Section 7.2, however. Although this plateau appears again between the GFP and the NGFP the corresponding value for D_s differs from the one observed in Section 7.2. Within the Einstein-Hilbert truncation we found $D_s = 4/3$ while the inclusion of R^2 leads to $D_s \simeq 1.5$. The difference is that this

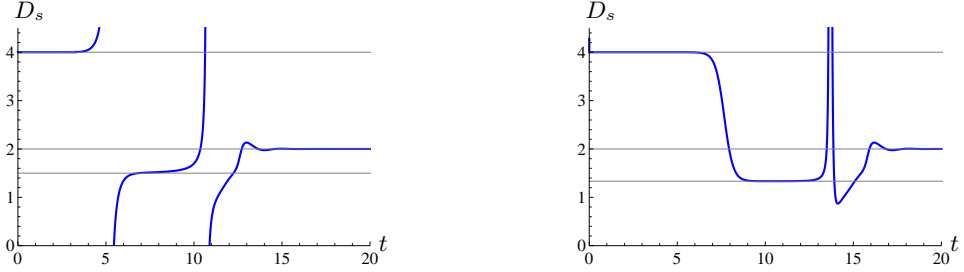


Figure 7.4: The spectral dimension corresponding to the trajectories A (left plot) and B (right plot) of Figure 6.8.

time the scaling behaviour k^δ with $\delta \simeq 3.3$ is not caused by the GFP but by the pole of the beta functions discussed extensively in Section 6.2. Between the NGFP and the GFP the trajectory A passes by very closely to this pole which leads to the formation of the semi-classical plateau.

The second plot in Figure 7.4 depicts the spectral dimension corresponding to trajectory B in Figure 6.8. Again we find a NGFP plateau with $D_s = 2$ at high energies and a classical plateau with $D_s = 4$ at low energies. This time the semi-classical plateau develops at $D_s = 4/3$ which is the value we found within the Einstein-Hilbert truncation. This indicates that the plateau is caused by the GFP and not by the pole as for trajectory A. Indeed, if we investigate the part of the trajectory where the intermediate plateau develops we find that this does not happen between the NGFP and the GFP. Here the situation is as follows. If we start at high energies close to the NGFP and flow towards the IR, the trajectory does not spend enough RG time in the vicinity of the pole to form a plateau. Right

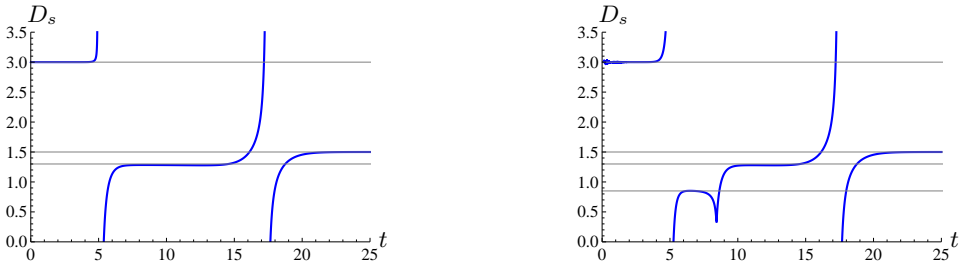


Figure 7.5: The spectral dimension corresponding to the trajectories A (left plot) and B (right plot) of Figure 6.6.

after passing by the GFP the semi-classical plateau depicted in the right plot of Figure 7.4 develops. In this region the GFP causes a k^4 scaling and we find the spectral dimension $D_s = 4/3$.

For completeness, we shall discuss the situation in three spacetime dimensions as well. The plots in Figure 7.5 show the scale-dependent spectral dimension corresponding to the trajectories A and B in Figure 6.6. The former is depicted in the left plot and shows three distinguished plateaus. In the UV we find the NGFP plateau corresponding to the scaling behaviour close to the NGFP₁^{3D}, which realises $D_s = D/2 = 1.5$. In the IR we find the classical plateau with $D_s = D = 3$ caused by a classical running of the couplings. The intermediate plateau develops at $D_s \simeq 1.3$. As in $D = 4$ this is caused by the trajectory running close to the pole.

The right plot in Figure 7.5 corresponds to trajectory B in Figure 6.6. It shows four distinguished plateaus where the very left is the classical one with $D_s = 3$ and the very right one is the NGFP plateau with $D_s = 1.5$. In between we find two semi-classical plateaus which are caused by the pole ($D_s \simeq 1.3$) and by the GFP ($D_s \simeq 0.85$) respectively.

Part III

Foliated Gravity

This part of the thesis is based on the publications
”Asymptotically Safe Lorentzian Gravity”,
by Elisa Manrique, Stefan Rechenberger and Frank Saueressig,
Phys.Rev.Lett., 106:251302, 2011,
”A functional renormalization group equation for foliated spacetimes”,
by Stefan Rechenberger and Frank Saueressig,
JHEP, 1303:010, 2013
and
”Renormalization group flows of Hořava-Lifshitz gravity at low
energies”,
by Adriano Contillo, Stefan Rechenberger and Frank Saueressig,
to appear.

Motivation

8.1 Field Content and Symmetry

In Part II of this thesis we discussed QEG within the metric formulation. This means we started from a path integral where we integrated over the spacetime metric $\tilde{g}_{\mu\nu}$ as the degrees of freedom describing the theory. The classical theory might be described by the Einstein-Hilbert action

$$S^{\text{EH}}[\tilde{g}_{\mu\nu}] = \frac{1}{16\pi G_{\text{N}}} \int d^D x \sqrt{\tilde{g}} \left({}^{(D)}R - 2\Lambda \right) \quad (8.1)$$

with the Ricci scalar in D dimensions ${}^{(D)}R$, the cosmological constant Λ and the Newton constant G_{N} . \tilde{g} denotes the determinant of the metric.

At the classical level, however, the gravitational degrees of freedom can be encoded in a different set of fields, without affecting the dynamics of the theory. A very well known example is the tetrad formulation where the metric is replaced with the vielbeins \tilde{e}_μ^a , by $\tilde{g}_{\mu\nu} = \eta_{ab} \tilde{e}_\mu^a \tilde{e}_\nu^b$. In this case the integration in the path integral would be over the vielbein fields instead of the metric. Other examples are unimodular gravity or the Arnowitt-Deser-Misner (ADM) decomposed version of GR. Within this part of the thesis we discuss the latter one, see [167–169]. Note that, even though the formulation of gravity in terms of different variables are classically equivalent, the same is not necessarily true at the quantum level. The rest of this chapter discusses the field content and the symmetry on the classical level. The quantisation is discussed in the following chapters.

The ADM decomposed formulation of gravity encodes the degrees of freedom in the lapse function \tilde{N} , the shift vector \tilde{N}^i and the spatial metric $\tilde{\sigma}_{ij}$. The relation between the metric formulation and this foliated version is given by the ADM decomposition, explained in detail in Appendix E. The final result of the appendix

is an expression for $\tilde{g}_{\mu\nu}$ in terms of \tilde{N} , \tilde{N}^i , $\tilde{\sigma}_{ij}$ (see (E.5)) and reads

$$\tilde{g}_{\mu\nu} = \begin{pmatrix} \varepsilon\tilde{N}^2 + \tilde{N}_i\tilde{N}^i & \tilde{N}_j \\ \tilde{N}_i & \tilde{\sigma}_{ij} \end{pmatrix}, \quad \tilde{g}^{\mu\nu} = \begin{pmatrix} \frac{1}{\varepsilon\tilde{N}^2} & -\frac{\tilde{N}^j}{\varepsilon\tilde{N}^2} \\ -\frac{\tilde{N}^i}{\varepsilon\tilde{N}^2} & \tilde{\sigma}^{ij} + \frac{\tilde{N}^i\tilde{N}^j}{\varepsilon\tilde{N}^2} \end{pmatrix}. \quad (8.2)$$

Here and in the following we denote spacetime indices with Greek symbols μ, ν, \dots and spatial indices on the slices of constant time τ are denoted by Latin labels i, j, \dots . The latter ones are raised and lowered with the spatial metric on the slices $\tilde{\sigma}_{ij}$. Therefore a spacetime vector v^μ reads, in the foliated notation, $v^\mu = (v^0, v^i)$. Note that the symbol ε , appearing in (8.2), is a signature parameter which distinguishes Euclidean ($\varepsilon = +1$) from Lorentzian ($\varepsilon = -1$) signature as explained in Appendix A.

The next question arising naturally would be: What does the classical action (8.1) look like when using the new variables? Since investigations of higher order truncations within the foliated formulation is above the scope of this thesis, it suffices to consider the classical Einstein-Hilbert action given in (8.1). First of all we encounter the square root of the determinant of the spacetime metric $\sqrt{\tilde{g}}$. Taking into account the parameter ε to define the signature we get

$$\sqrt{\tilde{g}} = \sqrt{\varepsilon}\tilde{N}\sqrt{\tilde{\sigma}}. \quad (8.3)$$

The second object depending on the spacetime metric is the D -dimensional scalar curvature ${}^{(D)}R$. The transformation to the new variables is not complicated but lengthy and thus we refrain from giving the detailed calculation here. The interested reader might find a detailed discussion in [170]. We just give the result in terms of the extrinsic curvature K_{ij} of the spatial slices

$$K_{ij} = \frac{1}{2\tilde{N}} \left(\partial_\tau \tilde{\sigma}_{ij} - \nabla_i \tilde{N}_j - \nabla_j \tilde{N}_i \right). \quad (8.4)$$

Here we denote the covariant derivative in d dimensions, constructed from the spatial metric $\tilde{\sigma}_{ij}$, as ∇_i . Introducing furthermore the d -dimensional scalar curvature ${}^{(d)}R$ leads us to the following decomposition of the D -dimensional Ricci scalar

$${}^{(D)}R = {}^{(d)}R - \frac{1}{\varepsilon} (K^{ij}K_{ij} - K^2). \quad (8.5)$$

This, in turn, leads us to the foliated formulation of the Einstein-Hilbert action (8.1), reading

$$S^{\text{fEH}} = \frac{\sqrt{\varepsilon}}{16\pi G_{\text{N}}} \int d^D x \sqrt{\tilde{\sigma}} \tilde{N} \left({}^{(d)}R - 2\Lambda - \frac{1}{\varepsilon} (K^{ij}K_{ij} - K^2) \right). \quad (8.6)$$

Here $K = \tilde{\sigma}^{ij}K_{ij}$ denotes the trace of the extrinsic curvature. Note that the three terms ${}^{(d)}R$, $K^{ij}K_{ij}$ and K^2 have to appear with the ratio of (8.5) to satisfy D -dimensional diffeomorphism invariance. As these symmetries will play a crucial role later on, it is worthwhile to discuss them in detail.

Classical GR, based on the Einstein-Hilbert action (8.1), is invariant with respect to spacetime diffeomorphisms $\text{Diff}(\mathcal{M})$, where \mathcal{M} denotes the spacetime manifold. Therefore, we ask the action within the metric formulation, (8.1), to be invariant under

$$\tilde{g}_{\mu\nu} \rightarrow \tilde{g}_{\mu\nu} + \delta\tilde{g}_{\mu\nu}, \quad \delta\tilde{g}_{\mu\nu} = \mathcal{L}_v \tilde{g}_{\mu\nu}. \quad (8.7)$$

Here \mathcal{L}_v denotes the Lie derivative with respect to the D -dimensional vector $v(x^\mu)$. To reformulate this in foliated terms we have to split the vector v into its components perpendicular and tangential to the spatial slices as

$$v^\mu(x^\mu) = (f(\tau, x^i), \zeta^i(\tau, x^i)), \quad f = t^\mu v_\mu, \quad \zeta^i = e^i_\mu v^\mu. \quad (8.8)$$

The definition of t^μ and e^i_μ , which are introduced in Appendix E, can be found in (E.1). Now we can insert (8.2) and (8.8) into (8.7) to get the variation of the lapse function \tilde{N} , the shift vector \tilde{N}^i and the spatial metric $\tilde{\sigma}_{ij}$ under $\text{Diff}(\mathcal{M})$. For completeness we give the variations of \tilde{N}_i and $\tilde{\sigma}^{ij}$ as well. The variations read

$$\begin{aligned} \delta\tilde{N} &= \partial_\tau(f\tilde{N}) + \zeta^k \partial_k \tilde{N} - \tilde{N} \tilde{N}^j \partial_j f, \\ \delta\tilde{N}^i &= \partial_\tau(f\tilde{N}^i) + \zeta^k \partial_k \tilde{N}^i - \tilde{N}^k \partial_k \zeta^i + \partial_\tau \zeta^i + \tilde{N}^i \tilde{N}^k \partial_k f + \varepsilon \tilde{N}^2 \tilde{\sigma}^{ik} \partial_k f, \\ \delta\tilde{N}_i &= \partial_\tau(f\tilde{N}_i) + \zeta^k \partial_k \tilde{N}_i + \tilde{N}_k \partial_i \zeta^k + \tilde{\sigma}_{ki} \partial_\tau \zeta^k + \tilde{N}_k \tilde{N}^k \partial_i f + \varepsilon \tilde{N}^2 \partial_i f, \\ \delta\tilde{\sigma}_{ij} &= f \partial_\tau \tilde{\sigma}_{ij} + \zeta^k \partial_k \tilde{\sigma}_{ij} + \tilde{\sigma}_{jk} \partial_i \zeta^k + \tilde{\sigma}_{ik} \partial_j \zeta^k + \tilde{N}_j \partial_i f + \tilde{N}_i \partial_j f, \\ \delta\tilde{\sigma}^{ij} &= f \partial_\tau \tilde{\sigma}^{ij} + \zeta^k \partial_k \tilde{\sigma}^{ij} - \tilde{\sigma}^{jk} \partial_k \zeta^i - \tilde{\sigma}^{ik} \partial_k \zeta^j - \tilde{\sigma}^{ik} \tilde{N}^j \partial_k f - \tilde{\sigma}^{jk} \tilde{N}^i \partial_k f. \end{aligned} \quad (8.9)$$

This variation acting on ${}^{(d)}R$, $K^{ij}K_{ij}$ and K^2 separately shows that it vanishes only if one combines them with the prefactors given in (8.5).

There are two important observations to make. Firstly, while $\text{Diff}(\mathcal{M})$ acts linearly on the spacetime metric $\tilde{g}_{\mu\nu}$ the action on the component fields \tilde{N} , \tilde{N}^i and $\tilde{\sigma}_{ij}$ is non linear. Secondly, the gauge freedom in (8.9) can be fixed with the proper-time gauge choice [171]

$$\tilde{N}(\tau, x^i) = 1, \quad \tilde{N}^i(\tau, x^i) = 0. \quad (8.10)$$

The residual freedom is a coordinate transformation satisfying $\partial_\tau f = 0$ and $\partial_\tau \zeta^i + \varepsilon \tilde{\sigma}^{ij} \partial_j f = 0$. This corresponds to the freedom of choosing a coordinate system on the initial slice of the foliation. At the level of the path integral this is fixed by the boundary conditions. The interested reader might find more details in [172, 173]. Possible surface effects are beyond the scope of this thesis and thus we do not consider this leftover freedom any further.

8.2 An Excursion to Hořava-Lifshitz Gravity

It is very well known that GR is perturbatively non-renormalisable, neither in the metric nor in the foliated formulation. Thus Hořava proposed a theory, called

Horava-Lifshitz Gravity (HLG), which uses foliation-preserving diffeomorphisms $\text{Diff}(\mathcal{M}, \Sigma)$, instead of $\text{Diff}(\mathcal{M})$, as the fundamental symmetry. Weakening the symmetry requirements makes it possible to include higher spatial derivatives without adding higher time derivatives and thus might render the theory perturbatively renormalisable. For the perturbative renormalisability one has to pay the price of a relaxation of the symmetry constraints. However, on observational scales we know that the world is invariant under $\text{Diff}(\mathcal{M})$. This can be matched by assuming that the fundamental symmetry is $\text{Diff}(\mathcal{M}, \Sigma)$ and the RG running reestablishes the diffeomorphism invariance at observational scales dynamically. This, in short, is the idea of HLG and the interested reader finds more details in [15, 16].

As it will play a crucial role in the following, we next discuss the foliation-preserving diffeomorphisms. The difference between $\text{Diff}(\mathcal{M})$ and $\text{Diff}(\mathcal{M}, \Sigma)$ is that, for the latter, the function f in (8.8) does not depend on space but is a function of time τ only. Since \tilde{N} and \tilde{N}^i can be interpreted as gauge fields of $\text{Diff}(\mathcal{M}, \Sigma)$ their dependencies should correspond to those of the generators f, ζ^i . Thus the lapse function as well should be space independent. This interpretation is called the projectable version of HLG. Another possibility would be to insist on the spacetime dependence of the lapse function. This would lead to the so-called non-projectable version of HLG. A comparison of these two cases to yet another version with non-relativistic general covariance can be found in [174].

In the following we will focus on the projectable version of HLG. In this case the variation of the component fields under $\text{Diff}(\mathcal{M}, \Sigma)$ results from (8.9) by asking f and \tilde{N} to be space-independent. It reads

$$\begin{aligned}
\delta\tilde{N} &= \partial_\tau(f\tilde{N}), \\
\delta\tilde{N}^i &= \partial_\tau(f\tilde{N}^i) + \zeta^k\partial_k\tilde{N}^i - \tilde{N}^k\partial_k\zeta^i + \partial_\tau\zeta^i, \\
\delta\tilde{N}_i &= \partial_\tau(f\tilde{N}_i) + \zeta^k\partial_k\tilde{N}_i + \tilde{N}_k\partial_i\zeta^k + \tilde{\sigma}_{ik}\partial_\tau\zeta^k, \\
\delta\tilde{\sigma}_{ij} &= f\partial_\tau\tilde{\sigma}_{ij} + \zeta^k\partial_k\tilde{\sigma}_{ij} + \tilde{\sigma}_{jk}\partial_i\zeta^k + \tilde{\sigma}_{ik}\partial_j\zeta^k, \\
\delta\tilde{\sigma}^{ij} &= f\partial_\tau\tilde{\sigma}^{ij} + \zeta^k\partial_k\tilde{\sigma}^{ij} - \tilde{\sigma}^{jk}\partial_k\zeta^i - \tilde{\sigma}^{ik}\partial_k\zeta^j.
\end{aligned} \tag{8.11}$$

Important to notice is that, under $\text{Diff}(\mathcal{M}, \Sigma)$, the variation acts linearly on the component fields. This observation makes the foliation-preserving diffeomorphism the natural symmetry for the Wetterich equation formulated for the component fields \tilde{N}, \tilde{N}^i and $\tilde{\sigma}_{ij}$. This will be explained in more detail later on. While gauge fixing with the proper-time gauge (8.10) the residual transformations $\partial_\tau f = 0$ and $\partial_\tau\zeta^i = 0$ are left. Again, this corresponds to the coordinate choice on the initial slice.

Now let us come back to the decomposition of the Einstein-Hilbert action (8.1). We have seen that the invariance under $\text{Diff}(\mathcal{M})$ requires the ratios in (8.5) between the d -dimensional Ricci scalar ${}^{(d)}R$ and the extrinsic curvature terms $K^{ij}K_{ij}$ and K^2 . However, if we consider the $\text{Diff}(\mathcal{M}, \Sigma)$ variations in (8.11) we realise that all

theory	theory space	gravitational fields	symmetry
mQEG	$\mathcal{T}^{\text{mQEG}}$	$\tilde{g}_{\mu\nu}(x^\mu)$	$\text{Diff}(\mathcal{M})$
fQEG	$\mathcal{T}^{\text{fQEG}}$	$\tilde{N}(\tau, x^i), \tilde{N}_i(\tau, x^i), \tilde{\sigma}_{ij}(\tau, x^i)$	$\text{Diff}(\mathcal{M})$
pHL	\mathcal{T}^{pHL}	$\tilde{N}(\tau), \tilde{N}_i(\tau, x^i), \tilde{\sigma}_{ij}(\tau, x^i)$	$\text{Diff}(\mathcal{M}, \Sigma)$
npHL	$\mathcal{T}^{\text{npHL}}$	$\tilde{N}(\tau, x^i), \tilde{N}_i(\tau, x^i), \tilde{\sigma}_{ij}(\tau, x^i)$	$\text{Diff}(\mathcal{M}, \Sigma)$

Table 8.1: Definition of the gravitational theory spaces \mathcal{T} corresponding to the metric (mQEG) and the foliated (fQEG) formulation of QEG and the projectable (pHL) and non-projectable (npHL) version of HLG. According to their precise field content and underlying symmetry group the latter constitute natural generalisations of the theory space underlying metric QEG.

three terms are invariant on their own. Thus relaxing the symmetry from $\text{Diff}(\mathcal{M})$ to $\text{Diff}(\mathcal{M}, \Sigma)$ allows us to take independent coupling constants in front of each invariant term. The generalisation of the Einstein-Hilbert action therefore reads

$$S^{\text{HL}} = \frac{\sqrt{\varepsilon}}{16\pi G_{\text{N}}} \int d^D x \sqrt{\tilde{\sigma}} \tilde{N} \left[{}^{(d)}R - 2\Lambda - \frac{1}{\varepsilon} (\lambda_1 K^{ij} K_{ij} - \lambda_2 K^2) \right]. \quad (8.12)$$

For $\lambda_1 = \lambda_2 = 1$ this action becomes S^{fEH} and is invariant under D -dimensional diffeomorphisms. Different values for λ_1 or λ_2 break this symmetry. As higher derivative terms are negligible in the IR, the action (8.12) constitutes a natural low-energy limit of HLG. Therefore it shall be called Hořava-Lifshitz action in the following. Note that, in [15, 16], the second part of this action, constructed out of the extrinsic curvature, was introduced as the most general kinetic term according to the generalised Wheeler-DeWitt metric. The other two terms would correspond to the potential in [15, 16].

Recalling that the lapse function \tilde{N} is just a gauge degree of freedom, we can rescale it and thus arrange the ratio between the d -dimensional Ricci scalar and the purely spatial extrinsic-curvature terms at our will. Thus we are left with only one additional coupling constant, which might be $\lambda = \lambda_2$ as in [15, 16]. Note that at a quantum level this argument is not true any more. More explicitly, it is possible to arrange the ratio at a single scale. However, the potentially different beta functions for the couplings λ_1 and λ_2 lead to a scale-dependent ratio between them.

Summarising this chapter, the Hořava-Lifshitz action (8.12) enables us to study $\text{Diff}(\mathcal{M})$ -invariant foliated Quantum Einstein Gravity (fQEG) by using $\lambda_1 = \lambda_2 = 1$. Its beta functions are derived in Chapter 10 and analysed in Section 11.1. Here we concentrate on the comparison of Euclidean and Lorentzian signature, see

[167, 168]. Furthermore, we are enabled to analyse $\text{Diff}(M, \Sigma)$ -invariant projectable HLG by using λ_1 and λ_2 arbitrary. In the next chapter we derive the corresponding beta functions. Note that the beta functions of fQEG arises as the limit $\lambda_1, \lambda_2 \rightarrow 1$ of the beta functions for projectable HLG. Here we restrict ourselves to one new coupling, $\lambda = \lambda_2$, and use $\lambda_1 = 1$ for technical simplicity. This new coupling breaks $\text{Diff}(\mathcal{M})$ invariance and thus enables us to investigate the breaking of $\text{Diff}(\mathcal{M})$ invariance for the low-energy limit of HLG. This is done in Section 11.2. In order to analyse the perturbative renormalisability of HLG one has to introduce higher powers of the d -dimensional Ricci scalar, constituting a further source of $\text{Diff}(\mathcal{M})$ breaking. However, this natural extension is beyond the scope of this thesis and shall be left for future work. The different theories are summarised in Table 8.1. This table opposes the metric formulation of QEG with its foliated formulation and the projectable and non-projectable version of HLG. Explicitly, the field content and symmetry corresponding to the different theories are contrasted. Moreover, the second row in Table 8.1 denotes the space of all action functionals invariant under the symmetry under consideration. The field content and the symmetry lead us to the following relation between these theory spaces

$$\mathcal{T}^{\text{mQEG}} = \mathcal{T}^{\text{fQEG}} \subset \mathcal{T}^{\text{pHL}} \subset \mathcal{T}^{\text{npHL}} . \quad (8.13)$$

In Part II of this thesis we discussed two truncations of the $\mathcal{T}^{\text{mQEG}}$, while the present part concentrates on the simplest truncation of $\mathcal{T}^{\text{fQEG}}$ and \mathcal{T}^{pHL} .

The Wetterich Equation for Foliated Spacetimes

Motivated by Hořava's idea, discussed in Section 8.2, we are interested in a theory which encodes the gravitational degrees of freedom in the lapse function \tilde{N} , the shift vector \tilde{N}^i and the spatial metric $\tilde{\sigma}_{ij}$. As the underlying symmetry group we choose foliation-preserving diffeomorphisms, $\text{Diff}(\mathcal{M}, \Sigma)$. This data defines the theory space of projectable HLG. In this chapter we construct the Wetterich equation capturing the RG flow on this space. Based on this novel flow equation we will derive the beta functions of the foliated Einstein-Hilbert truncation and a truncation governing the IR behaviour of HLG in Chapter 10.

Analogous to the metric construction we start from the partition function given by a gravitational path integral in terms of the ADM variables as

$$Z = \int \mathcal{D}\mu e^{-S^{\text{grav}} + S^{\text{source}}}. \quad (9.1)$$

Here S^{source} denotes the source terms corresponding to the decomposed fields and the measure $\mathcal{D}\mu$ denotes a functional integration with respect to the latter as well as a gauge fixing with the corresponding ghost contribution according to Appendix B.1. These are necessary to prevent the integration over gauge-equivalent field configurations. Moreover, S^{grav} denotes a generic $\text{Diff}(\mathcal{M}, \Sigma)$ -invariant gravitational action constructed from the component fields \tilde{N} , \tilde{N}^i and $\tilde{\sigma}_{ij}$. This class of actions is larger than in the metric case, as we are considering $\text{Diff}(\mathcal{M}, \Sigma)$ instead of $\text{Diff}(\mathcal{M})$. To preserve this symmetry on the quantum level we use the background field method described in Appendix B.2. This enables us to handle the symmetry during the RG flow and finally get an invariant effective action.

The first step of the background field method splits the quantum fields into fixed

but arbitrary background plus fluctuations around the latter. This split reads

$$\begin{aligned}\tilde{N}(\tau) &= \bar{N}(\tau) + \hat{N}(\tau), \\ \tilde{N}^i(\tau, x^i) &= \bar{N}^i(\tau, x^i) + \hat{N}^i(\tau, x^i), \\ \tilde{\sigma}_{ij}(\tau, x^i) &= \bar{\sigma}_{ij}(\tau, x^i) + \hat{\sigma}_{ij}(\tau, x^i).\end{aligned}\tag{9.2}$$

Collecting the fields in multiplets $\tilde{\chi} = \{\tilde{N}, \tilde{N}^i, \tilde{\sigma}_{ij}\}$, $\bar{\chi} = \{\bar{N}, \bar{N}^i, \bar{\sigma}_{ij}\}$ and $\hat{\chi} = \{\hat{N}, \hat{N}^i, \hat{\sigma}_{ij}\}$, these expressions can collectively be written as $\tilde{\chi} = \bar{\chi} + \hat{\chi}$. Here the fluctuations $\hat{\chi}$ are not assumed to be small in any sense. Note that we used a linear split in \tilde{N}^i and not \tilde{N}_i . As the indices are raised and lowered with $\bar{\sigma}_{ij}$ we get a non-trivial split in \tilde{N}_i and $\tilde{\sigma}^{ij}$.

According to Appendix B.2 the underlying symmetry variation δ can be split in two different ways. The first is called the quantum gauge transformation $\hat{\delta}$ and reads

$$\begin{aligned}\hat{\delta}\bar{N} &= 0, & \hat{\delta}\hat{N} &= \partial_\tau (f\tilde{N}), \\ \hat{\delta}\bar{N}^i &= 0, & \hat{\delta}\hat{N}^i &= \partial_\tau (f\tilde{N}^i) + \partial_t \zeta^i + \mathcal{L}_\zeta(\tilde{N}^i), \\ \hat{\delta}\bar{\sigma}_{ij} &= 0, & \hat{\delta}\hat{\sigma}_{ij} &= f\partial_\tau \tilde{\sigma}_{ij} + \mathcal{L}_\zeta(\tilde{\sigma}_{ij}).\end{aligned}\tag{9.3}$$

This is the symmetry to be fixed. Secondly we can introduce the background gauge transformation $\bar{\delta}$ as

$$\begin{aligned}\bar{\delta}\bar{N} &= \partial_\tau (f\bar{N}), & \bar{\delta}\hat{N} &= \partial_\tau (f\hat{N}), \\ \bar{\delta}\bar{N}^i &= \partial_\tau (f\bar{N}^i) + \partial_\tau \zeta^i + \mathcal{L}_\zeta(\bar{N}^i), & \bar{\delta}\hat{N}^i &= \partial_\tau (f\hat{N}^i) + \mathcal{L}_\zeta(\hat{N}^i), \\ \bar{\delta}\bar{\sigma}_{ij} &= f\partial_\tau \bar{\sigma}_{ij} + \mathcal{L}_\zeta(\bar{\sigma}_{ij}), & \bar{\delta}\hat{\sigma}_{ij} &= f\partial_\tau \hat{\sigma}_{ij} + \mathcal{L}_\zeta(\hat{\sigma}_{ij}),\end{aligned}\tag{9.4}$$

with the spatial Lie derivative with respect to ζ^i denoted by \mathcal{L}_ζ . This background gauge transformation is merely a technical tool. As explained in Appendix B.2 we demand the invariance under these transformations during the calculations and gain back the invariance with respect to the underlying symmetry at the end by setting the fluctuations to zero.

The next step consist of gauge fixing the quantum symmetry by introducing an appropriate gauge fixing and ghost term (see Appendix B.1 for more details). The gauge-fixing action should implement the background proper-time gauge $\hat{N}/\bar{N} = 0$, $\hat{N}^i/\bar{N} = 0$ and preserve the background symmetry. This can be achieved by

$$S^{\text{gf}} = \frac{1}{2}\sqrt{\varepsilon} \int d^D x \bar{N} \sqrt{\bar{\sigma}} \left[\frac{\hat{N}^2}{\alpha_L \bar{N}^2} + \frac{\hat{N}^i \bar{\sigma}_{ij} \hat{N}^j}{\alpha_S \bar{N}^2} \right].\tag{9.5}$$

The corresponding ghost action can be derived by calculating the quantum gauge transformation of the gauge condition and replacing the parameters f, ζ^i by the ghost fields ω, ω^i . The result has to be contracted with the corresponding anti-ghosts and an integration gives

$$S^{\text{gh}} = \sqrt{\varepsilon} \int d^D x \sqrt{\bar{\sigma}} \left[\bar{\omega} \partial_\tau (\tilde{N} \omega) + \bar{\omega}_i (\delta_j^i \partial_\tau - \delta_j^i \tilde{N}^k \partial_k + (\partial_j \tilde{N}^i)) \omega^j \right]. \quad (9.6)$$

The variation of the ghost fields under background transformations has to be chosen such that this ghost action is invariant. A straightforward calculation reveals that this might be achieved by using

$$\begin{aligned} \bar{\delta} \omega &= f \partial_\tau \omega - \omega \partial_\tau f, & \bar{\delta} \bar{\omega} &= f \partial_\tau \bar{\omega}, \\ \bar{\delta} \omega^j &= f \partial_\tau \omega^j + \mathcal{L}_\zeta(\omega^j), & \bar{\delta} \bar{\omega}_i &= f \partial_\tau \bar{\omega}_i + \mathcal{L}_\zeta(\bar{\omega}_i). \end{aligned} \quad (9.7)$$

Summarising these findings, the gauge-fixed partition function includes, besides the gravitational action itself, the gauge-fixing action (9.5), the ghost action (9.6) and the sources. It reads

$$Z = \int \mathcal{D}\hat{\chi} \mathcal{D}\bar{\omega} \mathcal{D}\omega \mathcal{D}\bar{\omega}_i \mathcal{D}\omega^i \exp[-S^{\text{grav}} - S^{\text{gf}} - S^{\text{gh}} + S^{\text{source}}]. \quad (9.8)$$

Here $\mathcal{D}\hat{\chi}$ denotes the integration over the lapse function, shift vector and spatial metric. The source term now includes sources for the ghosts, $\bar{\eta}, \eta, \bar{\eta}_i, \eta^i$, and reads

$$S^{\text{source}} = \sqrt{\varepsilon} \int d^D x \sqrt{\bar{\sigma}} \bar{N} (t \tilde{N} + t_i \tilde{N}^i + t^{ij} \tilde{\sigma}_{ij} + \bar{\eta} \omega + \bar{\omega} \eta + \bar{\eta}_i \omega^i + \bar{\omega}_i \eta^i). \quad (9.9)$$

Note that the invariance of the source term under background transformations can be achieved by choosing suitable variations for the sources. We refrain from giving them here explicitly, since they will not play an essential role in the following.

To get a scale-dependent partition function we insert a regulator term $-\Delta S_k$ into the exponent as explained in Chapter 2. First of all it should be quadratic in the fluctuation fields to allow for practical computations. For convenience we separate the gravitational field content from the ghosts by writing

$$\begin{aligned} \Delta S_k &= \frac{\sqrt{\varepsilon}}{2} \int d^D x \bar{N} \sqrt{\bar{\sigma}} \hat{\chi} \mathcal{R}_k^{\text{grav}}[\bar{\chi}] \hat{\chi} \\ &\quad + \sqrt{\varepsilon} \int d^D x \bar{N} \sqrt{\bar{\sigma}} (\bar{\omega}, \bar{\omega}_i) \mathcal{R}_k^{\text{gh}}[\bar{\chi}] (\omega, \omega^j)^{\text{T}}. \end{aligned} \quad (9.10)$$

Here we leave the cutoff operators $\mathcal{R}_k^{\text{grav}}$ and $\mathcal{R}_k^{\text{gh}}$ arbitrary for the time being. They will be specified later on and we just ask them to satisfy the conditions (2.3).

The derivation of the Wetterich equation then follows the manipulations outlined in Section 2.2. While performing the Legendre transformation to find the effective average action (EAA) we have to introduce the expectation values of the fluctuation fields $\chi^{\text{grav}} = (h, h^i, h_{ij}) = (\langle \hat{N} \rangle, \langle \hat{N}^i \rangle, \langle \hat{\sigma}_{ij} \rangle)$ and $\chi^{\text{gh}} = (\bar{c}, c, \bar{c}_i, c^i) = (\langle \bar{\omega} \rangle, \langle \omega \rangle, \langle \bar{\omega}_i \rangle, \langle \omega^i \rangle)$ for the gravitational fields and the ghosts respectively. As the final equation we find

$$\partial_t \Gamma_k = \frac{1}{2} \text{STr} \left[\left(\Gamma_k^{(2)} + \mathcal{R}_k \right)^{-1} \partial_t \mathcal{R}_k \right]. \quad (9.11)$$

Here the supertrace STr includes a trace over field space and all further internal indices as well as a momentum integration. Furthermore it encodes a minus sign for fermionic field contributions as e.g. the ghost fields. The second variation of Γ_k is given by

$$\left(\Gamma_k^{(2)} \right)_{ab} = (-1)^{[c]} \frac{1}{\varepsilon \bar{N}^2 \sqrt{\bar{\sigma}(x, \tau_x) \bar{\sigma}(y, \tau_y)}} \frac{\delta^2 \Gamma_k}{\delta \chi^a(x, \tau_x) \delta \chi^b(y, \tau_y)}. \quad (9.12)$$

Here the index $[c]$ is zero for commuting and one for anti-commuting fields respectively. The resulting background EAA is by construction invariant under background transformations. For vanishing fluctuation fields it reduces to the EAA, which in turn becomes the effective action Γ for $k \rightarrow 0$. The latter one is finally invariant under the supposed $\text{Diff}(\mathcal{M}, \Sigma)$ due to the limit of vanishing fluctuations as explained in Appendix B.2.

Flow Equations for Foliated Gravity

10.1 A Versatile Truncation

After deriving the Wetterich equation in the last section we will introduce a first truncation for an explicit analysis of a $\text{Diff}(\mathcal{M}, \Sigma)$ invariant theory. The necessity of using truncations has been explained in Chapter 2 and, to be precise, we will discuss in the following a truncation containing the monomials of the Hořava-Lifshitz action (8.12). This action will serve as an ansatz for the gravitational part of the EAA, Γ_k^{grav} , by inserting scale dependent coupling constants G_k for the Newton constant, Λ_k for the cosmological constant and λ_k for the coupling λ_2 potentially encoding an explicit breaking of the $\text{Diff}(\mathcal{M})$ symmetry. Note that we consider only λ_2 for technical simplicity. However, since it introduces an explicit invariance between space and time it is sufficient to investigate many interesting aspects. The consideration of the second coupling, λ_1 , appearing in (8.12) is beyond the scope of this thesis and shall be left for future work.

Besides the gravitational part, we have to add the gauge-fixing and ghost action which we approximate by their classical versions (9.5) and (9.6) respectively. Thus our truncation reads $\Gamma_k = \Gamma_k^{\text{grav}} + S^{\text{gf}} + S^{\text{gh}}$ with

$$\Gamma_k^{\text{grav}} = \frac{\sqrt{\varepsilon}}{16\pi G_k} \int d^D x N \sqrt{\sigma} \left[\frac{1}{\varepsilon} (K_{ij} K^{ij} - \lambda_k K^2) - {}^{(d)}R + 2\Lambda_k \right]. \quad (10.1)$$

The field N denotes the classical version of the quantum field \tilde{N} . Analogously we define N^i and σ_{ij} via

$$N = \bar{N} + \langle \hat{N} \rangle, \quad N^i = \bar{N}^i + \langle \hat{N}^i \rangle, \quad \sigma_{ij} = \bar{\sigma}_{ij} + \langle \hat{\sigma}_{ij} \rangle. \quad (10.2)$$

Depending on these fields the extrinsic curvature reads

$$K_{ij} = \frac{1}{2N} (\partial_\tau \sigma_{ij} - \nabla_i N_j - \nabla_j N_i). \quad (10.3)$$

The covariant derivative ∇ and the Ricci scalar ${}^{(d)}R$ are constructed from the spatial metric σ_{ij} . Here and in the following we omit the superscript d for the Ricci scalar since the D -dimensional version will not play any role.

The truncation (10.1) is a very versatile ansatz, as it allows for the investigation of two completely different aspects. The first appears in the limit $\lambda_k = 1$, which makes Γ_k^{grav} invariant under $\text{Diff}(\mathcal{M})$. Although the whole truncation is not invariant under spacetime diffeomorphisms, this foliated Einstein-Hilbert truncation serves as an approximation of a $\text{Diff}(\mathcal{M})$ invariant theory. Within this setting one can compare the results of the metric Einstein-Hilbert truncation with the Euclidean signature and the Lorentzian one of the foliated formulation by utilising the signature parameter ε . Besides the approximation of the usual Einstein-Hilbert truncation the ansatz (10.1), including the asymmetry coupling λ_k , serves as a low energy approximation of HLG, including all terms with two spatial derivatives. All terms with higher orders in spatial derivatives are subleading and thus do not contribute to the IR limit of HLG. The ansatz (10.1) then allows to test if the RG flow of HLG restores $\text{Diff}(\mathcal{M})$ dynamically and approaches classical GR in the IR.

The derivation of the beta functions encoding the scale dependence of the couplings contained in (10.1) proceeds as follows. Firstly, we observe that the calculation can be simplified considerably by two adaptations. The first is the use of Landau gauge. Choosing $\alpha_L, \alpha_S \rightarrow 0$, the gauge fixing action becomes two delta functions, $\delta(\hat{N})$ and $\delta(\hat{N}^i)$, under the path integral. Thus we can freeze \hat{N} and \hat{N}^i to zero. The second adaptation, simplifying the calculations, is the choice of a special background. This choice is almost arbitrary since the background is only a technical tool, serving as a bookkeeping device during the calculation. The only condition it has to match is that it should enable us to distinguish the different interaction monomials. For tracking the RG flow of the couplings contained in (10.1), the following choice suffices

$$\bar{N} = 1, \quad \bar{N}^i = 0, \quad \bar{\sigma}_{ij}(\tau, x) = \chi(\tau) \bar{\sigma}_{ij}(x)|_{S^d}. \quad (10.4)$$

Here, $\bar{\sigma}_{ij}(x)|_{S^d}$ is the metric of the time-independent d -dimensional sphere and in the following we denote $\bar{\sigma}_{ij}(\tau, x)$ by $\bar{\sigma}_{ij}$ for brevity. Whenever we use the time-independent sphere, the metric is marked with an index S^d . The maximal symmetry of the sphere S^d simplifies the Ricci tensor and the Riemann tensor to give

$$\bar{R}_{ij} = \frac{\bar{R}}{d} \bar{\sigma}_{ij}, \quad \bar{R}_{ijkl} = \frac{\bar{R}}{d(d-1)} (\bar{\sigma}_{ik} \bar{\sigma}_{jl} - \bar{\sigma}_{il} \bar{\sigma}_{jk}). \quad (10.5)$$

Note that here the curvature scalar \bar{R} is, in contrast to the considerations in Appendix C.2, time dependent. Explicitly the Ricci scalar is proportional to $\chi^{-1}(\tau)$. Evaluating the gravitational part of our truncation, (10.1), within the Landau

gauge and on this background we find

$$\Gamma_k^{\text{grav}}|_{\text{back}} = \frac{\sqrt{\varepsilon}}{16\pi G_k} \int d^D x \sqrt{\bar{\sigma}}|_{S^d} \chi^{d/2} \left[\frac{d\gamma^2}{4\varepsilon} (1 - d\lambda_k) - \frac{\bar{R}|_{S^d}}{\chi} + 2\Lambda_k \right] \quad (10.6)$$

with $\gamma = \partial_\tau \ln \chi$. Note that the $K_{ij}K^{ij}$ term and the K^2 term get the same proportionality. This shows that our background is sufficient to distinguish the extrinsic curvature terms from the intrinsic term but is not general enough to distinguish between the two extrinsic terms. Therefore within this background we can discuss three couplings. The cosmological constant Λ_k corresponds to the volume term, the Newton constant G_k is related to the scalar curvature term and the last coupling, λ_k , is associated with the parameter γ^2 .

The Landau gauge and the background (10.4) can be used to calculate the right hand side of the foliated Wetterich equation (9.11) within our truncation. We start with the second variation of the EAA with respect to the gravitational fields $\frac{\delta^2 \Gamma_k}{\delta \chi_{\text{grav}}^2}$. Note that due to the gauge fixing, the lapse function and shift vector are fixed and we are left with the spatial metric $\langle \hat{\sigma}_{ij} \rangle = h_{ij}$. The calculation of the second variations is lengthy but straightforward. Therefore we just give the result here and explain the details in Appendix F.1. For the following steps it is convenient to organise the terms quadratic in the fluctuations according to the components. Thus we write $\Gamma_k^{\text{grav}}[\sigma_{ij}] = \Gamma_k^{\text{grav}}[\bar{\sigma}_{ij}] + \frac{1}{2} \delta^2 \Gamma_k^{\text{grav}}[h_{ij}; \bar{\sigma}_{ij}] + \dots$. The terms linear in the fluctuations as well as terms with more than two powers of the fluctuation field are not required, since they do not enter into the present computation. The quadratic term separated by the field content as derived in Appendix F.1 reads

$$\delta^2 \Gamma_{\text{TT}}^{\text{grav}} = \frac{\sqrt{\varepsilon}}{16\pi G_k} \int d^D x \sqrt{\bar{\sigma}} \frac{1}{2} h_{ij}^{\text{TT}} \left[\Delta + C_{2\text{T}} \bar{R} - 2\Lambda_k - \frac{1}{\varepsilon} \partial_\tau^2 + \gamma \frac{4d\lambda_k - d - 4}{2\varepsilon} \partial_\tau + \gamma^2 \frac{d^2 \lambda_k + 4 - d}{4\varepsilon} \right] h^{\text{TT}ij}, \quad (10.7)$$

$$\delta^2 \Gamma_{\xi\xi}^{\text{grav}} = \frac{\sqrt{\varepsilon}}{16\pi G_k} \int d^D x \sqrt{\bar{\sigma}} \xi_i \left[\frac{d-2}{d} \bar{R} - 2\Lambda_k - \frac{1}{\varepsilon} \partial_\tau^2 + \gamma \frac{4d\lambda_k - d - 4}{2\varepsilon} \partial_\tau + \gamma^2 \frac{(d^2 + 4d)\lambda_k - d - 1}{4\varepsilon} \right] \xi^i, \quad (10.8)$$

$$\delta^2 \Gamma_{\zeta\zeta}^{\text{grav}} = \frac{\sqrt{\varepsilon}}{16\pi G_k} \int d^D x \sqrt{\bar{\sigma}} \frac{1}{2} \zeta \left[-C_0(\Delta - \bar{R}) - \frac{2(d-1)}{d} \Lambda_k - \frac{d-1}{d\varepsilon} \partial_\tau^2 + \gamma \frac{(d-1)(4d\lambda_k - d - 4)}{2d\varepsilon} \partial_\tau + \gamma^2 \frac{(d-1)((d^2 + 8d)\lambda_k - d - 8)}{4d\varepsilon} \right] \zeta, \quad (10.9)$$

$$\delta^2 \Gamma_{hh}^{\text{grav}} = \frac{\sqrt{\varepsilon}}{16\pi G_k} \int d^D x \sqrt{\bar{\sigma}} \frac{1}{2} h \left[-C_0 \Delta - \frac{(d-2)(d-4)}{2d^2} \bar{R} + \frac{d-2}{d} \Lambda_k + \frac{d\lambda_k - 1}{d\varepsilon} \partial_\tau^2 \right. \\ \left. - \gamma \frac{(d-4)(d\lambda_k - 1)}{2d\varepsilon} \partial_\tau - \gamma^2 \frac{(d^2 - 2d - 16)(d\lambda_k - 1)}{8d\varepsilon} \right] h, \quad (10.10)$$

$$\delta^2 \Gamma_{h\varsigma}^{\text{grav}} = -\frac{\sqrt{\varepsilon}}{16\pi G_k} \int d^D x \sqrt{\bar{\sigma}} C_0 h \left[\Delta^2 - \frac{1}{d-1} \bar{R} \Delta \right]^{1/2} \varsigma. \quad (10.11)$$

Here $\Delta = -\bar{\sigma}^{ij} \bar{\nabla}_i \bar{\nabla}_j$ denotes the background Laplacian, $C_0 = \frac{(d-2)(d-1)}{d^2}$ and $C_{2T} = \frac{d^2 - 3d + 4}{d(d-1)}$. Furthermore we used the TT decomposition [175] as well as a field redefinition [150]. The latter ones are described in detail in the appendix and can be summarised in

$$h_{ij} = h_{ij}^T + \frac{1}{d} \bar{\sigma}_{ij} h, \quad \bar{\sigma}^{ij} h_{ij}^T = 0 \quad (10.12)$$

with

$$h_{ij}^T = h_{ij}^{\text{TT}} + 2\bar{\nabla}_{(i} \left[\Delta - \frac{1}{d} \bar{R} \right]^{-1/2} \xi_{j)} + \left[\bar{\nabla}_i \bar{\nabla}_j - \frac{1}{d} \bar{\sigma}_{ij} \right] \left[\Delta \left(\Delta - \frac{1}{d-1} \bar{R} \right) \right]^{-1/2} \varsigma. \quad (10.13)$$

The second variations with respect to the component fields (10.7)-(10.11) are not yet diagonal, but we can handle the mixing term in the scalar sector as shown below. Note as well that $\delta^2 \Gamma_{\xi\xi}^{\text{grav}}$ is independent of the spatial Laplacian, since this will be important in the following. To complete the information about the second variation of the EAA we give the results for the ghost part. Here it is important that we used the Landau gauge and all fluctuating lapse functions and shift vectors vanish. This simplifies the ghost action (9.6) considerably and the part quadratic in the ghost fluctuations for vanishing background ghost fields reads

$$\delta^2 \Gamma_{\bar{c}c}^{\text{gh}} = \sqrt{\varepsilon} \int d^D x \sqrt{\bar{\sigma}} \bar{c} \partial_\tau c, \quad \delta^2 \Gamma_{\bar{c}^i c_j}^{\text{gh}} = \sqrt{\varepsilon} \int d^D x \sqrt{\bar{\sigma}} \bar{c}^i \partial_\tau c_j. \quad (10.14)$$

As we have seen for $\delta^2 \Gamma_{\xi\xi}^{\text{grav}}$ we do not get any dependencies on the spatial Laplacian.

After gathering all information for $\Gamma_k^{(2)}$ the next object on the right hand side of (9.11) is the regulator \mathcal{R}_k . This regulator should serve mainly two purposes. First it should implement a momentum-shell-wise integration and second it should act as an IR regulator. The only restrictions for the form of the regulator is the invariance under background transformations (9.4). Note that this symmetry allows us to handle the fluctuations in spatial and time direction separately. We use this and introduce a regulator \mathcal{R}_k which is purely spatial and thus regulates only the spatial fluctuations. The fluctuations in time direction will be considered afterwards. One advantage of this treatment is that we can investigate Lorentzian signatures. This is very hard for spacetime-symmetric regulators since they have

to be positive definite for all values of k . Such regulators have been investigated in [176].

Now we can have a closer look at the cutoff term \mathcal{R}_k . First of all we separate \mathcal{R}_k into the matrix part (in field space) and a scalar function R_k as

$$[\mathcal{R}_k]_{ij} = [Z_k]_{ij} R_k = [Z_k]_{ij} k^2 R^{(0)}\left(\frac{\Delta}{k^2}\right). \quad (10.15)$$

We choose a cutoff of Type I according to the nomenclature in [121]. This prescription constructs \mathcal{R}_k in such a way that Laplacians in $\Gamma_k^{(2)}$ are dressed up with the k -dependent mass term R_k according to $\Delta \rightarrow P_k = \Delta + R_k$. Note that all terms independent of the spatial Laplacian do not get any regulator contributions and therefore drop out of the right hand side of the flow equation (9.11). Thus we get no ghost contributions and no vector contributions. We are left with the following regulator

$$\mathcal{R}_k = \begin{pmatrix} \mathcal{R}_k^{\text{TT}} & & \\ & \mathcal{R}_k^{hh} & \mathcal{R}_k^{h\zeta} \\ & \mathcal{R}_k^{\zeta h} & \mathcal{R}_k^{\zeta\zeta} \end{pmatrix} \quad (10.16)$$

with

$$\begin{aligned} \mathcal{R}_k^{hh} &= \mathcal{R}_k^{\zeta\zeta} = -\frac{1}{32\pi G_k} C_0 R_k, \\ \mathcal{R}_k^{\zeta h} &= \mathcal{R}_k^{h\zeta} = -\frac{1}{32\pi G_k} C_0 \left[\left(P_k^2 - \frac{1}{d-1} \bar{R} P_k \right)^{1/2} - \left(\Delta^2 - \frac{1}{d-1} \bar{R} \Delta \right)^{1/2} \right], \\ \mathcal{R}_k^{\text{TT}} &= \frac{1}{32\pi G_k} \mathbb{1}_{2\text{T}} R_k. \end{aligned} \quad (10.17)$$

Here $\mathbb{1}_{2\text{T}}$ denotes the $d_{2\text{T}}$ -dimensional unit matrix with $d_{2\text{T}} = \frac{1}{2}(d+1)(d-2)$. The scalar profile function $R^{(0)}$, interpolating smoothly between $R^{(0)}(0) = 1$ and $R^{(0)}(\infty) = 0$, is kept arbitrary here and will be specified to the optimised version later on.

Combining the second variations (10.7)-(10.11) and the regulator (10.16) we can write the foliated Wetterich equation (9.11) as

$$\partial_t \Gamma_k = \mathcal{T}_{\text{TT}} + \mathcal{T}_{\text{scalar}} \quad (10.18)$$

with the TT part

$$\mathcal{T}_{\text{TT}} = \frac{32\pi G_k}{2} \text{Tr}_D \left[\left(P_k + C_{2\text{T}} \bar{R} - 2\Lambda_k - \frac{1}{\varepsilon} \partial_\tau^2 + \gamma \frac{4d\lambda_k - d - 4}{2\varepsilon} \partial_\tau + \gamma^2 \frac{d^2 \lambda_k + 4 - d}{4\varepsilon} \right)^{-1} \partial_t \mathcal{R}_k^{\text{TT}} \right]. \quad (10.19)$$

The scalar part is a bit more involved since it is not diagonal. However we can just treat the scalar part as matrix valued in field space to find

$$\begin{aligned} \mathcal{T}_{\text{scalar}} &= \frac{1}{2} \text{Tr}_D \left[\left(\begin{array}{cc} \Gamma_{hh}^{(2)} & \Gamma_{h\zeta}^{(2)} \\ \Gamma_{\zeta h}^{(2)} & \Gamma_{\zeta\zeta}^{(2)} \end{array} \right)^{-1} \partial_t \begin{pmatrix} \mathcal{R}_k^{hh} & \mathcal{R}_k^{h\zeta} \\ \mathcal{R}_k^{\zeta h} & \mathcal{R}_k^{\zeta\zeta} \end{pmatrix} \right] \\ &= \frac{1}{2} \text{Tr}_D \left[\frac{\Gamma_{\zeta\zeta}^{(2)} \partial_t \mathcal{R}_k^{\zeta\zeta} + \Gamma_{hh}^{(2)} \partial_t \mathcal{R}_k^{hh} - 2\Gamma_{h\zeta}^{(2)} \partial_t \mathcal{R}_k^{h\zeta}}{\Gamma_{hh}^{(2)} \Gamma_{\zeta\zeta}^{(2)} - \Gamma_{h\zeta}^{(2)} \Gamma_{\zeta h}^{(2)}} \right]. \end{aligned} \quad (10.20)$$

Here the index D at the traces highlights that the momentum integral, corresponding to it, is actually D -dimensional.

10.2 Evaluating the Functional Traces

Up to this point we regulated only the spatial fluctuations but ignored the fluctuations in time direction. As promised in the last section we will treat them separately here. For this purpose we follow a completely different approach compared to the regulator insertion. We follow the lines of finite-temperature flow equations [176–178] and introduce a finite length β of the time direction with periodic boundary conditions. This can be used to Fourier expand the τ -dependent fields with a discrete Fourier transformation

$$\phi(\tau, x) = \sum_{n=-\infty}^{\infty} \phi_n(x) e^{2\pi i n \tau / \beta} \quad \Rightarrow \quad \phi_n(x) = \frac{1}{\beta} \int_0^\beta d\tau \phi(\tau, x) e^{-2\pi i n \tau / \beta}. \quad (10.21)$$

The complex coefficients $\phi_n(x)$ satisfy the reality constraint $\phi_n(x) = \phi_{-n}^*(x)$. Note the right hand side of the foliated Wetterich equation (9.11) contains τ integrals (if we use the heat-kernel expansion (C.4)) as well as τ derivatives. Furthermore we encounter τ -dependent backgrounds which might be the volume, the volume multiplied with the Ricci scalar and the volume multiplied with $\gamma^2 = (\partial_\tau \ln \chi)^2$. To analyse the Fourier transform of the right hand side we specify the background to be slowly varying in time. Thus we use

$$\begin{aligned} \chi(\tau) &= \exp\left(-\frac{\tau}{\theta}\right), \quad \Rightarrow \quad \bar{R} = \bar{R}|_{S^d} \exp\left(\frac{\tau}{\theta}\right) \\ \Rightarrow \int d^d x \sqrt{\bar{\sigma}} &= \int d^d x \sqrt{\bar{\sigma}|_{S^d}} \exp\left(-\frac{d\tau}{2\theta}\right), \quad \gamma = -\frac{1}{\theta} \end{aligned} \quad (10.22)$$

where the terms with a lower index S^d are evaluated on the time-independent, d -dimensional sphere. Here the time constant θ is chosen as $\theta \gg \beta$. Note that we are using a non-periodic function $\chi(\tau)$ on a periodic manifold. However, the background is just a tool and does not have a physical interpretation. Thus we keep

this background τ dependence with a discontinuity at $\tau = 0 = \beta$. Using (10.22) we can perform the following approximation

$$\begin{aligned}\sqrt{\bar{\sigma}} &= \sqrt{\bar{\sigma}|_{S^d}} e^{-d\tau/2\theta} = \sqrt{\bar{\sigma}|_{S^d}} + \mathcal{O}\left(\frac{\tau}{\theta}\right), \\ \sqrt{\bar{\sigma}} \bar{R} &= \sqrt{\bar{\sigma}|_{S^d}} \bar{R}|_{S^d} e^{-(d-2)\tau/2\theta} = \sqrt{\bar{\sigma}|_{S^d}} \bar{R}|_{S^d} + \mathcal{O}\left(\frac{\tau}{\theta}\right), \\ \sqrt{\bar{\sigma}} \gamma^2 &= \sqrt{\bar{\sigma}|_{S^d}} e^{-d\tau/2\theta} \frac{1}{\theta^2} = \sqrt{\bar{\sigma}|_{S^d}} \frac{1}{\theta^2} + \mathcal{O}\left(\frac{\tau}{\theta}\right).\end{aligned}\tag{10.23}$$

Here we keep only terms of order τ^0 . Higher orders in τ are beyond our truncation and within the order τ^0 the parameter θ suffices to discriminate between the extrinsic and intrinsic terms in our truncation.

The trace over time-like fluctuations and the time derivative turn into

$$\text{Tr}_D \rightarrow \sqrt{\varepsilon} \sum_{n=-\infty}^{\infty} \text{Tr}_d, \quad \partial_\tau \rightarrow \imath \left(\frac{2\pi n}{\beta} \right).\tag{10.24}$$

Here Tr_d denotes the leftover trace which contains the spatial operator trace and the trace in field space. Since all the traces appearing in the following are d -dimensional, the index d will be suppressed. The last adaptation due to the discretisation affects the second variations $\Gamma_k^{(2)}$. So far this denoted the second variation with respect to the τ -dependent fields and changes now to become the second variation with respect to the field modes. For quadratic terms we find

$$\int d\tau \phi(\tau) \phi(\tau) = \beta \sum_n \phi_n \phi_{-n}\tag{10.25}$$

and thus the second variations receive an additional prefactor β . The same holds for the regulator as it was adapted to the second variation.

Finally we have to explain, how this discretisation is able to implement a cutoff. Note that the finite length of the time direction automatically acts as a IR cutoff and a UV cutoff can be implemented by simply restricting the sum over Matsubara modes. Thus the Fourier transformation gives us an alternative implementation to the regulator insertion used in the spatial direction.

If we evaluate the derivative with respect to the RG time t on the left hand side of the FRGE (9.11) and take into account the special background (10.22) we find that (10.6) becomes

$$\partial_t \Gamma_k = \frac{\sqrt{\varepsilon}}{16\pi} \int d^d x \sqrt{\bar{\sigma}|_{S^d}} \left[\frac{d\gamma^2}{4\varepsilon} \left(\partial_t \frac{\beta}{G_k} - d \partial_t \frac{\beta \lambda_k}{G_k} \right) - \bar{R}|_{S^d} \partial_t \frac{\beta}{G_k} + 2 \partial_t \frac{\beta \Lambda_k}{G_k} \right]\tag{10.26}$$

where we evaluated the t derivative at vanishing fluctuations. Note that we used the expansion (10.23) and furthermore evaluated the τ integral, leading to a factor

β . Since we would like to keep the possibility of a t -dependent time-interval length, we moved this factor under the t derivatives. As we have seen in (10.6), the running couplings are encoded in the coefficients of the terms proportional to a constant, proportional to R and proportional to γ^2 .

Finally we are interested in the beta functions of the coupling constants of our truncation. The flow equation for the Newton constant G_k can be found by projections onto the terms proportional to \bar{R} . The one for the cosmological constant Λ_k follows from the constant terms and finally the flow equation for the asymmetry coupling λ_k can be found by projecting onto terms proportional to γ^2 . All higher orders in \bar{R} and γ are outside the truncation and can be dropped. This can be used to evaluate the right hand side (10.18). Before analysing the scalar contribution we start with an expansion of the denominator of the transverse traceless part which is given in (10.19) and has the form

$$\mathcal{T}_{\text{TT}} = \frac{1}{2}\sqrt{\varepsilon} \sum_n \text{Tr}_{2\text{T}} \left[\frac{\partial_t(\beta Z_{\text{N}k} R_k)}{\beta Z_{\text{N}k}} \frac{1}{P_k + b_1 + b_2 \bar{R} + b_3 \gamma + b_4 \gamma^2} \right]. \quad (10.27)$$

Here we introduced the wave function renormalisation $Z_{\text{N}k}$ carrying the running of the inverse of the Newton constant, $G_k = Z_{\text{N}k}^{-1} G_0$. The coefficients b_1, \dots, b_4 are given by

$$\begin{aligned} b_1 &= -2\Lambda_k + \frac{1}{\varepsilon} \left(\frac{2\pi n}{\beta} \right)^2, & b_2 &= C_{2\text{T}}, \\ b_3 &= i \frac{4d\lambda_k - d - 4}{2\varepsilon} \left(\frac{2\pi n}{\beta} \right), & b_4 &= \frac{d^2 \lambda_k + 4 - d}{4\varepsilon}. \end{aligned} \quad (10.28)$$

The expansion in \bar{R} and γ leads to

$$\begin{aligned} \mathcal{T}_{\text{TT}} &= \frac{1}{2}\sqrt{\varepsilon} \sum_n \text{Tr}_{2\text{T}} \left[\frac{\partial_t(\beta Z_{\text{N}k} R_k)}{\beta Z_{\text{N}k}} \left(\frac{1}{P_k + b_1} - \frac{b_2}{(P_k + b_1)} \bar{R} \right. \right. \\ &\quad \left. \left. - \frac{b_4}{(P_k + b_1)^2} \gamma^2 + \frac{b_3^2}{(P_k + b_1)^3} \gamma^2 \right) \right] + \dots \quad (10.29) \end{aligned}$$

Here and in the following, the dots denote irrelevant terms, not contributing to the present truncation. Now all appearing traces are of the form discussed in Appendix C. Therefore we can write the result in terms of the threshold functions Φ given in (C.31). For convenience we again combine them to $q_n^{p,q}(w) = \Phi_n^{p,q}(w) - \frac{1}{2}\eta_N \bar{\Phi}_n^{p,q}(w)$ with the anomalous dimension of the Newton constant given by $\eta_N = -\partial_t \ln(\beta Z_{\text{N}k})$. The result reads

$$\begin{aligned} \mathcal{T}_{\text{TT}} &= \frac{d_{2\text{T}} \sqrt{\varepsilon}}{(4\pi)^{d/2}} \sum_n \int d^d x \sqrt{\sigma} k^d \left[q_{d/2}^{1,0} + \frac{\bar{R}}{k^2} \left(\frac{(d+2)(d-5)}{6(d-1)(d-2)} q_{d/2-1}^{1,0} - C_{2\text{T}} q_{d/2}^{2,0} \right) \right. \\ &\quad \left. + \frac{\gamma^2}{k^2} \left(-\frac{(4d\lambda_k - d - 4)^2}{4} \left(\frac{2\pi n}{\beta k} \right)^2 q_{d/2}^{3,0} - \frac{d^2 \lambda_k + 4 - d}{4\varepsilon} q_{d/2}^{2,0} \right) \right] + \dots \quad (10.30) \end{aligned}$$

Two comments are in order. Firstly, a term proportional to $\delta_{d,2}$, given in Appendix C.3, is ignored since we will concentrate on $d = 3$ later on. Secondly (10.30) differs from the expression given in [168], where the wrong heat-kernel coefficients have been used. All q functions in (10.30) are evaluated at

$$w_{2\Gamma} = -2\bar{\Lambda}_k + \frac{1}{\varepsilon}m^2n^2 \quad (10.31)$$

with the dimensionless cosmological constant $\bar{\Lambda}_k$ and the Kaluza-Klein mass m defined as

$$\bar{\Lambda}_k = \frac{\Lambda_k}{k^2}, \quad m = \frac{2\pi}{\beta k}, \quad \bar{G}_k = G_k k^{d-1}. \quad (10.32)$$

For completeness we also defined the dimensionless Newton constant \bar{G}_k via a multiplication with a suitable power of the scale k .

The scalar trace can be evaluated along the lines of the TT calculation. However it is more involved and very lengthy. Thus the details have been relegated to Appendix F.2. At this point we just state the final result

$$\begin{aligned} \mathcal{T}_{\text{scalar}} = & -\frac{2\sqrt{\varepsilon}}{(4\pi)^{d/2}} \sum_n \int d^d x \sqrt{\sigma} k^d \left[a_1 q_{d/2}^{1,0} \right. \\ & + \frac{\bar{R}}{k^2} \left(\frac{a_1}{6} q_{d/2-1}^{1,0} + a_2 X q_{d/2}^{1,0} + (a_3 + a_4 m^2 n^2) X q_{d/2}^{2,0} + a_5 X q_{d/2}^{2,-1} \right) \\ & + \frac{\gamma^2}{k^2} \left(a_6 X q_{d/2}^{1,0} + (a_7 + a_8 m^2 n^2 + a_9 X m^2 n^2 + a_{10} X m^4 n^4) X q_{d/2}^{2,0} \right. \\ & + (a_{11} + a_{12} X m^2 n^2) X q_{d/2}^{2,-1} \\ & + (a_{13} + a_{14} m^2 n^2 + a_{15} m^4 n^4) X^2 m^2 n^2 q_{d/2}^{3,0} \\ & \left. + (a_{16} + a_{17} m^2 n^2) X^2 m^2 n^2 q_{d/2}^{3,-1} + a_{18} X^2 m^2 n^2 q_{d/2}^{3,-2} \right) + \dots \quad (10.33) \end{aligned}$$

Here all q functions are understood to be evaluated at

$$w_0 = \frac{1}{\bar{\Lambda}_k - \frac{1-\lambda_k}{\varepsilon} m^2 n^2} \left(-2\bar{\Lambda}_k^2 + \frac{d-4+2d\lambda_k}{(d-2)\varepsilon} \bar{\Lambda}_k m^2 n^2 - \frac{(d\lambda_k-1)}{(d-2)} m^4 n^4 \right). \quad (10.34)$$

The prefactors a_1, \dots, a_{18} depend on the dimension and the coupling constants and are given in (F.26).

At this stage, we are left with the sums over the Matsubara modes in (10.30) and (10.33). These can be evaluated analytically as explained in Appendix F.3. The result can be given in terms of the summed threshold functions T and S defined

in this appendix and reads

$$\begin{aligned}
\mathcal{T}_{\text{TT}} &= \frac{d_{2\text{T}}\sqrt{\varepsilon}}{(4\pi)^{d/2}} \int d^d x \sqrt{\bar{\sigma}} k^d \left[T_{d/2}^{1,0} + \frac{\bar{R}}{k^2} \left(\frac{(d+2)(d-5)}{6(d-1)(d-2)} T_{d/2-1}^{1,0} - C_{2\text{T}} T_{d/2}^{2,0} \right) \right. \\
&\quad \left. - \frac{\gamma^2}{k^2} \left(\frac{(4d\lambda_k - d + 4)^2}{4} T_{d/2}^{3,1} + \frac{d^2 \lambda_k + 4 - d}{4\varepsilon} T_{d/2}^{2,0} \right) \right], \\
\mathcal{T}_{\text{scalar}} &= - \frac{2\sqrt{\varepsilon}}{(4\pi)^{d/2}} \int d^d x \sqrt{\bar{\sigma}} k^d \left[a_1 S_{d/2,0}^{1,0} \right. \\
&\quad + \frac{\bar{R}}{k^2} \left(\frac{a_1}{6} S_{d/2-1,0}^{1,0} + a_2 S_{d/2,1}^{1,0} + (a_3 + a_5) S_{d/2,1}^{2,0} + a_4 S_{d/2,1}^{2,1} \right) \\
&\quad + \frac{\gamma^2}{k^2} \left(a_6 S_{d/2,1}^{1,0} + (a_7 + a_{11}) S_{d/2,1}^{2,0} + a_8 S_{d/2,1}^{2,1} + (a_9 + a_{12}) S_{d/2,2}^{2,1} \right. \\
&\quad \left. + a_{10} S_{d/2,2}^{2,2} + (a_{13} + a_{16} + a_{18}) S_{d/2,2}^{3,1} + (a_{14} + a_{17}) S_{d/2,2}^{3,2} + a_{15} S_{d/2,2}^{3,3} \right) \left. \right]. \tag{10.35}
\end{aligned}$$

This final right hand side, given in terms of the summed q functions T and S , has to be compared to the left hand side (10.26). Evaluated at vanishing fluctuations the latter one reads

$$\begin{aligned}
\partial_t \Gamma_k &= \frac{\sqrt{\varepsilon}}{16\pi G_0} \int d^d x \sqrt{\bar{\sigma}}|_{S^d} \left[\frac{d\gamma^2}{4\varepsilon} (\partial_t(\beta Z_{Nk}) - d\partial_t(\beta Z_{Nk}\lambda_k)) \right. \\
&\quad \left. - \partial_t(\beta Z_{Nk})\bar{R}|_{S^d} + 2\partial_t(\beta Z_{Nk}\Lambda_k) \right] \tag{10.36}
\end{aligned}$$

where we replaced $G_k = G_0/Z_{Nk}$. Again the index S^d denotes the evaluation on the time-independent, d -dimensional sphere. For convenience we switch to dimensionless coupling constants (10.32). Therefore the beta function for the dimensionless Newton constant can be given as

$$\partial_t \bar{G}_k = (d-1 + \eta_N + \frac{\partial_t \beta}{\beta}) \bar{G}_k \tag{10.37}$$

with the anomalous dimension $\eta_N = -\partial_t \ln(\beta Z_{Nk})$. For the derivation of the beta function for the cosmological constant we compare the terms proportional to the volume on the left (10.36) and the right hand side (10.35) of the Wetterich equation. We find

$$\begin{aligned}
\frac{\partial_t(\beta Z_{Nk}\Lambda_k)}{\beta Z_{Nk}} &= \partial_t \Lambda_k - \eta_N \Lambda_k = \frac{2\bar{G}_k}{(4\pi)^{d/2-1}\beta} k \left[d_{2\text{T}} T_{d/2}^{1,0} - 2a_1 S_{d/2,0}^{1,0} \right] \\
&\Rightarrow \partial_t \bar{\Lambda}_k = (\eta_N - 2)\bar{\Lambda}_k + \frac{4m\bar{G}_k}{(4\pi)^{d/2}} \left[d_{2\text{T}} T_{d/2}^{1,0} - 2a_1 S_{d/2,0}^{1,0} \right]. \tag{10.38}
\end{aligned}$$

Next we are interested in the beta function of the anisotropy parameter λ_k . This is derived by the comparison of the terms proportional to γ^2 . We find

$$\begin{aligned} \partial_t \lambda_k = & \frac{d\lambda_k - 1}{d} \eta_N - \frac{32\varepsilon m \bar{G}_k}{d^2 (4\pi)^{d/2}} \left[d_{2T} \left(-\frac{(4d\lambda_k - d + 4)^2}{4} T_{d/2}^{3,1} - \frac{d^2 \lambda_k + 4 - d}{4\varepsilon} T_{d/2}^{2,0} \right) \right. \\ & - 2 \left(a_6 S_{d/2,1}^{1,0} + (a_7 + a_{11}) S_{d/2,1}^{2,0} + a_8 S_{d/2,1}^{2,1} + (a_9 + a_{12}) S_{d/2,2}^{2,1} + a_{10} S_{d/2,2}^{2,2} \right. \\ & \left. \left. + (a_{13} + a_{16} + a_{18}) S_{d/2,2}^{3,1} + (a_{14} + a_{17}) S_{d/2,2}^{3,2} + a_{15} S_{d/2,2}^{3,3} \right) \right]. \quad (10.39) \end{aligned}$$

The anomalous dimension on the other hand is derived by a comparison of the terms proportional to \bar{R} on the left (10.36) and the right hand side (10.35) and reads

$$\begin{aligned} \eta_N = & \frac{8m \bar{G}_k}{(4\pi)^{d/2}} \left[d_{2T} \left(\frac{(d+2)(d-5)}{6(d-1)(d-2)} T_{d/2-1}^{1,0} - C_{2T} T_{d/2}^{2,0} \right) \right. \\ & \left. - 2 \left(\frac{a_1}{6} S_{d/2-1,0}^{1,0} + a_2 S_{d/2,1}^{1,0} + (a_3 + a_5) S_{d/2,1}^{2,0} + a_4 S_{d/2,1}^{2,1} \right) \right]. \quad (10.40) \end{aligned}$$

Note that the S and T functions, defined in (F.50) and (F.34) respectively, depend on η_N . Splitting S and T into Ψ , $\tilde{\Psi}$, Υ and $\tilde{\Upsilon}$ defined in Appendix F.3 leads to

$$\eta_N = \frac{m \bar{G}_k B_1(\bar{\Lambda}_k, \lambda_k)}{1 + m \bar{G}_k B_2(\bar{\Lambda}_k, \lambda_k)} \quad (10.41)$$

with

$$\begin{aligned} B_1 = & \frac{8}{(4\pi)^{d/2}} \left[-2 \left(\frac{a_1}{6} \Psi_{d/2-1,0}^{1,0} + a_2 \Psi_{d/2,1}^{1,0} + (a_3 + a_5) \Psi_{d/2,1}^{2,0} + a_4 \Psi_{d/2,1}^{2,1} \right) \right. \\ & \left. + d_{2T} \left(\frac{(d+2)(d-5)}{6(d-1)(d-2)} \Upsilon_{d/2-1}^{1,0} - C_{2T} \Upsilon_{d/2}^{2,0} \right) \right] \\ B_2 = & \frac{4}{(4\pi)^{d/2}} \left[-2 \left(\frac{a_1}{6} \tilde{\Psi}_{d/2-1,0}^{1,0} + a_2 \tilde{\Psi}_{d/2,1}^{1,0} + (a_3 + a_5) \tilde{\Psi}_{d/2,1}^{2,0} + a_4 \tilde{\Psi}_{d/2,1}^{2,1} \right) \right. \\ & \left. + d_{2T} \left(\frac{(d+2)(d-5)}{6(d-1)(d-2)} \tilde{\Upsilon}_{d/2-1}^{1,0} - C_{2T} \tilde{\Upsilon}_{d/2}^{2,0} \right) \right]. \quad (10.42) \end{aligned}$$

Finally we arrived at a non-linear system of beta functions for the dimensionless Newton constant \bar{G}_k , the dimensionless cosmological constant $\bar{\Lambda}_k$ and the asymmetry parameter λ_k which reads

$$\begin{aligned} \partial_t \bar{G}_k &= \beta_{\bar{G}}(\bar{G}_k, \bar{\Lambda}_k, \lambda_k, m), \\ \partial_t \bar{\Lambda}_k &= \beta_{\bar{\Lambda}}(\bar{G}_k, \bar{\Lambda}_k, \lambda_k, m), \\ \partial_t \lambda_k &= \beta_{\lambda}(\bar{G}_k, \bar{\Lambda}_k, \lambda_k, m). \end{aligned} \quad (10.43)$$

Note that the beta functions here, in contrast to the metric formulation, depend parametrically on the Kaluza-Klein mass m . The explicit expressions are given in (10.37), (10.38) and (10.39). They read

$$\begin{aligned}
\beta_{\bar{G}} &= (d-1 + \eta_N + \frac{\partial_t \beta}{\beta}) \bar{G}_k, \\
\beta_{\bar{\Lambda}} &= (\eta_N - 2) \bar{\Lambda}_k + \frac{4m\bar{G}_k}{(4\pi)^{d/2}} \left[d_{2T} T_{d/2}^{1,0} - 2a_1 S_{d/2,0}^{1,0} \right], \\
\beta_{\lambda} &= \frac{d\lambda_k - 1}{d} \eta_N - \frac{32\varepsilon m \bar{G}_k}{d^2 (4\pi)^{d/2}} \left[d_{2T} \left(-\frac{(4d\lambda_k - d - 4)^2}{4} T_{d/2}^{3,1} - \frac{d^2 \lambda_k + 4 - d}{4\varepsilon} T_{d/2}^{2,0} \right) \right. \\
&\quad - 2 \left(a_6 S_{d/2,1}^{1,0} + (a_7 + a_{11}) S_{d/2,1}^{2,0} + a_8 S_{d/2,1}^{2,1} + (a_9 + a_{12}) S_{d/2,2}^{2,1} + a_{10} S_{d/2,2}^{2,2} \right. \\
&\quad \left. \left. + (a_{13} + a_{16} + a_{18}) S_{d/2,2}^{3,1} + (a_{14} + a_{17}) S_{d/2,2}^{3,2} + a_{15} S_{d/2,2}^{3,3} \right) \right]. \quad (10.44)
\end{aligned}$$

This set of beta functions represents a novel type of flow equations and constitutes a main result of this thesis. The first novelty is encoded in the ε dependence and enables us to analyse the effect of different signatures. The second novelty is the inclusion of an explicit asymmetry between space and time allowing us to discuss the low-energy behaviour of HLG in the next chapter.

RG Flows of Foliated Gravity

11.1 Phase Diagram of the Foliated Einstein-Hilbert Truncation

The last chapter was dedicated to the derivation of the beta functions for foliated gravity. The resulting system of flow equations is given in (10.43). The properties of it shall be analysed within this section in the symmetric limit $\lambda_k = 1$. Thus, we discuss the beta functions corresponding to the foliated Einstein-Hilbert truncation containing two couplings, the Newton constant and the cosmological constant. The most obvious difference to the metric formulation is the parametric dependence on the Kaluza-Klein mass m . In (10.32) it is given as $m = \frac{2\pi}{\beta k}$ and thus depends on both the size of the time circle and the RG scale k . Within an Asymptotic Safety scenario one would expect that m finds a fixed point m^* for $k \rightarrow \infty$. In the following we will concentrate on two different options. The first is given by constant length of the time circle β and thus is called the Gaussian fixed-point scenario, since $m \rightarrow m^* = 0$ for $k \rightarrow \infty$. The second scenario approximates the Kaluza-Klein mass at all scales by a supposed NGFP value $m = m^* \neq 0$. This scenario is called floating fixed-point scenario and passes a k dependence to the length of the time circle β .

Notably, the beta functions of the foliated case are much more complicated than the ones encountered in metric gravity. Foremost, this complicated structure arises due to the summation of Matsubara modes. According to (F.29) we find hyperbolic functions, well defined on the entire real axis, or trigonometric functions, giving rise to poles depending on the argument. In Appendix F.3 we have seen that the argument is either \arg_{2T} for TT sector or \arg_{\pm} for the scalar sector. These

ε	$\bar{\Lambda}_k < -4C_0$	$-4C_0 < \bar{\Lambda}_k < 1/2$	$1/2 < \bar{\Lambda}_k$
+1	hyperbolic	mixture	trigonometric
-1	trigonometric	mixture	hyperbolic

Table 11.1: The analytic structure of the beta functions is given in terms of the signature of spacetime ε and the value of the cosmological constant $\bar{\Lambda}_k$. We distinguish the regions where the beta functions are constructed from hyperbolic or trigonometric functions only or contain both types of terms.

arguments read

$$\begin{aligned} \arg_{2T} &= \frac{\pi}{m} \sqrt{\varepsilon(1 - 2\bar{\Lambda}_k)}, \\ \arg_{\pm} &= \pi \sqrt{\frac{\varepsilon \bar{\Lambda}_k}{m^2} \left(\frac{3d-4}{2(d-1)} \pm \sqrt{\left(\frac{3d-4}{2(d-1)} \right)^2 + \frac{(d-2)(1-2\bar{\Lambda}_k)}{(d-1)\Lambda_k}} \right)}. \end{aligned} \quad (11.1)$$

The analytic structure arising from these arguments depends on the signature and the value of the cosmological constant and is collected in Table 11.1. For $\bar{\Lambda}_k > 1/2$ the argument of the hyperbolic functions, \arg_{2T} , becomes imaginary for Euclidean and real for Lorentzian signature. The converse holds for the argument of the trigonometric functions, \arg_{\pm} . Therefore the beta functions become trigonometric for Euclidean signature and hyperbolic for Lorentzian signature. Next we can discuss the case $\bar{\Lambda}_k < -4C_0$. There we find that \arg_{2T} is real or imaginary for Euclidean and Lorentzian signature respectively. Again we find the converse for \arg_{\pm} and therefore, the beta functions become hyperbolic for Euclidean and trigonometric for Lorentzian signature. Between $\bar{\Lambda}_k = -4C_0$ and $\bar{\Lambda}_k = 1/2$ we find a mixture of trigonometric and hyperbolic functions.

Let us elaborate a bit more on the central region $-4C_0 < \bar{\Lambda}_k < 1/2$, as this is the most interesting one in the metric formulation. For the sake of comparison to the latter we concentrate on $\varepsilon = +1$. In (11.1) we see that the TT sector contributes hyperbolic function, while the pole-producing trigonometric functions originate from the scalar sector. Tracing back the reason for that we find that it relates to the wrong relative sign between the kinetic and potential part of the conformal mode. This is the conformal factor problem, very well known in the metric formulation. We expect that it will be cured by higher-derivative terms, not considered in the present truncation.

After discussing the analytic structure of the beta functions we can discuss consequences of hyperbolic and trigonometric structures in more detail. We start

with the Gaussian fixed-point scenario corresponding to a constant time-interval length β . The most interesting case, of course, is the decompactification limit $\beta \rightarrow \infty$, as it leads us to a familiar D -dimensional spacetime. In this limit the Matsubara sums in (F.29) become continuous integrals and thus the trigonometric functions lead to divergent expressions. According to Table 11.1 we find well defined beta functions only in two regions, $\bar{\Lambda}_k < -4C_0$ in Euclidean and $\bar{\Lambda}_k > 1/2$ in Lorentzian signature. In these two regions a numerical analysis did not reveal any NGFP suitable for an Asymptotic Safety scenario. This complies with the expectation, as the interesting region, according to the metric analysis, is the central one.

Although the decompactification limit did not reveal any fixed point we might find some in the opposite limit $\beta \rightarrow 0$. Within this compactification limit the time circle collapses. Consequently, the Matsubara modes become infinitely heavy and decouple. This, in turn, leads us to an essentially d -dimensional flow. As we are effectively reducing the dimension, we have to redefine the Newton constant via

$$G_k^{(d)} = G_k^{(D)} \beta^{-1} \quad \Rightarrow \quad \bar{G}_k^{(d)} = \frac{m}{2\pi} \bar{G}_k^{(D)} \quad (11.2)$$

to capture the correct physics. The beta function for $\bar{G}_k^{(d)}$ can be derived from the one for $\bar{G}_k^{(D)}$ easily and finally applying the compactification limit $m \rightarrow \infty$ leads to

$$\partial_t \bar{G}_k^{(d)} = \beta_{\bar{G}}^{(d)}(\bar{G}_k^{(d)}, \bar{\Lambda}_k), \quad \partial_t \bar{\Lambda}_k = \beta_{\bar{\Lambda}}^{(d)}(\bar{G}_k^{(d)}, \bar{\Lambda}_k) \quad (11.3)$$

with

$$\begin{aligned} \beta_{\bar{G}}^{(d)} &= \left(d - 2 + \eta_N^{(d)} \right) \bar{G}_k^{(d)}, \\ \beta_{\bar{\Lambda}}^{(d)} &= \left(\eta_N^{(d)} - 2 \right) \bar{\Lambda}_k + \frac{2\bar{G}_k^{(d)}}{(4\pi)^{d/2-1}} \left(d_{2T} + 1 \right) \left(\Phi_{d/2}^{1,0} - \frac{1}{2} \eta_N^{(d)} \tilde{\Phi}_{d/2}^{1,0} \right). \end{aligned} \quad (11.4)$$

Here the threshold functions Φ and $\tilde{\Phi}$ are defined in (C.32) and evaluated at $-2\bar{\Lambda}_k$. Furthermore the d -dimensional anomalous dimension $\eta_N^{(d)}$ reads

$$\eta_N^{(d)} = \frac{2\pi \bar{G}_k^{(d)} B_1(\bar{\Lambda}_k)}{1 + 2\pi \bar{G}_k^{(d)} B_2(\bar{\Lambda}_k)} \quad (11.5)$$

with the functions B_1 and B_2 given as

$$\begin{aligned} B_1 &= \frac{8}{(4\pi)^{d/2}} \left[\left(1 + \frac{(d-5)(d+2)(d+1)}{12(d-1)} \right) \Phi_{d/2-1}^{1,0} - \frac{d-2}{2d\bar{\Lambda}_k} \Phi_{d/2}^{1,0} \right. \\ &\quad \left. - \left(\frac{(d+1)(d-2)(d^2-3d+4)}{2d(d-1)} + \frac{(d-3)4\bar{\Lambda}_k-d+2}{2d\bar{\Lambda}_k} \right) \Phi_{d/2}^{2,0} \right] \\ B_2 &= \frac{4}{(4\pi)^{d/2}} \left[\left(1 + \frac{(d-5)(d+2)(d+1)}{12(d-1)} \right) \tilde{\Phi}_{d/2-1}^{1,0} - \frac{d-2}{2d\bar{\Lambda}_k} \tilde{\Phi}_{d/2}^{1,0} \right. \\ &\quad \left. - \left(\frac{(d+1)(d-2)(d^2-3d+4)}{2d(d-1)} + \frac{(d-3)4\bar{\Lambda}_k-d+2}{2d\bar{\Lambda}_k} \right) \tilde{\Phi}_{d/2}^{2,0} \right]. \end{aligned} \quad (11.6)$$

d	$\bar{G}_*^{(d)}$	$\bar{\Lambda}_*$	τ_*	$\theta_{1,2}$	τ_*^{comp}	$\theta_{1,2}^{\text{comp}}$
3	0.19	0.13	0.005	$1.77 \pm 1.10i$	-	-
4	0.76	0.21	0.16	$2.81 \pm 3.03i$	0.14	$1.48 \pm 3.04i$
5	3.24	0.24	0.53	$4.32 \pm 4.89i$	0.48	$2.69 \pm 5.15i$
6	15.7	0.26	1.03	$6.20 \pm 6.66i$	0.96	$4.33 \pm 7.14i$
7	86.1	0.28	1.66	$8.37 \pm 8.36i$	1.54	$6.27 \pm 9.05i$

Table 11.2: Fixed point values, the universal product τ_* and corresponding critical exponents of the compactification limit within the foliated Einstein-Hilbert truncation for $3 \leq d \leq 7$. Remarkably the results are very similar to the results obtained in the metric formulation [179]. For comparison the latter are given in the last two columns.

Here again the threshold functions are evaluated at $-2\bar{\Lambda}_k$.

We find that the beta functions simplified considerably. Explicitly the signature dependence dropped out completely. This was expected as the information about the signature is stored in the time circle, which collapsed. Note that the simplified beta functions are governed by the spatial TT metric and a scalar field, as the transverse spatial vector within the York decomposition did not contribute. Thus the decoupling of the latter, which was somewhat surprising at the beginning, is necessary to find the d -dimensional gravity in the compactification limit.

Next, we determine the FPs of the flow equations (11.3), since these are central for establishing a possible Asymptotic Safety scenario. First of all we find the obvious GFP at the origin $(\bar{G}_k^{(d)}, \bar{\Lambda}_k) = (0, 0)$. Besides this trivial fixed point we find a NGFP. For $3 \leq d \leq 7$ its values and the corresponding critical exponents are given in Table 11.2. The critical exponents have been calculated as explained in Chapter 3. Furthermore, the universal scaling variable

$$\tau_* = \bar{\Lambda}_* \left(\bar{G}_*^{(d)} \right)^{2/(d-2)} \quad (11.7)$$

is given. Notably the results given in Table 11.2 are very similar to known results, which have been obtained within the metric Einstein-Hilbert truncation [179]. Thus it is very likely that the two descriptions correspond to the same universality class. To fortify this statement we can investigate the phase diagram resulting from the beta functions (11.3) in $d = 4$, given in Figure 11.1. The comparison of it to the phase diagram in Figure 6.1 corresponding to the metric formulation shows that these two phase diagrams are virtually indistinguishable. The main difference is the slight change of the pole structure. Most importantly, we find again the Type

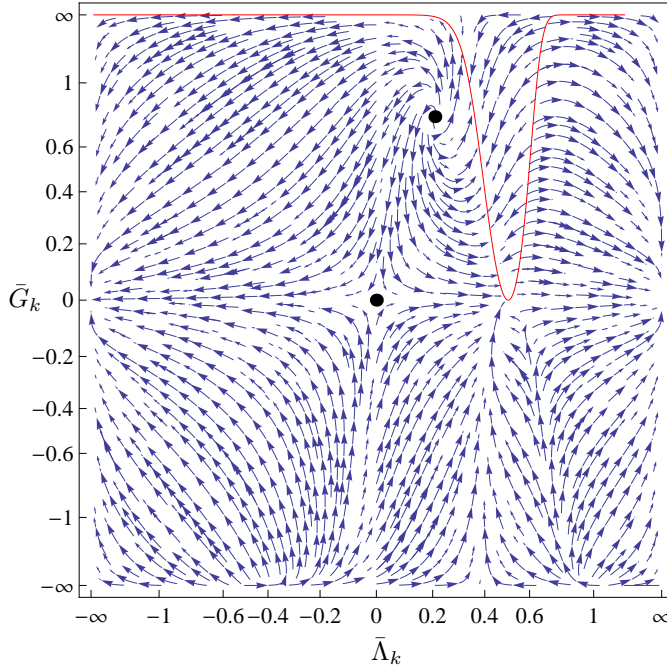


Figure 11.1: The phase diagram of the foliated Einstein-Hilbert truncation in the compactification limit for $d = 4$. The pole of diverging anomalous dimension $\eta_N^{(d)}$ is depicted in red and the arrows point from UV to IR.

IIIa trajectories, starting close to the NGFP, passing by close to the GFP and staying at positive cosmological constant.

Up to this point we considered the Gaussian fixed-point scenario of constant β . As mentioned above, the property of NGFPs that dimensionless couplings become constant motivates to also study the case of a constant Kaluza-Klein mass m . This floating fixed point scenario is interesting, since a constant m leads to β proportional to the inverse of the RG scale k . Thus the time circle decompactifies in the IR as it is necessary for a theory reproducing GR at low energies. At high energies on the other hand the time circle collapses and the situation is likely to be similar to the compactification limit discussed above. According to Figure 11.1 the most interesting parameter range would therefore be $0 < \bar{\Lambda}_k < 1/2$, where the NGFP arising in the metric formulation is situated. However, Table 11.1 states that this region is potentially troublesome. Therefore we elaborate on the pole

ε	\bar{G}_*	$\bar{\Lambda}_*$	$\bar{G}_*\bar{\Lambda}_*$	$\theta_{1,2}$
+1	0.18	0.13	0.023	$1.78 \pm 1.06i$
-1	0.20	0.13	0.026	$1.75 \pm 1.13i$

Table 11.3: Fixed point values, universal product and corresponding critical exponents within the foliated Einstein-Hilbert truncation for $m = 2\pi$ in $d = 3$.

structure a bit more detailed, before analysing possible NGFPs.

To start with, we discuss \arg_{2T} given in (11.1). For Euclidean signature it is real if $\bar{\Lambda}_k < 1/2$ and thus not troublesome since it is the argument of hyperbolic functions. In Lorentzian signature on the other hand \arg_{2T} becomes imaginary and therefore the hyperbolic function turns into a trigonometric one potentially leading to poles. These poles appear if the argument becomes $n\pi$ with n an integer number. Therefore they appear at

$$\bar{\Lambda}_k = -\frac{1}{4}m^2n^2 + \frac{1}{2}. \quad (11.8)$$

Thus the interesting region $0 < \bar{\Lambda}_k < 1/2$ is free of poles, as long as $m > \sqrt{2}$. For a better understanding the physical interpretation of these poles is in order. Their appearance is caused by the propagator going onshell. Denoting the mass with M its typical structure is $\varepsilon m^2 n^2 + \vec{p}^2 + M^2$. As the poles appear if this expression vanishes they are found only for Lorentzian signature.

A similar analysis for the scalar sector shows that the central region is free of divergences as long as

$$m > \sqrt{\frac{3d-4}{2(d-1)}}. \quad (11.9)$$

Combining this critical value for the Kaluza-Klein mass m with the critical value $\sqrt{2}$ from the TT sector shows that $\sqrt{2}$ constitutes the critical limit if we assume $d \geq 2$.

As an example let us discuss the specific case $d = 3, m = 2\pi$. Within this setting the interesting region does not show any divergences of the beta functions. Therefore we can investigate the corresponding flow equations without considering potentially ill-defined regions. Remarkably we find a NGFP in both signatures. The FP values and the corresponding critical exponents are given in Table 11.3. As the beta functions are well defined between $\bar{\Lambda}_k = 0$ and $\bar{\Lambda}_k = 1/2$ we can draw the phase diagram restricted to this region. It is given in Figure 11.2 for Euclidean as well as Lorentzian signature. Notably the difference between the two

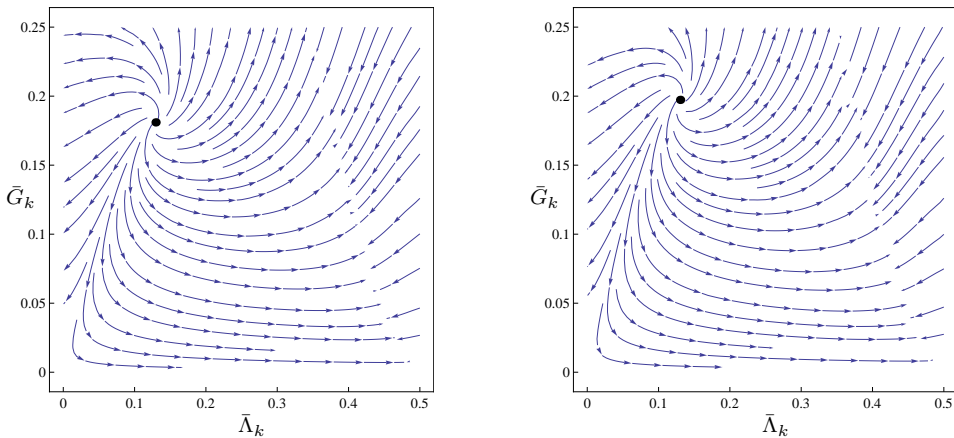


Figure 11.2: The phase diagram of the foliated Einstein-Hilbert truncation for $m = 2\pi$ in $d = 3$. The left plot shows the result within the Euclidean signature and the right plot depicts the result for the Lorentzian signature. The NGFP is depicted as a black dot and the arrow point towards low energies.

plots is only marginal. The main difference results from the diverse FP values given in Table 11.3. Moreover the resulting plots are very similar to the first quadrant of the phase diagram resulting from the compactification limit, given in Figure 11.1, and the one resulting from the metric formulation, given in Figure 6.1. This demonstrates that the signature effects play a sub-dominant role and therefore supports the mainly Euclidean results obtained in the past. Additionally our foliated setting gives further support for the results of the metric formulation.

However, the specific value $m = 2\pi$ was chosen without any physical input and therefore it is worth discussing the changes resulting from a varying Kaluza-Klein mass m . Sticking to $d = 3$, the region $0 < \bar{\Lambda}_k < 1/2$ is free of divergences within the beta functions as long as $m > \sqrt{2}$. Evaluating the fixed point values and the corresponding critical exponents for various values of m leads to the results shown in Figure 11.3. In the upper left plot the FP values for the D -dimensional Newton constant $\bar{G}_k^{(D)}$ and the cosmological constant $\bar{\Lambda}_k$ are depicted. Here the blue dots correspond to Euclidean and the red dots to the Lorentzian signature. It is visible that for increasing Kaluza-Klein mass m the FP values converge towards each other. This is expected, since increasing m is related to decreasing time circle and therefore signature effects are expected to be less important. The upper right plot depicts the corresponding critical exponents, where we decomposed the complex valued exponents according to $\theta_{1/2} = \theta' \pm \theta''$. Again the resulting values approach

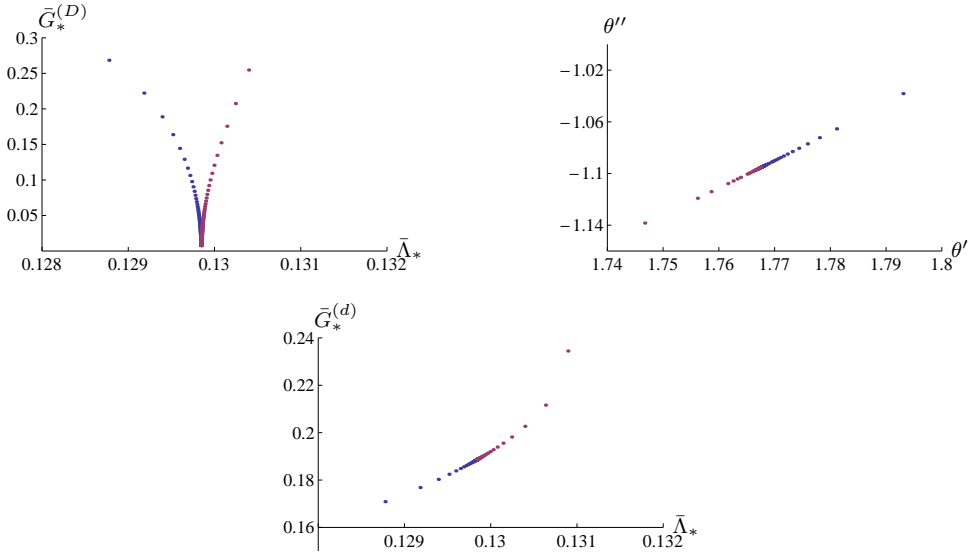


Figure 11.3: The upper left plot shows the FP values depending on m for Lorentzian (red dots) as well as Euclidean (blue dots) signature. For increasing Kaluza-Klein mass the FP values for the different signatures approach each other. The upper right plot shows the m dependence of the real part (θ') and the imaginary part (θ'') of the corresponding critical exponents. The lower plot depicts the m dependence of the FP values for the cosmological constant and the d -dimensional Newton constant.

each other for increasing m . Notably the FP value for $\bar{G}_k^{(D)}$ tends towards $\bar{G}_k^{(D)} = 0$ for larger masses m . This can be understood as a hint that one has to change to the d -dimensional version $\bar{G}_k^{(d)}$, since we are approaching the compactification limit. The m dependence for the d -dimensional Newton constant and the cosmological constant is depicted in the lower plot of Figure 11.3. For very large masses m the m -dependent NGFP converges to the FP evaluated in the compactification limit given in Table 11.2.

In summary, we discussed the beta functions of the foliated Einstein-Hilbert truncation within two scenarios. The Gaussian fixed-point scenario uses a constant time-interval length β and we concentrated on the limits $\beta \rightarrow \infty$ and $\beta \rightarrow 0$. The former did not reveal a NGFP due to divergent expressions within the beta functions. Recalling that the ill-definiteness in the central region is related to the conformal factor problem, one should not interpret this as a failure of Asymptotic

Safety. In contrast it is a hint that the simple Einstein-Hilbert truncation might be insufficient within this treatment. Nevertheless, the inclusion of higher derivative terms is beyond the scope of this thesis and shall be postponed to future work. Within the compactification limit $\beta \rightarrow 0$ the situation was found to be independent of the signature and similar to the metric case in three spacetime dimensions.

Within the floating fixed-point scenario the results were found to depend on the Kaluza-Klein mass m and tend towards those of the compactification limit for $m \rightarrow \infty$. For finite m the signature plays a sub-dominant role. All these results support the possibility that the foliated and the metric formulation of QEG are in the same universality class.

11.2 Phase Diagram of Hořava-Lifshitz Gravity

After studying the RG flow of the foliated Einstein-Hilbert truncation we now enlarge the truncation space under consideration by including the asymmetry coupling λ_k . As discussed above, this setting corresponds to the low-energy limit of projectable HLG. Therefore the asymmetry between space and time should be small and we concentrate on values for $\bar{\lambda}_k$ close to $\bar{\lambda}_k = 1$. The fixed point proposed by Hořava will not be considered here, since this requires the introduction of higher spatial-derivative terms which are beyond our truncation.

In Section 11.1 we have seen that the situation changes only slightly by varying the dimension. Therefore we restrict ourselves, for simplicity, within this section to $d = 3$. This is the most interesting case as it corresponds to a four-dimensional spacetime. As we did in the last section, we start to discuss the analytic structure of the beta functions. Again these are constructed from trigonometric and hyperbolic functions with the respective arguments \arg_{\pm} and $\arg_{2\Gamma}$. These depend on the Kaluza-Klein mass m , the cosmological constant $\bar{\Lambda}_k$ and the asymmetry coupling $\bar{\lambda}_k$ and read

$$\begin{aligned} \arg_{2\Gamma} &= \frac{\pi}{m} \sqrt{\varepsilon(1 - 2\bar{\Lambda}_k)}, \\ \arg_{\pm} &= \pi \sqrt{\frac{(1-6\lambda_k)\bar{\Lambda}_k+1-\lambda_k}{(1-3\lambda_k)2\varepsilon m^2} \pm \sqrt{\left(\frac{(1-6\lambda_k)\bar{\Lambda}_k+1-\lambda_k}{(1-3\lambda_k)2m^2}\right)^2 - \frac{\bar{\Lambda}_k(1-2\bar{\Lambda}_k)}{(1-3\lambda_k)m^4}}}. \end{aligned} \quad (11.10)$$

In the limit $\bar{\lambda}_k = 1$ they reduce to (11.1). These arguments might turn imaginary and thus change the trigonometric into hyperbolic functions and vice versa. This leads us to the analytic structure of the beta functions given in Table 11.4. As in Section 11.1 we find only trigonometric functions for $\bar{\Lambda}_k > 1/2$ in Euclidean or for $\bar{\Lambda}_k < \bar{\Lambda}^{\text{crit}}(\lambda_k)$ in Lorentzian signature. The situation is inverted for hyperbolic

ε	$\bar{\Lambda}_k < \bar{\Lambda}^{\text{crit}}(\lambda_k)$	$\bar{\Lambda}^{\text{crit}}(\lambda_k) < \bar{\Lambda}_k < 1/2$	$1/2 < \bar{\Lambda}_k$
+1	hyperbolic	mixture	trigonometric
-1	trigonometric	mixture	hyperbolic

Table 11.4: Analytic structure of the beta functions for the low-energy limit of HLG in $d = 3$. Depending on the signature and the cosmological constant they are constructed out of trigonometric functions, hyperbolic functions or a mixture. The critical value $\bar{\Lambda}_k^{\text{crit}}$ depends on λ_k and is given in (11.11).

functions and the critical value for the dimensionless cosmological constant reads

$$\bar{\Lambda}^{\text{crit}} = \frac{1 + \lambda_k - 6\lambda_k^2 + 2\sqrt{2} \sqrt{-1 + 7\lambda_k - 16\lambda_k^2 + 12\lambda_k^3}}{9(1 - 4\lambda_k + 4\lambda_k^2)}. \quad (11.11)$$

For $\bar{\Lambda}^{\text{crit}}(\lambda_k) < \bar{\Lambda}_k < 1/2$ we find a mixture of trigonometric and hyperbolic functions. Notably the situation is completely analogous to Section 11.1 and we find again that the interesting region $0 < \bar{\Lambda}_k < 1/2$ contains a mixture. For a better visualisation the analytic structure is depicted in Figure 11.4.

Although we find a mixture it might be possible that this region is free of poles if the poles produced by the trigonometric functions are outside this region. As the argument \arg_{2T} did not change compared to Section 11.1 we find again that m has to be larger than $\sqrt{2}$ to get poles of trigonometric functions at $\bar{\Lambda}_k > 1/2$. The

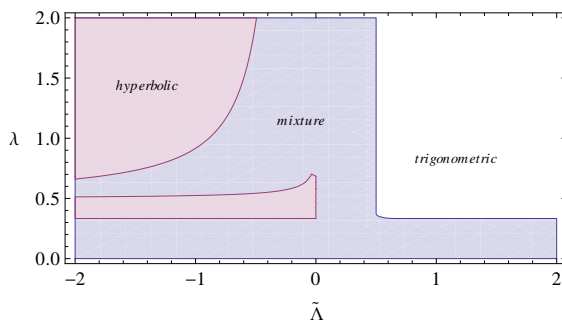


Figure 11.4: Analytic structure of the beta functions for the low-energy limit of HLG in $d = 3$ depending on the dimensionless cosmological constant $\bar{\Lambda}$ and the asymmetry coupling λ .

ε	\bar{G}_*	$\bar{\Lambda}_*$	$\bar{\lambda}_*$	$\theta_{1,2}$	θ_3
+1	0.18	0.13	0.44	$1.79 \pm 1.11i$	2.40
-1	0.20	0.12	0.44	$1.74 \pm 1.08i$	2.48

Table 11.5: NGFP values and corresponding critical exponents within the low-energy limit of HLG for $m = 2\pi$ in $d = 3$.

same analysis for the second argument gives us

$$m > \frac{\sqrt{8\bar{\lambda}_k - 3}}{\sqrt{2(3\bar{\lambda}_k - 1)}}, \quad (11.12)$$

which is smaller than $\sqrt{2}$ if we are close to $\bar{\lambda}_k = 1$. Thus choosing $m > \sqrt{2}$ is sufficient to find a region $0 < \bar{\Lambda}_k < 1/2$ without poles.

As an example we can choose again $m = 2\pi$ and search for fixed points. First of all the beta functions give rise to a GFP. It is situated at

$$\text{GFP:} \quad (\bar{G}_*, \bar{\Lambda}_*, \bar{\lambda}_*) = (0, 0, 1). \quad (11.13)$$

Besides this GFP it is worth searching for a NGFP, since the high-energy behaviour of our truncation might be interesting in comparison to the symmetric discussion of Section 11.1 and also as a benchmark for future results including higher derivative terms. Specifying $d = 3$ and $m = 2\pi$, the beta functions give rise to a novel NGFP for Lorentzian as well as Euclidean signature. Their values and the corresponding critical exponents are given in Table 11.5. We find that this NGFP is UV-attractive in all three directions and the FP values as well as the critical exponents differ only slightly while changing the signature. This difference again decreases if we increase the Kaluza-Klein mass m . The FP values and the critical exponents depending on m are depicted in Figure 11.5. It is very well visible that for increasing mass m the Euclidean and the Lorentzian signature approach each other. Explicitly, the values of $\bar{G}_k^{(d)}$ and $\bar{\Lambda}_k$ and the critical exponents $\theta_{1/2}$ tend towards the values of the compactification limit discussed in Section 11.1 (see Table 11.2). Moreover, the third critical exponent approaches $\theta_3 = 2.44$. The last plot in Figure 11.5 illustrates two facts. First, as one would expect from the other plots, the signature dependence vanishes for large Kaluza-Klein masses m . Second, unexpectedly the decompactification limit $m \rightarrow 0$, corresponding to $\beta \rightarrow 0$, does not lead to a FP $\bar{\lambda}_k = 1$. In contrast, the FP known from the compactification limit in the symmetric analysis is lifted to $\bar{\lambda}^* = 0.44$.

At this point, a closer analysis of the plane $\bar{\lambda}_k = 1$ is in order. For simplicity we restrict ourselves to the case of Euclidean signature with $m = 2\pi$ and $d = 3$. In

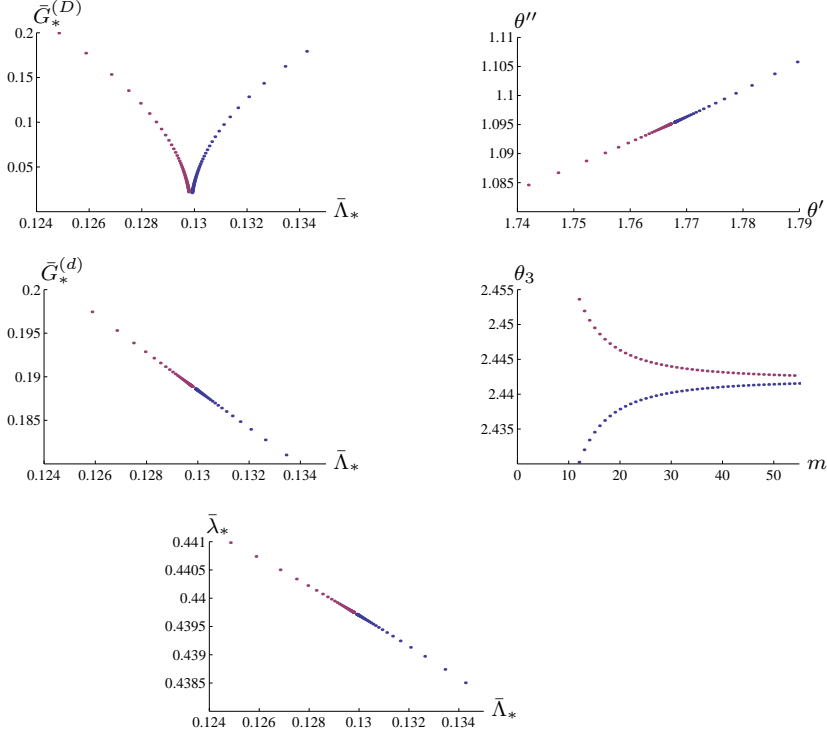


Figure 11.5: Properties of the NGFP emerging in projectable HLG for Lorentzian (red dots) as well as Euclidean (blue dots) signature. The upper left plot shows the FP values of the D -dimensional Newton constant and the cosmological constant depending on m . For increasing Kaluza-Klein mass the FP values for the different signatures approach each other. The upper right plot shows the m dependence of the real part (θ') and the imaginary part (θ'') of the corresponding critical exponents $\theta_{1/2}$. The middle left plot depicts the m dependence of the FP values for the cosmological constant and the d -dimensional Newton constant and the middle right plot shows the m dependence of the third critical exponent. The lowest plot finally depicts the FP values for the cosmological constant and the asymmetry coupling. Again the values for the different signatures approach each other for increasing m .

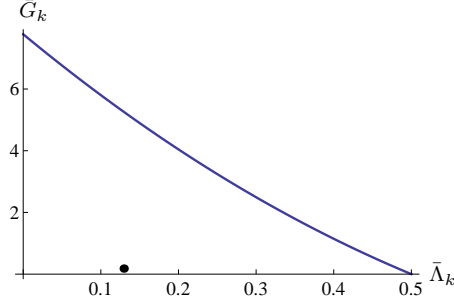


Figure 11.6: Line of vanishing $\beta_{\bar{\chi}}$ for $\bar{\lambda}_k = 1$, $m = 2\pi$ and $\varepsilon = 1$. The black dot denotes the NGFP_{sym}, where $\beta_{\bar{\chi}}$ does not vanish.

In Section 11.1 we found a NGFP in the symmetric limit given in Table 11.3. In the following it shall be denoted by

$$\text{NGFP}_{\text{sym}} : (\bar{G}_*, \bar{\Lambda}_*) = (0.18, 0.13). \quad (11.14)$$

Evaluating the third beta function at this point we find $\beta_{\bar{\chi}} = -1.35$. Thus the hypersurface $\bar{\lambda}_k = 1$ is *not* invariant under RG flows. However, there are points in the plane $\bar{\lambda}_k = 1$ where $\beta_{\bar{\chi}}$ vanishes. Within the most interesting region $0 < \bar{\Lambda}_k < 1/2$ it is actually a line, depicted in Figure 11.6. Notably this line passes by the NGFP_{sym} with quite some distance. However, for different values of m this line looks different. More precisely, for increasing m the line is lowered. However, for increasing m the NGFP_{sym} is lowered as well. Thus there is no NGFP in the three-dimensional theory space for $\bar{\lambda}_k = 1$ and $0 < \bar{\Lambda}_k < 1/2$.

Besides a NGFP, the attraction of trajectories towards the symmetric plane might be achieved by the GFP (11.13). In order to analyse the behaviour of the RG flow in the vicinity of this GFP we linearise the beta functions. Therefore we expand them around $\bar{\lambda}_k = 1$ and expand the two lowest coefficients in \bar{G}_k and $\bar{\Lambda}_k$. The result reads

$$\begin{aligned} \beta_{\bar{G}} &\approx A_0^{\bar{G}} + A_1^{\bar{G}} (\bar{\lambda}_k - 1) \\ \beta_{\bar{\Lambda}} &\approx A_0^{\bar{\Lambda}} + A_1^{\bar{\Lambda}} (\bar{\lambda}_k - 1) \\ \beta_{\bar{\chi}} &\approx A_0^{\bar{\chi}} + A_1^{\bar{\chi}} (\bar{\lambda}_k - 1) \end{aligned} \quad (11.15)$$

with

$$A_0^{\bar{G}} = \bar{G}, \quad A_1^{\bar{G}} = 0, \quad A_0^{\bar{\Lambda}} = \frac{2}{3} \left(\frac{\bar{G}m}{\pi^2} - 3\bar{\Lambda} + \frac{2\bar{G}}{\pi \tanh(\frac{\pi}{m})} \right), \quad A_1^{\bar{\Lambda}} = -\frac{\bar{G}}{9m}, \quad (11.16)$$

and

$$\begin{aligned}
A_0^{\bar{\lambda}} &= -\frac{\bar{G}}{9} \left(\frac{46m}{\pi^2} + \frac{28\pi^2}{45m^3} + \frac{32\pi^4}{2835m^5} \right. \\
&\quad \left. - \frac{13}{3\pi \tanh(\frac{\pi}{m})} - \frac{73}{3m \sin^2(\frac{\pi}{m})} + \frac{98\pi}{3m^2 \tanh(\frac{\pi}{m}) \sin^2(\frac{\pi}{m})} \right), \\
A_1^{\bar{\lambda}} &= -\frac{\bar{G}}{3} \left(\frac{199m}{9\pi^2} + \frac{1}{9m} + \frac{74\pi^2}{135m^3} + \frac{104\pi^4}{2835m^5} + \frac{8\pi^6}{14175m^7} \right. \\
&\quad \left. - \frac{10}{\pi \tanh(\frac{\pi}{m})} - \frac{20}{m \sin^2(\frac{\pi}{m})} + \frac{112\pi}{3m^2 \tanh(\frac{\pi}{m}) \sin^2(\frac{\pi}{m})} \right). \quad (11.17)
\end{aligned}$$

This linearisation shows that the GFP indeed is a fixed point, as $\beta_{\bar{\lambda}}$ vanishes as well. Nevertheless, as soon as we leave the GFP the running in direction of $\bar{\lambda}_k$ sets in. Thus the plane $\bar{\lambda}_k = 1$ is not a fixed plane. The running in direction of $\bar{\lambda}_k$ can be minimised by choosing a suitable value for the Kaluza-Klein mass m . Demanding

$$\left. \frac{d}{dm} A_0^{\bar{\lambda}} \right|_{m=m_{\text{crit}}} = 0 \quad (11.18)$$

we find the critical value numerically to be $m_{\text{crit}} = 1.31$.

For illustrative purposes we specify to this critical value for the Kaluza-Klein mass in the following. Within this setup we can find trajectories emanating from the NGFP with a crossover to the GFP. A sample of such trajectories is depicted in Figure 11.7. This plot of the three dimensional theory space shows the NGFP at the bottom as the origin of all trajectories. The hypersurface $\bar{\lambda}_k = 1$ is highlighted and the trajectories on the right side of the plot pierce through it in the vicinity of the GFP. If they pass by the GFP very close and spend a sufficiently large RG time in the vicinity of $\bar{\lambda}_k = 1$ they might develop a classical regime. As an example we consider the highlighted trajectory running close to $\bar{G}_k = 0$ in the IR a bit further. The scale dependence of the dimensionful couplings corresponding to this trajectory are depicted in Figure 11.8. The first two plots show the RG running of the dimensionful Newton constant \bar{G}_k and the dimensionful cosmological constant $\bar{\Lambda}_k$. At low energies, corresponding to small RG time t , they develop a scale-independent value over a long range of scales. This is required for the formation of a classical regime. The corresponding values achieved in this regime depend on the starting values at high energies and might be tuned to values compatible with observations. The third plot in Figure 11.8 shows the scale dependence of the asymmetry coupling λ . At small scales this coupling turns towards $\lambda = 1$ and stays at this value for a long RG time. This is another requirement for a classical regime. Notably the running of the asymmetry coupling seems to be monotonic which might be related to the c-theorem.

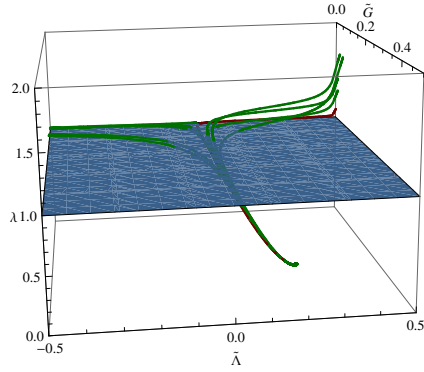


Figure 11.7: Depicted is a sample of trajectories in the Euclidean setting for $d = 3$ and $m = m_{\text{crit}}$. They emanate from the NGFP and pass by the GFP very close. This behaviour allows for a long classical IR regime where GR constitutes a good approximation.

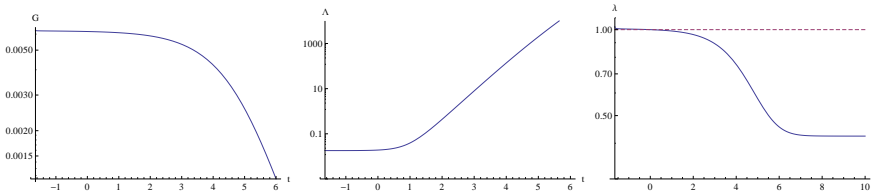


Figure 11.8: Depicted is the scale dependence of the dimensionful couplings corresponding to the highlighted trajectory in Figure 11.7.

Summarising, we found trajectories which emanate from a NGFP and thus are candidates for an Asymptotic Safety scenario. Furthermore they provide a crossover from the NGFP to the GFP. The latter attracts the trajectories to the plane $\bar{\lambda}_k = 1$. Therefore a classical regime develops where GR constitutes a good approximation. This constitutes a quantum theory of gravity which breaks diffeomorphism invariance at high energies and reestablishes it dynamically at low energies via the RG flow. This marks the most remarkable result of this thesis.

Conclusion and Outlook

In this thesis we performed a Functional Renormalisation Group (FRG) analysis of Quantum Einstein Gravity (QEG) and projectable Hořava-Lifshitz gravity (HLG). The central aim is to establish a consistent and predictive theory of Quantum Gravity (QG) within the framework of Quantum Field Theory (QFT). The validity of such a construction requires

- a) a fixed point of the Renormalisation Group (RG) flow which controls the theory's UV behaviour and renders physical quantities safe from unphysical divergences,
- b) a finite number of relevant parameters ensuring the predictivity of the construction,
- c) the emergence of a classical limit which connects the theory to the experimental successes of General Relativity (GR).

This work presented novel insights to all three of these points. We start to summarise our findings for metric gravity before highlighting the results for projectable HLG.

Within the QEG we derived the beta functions for the Einstein-Hilbert truncation. Explicitly, we used the York decomposition for the metric fluctuations as it was done for the first time in [150]. The ghost sector on the other hand was treated along the lines of the pioneering work [114]. These beta functions give rise to a single non-Gaussian fixed point (NGFP) with all the properties required for Asymptotic Safety. To complete this scenario it is necessary to find a trajectory in theory space which connects the NGFP with a suitable low-energy limit. In order to identify such a trajectory we discussed in detail the pole structure in the theory space to find the points where the beta functions are ill defined. The resulting division of the theory space led to a complete classification of all possible trajectories, see Figure 6.1, and extends considerably earlier results [148]. The class containing

the trajectory connecting the NGFP with a suitable classical regime was found as well and is called Type IIIa.

This investigation laid the groundwork for a similar study, also including the higher-derivative operator $\beta_k R^2$. The beta functions of this so-called R^2 truncation have been derived in [117–119]. Therefore, we did not present all details, but concentrated on the main steps for giving the resulting flow equations. The detailed analysis of the flow pattern corresponding to these beta functions was done for the first time and constitutes one of the main results of this thesis. Part of the results have been published in [31] and the thesis extended the discussion of the singular loci contained in the beta functions considerably. As expected the beta functions possess a Gaussian fixed point (GFP). Notably it is found to be situated at vanishing b_k , where $b_k = \frac{1}{\beta_k}$. In three and four spacetime dimensions the beta functions additionally give rise to four and two NGFPs respectively. Focusing on $D = 3$, it was shown that one NGFP is separated from the others by a singular locus. As a consequence the latter can not be connected to a suitable low energy regime. The first NGFP on the other hand can be connected to a regime where classical General Relativity (GR) is a good approximation. This identifies this fixed point as the one featuring Asymptotic Safety. Exemplary trajectories connected to it are depicted in Figure 6.6.

In four spacetime dimensions the situation was found to be more complicated. The reason is a second singular locus, introduced by the zero-modes of the York decomposition. Besides the new pole and the GFP we find two NGFPs, situated close to each other. One of them corresponds to the NGFP found in the original work [117–119] and both are separated by the singular locus. Unfortunately the second singular locus lies very close to the first one and one of the NGFPs is located between them. Thus the evaluation of trajectories is extremely hard. However, the second pole results from the York decomposition, which is just a technical tool. Assuming this to be a technical artefact we turned off the zero-mode contributions responsible for the troublesome pole as a first approximation. This simplification caused the vanishing of one of the two NGFPs. More explicitly, the one known from the original work disappeared. Remarkably, the surviving NGFP and its critical exponents fit better into the table of higher polynomial $f(R)$ truncations and can be used for the construction of an Asymptotic Safety scenario. As this scenario requires the connection of this NGFP to a suitable low energy regime via a trajectory in theory space we discussed some of them and depicted a selection of the most interesting ones in Figure 6.8. Notably it is easy to find trajectories where the corresponding R^2 couplings are compatible with experimental bounds [180,181]. Furthermore it is worth mentioning that the R^2 coupling of the trajectory describing our universe changes sign during the RG running.

As a first application of our classification we analysed the spectral dimension of the effective QEG spacetimes. Within this thesis we started with recapitulating the

results of [30]. There it was shown that the spectral dimension, if the definition is generalised to a scale-dependent version, changes with the RG scale. Explicitly the authors analysed the spectral dimension along some specific trajectories within the Einstein-Hilbert truncation. They found that a trajectory describing our universe would develop a classical plateau, extending over a large range of scales, where the spectral dimension is the topological dimension of the manifold. This behaviour is triggered by the typical running of the dimensionless cosmological constant in the classical regime. Furthermore they showed that fixed points might cause a plateau structure as well. Explicitly the NGFP causes a plateau with spectral dimension equal to $D/2$, where D denotes the spacetime dimension. Another plateau with spectral dimension equal to $2D/(2+D)$ is caused by the GFP. Notably, a reasonable agreement between the results of Causal Dynamical Triangulations and QEG was found.

As the second novelty contained in this thesis we extended this analysis to the R^2 truncation. The results have been published in [31]. Most importantly we have been able to confirm the NGFP plateau with spectral dimension equal to $D/2$ and the classical plateau with spectral dimension equal to D . The intermediate regime revealed a novel possible cause for the development of a plateau with constant spectral dimension over a long range of scales. Besides the fixed points, a singular locus can produce such a behaviour. In this sense we have shown that it is possible to find two intermediate regimes, one corresponding to the GFP and one to the singular locus. As a drawback, the resulting scale-dependent spectral dimension develops poles. However, these poles appear between the plateaus and since the spectral dimension is well defined in regimes where it is approximately constant, no physical meaning should be attributed to these poles.

Besides the metric formulation, we used the Functional Renormalisation Group Equation (FRGE) in a foliated setup for the first investigation of RG flows on the theory space of projectable HLG. This theory proposes the introduction of an explicit asymmetry between space and time to save perturbative renormalisability. First results of this foliated formulation have been published in [167], the corresponding technical details for the derivation of the flow equations are published in [168] and a third work [169] is currently in progress. Within this new formulation the spacetime metric was decomposed according to the Arnowitt-Deser-Misner formalism. The gravitational degrees of freedom are then carried by the lapse function, the shift vector and the spatial metric. Although the formulation of gravity within these new fields is classically equivalent to GR, it might differ at the quantum level. The natural symmetry of the theory space constructed from the new variables is the invariance under foliation-preserving diffeomorphisms which build a subgroup of the spacetime diffeomorphisms.

We started by deriving the FRGE for foliated spacetimes. Therefore we introduced an alternative formulation for regulating the quantum fluctuations in time

direction as it is known in finite temperature field theory. In contrast to the usual regulator insertion we used a finite length of the time direction β which becomes a circle by introducing periodic boundary conditions. The spatial quantum fluctuations have been regulated in the standard way by introducing a regulator insertion. This construction resulted in a flow equation for the projectable version of Hořava-Lifshitz Gravity.

Building on the FRGE we studied the RG flow of the foliated Einstein-Hilbert truncation (10.1). It contains a volume term, an intrinsic curvature term and two extrinsic curvature terms. These three terms have to appear with a specific ratio to preserve the D -dimensional diffeomorphism invariance. The inclusion of an asymmetry coupling λ_k enabled us to change the ratio between the intrinsic and the extrinsic part of the truncation. Thus for $\lambda_k = 1$ the gravitational part of our truncation is diffeomorphism invariant and $\lambda_k \neq 1$ breaks this symmetry explicitly and leads to an invariance under foliation preserving diffeomorphisms. The beta functions have been derived for the latter case and the former can be found in the limit $\lambda_k = 1$. Notably the foliated framework enabled us to introduce a signature parameter ε , which was used to switch from Euclidean ($\varepsilon = +1$) to Lorentzian signature ($\varepsilon = -1$). Thus, the resulting beta functions depend on the coupling constants themselves as well as on the signature parameter ε and the Kaluza-Klein mass m . The latter is proportional to the inverse of the length of the time interval β . Thus we found a scale dependence of m or respectively β without any further information in form of an additional beta function.

These flow equations of the foliated formulation have been discussed first in the limit $\lambda_k = 1$ where we kept ε as a free parameter. We analysed the analytic structure and found that it depends on the signature as well as on the value of the cosmological constant. Depending on them the beta functions might be constructed of trigonometric or hyperbolic functions only. There is also a region, where the flow equations are constructed from both types of functions. As the scale dependence of the Kaluza-Klein mass m or respectively the time-interval length β was still at our disposal we used first a scale-independent β . More explicitly we discussed the compactification limit $\beta \rightarrow 0$ and the decompactification limit $\beta \rightarrow \infty$. The latter one did not reveal any suitable fixed points that could give rise to Asymptotic Safety. In the former limit however, the dependence on trigonometric and hyperbolic functions of the flow equations vanishes and the simplified beta functions indeed give rise to a NGFP. As the time circle collapses in this limit we found an effectively $(D-1)$ -dimensional theory and the signature dependence disappeared. The resulting fixed points have been compared to known results in various dimensions and showed an excellent agreement with previous computations using the metric formulation. The numerical differences are of the typical size expected from working with different choices of the regulator.

As a second scenario we analysed the beta functions for scale-independent mass m . Again we found a NGFP whose properties depend on this parameter. In the limit of $m \rightarrow \infty$ the NGFP turned into the one found in the compactification limit. As an example we analysed the system with $m = 2\pi$ in detail. We found that the corresponding phase space shows only minor difference between the Euclidean and the Lorentzian version. Moreover, both are similar to the phase space known from the metric formulation. This demonstrates that the signature plays a minor role for the high energy behaviour of Quantum Einstein Gravity. This statement constitutes the next main result of this thesis.

The final topic addressed in this thesis is the low-energy limit of projectable HLG. Again we started with the analysis of the analytic structure of the flow equations and found that it is similar to the one encountered for $\bar{\lambda}_k = 1$. Next, the discussion of the scenario with a scale-independent Kaluza-Klein mass m revealed a NGFP. This seems to be the fixed point found in the limit $\bar{\lambda}_k = 1$, lifted to a value of $\bar{\lambda}_k \neq 1$. For increasing m the fixed-point values for the Lorentzian and the Euclidean signature tend towards each other. In the compactification limit the signature dependence again vanishes. We showed that the Newton constant and the cosmological constant find the fixed-point values of the foliated Einstein-Hilbert truncation in this limit, but the fixed-point value of the asymmetry coupling $\bar{\lambda}_k$ does not approach $\bar{\lambda}_k = 1$. Moreover, we demonstrated explicitly that the Gaussian fixed point can be used as an attractor for trajectories of asymmetric theories. Choosing suitable starting values, these trajectories can develop a classical regime where General Relativity constitutes a good approximation. This statement constitutes another important result of this thesis.

Besides the results obtained in this thesis the techniques and insights obtained here can be used to investigate further interesting questions. One interesting task for future work would be an alternative calculation of the beta functions for the R^2 truncation within the metric formulation of Quantum Einstein Gravity. A derivation which circumvents the York decomposition is likely to find beta functions without the second singular locus and might shed some light on the fate of the second NGFP found in four dimensions. Within this truncation it might also be interesting to investigate cosmological consequences of the observed effect as the running of the R^2 coupling or the change of the sign of the cosmological constant.

The novel FRGE for gravity on foliated spacetimes also opens up a wide range of possible applications. The most interesting one is the inclusion of higher orders in the spatial curvature within the truncation in order to investigate the high energy behaviour of Hořava-Lifshitz Gravity as well. Based on this extension the open question concerning the conjectured perturbative renormalisability of HLG may finally be settled.

Notation and Conventions

In the following we will summarise the notations and conventions used throughout the thesis.

Most importantly we set the Planck constant \hbar and the speed of light c equal to one for simplicity. This simplifies many equations considerably and is commonly used throughout the cited literature. Using this convention, the following identities for the units hold

$$\hbar = 1 = c \quad \Rightarrow \quad [\text{length}] = [\text{time}] = [\text{mass}]^{-1} = [\text{energy}]^{-1}. \quad (\text{A.1})$$

This thesis discusses gravitational theories and thus we have to fix some conventions for the curved spacetime. The first difference to standard notation is the nomenclature of the dimension. As we frequently encounter the spacetime dimension as well as the spatial dimension we denote the former by D and the latter by d . The second important convention considers the metric itself. Throughout the high-energy-physics literature mainly the timelike convention for the metric is used, which is $(+, -, -, \dots)$. However, the GR literature is dominated by the spacelike convention $(-, +, +, \dots)$. Within this thesis we stick to the latter one in order to save ε 's which are used to switch the signature. Thus we utilise the following

$$\text{signature: } (\varepsilon, +, +, \dots), \quad \varepsilon = \begin{cases} +1 & \text{Euclidean} \\ -1 & \text{Lorentzian} \end{cases}. \quad (\text{A.2})$$

Note that in Part II we are using the spacetime metric $g_{\mu\nu}$ and its inverse $g^{\mu\nu}$ defined via $g_{\mu\nu}g^{\nu\rho} = \delta_{\mu}^{\rho}$, where δ_{μ}^{ρ} denotes the Kronecker delta. However, in Part III the spatial metric, denoted by σ_{ij} , and its inverse σ^{ij} with $\sigma_{ij}\sigma^{jk} = \delta_i^k$ is used. Throughout the thesis we will employ Greek indices for spacetime coordinates and Latin indices for purely spatial coordinates.

For the spacetime metric $g_{\mu\nu}$ we define the Christoffel symbols $\Gamma_{\mu\nu}^{\lambda}$ and the

Constant	$D_{2\text{T}}$	$d_{2\text{T}}$	C_0	$C_{2\text{T}}$
Definition	$\frac{(D+1)(D-2)}{2}$	$\frac{(d+1)(d-2)}{2}$	$\frac{(d-2)(d-1)}{d^2}$	$\frac{d^2-3d+4}{d(d-1)}$

Table A.1: List of frequently used constants.

Riemann tensor $R_{\mu\nu\rho}{}^\lambda$ according to

$$\begin{aligned}\Gamma_{\mu\nu}{}^\lambda &= \frac{1}{2}g^{\lambda\sigma}(\partial_\mu g_{\nu\sigma} + \partial_\nu g_{\mu\sigma} - \partial_\sigma g_{\mu\nu}), \\ R_{\mu\nu\rho}{}^\lambda &= \partial_\nu \Gamma_{\mu\rho}{}^\lambda - \partial_\mu \Gamma_{\nu\rho}{}^\lambda + \Gamma_{\mu\rho}{}^\sigma \Gamma_{\nu\sigma}{}^\lambda - \Gamma_{\nu\rho}{}^\sigma \Gamma_{\mu\sigma}{}^\lambda.\end{aligned}\tag{A.3}$$

Finally, the Ricci tensor and the Ricci scalar are the contractions of the Riemann tensor and read $R_{\mu\nu} = R_{\mu\lambda\nu}{}^\lambda$ and $R = g^{\mu\nu} R_{\mu\nu}$. The last frequently used object is the covariant derivative, which we call ∇_μ . Its commutator is related to the Riemann tensor via

$$\begin{aligned}[\nabla_\mu, \nabla_\nu]A_\lambda &= R_{\mu\nu\lambda}{}^\rho A_\rho, \\ [\nabla_\mu, \nabla_\nu]H_{\lambda\sigma} &= R_{\mu\nu\lambda}{}^\rho H_{\rho\sigma} + R_{\mu\nu\sigma}{}^\rho H_{\lambda\rho},\end{aligned}\tag{A.4}$$

where A_μ is an arbitrary 1-form and $H_{\lambda\sigma}$ denotes a $(0,2)$ tensor. The objects corresponding to the spatial metric are defined analogously.

This thesis uses the FRGE for the EAA and thus we have to handle different versions of the same field. First of all we use the quantum fields which are marked with a tilde on top. The quantum spacetime metric e.g. reads $\tilde{g}_{\mu\nu}$. As we are using the background field method (see Appendix B.2), the quantum fields are split into background fields and fluctuations. The former are marked with a bar on top and the latter with a hat. Thus the quantum spacetime metric splits according to $\tilde{g}_{\mu\nu} = \bar{g}_{\mu\nu} + \hat{g}_{\mu\nu}$. Finally, our main object of interest is the EAA and therefore we use the averaged fields. These are not marked at all and the averaged spacetime metric, as an example, is denoted by $h_{\mu\nu} = \langle \hat{g}_{\mu\nu} \rangle$. Note that this notation differs from the one usually used in the literature.

For those who just skim the thesis we give an overview over some frequently used constants defined in the text, so the reader does not have to search for their definition. The list can be found in Table A.1.

Gauge Symmetry and Quantisation

B.1 The Faddeev-Popov Method

This appendix is dedicated to the treatment of gauge symmetries within the path integral approach. Let us begin by briefly discussing the problem. The physical information of a theory can be extracted completely out of the partition function

$$Z[J] = \int \mathcal{D}\tilde{\varphi} \exp \left[-S[\tilde{\varphi}] + \int d^D x J(x) \tilde{\varphi}(x) \right], \quad (\text{B.1})$$

Here $\tilde{\varphi}$ denotes the field content of our theory, J is the corresponding source and $S[\tilde{\varphi}]$ is the classical action. In case, the theory under consideration possesses a gauge symmetry, this partition function is ill-defined since we are integrating over gauge-equivalent field configurations. As these are describing the same physics we would like to count only one per set of gauge-equivalent configuration within the path integral. This can be achieved along the line proposed by Faddeev and Popov in 1967 [182]. In the following we will summarise this idea and thereby follow [82].

Let us denote the spacetime-dependent parameter of the gauge transformation with $\gamma(x)$, and $G[\tilde{\varphi}]$ shall be the functional which fixes the gauge by demanding $G[\tilde{\varphi}] = 0$. In order to single out one field configuration from the orbit of physically equivalent ones we would like to insert a $\delta(G[\tilde{\varphi}])$ under the path integral. Without changing the partition function this can be done by inserting a 1 which we write as

$$1 = \int \mathcal{D}\gamma(x) \delta(G[\tilde{\varphi}]) \det \left(\frac{\delta G(\tilde{\varphi}^\gamma)}{\delta \gamma} \right), \quad (\text{B.2})$$

with $\tilde{\varphi}^\gamma$ denoting the transformed field. This expression is nothing but a generalisation of $1 = \int dx \delta(f(x)) |\partial f / \partial x|$. Note that, as long as G is linear, the determinant is independent of γ and thus the integration with respect to γ gives

just a normalisation \mathcal{N} . If we insert this expression into the partition function we find

$$\begin{aligned} Z &= \mathcal{N} \int \mathcal{D}\tilde{\varphi} e^{-S[\tilde{\varphi}] + \int d^D x J \tilde{\varphi}} \delta(G(\tilde{\varphi})) \det\left(\frac{\delta G(\tilde{\varphi}^\gamma)}{\delta \gamma}\right) \\ &= \mathcal{N} \int \mathcal{D}\tilde{\varphi} \mathcal{D}\bar{\omega} \mathcal{D}\omega e^{-S[\tilde{\varphi}] - \int \frac{G^* G}{2\alpha} - \int \bar{\omega} \mathcal{M} \omega + \int (J \tilde{\varphi} + \bar{\eta} \omega + \bar{\omega} \eta)}. \end{aligned} \quad (\text{B.3})$$

Here we exponentiated the determinant by introducing the Grassmann valued ghost and anti-ghost fields $\omega, \bar{\omega}$, including the corresponding sources $\bar{\eta}, \eta$. We introduced \mathcal{M} as an abbreviation for $\delta G(\tilde{\varphi}^\gamma)/\delta \gamma$ and suppressed the measure $d^D x$ of the exponentiated integrals. Furthermore we replaced the delta distribution with $\exp[-\int \frac{G^* G}{2\alpha}]$ where α is called gauge parameter. Typical gauges are the Landau gauge $\alpha \rightarrow 0$ or the Feynman-'t Hooft gauge $\alpha \rightarrow 1$.

The partition function (B.3) now can serve as a starting point for further investigations, since the unphysical overcounting of equivalent field configurations is controlled by the introduction of the gauge-fixing action $S^{\text{gf}} = \int \frac{G^* G}{2\alpha}$ and the corresponding ghost action $S^{\text{gh}} = \int \bar{\omega} \mathcal{M} \omega$.

B.2 The Background Field Method

In Appendix B.1 we have seen that the quantisation of a gauge theory within the path-integral formalism asks for the introduction of a gauge-fixing and a ghost term. By construction these terms explicitly break the underlying gauge symmetry, as e.g. in Landau-gauge QCD, where the gauge condition reads $\partial_\mu A^\mu = 0$. Nevertheless, any observable quantity will be independent of the chosen gauge. On the other hand, quantities without a physical interpretation, as e.g. Green functions, will not be invariant. Especially Green functions, instead of respecting the gauge symmetry, satisfy Slavnov-Taylor identities.

At the level of the EAA the gauge symmetry leads to modified Ward identities, derived as follows. Starting point is the scale-dependent partition function

$$Z_k[J] = \int \mathcal{D}\tilde{\Phi} \exp\left[-S[\tilde{\Phi}] - \Delta S_k[\tilde{\Phi}] + \int d^D x J(x) \tilde{\Phi}(x)\right]. \quad (\text{B.4})$$

Here $\tilde{\Phi}$ denotes the field content of the theory. Thus it includes the field of the microscopic action as well as the ghost fields, appearing due to the Faddeev-Popov method. The corresponding sources are summarised as J and we added the regulator term $\Delta S_k[\tilde{\Phi}]$. Assuming that the field $\tilde{\Phi}$ transforms as $\tilde{\Phi} \rightarrow \tilde{\Phi} + \delta\tilde{\Phi}$ and that the measure of the path integral is invariant, the variation of (B.4) reads

$$0 = \int \mathcal{D}\tilde{\Phi} \left(-\frac{\delta(S[\tilde{\Phi}] + \Delta S_k[\tilde{\Phi}])}{\delta\tilde{\Phi}} \delta\tilde{\Phi} + J \delta\tilde{\Phi} \right) e^{-S - \Delta S_k + \int d^D x J \tilde{\Phi}}. \quad (\text{B.5})$$

Explicitly, we are not interested in the properties of the k -dependent partition function but of the EAA. Thus we have to switch to the k -dependent Schwinger functional $W_k[J] = \ln Z_k[J]$ and perform the Legendre transformation thereof. Starting with (B.5) we find

$$\begin{aligned} 0 &= \frac{1}{Z_k} \int \mathcal{D}\tilde{\Phi} \left(-\frac{\delta(S[\tilde{\Phi}] + \Delta S_k[\tilde{\Phi}])}{\delta\tilde{\Phi}} \delta\tilde{\Phi} + J \delta\tilde{\Phi} \right) e^{-S - \Delta S_k + \int d^D x J \tilde{\Phi}} \\ &= - \left\langle \frac{\delta(S + \Delta S_k)}{\delta\tilde{\Phi}} \delta\tilde{\Phi} \right\rangle_J + e^{-W_k[J]} \int d^D x J \delta\tilde{\Phi} \Big|_{\tilde{\Phi} = \frac{\delta}{\delta J}} e^{W_k[J]}. \end{aligned} \quad (\text{B.6})$$

The Legendre transformation of this at the supremum of the source, J_{sup} , reads

$$\begin{aligned} 0 &= - \left\langle \frac{\delta(S + \Delta S_k)}{\delta\tilde{\Phi}} \delta\tilde{\Phi} \right\rangle_{J_{\text{sup}}} + \int d^D x \frac{\delta\Gamma[\Phi]}{\delta\Phi} \delta\Phi + \delta\Delta S_k \\ &\Rightarrow \delta\Gamma_k = \langle \delta(S + \Delta S_k) \rangle_{J_{\text{sup}}} - \delta\Delta S_k. \end{aligned} \quad (\text{B.7})$$

Here Φ denotes the expectation value of $\tilde{\Phi}$ and Γ_k is the EAA. The final result in (B.7) is called modified Ward identity and includes the ordinary Ward identity,

$$\delta\Gamma = \langle \delta S \rangle_{J_{\text{sup}}}, \quad (\text{B.8})$$

as the limit $k \rightarrow 0$. An equivalent expression is true at any scale for symmetric regulator terms. However, in general the regulator term is non symmetric and thus, the initial conditions in the UV have to be chosen such that the non-symmetric terms at the initial point are cancelled during the flow towards the IR. This is anything but simple. To circumvent this problem, and the problem of non-covariant S due to gauge-fixing and ghost terms, one can use the Background Field Method (BFM) explained in the following. For an introduction see [183]. In the context of the FRG, the interested reader might also be referred to [91] or, for gravitational theories, [184].

The BFM is a tool which enables us to retain the gauge symmetry for non-observable quantities and we will concentrate on the example of the EAA. As the name suggests a crucial ingredient is the background field. We split the quantum field $\tilde{\Phi}$ into an arbitrary, non-dynamical background $\bar{\Phi}$ and fluctuations $\hat{\Phi}$ around it via $\tilde{\Phi} = \bar{\Phi} + \hat{\Phi}$. Now the functional integration over the quantum field is replaced by an integration over the fluctuations, which are not assumed to be small in any sense. The variation $\tilde{\Phi} \rightarrow \tilde{\Phi} + \delta\tilde{\Phi}$ can be decomposed in different ways

$$\text{Quantum:} \quad \hat{\Phi} \rightarrow \hat{\Phi} + \hat{\delta}\hat{\Phi}, \quad \bar{\Phi} \rightarrow \bar{\Phi} \quad (\text{B.9})$$

$$\text{Background:} \quad \hat{\Phi} \rightarrow \hat{\Phi} + \bar{\delta}\hat{\Phi}, \quad \bar{\Phi} \rightarrow \bar{\Phi} + \bar{\delta}\bar{\Phi} \quad (\text{B.10})$$

where $\delta\tilde{\Phi} = \hat{\delta}\hat{\Phi} = \bar{\delta}(\bar{\Phi} + \hat{\Phi})$. We call (B.9) the quantum gauge transformations and (B.10) background gauge transformations. Note that the former is the one which

has to be fixed, while the latter is an auxiliary symmetry and should merely be treated as a technical tool. The next step is to find a classical action (including gauge-fixing and ghost term) which breaks the quantum gauge transformation but is invariant under the background version. To use again the above example, we can replace the Landau gauge condition $\partial_\mu A^\mu = 0$ by the Landau-DeWitt condition $\bar{\nabla}_\mu \hat{A}^\mu = 0$ with the fluctuation \hat{A} and the covariant derivative $\bar{\nabla}_\mu$ constructed from the background field \bar{A}_μ . The ghost action can be adapted similarly.

Starting from the k -dependent partition function (this time with an integration with respect to $\hat{\phi}$) we finally get the so-called Background Effective Average Action (BEAA) $\Gamma_k[\Phi, \bar{\Phi}]$. This, in contrast to the standard EAA, depends on the background field $\bar{\Phi}$ and the classical field reads $\Phi = \bar{\Phi} + \langle \hat{\Phi} \rangle$. Note that the BEAA breaks the quantum gauge transformation (B.9) but preserves the background gauge transformation (B.10) if we adapt the regulator term, ΔS_k , such that it preserves (B.10). This gives us RG flows invariant under the background gauge transformations. In the limit $k \rightarrow 0$ we find the Background Effective Action (BEA) $\Gamma[\Phi, \bar{\Phi}]$ explicitly depending on the background $\bar{\Phi}$. Setting $\Phi = \bar{\Phi}$, the invariance of the BEA under (B.10) implies that the EA is invariant under the initial gauge symmetry

$$0 = \bar{\delta}\Gamma[\Phi, \bar{\Phi}]|_{\Phi=\bar{\Phi}} = \delta\Gamma[\Phi]. \quad (\text{B.11})$$

We refrain from giving an explicit proof that the BEA at $\Phi = \bar{\Phi}$ indeed is the usual EA. For more details see e.g. [91] and references therein.

Summarising the BFM, we start by introducing an arbitrary, non-dynamical background field. We impose that the classical, gauge-fixed action (including ΔS_k) is invariant under background gauge transformations (B.10). Finally, after integrating towards the IR, we identify the background with the expectation value of the quantum field to find an EA, which is invariant under the initial gauge symmetry.

The Heat-Kernel Technique

C.1 The Early-Time Expansion

The main technical tool of this thesis is the Wetterich equation (2.15). On the right hand side we encounter operator traces over functions of the covariant Laplacian Δ . In the following we will stick to a general D -dimensional metric $g_{\mu\nu}$ and follow the appendices in [119] and [121]. However, the d -dimensional analog, used in Part III, can be obtained easily by replacing D by d .

Generally, we encounter traces of the form $\text{Tr}[W(\Delta)]$ where Tr denotes an operator trace as well as a trace in field space. The Laplace operator acts on the metric $g_{\mu\nu}$ which can be expanded in terms of its eigenfunctions [185, 186]. Denoting the eigenvalues with Λ_n , this leads to

$$\text{Tr}[W(\Delta)] = \text{tr} \sum_n W(\Lambda_n) \quad (\text{C.1})$$

with tr denoting the left-over trace in field space. However, it is extremely hard to solve the traces this way. Thus, we will use an approximation called the early-time expansion also known as the heat-kernel expansion [165, 166].

Before we give the explicit form of this expansion we define the Laplace-anti transform $\tilde{W}(s)$ for the general function W according to

$$W(z) = \int_0^\infty ds \tilde{W}(s) e^{-zs}. \quad (\text{C.2})$$

Note that for functions W encountered in this thesis it is a well-defined transformation. Using (C.2) we can rewrite the trace such that, instead of the trace of the general function W , we now have to handle the trace of the heat kernel $e^{-s\Delta}$

$$\text{Tr}[W(\Delta)] = \int_0^\infty ds \tilde{W}(s) \text{Tr}[e^{-s\Delta}]. \quad (\text{C.3})$$

Although we find Laplace operators of the form $\Delta = -\nabla^2$ throughout the main text, it is easy, useful, and indeed necessary (see Appendix C.3), to generalise to a dependence on $\Delta + qR$. Here q is a real number and R denotes the scalar curvature. In order to evaluate the trace of the heat kernel we use the early-time expansion [165, 166] which reads in general

$$\mathrm{Tr} \left[e^{-s(\Delta+qR)} \right] = \frac{1}{(4\pi s)^{D/2}} \int d^D x \sqrt{g} \left[\mathrm{tr} a_0 + s \mathrm{tr} a_2 + s^2 \mathrm{tr} a_4 + \dots \right]. \quad (\text{C.4})$$

Here again tr denotes the left-over trace in field space and the a_i are the heat-kernel coefficients. The first two of them read

$$a_1 = \mathbb{1}, \quad a_2 = \left(\frac{1}{6} - q \right) R \mathbb{1} \quad (\text{C.5})$$

with $\mathbb{1}$ being the unit matrix in field space. Therefore we find $\mathrm{tr} \mathbb{1}$ to be 1, D and $\frac{D}{2}(D+1)$ for scalars, vectors and symmetric tensors, respectively.

However, the heat-kernel coefficients differ from those given in (C.5), if we consider fields with constraints. In Appendix C.2 we explain, how such constraints enter our calculations. Afterwards, in Appendix C.3, we derive the new coefficients.

C.2 The York Decomposition and Spherical Backgrounds

This appendix introduces a decomposition of the metric fluctuations which is used in Part II and Part III of this thesis. It is the so-called transverse-traceless (TT) or York decomposition [175]. Note that in Part II the fluctuation of the spacetime metric, $h_{\mu\nu}$, is decomposed while in Part III the fluctuation of the spatial metric, h_{ij} , is decomposed. The explanation here will concentrate on the spacetime-metric case in the sense that we use indices μ, ν, \dots and D for the dimension. However the purely spatial version is analog and can be achieved by using spatial indices and dimension d instead.

The York decomposition is used to evaluate the right hand side of the Wetterich equation (2.15), which consists of traces of functions of operator structures as discussed in Appendix C.1. Although it simplifies the inversion of the operator structure $\Gamma_k^{(2)} + \mathcal{R}_k$ one has to be careful, while evaluating the functional traces.

The most important operator within our calculation is the Laplacian $\Delta = -\nabla^2$. Here ∇_μ denotes the covariant derivative with respect to the metric, which we split into a fixed background metric $\bar{g}_{\mu\nu}$ and fluctuations around it $h_{\mu\nu}$. The TT decomposition of the latter reads

$$h_{\mu\nu} = h_{\mu\nu}^{\mathrm{TT}} + \bar{\nabla}_\mu \xi_\nu + \bar{\nabla}_\nu \xi_\mu + \bar{\nabla}_\mu \bar{\nabla}_\nu \varsigma - \frac{1}{D} \bar{g}_{\mu\nu} \bar{\nabla}^2 \varsigma + \frac{1}{D} \bar{g}_{\mu\nu} \phi. \quad (\text{C.6})$$

Here D denotes the spacetime dimension and $\bar{\nabla}_\mu$ is the covariant derivative with respect to the background metric $\bar{g}_{\mu\nu}$. Furthermore $h_{\mu\nu}^{\text{TT}}$ denotes the transverse traceless part of the metric, ϕ is the trace and ξ_μ is a transverse vector. Thus we have

$$\bar{g}^{\mu\nu}h_{\mu\nu}^{\text{TT}} = 0, \quad \bar{\nabla}^\mu h_{\mu\nu}^{\text{TT}} = 0, \quad \bar{\nabla}^\mu \xi_\mu = 0, \quad \bar{g}^{\mu\nu}h_{\mu\nu} = \phi. \quad (\text{C.7})$$

Having a closer look at the decomposition (C.6) we find that not all vectors ξ_μ and not all scalars ς contribute to the physical field $h_{\mu\nu}$. The ones which do not contribute are those satisfying the Killing equation and the conformal Killing equation, respectively

$$\bar{\nabla}_\mu \xi_\nu + \bar{\nabla}_\nu \xi_\mu = 0, \quad \bar{\nabla}_\mu \bar{\nabla}_\nu \varsigma - \frac{1}{D} \bar{g}_{\mu\nu} \bar{\nabla}^2 \varsigma = 0. \quad (\text{C.8})$$

Note that the solution of these equations depends on the background. This will become important if we calculate e.g. traces in field space on a spherical background.

Within this thesis the appearing traces are evaluated on special backgrounds. These are maximally symmetric, compact spaces with constant curvature \bar{R} . Thus the Riemann tensor and Ricci tensor assume the form

$$\bar{R}_{\mu\nu\rho\sigma} = \frac{\bar{R}}{D(D-1)} (\bar{g}_{\mu\rho} \bar{g}_{\nu\sigma} - \bar{g}_{\mu\sigma} \bar{g}_{\nu\rho}), \quad \bar{R}_{\mu\nu} = \frac{\bar{R}}{D} \bar{g}_{\mu\nu}. \quad (\text{C.9})$$

Here the Ricci scalar \bar{R} is a constant and related to the radius of the sphere by

$$\bar{R} = \frac{D(D-1)}{r^2}, \quad \int d^D x \sqrt{\bar{g}} = \frac{\Gamma(D/2)}{\Gamma(D)} (4\pi r^2)^{D/2}. \quad (\text{C.10})$$

The second part of this equation relates the volume to the radius via the Gamma function Γ .

Coming back to the trace of the decomposed metric we can now expand the component fields in terms of the spherical harmonics T^{lm} , T_μ^{lm} and $T_{\mu\nu}^{lm}$. These constitute eigenfunctions of the covariant background Laplacian $\Delta = -\bar{\nabla}^2$ and form an orthogonal basis. Therefore we find

$$\begin{aligned} \Delta T^{lm}(x) &= \Lambda_l(D, 0) T^{lm}(x), \\ \Delta T_\mu^{lm}(x) &= \Lambda_l(D, 1) T_\mu^{lm}(x), \\ \Delta T_{\mu\nu}^{lm}(x) &= \Lambda_l(D, 2) T_{\mu\nu}^{lm}(x). \end{aligned} \quad (\text{C.11})$$

The eigenvalues $\Lambda_l(D, s)$ depend on the spin s of the field and correspond to the Laplacian acting on this field. Thus l takes the values $s, s+1, \dots$ and m counts the multiplicity $D_l(D, s)$ of the degenerate eigenvalues. The eigenvalues and degeneracies have been derived in [185, 186] and are given in Table C.1.

s	$\Lambda_l(D, s)$	$D_l(D, s)$	l
0	$\frac{l(l+D-1)}{D(D-1)} \bar{R}$	$\frac{(2l+D-1)(l+D-2)!}{l!(D-1)!}$	$0, 1, \dots$
1	$\frac{l(l+D-1)-1}{D(D-1)} \bar{R}$	$\frac{l(l+D-1)(2l+D-1)(l+D-3)!}{(D-2)!(l+1)!}$	$1, 2, \dots$
2	$\frac{l(l+D-1)-2}{D(D-1)} \bar{R}$	$\frac{(D+1)(D-2)(l+D)(l-1)(2l+D-1)(l+D-3)!}{2(D-1)!(l+1)!}$	$2, 3, \dots$

Table C.1: Eigenvalues $\Lambda_l(D, s)$ and degeneracies $D_l(D, s)$ of the background Laplace operator $\Delta = -\bar{\nabla}^2$ acting on fields with spin s .

Using (C.11), the expansions of the scalar (spin-0) field ϕ and the spin-2 field $h_{\mu\nu}^{\text{TT}}$ read

$$\phi(x) = \sum_{l=0}^{\infty} \sum_{m=1}^{D_l(D,0)} \phi_{lm} T^{lm}(x), \quad h_{\mu\nu}^{\text{TT}}(x) = \sum_{l=2}^{\infty} \sum_{m=1}^{D_l(D,2)} h_{lm}^{\text{TT}} T_{\mu\nu}^{lm}(x). \quad (\text{C.12})$$

The situation changes if we consider the spin 0 field ς . Here we have to exclude those modes satisfying the conformal Killing equation (C.8). Thus, in comparison to the expansion of ϕ we find

$$\varsigma(x) = \sum_{l=2}^{\infty} \sum_{m=1}^{D_l(D,0)} \varsigma_{lm} T^{lm}(x). \quad (\text{C.13})$$

The expansion of the spin 1 field ξ_μ has to be treated similarly. The expansion does not start at $l = 0$, as we have to exclude the solutions of the Killing equation (C.8). Thus we find

$$\xi_\mu(x) = \sum_{l=2}^{\infty} \sum_{m=1}^{D_l(D,1)} \xi_{lm} T_\mu^{lm}(x). \quad (\text{C.14})$$

For more details see e.g. [119] and references therein. These exclusions within the expansion of ς and ξ_μ will become important when we evaluate traces of the Laplacian acting on these constrained fields (see Appendix C.3).

C.3 Heat-Kernel Coefficients for Fields with Constraints

In Appendix C.1 we explained how to evaluate the traces appearing on the right hand side of the Wetterich equation with the heat-kernel expansion. Afterwards

we discussed in Appendix C.2 the York decomposition of the metric fluctuations and we had to deal with unphysical zero modes. In the following we will elaborate on the consequences of the decomposition for the heat-kernel coefficients.

As we did in Appendix C.2, we use the background split of the metric into the background metric $\bar{g}_{\mu\nu}$ and fluctuations $h_{\mu\nu}$, where the background is specified to the spherical one explained in (C.9).

According to (C.3), the main task is to evaluate the trace of the heat kernel $\text{Tr} \exp[-s\Delta]$. Here the background Laplacian Δ acts on the metric fluctuations which we decompose, according to the York decomposition (C.6), into the TT part $h_{\mu\nu}^{\text{TT}}$, transverse vectors ξ_μ and scalars ζ and ϕ . As discussed in Appendix C.2, ξ_μ and ζ are constrained fields in the sense that those modes satisfying the Killing equation and conformal Killing equation (C.8) do not contribute to the full metric. This effects the heat-kernel expansion considerably and the consequences will be explained in the following.

Acting with the Laplacian on the Killing equation and using the commutation relation we find

$$\Delta(\bar{\nabla}_\mu \xi_\nu + \bar{\nabla}_\nu \xi_\mu) = \bar{\nabla}_\mu \left(\Delta - \frac{D+1}{D(D-1)} \bar{R} \right) \xi_\nu + \bar{\nabla}_\nu \left(\Delta - \frac{D+1}{D(D-1)} \bar{R} \right) \xi_\mu. \quad (\text{C.15})$$

Correspondingly we find for the conformal Killing equation

$$\Delta(\bar{\nabla}_\mu \bar{\nabla}_\nu + \frac{1}{D} \bar{g}_{\mu\nu} \Delta) \zeta = (\bar{\nabla}_\mu \bar{\nabla}_\nu + \frac{1}{D} \bar{g}_{\mu\nu} \Delta) \left(\Delta - \frac{2}{D-1} \bar{R} \right) \zeta. \quad (\text{C.16})$$

This helps us to rewrite $\text{Tr} [e^{-s\Delta}]$, where the Laplacian acts on the metric, as a sum over traces where the Laplacian acts on the component fields. This sum of traces reads

$$\begin{aligned} \text{Tr} e^{-s\Delta} \Big|_h = & \text{Tr} e^{-s\Delta} \Big|_{h^{\text{TT}}} + \text{Tr} e^{-s\Delta} \Big|_\phi + \text{Tr} e^{-s(\Delta - \frac{D+1}{D(D-1)} \bar{R})} \Big|_\xi + \text{Tr} e^{-s(\Delta - \frac{2}{D-1} \bar{R})} \Big|_\zeta \\ & - e^{s \frac{2}{D-1} \bar{R}} - (D+1) e^{s \frac{1}{D-1} \bar{R}} - \frac{D(D+1)}{2} e^{s \frac{2}{D(D-1)} \bar{R}} \end{aligned} \quad (\text{C.17})$$

where the terms in the second line take into account that the Killing vectors do not contribute to the full metric. This gives us an expression for the trace with respect to the constrained field $h_{\mu\nu}^{\text{TT}}$ depending on the traces with respect to the unconstrained fields $h_{\mu\nu}$, ϕ , ζ and the transverse vector ξ_μ . The latter is constrained as well and we can use a similar trick to express the corresponding trace in terms of unconstrained traces.

Considering a vector field $A_\mu = A_\mu^{\text{T}} + \bar{\nabla}_\mu \varphi$, split into transverse part A_μ^{T} and longitudinal part $\bar{\nabla}_\mu \varphi$, we can use

$$\Delta \bar{\nabla}_\mu \varphi = \bar{\nabla}_\mu \left(\Delta - \frac{\bar{R}}{D} \right) \varphi \quad (\text{C.18})$$

to find

$$\mathrm{Tr} e^{-s\Delta}|_A = \mathrm{Tr} e^{-s\Delta}|_{A_T} + \mathrm{Tr} e^{-s(\Delta - \frac{\bar{R}}{D})} \Big|_{\varphi} - e^{s\frac{\bar{R}}{D}} \quad (\text{C.19})$$

where the last term again takes into account that constant scalars do not contribute. Reordering this result gives us the trace with respect to transverse vectors in terms of scalar traces and unconstrained vector traces. This can be inserted into (C.17) to result in an expression for the trace with respect to transverse traceless tensors in terms of unconstrained traces.

$$\begin{aligned} \mathrm{Tr} e^{-s\Delta}|_{h_{TT}} = & \mathrm{Tr} e^{-s\Delta}|_h - \mathrm{Tr} e^{-s\Delta}|_{\phi} - \mathrm{Tr} e^{-s(\Delta - \frac{D+1}{D(D-1)}\bar{R})} \Big|_A \\ & + (D+1)e^{s\frac{1}{D-1}\bar{R}} + \frac{D(D+1)}{2}e^{s\frac{2}{D(D-1)}\bar{R}}. \end{aligned} \quad (\text{C.20})$$

Note that, due to these manipulations we now encounter traces of the form $\mathrm{Tr} e^{-s(\Delta + q\bar{R})}$ with a constant q , instead of $\mathrm{Tr} e^{-s\Delta}$. We discussed traces of this form in Appendix C.1 and their expansion is given in (C.4). Inserting (C.4) into (C.20) we find

$$\begin{aligned} \mathrm{Tr} e^{-s\Delta}|_{h_{TT}} = & \frac{1}{(4\pi s)^{D/2}} \int d^D x \sqrt{\bar{g}} \left[D_{2T} + s\bar{R} \frac{(D+2)(D+1)(D-5)}{12(D-1)} \right] \\ & + (D+1)e^{s\frac{1}{D-1}\bar{R}} + \frac{D(D+1)}{2}e^{s\frac{2}{D(D-1)}\bar{R}} \end{aligned} \quad (\text{C.21})$$

with $D_{2T} = \frac{(D-2)(D+1)}{2}$, where we suppressed terms of order \bar{R}^2 and higher.

To adapt the terms in the second line we can insert a clever choice of a "1", which gives us the integral. Thus we use (C.10) and insert

$$1 = \int d^D x \sqrt{\bar{g}} \frac{\Gamma(D)}{\Gamma(\frac{D}{2})} \frac{1}{(4\pi)^{D/2}} \left(\frac{\bar{R}}{D(D-1)} \right)^{D/2}. \quad (\text{C.22})$$

Next, we expand the exponential in the second line of (C.21) in terms of \bar{R} as $\sum_m b_m \bar{R}^m$ and keep only the two lowest orders. Therefore we have to use those coefficients b_m with $D/2 + m = 0, 1$. Thus we get a contribution to \bar{R}^1 for $D = 2, m = 0$. The new term is $s\bar{R} \frac{(D+2)(D+1)3\delta_{D,2}}{12(D-1)}$ and thus we obtain

$$\mathrm{Tr} e^{-s\Delta}|_{h_{TT}} = \frac{1}{(4\pi s)^{D/2}} \int d^D x \sqrt{\bar{g}} \left[D_{2T} + s\bar{R} \frac{(D+2)(D+1)(D-5+3\delta_{D,2})}{12(D-1)} \right]. \quad (\text{C.23})$$

Note that one gets further terms proportional to $\delta_{D,4}$ if one takes into account \bar{R}^2 terms. This is very important for the discussion in Section 5.2.

field	tr a_0	tr a_2
S	1	$\frac{1}{6}\bar{R}$
V	D	$\frac{D}{6}\bar{R}$
TV	$D - 1$	$\frac{(D+2)(D-3)+6\delta_{D,2}}{6D}\bar{R}$
ST	$\frac{D(D+1)}{2}$	$\frac{D(D+1)}{12}\bar{R}$
STTT	$\frac{(D-2)(D+1)}{2}$	$\frac{(D+1)(D+2)(D-5+3\delta_{D,2})}{12(D-1)}\bar{R}$

Table C.2: The first two heat-kernel coefficients of the Laplacian on spherical backgrounds for scalars (S), vectors (V), transverse vectors (TV), symmetric tensors (ST) and symmetric transverse traceless tensors (STTT).

The derivation for the trace with respect to the constrained transverse vector is completely analog and thus we skip the details and just give the result. It reads

$$\mathrm{Tr} e^{-s\Delta}\Big|_{\xi} = \frac{1}{(4\pi s)^{D/2}} \int d^D x \sqrt{g} \left[D - 1 + s\bar{R} \frac{(D+2)(D-3)+6\delta_{D,2}}{6D} \right]. \quad (\text{C.24})$$

To summarise, Table C.2 lists the two lowest heat-kernel coefficients for constrained as well as unconstrained fields. The third coefficient, relevant for the R^2 truncation, can be found in Table C.3. For more details see e.g. [121].

At the end of this appendix we will discuss the effective changes appearing while excluding the lowest eigenmodes of the trace. This is necessary for constrained fields, since the lowest modes are unphysical, as discussed in Appendix C.2. Explicitly we will encounter constrained scalar traces which we denote by $\mathrm{Tr}''_{(0)}$ and constrained traces with respect to transverse vectors, denoted by $\mathrm{Tr}'_{(1T)}$. Here the number of primes n , counts the number of modes excluded

$$\mathrm{Tr}'\dots'[W(\Delta)] = \mathrm{Tr}[W(\Delta)] - \mathrm{tr} \sum_{l \in \{l_1, \dots, l_n\}} D_l(D, s) W(\Lambda_l(D, s)) \quad (\text{C.25})$$

with l counting the excluded modes, s denoting the spin of the field and $\Lambda_l(D, s)$ and $D_l(D, s)$ the eigenvalues and degeneracy respectively. The latter ones are given in Table C.1. Since the eigenvalues are functions of the scalar curvature \bar{R} we can perform an expansion and keep only the lowest order (sufficient for the Einstein-Hilbert truncation). For higher orders see e.g. [119]. Taking into account the \bar{R}

field	$\text{tr } a_4$
S	$\frac{5D^2-7D+6}{360D(D-1)} \bar{R}^2$
V	$\frac{5D^3-7D^2+6D-60}{360D(D-1)} \bar{R}^2$
TV	$\frac{5D^4-12D^3-47D^2-186D+180+360\delta_{D,2}+720\delta_{D,4}}{360D^2(D-1)} \bar{R}^2$
ST	$\frac{5D^4-2D^3-D^2-114D-240}{720D(D-1)} \bar{R}^2$
STTT	$\frac{(D+1)(5D^4-22D^3-83D^2-392D-228+1440\delta_{D,2}+3240\delta_{D,4})}{720D(D-1)^2} \bar{R}^2$

Table C.3: The third heat-kernel coefficients of the Laplacian on spherical backgrounds for scalars (S), vectors (V), transverse vectors (TV), symmetric tensors (ST) and symmetric transverse traceless tensors (STTT).

dependence of the volume element we find

$$\begin{aligned} \text{Tr}'_{(1T)}[W(\Delta)] &= \text{Tr}_{(1T)}[W(\Delta)] - \frac{\delta_{D,2}}{8\pi} \int d^D x \sqrt{g} 3W(0)\bar{R}, \\ \text{Tr}''_{(0)}[W(\Delta)] &= \text{Tr}_{(0)}[W(\Delta)] - \frac{\delta_{D,2}}{2\pi} \int d^D x \sqrt{g} W(0)\bar{R}. \end{aligned} \quad (\text{C.26})$$

Again we find contributions proportional to $\delta_{D,2}$. However, considering higher orders in the truncation one finds further terms. Within the R^2 truncation, for example, terms proportional to $\delta_{D,4}$ occur, as explained in [119].

C.4 The Threshold Functions

After evaluating the trace over the heat kernel we are left with an integral over $\tilde{W}(s)$. For convenience we introduce so-called threshold functions and evaluate them for a specific cutoff.

Inserting (C.23) and (C.24) into (C.2) gives us an expansion of the sought-after trace in the background Ricci scalar

$$\begin{aligned} \text{Tr}[W(\Delta)]_{h\text{TT}} &= \\ &= \frac{1}{(4\pi)^{D/2}} \int_x \int_0^\infty ds s^{-D/2} \tilde{W}(s) \left[\frac{(D-2)(D+1)}{2} + s\bar{R} \frac{(D+2)(D+1)(D-5+3\delta_{D,2})}{12(D-1)} \right] \\ &= \frac{1}{(4\pi)^{d/2}} \int_x \left[\frac{(D-2)(D+1)}{2} Q_{D/2}[W] + \frac{(D+2)(D+1)(D-5+3\delta_{D,2})}{12(D-1)} \bar{R} Q_{D/2-1}[W] \right] \end{aligned}$$

$$\begin{aligned}
\text{Tr} [W(\Delta)]_\xi &= \frac{1}{(4\pi)^{D/2}} \int_x \int_0^\infty ds s^{-D/2} \tilde{W}(s) \left[D - 1 + s \bar{R} \frac{(D+2)(D-3)+6\delta_{D,2}}{6D} \right] \\
&= \frac{1}{(4\pi)^{d/2}} \int_x \left[(D-1) Q_{D/2}[W] + \frac{(D+2)(D-3)+6\delta_{D,2}}{6D} \bar{R} Q_{D/2-1}[W] \right]
\end{aligned} \tag{C.27}$$

where we introduced the Q functional as the standard nomenclature in the literature. This is a Mellin transform and defined as

$$Q_l[W] = \int_0^\infty ds s^{-l} \tilde{W}(s) = \frac{1}{\Gamma(l)} \int_0^\infty dz z^{l-1} W(z). \tag{C.28}$$

Here the second equality holds only for positive l and $\Gamma(l)$ is the gamma function.

During our analysis in Part II and Part III we find W functions of a special form. Restricting to this form we can evaluate the traces even further. The appearing W functions have the pattern

$$W_1^{p,q}(w) = \frac{\partial_t R_k}{(P_k + w)^p (P_k)^q}, \quad W_2^{p,q}(w) = \frac{R_k}{(P_k + w)^p (P_k)^q}. \tag{C.29}$$

In the main text we already defined $P_k = \Delta + R_k$ and $R_k = k^2 R^{(0)}(\Delta/k^2)$. Inserting this into (C.28) leads to

$$\begin{aligned}
Q_l[W_1^{p,q}] &= 2k^{2(l-p-q+1)} \Phi_l^{p,q}(w/k^2), \\
Q_l[W_2^{p,q}] &= k^{2(l-p-q+1)} \tilde{\Phi}_l^{p,q}(w/k^2)
\end{aligned} \tag{C.30}$$

with the threshold functions Φ and $\tilde{\Phi}$ defined as

$$\begin{aligned}
\Phi_l^{p,q}(w) &= \frac{1}{\Gamma(l)} \int_0^\infty dz z^{l-1} \frac{R^{(0)}(z) - z R^{(0)'(z)}}{(z + R^{(0)}(z) + w)^p (z + R^{(0)}(z))^q}, \\
\tilde{\Phi}_l^{p,q}(w) &= \frac{1}{\Gamma(l)} \int_0^\infty dz z^{l-1} \frac{R^{(0)}(z)}{(z + R^{(0)}(z) + w)^p (z + R^{(0)}(z))^q}.
\end{aligned} \tag{C.31}$$

Here the profile function $R^{(0)}$ is kept arbitrary. However, throughout this thesis we will stick to the optimised cutoff introduced by Litim [84, 85]. It reads $R^{(0)}(z) = (1-z)\theta(1-z)$ with the Heaviside step function θ . Using this regulator the threshold functions can be analytically determined to

$$\Phi_l^{p,q}(w) = \frac{1}{\Gamma(l+1)} \frac{1}{(1+w)^p}, \quad \tilde{\Phi}_l^{p,q}(w) = \frac{1}{\Gamma(l+2)} \frac{1}{(1+w)^p}. \tag{C.32}$$

For the beta functions of the R^2 truncation in Section 5.2 we need a generalisation of the threshold functions Φ and $\tilde{\Phi}$ [119]. Their definition is given by

$$\begin{aligned}\Psi_{l,m}^{p,q}(v,w) &= \frac{(-1)^i}{\Gamma(l+i)} \int_0^\infty dz z^{l+i-1} \\ &\frac{\partial^i}{\partial z^i} \frac{(z + R^{(0)}(z))^m (R^{(0)}(z) - zR^{(0)'(z)})}{(z + R^{(0)}(z) + w)^p (32\pi v (z + R^{(0)}(z))^2 - \frac{D-2}{2(D-1)}(z + R^{(0)}(z) + w))^q}, \\ \tilde{\Psi}_{l,m,n}^{p,q}(v,w) &= \frac{(-1)^i}{\Gamma(l+i)} \int_0^\infty dz z^{l+i-1} \\ &\frac{\partial^i}{\partial z^i} \frac{(z + R^{(0)}(z))^m (2z + R^{(0)}(z))^n R^{(0)}(z)}{(z + R^{(0)}(z) + w)^p (32\pi v (z + R^{(0)}(z))^2 - \frac{D-2}{2(D-1)}(z + R^{(0)}(z) + w))^q}\end{aligned}\tag{C.33}$$

where i is non-negative and has to satisfy $i > -l$. Note that the threshold functions Φ , $\tilde{\Phi}$ and Ψ , $\tilde{\Psi}$ are related by $\Phi_l^{p,0}(w) = \Psi_{l,0}^{p,0}(v,w)$ and $\tilde{\Phi}_l^{p,0}(w) = \tilde{\Psi}_{l,0,0}^{p,0}(v,w)$. The definitions of the generalised threshold functions simplify if we use the optimised cutoff. In this case we find

$$\begin{aligned}\Psi_{l,m}^{p,q}(v,w) &= \frac{1}{\Gamma(l+1)} \frac{1}{(1+w)^p (32\pi v - \frac{D-2}{2(D-1)}(1+w))^q} \\ \tilde{\Psi}_{l,m,0}^{p,q}(v,w) &= \frac{1}{\Gamma(l+2)} \frac{1}{(1+w)^p (32\pi v - \frac{D-2}{2(D-1)}(1+w))^q} \\ \tilde{\Psi}_{l,m,1}^{p,q}(v,w) &= \frac{2}{(l+2)\Gamma(l+1)} \frac{1}{(1+w)^p (32\pi v - \frac{D-2}{2(D-1)}(1+w))^q}.\end{aligned}\tag{C.34}$$

Here we just give the expressions for $\tilde{\Psi}_{l,m,n}^{p,q}$ with $n = 0, 1$, since these are the only ones needed.

The Coefficient Functions for the R^2 Truncation

This appendix summarises the building blocks of the beta functions, capturing the RG flow of the R^2 truncation, studied in [117–119]. The coefficient functions A_i , B_i and C_i , depend on the coupling constants \bar{G}_k , $\bar{\Lambda}_k$ and $\bar{\beta}_k$. Furthermore, they contain dimension-dependent factors h_i given below and are given in terms of the threshold functions Φ , $\tilde{\Phi}$, Ψ and $\tilde{\Psi}$, which are defined in (C.32) and (C.34). The coefficient functions A_i read¹

$$\begin{aligned}
 A_1 = & -2\bar{\Lambda}_k + \frac{2\bar{G}_k}{(4\pi)^{\frac{D}{2}-1}} \left(h_8 \Phi_{D/2}^1(-2\bar{\Lambda}_k) - 2D \Phi_{d/2}^1(0) \right. \\
 & + 64\pi \bar{G}_k \bar{\beta}_k \Psi_{D/2,1}^{0,1}(\bar{G}_k \bar{\beta}_k, -2\bar{\Lambda}_k) - h_1 \Psi_{D/2,0}^{0,1}(\bar{G}_k \bar{\beta}_k, -2\bar{\Lambda}_k) \\
 & \left. + 32\pi \bar{G}_k \bar{\beta}_k \Psi_{D/2,2}^{1,1}(\bar{G}_k \bar{\beta}_k, -2\bar{\Lambda}_k) \right), \tag{D.1}
 \end{aligned}$$

$$\begin{aligned}
 A_2 = & \bar{\Lambda}_k - \frac{\bar{G}_k}{(4\pi)^{\frac{D}{2}-1}} \left(h_8 \tilde{\Phi}_{D/2}^1(-2\bar{\Lambda}_k) - h_1 \tilde{\Psi}_{D/2,0,0}^{0,1}(\bar{G}_k \bar{\beta}_k, -2\bar{\Lambda}_k) \right. \\
 & \left. + 32\pi \bar{G}_k \bar{\beta}_k \tilde{\Psi}_{D/2,2,0}^{1,1}(\bar{G}_k \bar{\beta}_k, -2\bar{\Lambda}_k) \right), \tag{D.2}
 \end{aligned}$$

$$A_3 = -\frac{8\bar{G}_k^2 \bar{\beta}_k}{(4\pi)^{\frac{D}{2}-2}} \tilde{\Psi}_{D/2,0,1}^{0,1}(\bar{G}_k \bar{\beta}_k, -2\bar{\Lambda}_k). \tag{D.3}$$

¹Note that the sign of the second term in A_2 differs between the preprint version and the published version of [119]. Here we use the correct sign, which appears in the published version.

The coefficient functions B_i and C_i on the other hand read²

$$\begin{aligned}
B_1 = & \frac{4}{(4\pi)^{\frac{D}{2}-1}} \left[h_9 \Phi_{D/2-1}^1(-2\bar{\Lambda}_k) + h_{10} \Phi_{D/2-1}^1(0) \right. \\
& + \frac{32\pi \bar{G}_k \bar{\beta}_k}{3} \Psi_{D/2-1,1}^{0,1}(\bar{G}_k \bar{\beta}_k, -2\bar{\Lambda}_k) - \frac{1}{6} h_1 \Psi_{D/2-1,0}^{0,1}(\bar{G}_k \bar{\beta}_k, -2\bar{\Lambda}_k) \\
& + \frac{16\pi \bar{G}_k \bar{\beta}_k}{3} \Psi_{D/2-1,2}^{1,1}(\bar{G}_k \bar{\beta}_k, -2\bar{\Lambda}_k) - 32\pi \bar{G}_k \bar{\beta}_k h_{11} \Phi_{D/2}^1(-2\bar{\Lambda}_k) \\
& + 32\pi \bar{G}_k \bar{\beta}_k h_{11} \Psi_{D/2,1}^{2,0}(\bar{G}_k \bar{\beta}_k, -2\bar{\Lambda}_k) + h_{12} \Phi_{D/2}^2(-2\bar{\Lambda}_k) + h_{13} \Phi_{D/2}^2(0) \\
& + 32\pi \bar{G}_k \bar{\beta}_k h_{19} \Psi_{D/2,1}^{1,1}(\bar{G}_k \bar{\beta}_k, -2\bar{\Lambda}_k) + h_4 \Psi_{D/2,0}^{1,1}(\bar{G}_k \bar{\beta}_k, -2\bar{\Lambda}_k) \\
& + 32\pi \bar{G}_k \bar{\beta}_k h_3 \Psi_{D/2,0}^{0,1}(\bar{G}_k \bar{\beta}_k, -2\bar{\Lambda}_k) - (32\pi \bar{G}_k \bar{\beta}_k)^2 h_{19} \Psi_{D/2,3}^{1,2}(\bar{G}_k \bar{\beta}_k, -2\bar{\Lambda}_k) \\
& - 64\pi \bar{G}_k \bar{\beta}_k h_4 \Psi_{D/2,2}^{1,2}(\bar{G}_k \bar{\beta}_k, -2\bar{\Lambda}_k) - 2(32\pi \bar{G}_k \bar{\beta}_k)^2 h_3 \Psi_{D/2,2}^{0,2}(\bar{G}_k \bar{\beta}_k, -2\bar{\Lambda}_k) \\
& + 32\pi \bar{G}_k \bar{\beta}_k h_1 h_{19} \Psi_{D/2,1}^{0,2}(\bar{G}_k \bar{\beta}_k, -2\bar{\Lambda}_k) + h_1 h_4 \Psi_{D/2,0}^{0,2}(\bar{G}_k \bar{\beta}_k, -2\bar{\Lambda}_k) \\
& \left. - (32\pi \bar{G}_k \bar{\beta}_k)^2 h_2 \Psi_{D/2,4}^{2,2}(\bar{G}_k \bar{\beta}_k, -2\bar{\Lambda}_k) \right], \tag{D.4}
\end{aligned}$$

$$\begin{aligned}
B_2 = & - \frac{2}{(4\pi)^{\frac{D}{2}-1}} \left[h_9 \tilde{\Phi}_{D/2-1}^1(-2\bar{\Lambda}_k) - \frac{1}{6} h_1 \tilde{\Psi}_{D/2-1,0,0}^{0,1}(\bar{G}_k \bar{\beta}_k, -2\bar{\Lambda}_k) \right. \\
& + \frac{16\pi \bar{G}_k \bar{\beta}_k}{3} \tilde{\Psi}_{D/2-1,2,0}^{1,1}(\bar{G}_k \bar{\beta}_k, -2\bar{\Lambda}_k) + 32\pi \bar{G}_k \bar{\beta}_k h_{11} \tilde{\Psi}_{D/2,1,0}^{2,0}(\bar{G}_k \bar{\beta}_k, -2\bar{\Lambda}_k) \\
& + h_{12} \tilde{\Phi}_{D/2}^2(-2\bar{\Lambda}_k) + 32\pi \bar{G}_k \bar{\beta}_k h_3 \tilde{\Psi}_{D/2,1,0}^{1,1}(\bar{G}_k \bar{\beta}_k, -2\bar{\Lambda}_k) \\
& + h_4 \tilde{\Psi}_{D/2,0,0}^{1,1}(\bar{G}_k \bar{\beta}_k, -2\bar{\Lambda}_k) - (32\pi \bar{G}_k \bar{\beta}_k)^2 h_3 \tilde{\Psi}_{D/2,3,0}^{1,2}(\bar{G}_k \bar{\beta}_k, -2\bar{\Lambda}_k) \\
& - 64\pi \bar{G}_k \bar{\beta}_k h_4 \tilde{\Psi}_{D/2,2,0}^{1,2}(\bar{G}_k \bar{\beta}_k, -2\bar{\Lambda}_k) + 32\pi \bar{G}_k \bar{\beta}_k h_1 h_3 \tilde{\Psi}_{D/2,1,0}^{0,2}(\bar{G}_k \bar{\beta}_k, -2\bar{\Lambda}_k) \\
& \left. + h_1 h_4 \tilde{\Psi}_{D/2,0,0}^{0,2}(\bar{G}_k \bar{\beta}_k, -2\bar{\Lambda}_k) - (32\pi \bar{G}_k \bar{\beta}_k)^2 h_2 \tilde{\Psi}_{D/2,4,0}^{2,2}(\bar{G}_k \bar{\beta}_k, -2\bar{\Lambda}_k) \right], \tag{D.5}
\end{aligned}$$

$$\begin{aligned}
B_3 = & - \frac{2}{(4\pi)^{\frac{D}{2}-1}} \left[\frac{16\pi \bar{G}_k \bar{\beta}_k}{3} \tilde{\Psi}_{D/2-1,0,1}^{0,1}(\bar{G}_k \bar{\beta}_k, -2\bar{\Lambda}_k) - 32\pi \bar{G}_k \bar{\beta}_k h_{11} \tilde{\Phi}_{D/2}^1(-2\bar{\Lambda}_k) \right. \\
& + 32\pi \bar{G}_k \bar{\beta}_k h_2 \tilde{\Psi}_{D/2,0,1}^{1,1}(\bar{G}_k \bar{\beta}_k, -2\bar{\Lambda}_k) + 32\pi \bar{G}_k \bar{\beta}_k h_3 \tilde{\Psi}_{D/2,0,0}^{0,1}(\bar{G}_k \bar{\beta}_k, -2\bar{\Lambda}_k) \\
& - (32\pi \bar{G}_k \bar{\beta}_k)^2 h_2 \tilde{\Psi}_{D/2,2,1}^{1,2}(\bar{G}_k \bar{\beta}_k, -2\bar{\Lambda}_k) - (32\pi \bar{G}_k \bar{\beta}_k)^2 h_3 \tilde{\Psi}_{D/2,1,1}^{0,2}(\bar{G}_k \bar{\beta}_k, -2\bar{\Lambda}_k) \\
& \left. - 32\pi \bar{G}_k \bar{\beta}_k h_4 \tilde{\Psi}_{D/2,0,1}^{0,2}(\bar{G}_k \bar{\beta}_k, -2\bar{\Lambda}_k) \right], \tag{D.6}
\end{aligned}$$

²Again a discrepancy between the preprint version and the published version of [119] appears in the second term of B_1 . We used the correct sign, which appeared in the preprint version. Furthermore, the preprint version contains a typing error. Instead of the factor h_3 in the 10th term of C_2 the factor h_{19} appears. Here we corrected this misprint.

$$\begin{aligned}
C_1 = & (4\pi)^{-\frac{D}{2}} \left[h_{14} \Phi_{D/2-2}^1(-2\bar{\Lambda}_k) - h_{16} \Phi_{D/2-2}^1(0) \right. \\
& + 64\pi \bar{G}_k \bar{\beta}_k h_{15} \Psi_{D/2-2,1}^{0,1}(\bar{G}_k \bar{\beta}_k, -2\bar{\Lambda}_k) - h_1 h_{15} \Psi_{D/2-2,0}^{0,1}(\bar{G}_k \bar{\beta}_k, -2\bar{\Lambda}_k) \\
& + 32\pi \bar{G}_k \bar{\beta}_k h_{15} \Psi_{D/2-2,2}^{1,1}(\bar{G}_k \bar{\beta}_k, -2\bar{\Lambda}_k) - 32\pi \bar{G}_k \bar{\beta}_k h_{17} \Phi_{D/2-1}^1(-2\bar{\Lambda}_k) \\
& + \frac{16\pi \bar{G}_k \bar{\beta}_k}{3} h_3 \Psi_{D/2-1,0}^{0,1}(\bar{G}_k \bar{\beta}_k, -2\bar{\Lambda}_k) + \frac{16\pi \bar{G}_k \bar{\beta}_k}{3} h_{19} \Psi_{D/2-1,1}^{1,1}(\bar{G}_k \bar{\beta}_k, -2\bar{\Lambda}_k) \\
& + \frac{1}{6} h_4 \Psi_{D/2-1,0}^{1,1}(\bar{G}_k \bar{\beta}_k, -2\bar{\Lambda}_k) + 32\pi \bar{G}_k \bar{\beta}_k h_{17} \Psi_{D/2-1,1}^{2,0}(\bar{G}_k \bar{\beta}_k, -2\bar{\Lambda}_k) \\
& - h_{18} \Phi_{D/2-1}^2(-2\bar{\Lambda}_k) - h_{20} \Phi_{D/2-1}^2(0) - \frac{(32\pi \bar{G}_k \bar{\beta}_k)^2}{6} h_{19} \Psi_{D/2-1,3}^{1,2}(\bar{G}_k \bar{\beta}_k, -2\bar{\Lambda}_k) \\
& - \frac{32\pi \bar{G}_k \bar{\beta}_k}{3} h_4 \Psi_{D/2-1,2}^{1,2}(\bar{G}_k \bar{\beta}_k, -2\bar{\Lambda}_k) - \frac{(32\pi \bar{G}_k \bar{\beta}_k)^2}{3} h_3 \Psi_{D/2-1,2}^{0,2}(\bar{G}_k \bar{\beta}_k, -2\bar{\Lambda}_k) \\
& + \frac{16\pi \bar{G}_k \bar{\beta}_k}{3} h_1 h_{19} \Psi_{D/2-1,1}^{0,2}(\bar{G}_k \bar{\beta}_k, -2\bar{\Lambda}_k) + \frac{1}{6} h_1 h_4 \Psi_{D/2-1,0}^{0,2}(\bar{G}_k \bar{\beta}_k, -2\bar{\Lambda}_k) \\
& - \frac{(32\pi \bar{G}_k \bar{\beta}_k)^2}{6} h_2 \Psi_{D/2-1,4}^{2,2}(\bar{G}_k \bar{\beta}_k, -2\bar{\Lambda}_k) - (32\pi \bar{G}_k \bar{\beta}_k)^2 h_{11} \Psi_{D/2,1}^{2,0}(\bar{G}_k \bar{\beta}_k, -2\bar{\Lambda}_k) \\
& + 32\pi \bar{G}_k \bar{\beta}_k h_{25} \Phi_{D/2}^2(-2\bar{\Lambda}_k) + (32\pi \bar{G}_k \bar{\beta}_k)^2 h_{11} \Psi_{D/2,2}^{3,0}(\bar{G}_k \bar{\beta}_k, -2\bar{\Lambda}_k) \\
& - 32\pi \bar{G}_k \bar{\beta}_k h_{11} h_{21} \Psi_{D/2,1}^{3,0}(\bar{G}_k \bar{\beta}_k, -2\bar{\Lambda}_k) + h_{23} \Phi_{D/2}^3(-2\bar{\Lambda}_k) + h_{24} \Phi_{D/2}^3(0) \\
& - (32\pi \bar{G}_k \bar{\beta}_k)^2 h_2 \Psi_{D/2,1}^{1,1}(\bar{G}_k \bar{\beta}_k, -2\bar{\Lambda}_k) + 32\pi \bar{G}_k \bar{\beta}_k h_2 h_{26} \Psi_{D/2,0}^{1,1}(\bar{G}_k \bar{\beta}_k, -2\bar{\Lambda}_k) \\
& + (32\pi \bar{G}_k \bar{\beta}_k)^3 h_2 \Psi_{D/2,3}^{1,2}(\bar{G}_k \bar{\beta}_k, -2\bar{\Lambda}_k) - (32\pi \bar{G}_k \bar{\beta}_k)^2 h_{27} \Psi_{D/2,2}^{1,2}(\bar{G}_k \bar{\beta}_k, -2\bar{\Lambda}_k) \\
& + 32\pi \bar{G}_k \bar{\beta}_k h_4 (d) h_{28} \Psi_{D/2,1}^{1,2}(\bar{G}_k \bar{\beta}_k, -2\bar{\Lambda}_k) - \frac{3}{2} h_4^2 \Psi_{D/2,0}^{1,2}(\bar{G}_k \bar{\beta}_k, -2\bar{\Lambda}_k) \\
& - (32\pi \bar{G}_k \bar{\beta}_k)^2 h_{29} \Psi_{D/2,1}^{0,2}(\bar{G}_k \bar{\beta}_k, -2\bar{\Lambda}_k) - 32\pi \bar{G}_k \bar{\beta}_k h_4 h_{26} \Psi_{D/2,0}^{0,2}(\bar{G}_k \bar{\beta}_k, -2\bar{\Lambda}_k) \\
& + \frac{(32\pi \bar{G}_k \bar{\beta}_k)^3}{2} h_2 \Psi_{D/2,4}^{2,2}(\bar{G}_k \bar{\beta}_k, -2\bar{\Lambda}_k) + \frac{2(32\pi \bar{G}_k \bar{\beta}_k)^2}{3} h_2 h_{28} \Psi_{D/2,3}^{2,2}(\bar{G}_k \bar{\beta}_k, -2\bar{\Lambda}_k) \\
& - 48\pi \bar{G}_k \bar{\beta}_k h_2 h_4 \Psi_{D/2,2}^{2,2}(\bar{G}_k \bar{\beta}_k, -2\bar{\Lambda}_k) + 2(32\pi \bar{G}_k \bar{\beta}_k)^3 h_3^2 \Psi_{D/2,3}^{0,3}(\bar{G}_k \bar{\beta}_k, -2\bar{\Lambda}_k) \\
& - 3(32\pi \bar{G}_k \bar{\beta}_k)^2 h_1 h_3 h_{30} \Psi_{D/2,2}^{0,3}(\bar{G}_k \bar{\beta}_k, -2\bar{\Lambda}_k) \\
& + \frac{64\pi \bar{G}_k \bar{\beta}_k}{3} h_1 h_4 h_{28} \Psi_{D/2,1}^{0,3}(\bar{G}_k \bar{\beta}_k, -2\bar{\Lambda}_k) - h_1 h_4^2 \Psi_{D/2,0}^{0,3}(\bar{G}_k \bar{\beta}_k, -2\bar{\Lambda}_k) \\
& + 3(32\pi \bar{G}_k \bar{\beta}_k)^3 h_3 h_{30} \Psi_{D/2,4}^{1,3}(\bar{G}_k \bar{\beta}_k, -2\bar{\Lambda}_k) \\
& - \frac{4(32\pi \bar{G}_k \bar{\beta}_k)^2}{3} h_4 h_{28} \Psi_{D/2,3}^{1,3}(\bar{G}_k \bar{\beta}_k, -2\bar{\Lambda}_k) + 96\pi \bar{G}_k \bar{\beta}_k h_4^2 \Psi_{D/2,2}^{1,3}(\bar{G}_k \bar{\beta}_k, -2\bar{\Lambda}_k) \\
& - \frac{2(32\pi \bar{G}_k \bar{\beta}_k)^3}{3} h_2 h_{28} \Psi_{D/2,5}^{2,3}(\bar{G}_k \bar{\beta}_k, -2\bar{\Lambda}_k) \\
& + 3(32\pi \bar{G}_k \bar{\beta}_k)^2 h_2 h_4 \Psi_{D/2,4}^{2,3}(\bar{G}_k \bar{\beta}_k, -2\bar{\Lambda}_k) \\
& + (32\pi \bar{G}_k \bar{\beta}_k)^3 h_2^2 \Psi_{D/2,6}^{3,3}(\bar{G}_k \bar{\beta}_k, -2\bar{\Lambda}_k) \\
& \left. + \left(-\frac{1}{2} R^{(0)'}(0) - \frac{96\pi \bar{G}_k \bar{\beta}_k}{(1-2\bar{\Lambda}_k)} + \frac{11R^{(0)'}(0)+192\pi \bar{G}_k \bar{\beta}_k}{2(1-2\bar{\Lambda}_k)^2} \right) \delta_{D,2} \right]
\end{aligned}$$

$$+ \left(\frac{288\pi\bar{G}_k\bar{\beta}_k-1}{4(144\pi\bar{G}_k\bar{\beta}_k-(1-2\bar{\Lambda}_k))} + \frac{1}{4(1-2\bar{\Lambda}_k)} - \frac{96\pi\bar{G}_k\bar{\beta}_k-1}{2(96\pi\bar{G}_k\bar{\beta}_k-(1-2\bar{\Lambda}_k))} - \frac{24\pi\bar{G}_k\bar{\beta}_k}{(1-2\bar{\Lambda}_k)(96\pi\bar{G}_k\bar{\beta}_k-(1-2\bar{\Lambda}_k))} \right) \delta_{D,4} \Big], \quad (\text{D.7})$$

$$\begin{aligned}
C_2 = & -\frac{1}{2(4\pi)^{\frac{D}{2}}} \left[h_{14} \tilde{\Phi}_{D/2-2}^1(-2\bar{\Lambda}_k) - h_1 h_{15} \tilde{\Psi}_{D/2-2,0,0}^{0,1}(\bar{G}_k\bar{\beta}_k, -2\bar{\Lambda}_k) \right. \\
& + 32\pi\bar{G}_k\bar{\beta}_k h_{15} \tilde{\Psi}_{D/2-2,2,0}^{1,1}(\bar{G}_k\bar{\beta}_k, -2\bar{\Lambda}_k) + \frac{16\pi\bar{G}_k\bar{\beta}_k}{3} h_3 \tilde{\Psi}_{D/2-1,1,0}^{1,1}(\bar{G}_k\bar{\beta}_k, -2\bar{\Lambda}_k) \\
& + \frac{1}{6} h_4 \tilde{\Psi}_{D/2-1,0,0}^{1,1}(\bar{G}_k\bar{\beta}_k, -2\bar{\Lambda}_k) + 32\pi\bar{G}_k\bar{\beta}_k h_{17} \tilde{\Psi}_{D/2-1,1,0}^{2,0}(\bar{G}_k\bar{\beta}_k, -2\bar{\Lambda}_k) \\
& - h_{18} \tilde{\Phi}_{D/2-1}^2(-2\bar{\Lambda}_k) - \frac{(32\pi\bar{G}_k\bar{\beta}_k)^2}{6} h_3 \tilde{\Psi}_{D/2-1,3,0}^{1,2}(\bar{G}_k\bar{\beta}_k, -2\bar{\Lambda}_k) \\
& - \frac{32\pi\bar{G}_k\bar{\beta}_k}{3} h_4 \tilde{\Psi}_{D/2-1,2,0}^{1,2}(\bar{G}_k\bar{\beta}_k, -2\bar{\Lambda}_k) + \frac{16\pi\bar{G}_k\bar{\beta}_k}{3} h_1 h_3 \tilde{\Psi}_{D/2-1,1,0}^{0,2}(\bar{G}_k\bar{\beta}_k, -2\bar{\Lambda}_k) \\
& + \frac{1}{6} h_1 h_4 \tilde{\Psi}_{D/2-1,0,0}^{0,2}(\bar{G}_k\bar{\beta}_k, -2\bar{\Lambda}_k) - \frac{(32\pi\bar{G}_k\bar{\beta}_k)^2}{6} h_2 \tilde{\Psi}_{D/2-1,4,0}^{2,2}(\bar{G}_k\bar{\beta}_k, -2\bar{\Lambda}_k) \\
& + 32\pi\bar{G}_k\bar{\beta}_k h_{22} \tilde{\Phi}_{D/2}^2(-2\bar{\Lambda}_k) + (32\pi\bar{G}_k\bar{\beta}_k)^2 h_{11} \tilde{\Psi}_{D/2,2,0}^{3,0}(\bar{G}_k\bar{\beta}_k, -2\bar{\Lambda}_k) \\
& - 32\pi\bar{G}_k\bar{\beta}_k h_{11} h_{21} \tilde{\Psi}_{D/2,1,0}^{3,0}(\bar{G}_k\bar{\beta}_k, -2\bar{\Lambda}_k) + h_{23} \tilde{\Phi}_{D/2}^3(-2\bar{\Lambda}_k) \\
& + 32\pi\bar{G}_k\bar{\beta}_k h_6 \tilde{\Psi}_{D/2,0,0}^{1,1}(\bar{G}_k\bar{\beta}_k, -2\bar{\Lambda}_k) - (32\pi\bar{G}_k\bar{\beta}_k)^2 h_7 \tilde{\Psi}_{D/2,2,0}^{1,2}(\bar{G}_k\bar{\beta}_k, -2\bar{\Lambda}_k) \\
& - 96\pi\bar{G}_k\bar{\beta}_k h_3 h_4 \tilde{\Psi}_{D/2,1,0}^{1,2}(\bar{G}_k\bar{\beta}_k, -2\bar{\Lambda}_k) - \frac{3}{2} h_4^2 \tilde{\Psi}_{D/2,0,0}^{1,2}(\bar{G}_k\bar{\beta}_k, -2\bar{\Lambda}_k) \\
& + 32\pi\bar{G}_k\bar{\beta}_k h_1 h_6 \tilde{\Psi}_{d/2,0,0}^{0,2}(\bar{G}_k\bar{\beta}_k, -2\bar{\Lambda}_k) + \frac{(32\pi\bar{G}_k\bar{\beta}_k)^3}{2} h_2 \tilde{\Psi}_{D/2,4,0}^{2,2}(\bar{G}_k\bar{\beta}_k, -2\bar{\Lambda}_k) \\
& - 2(32\pi\bar{G}_k\bar{\beta}_k)^2 h_2 h_3 \tilde{\Psi}_{D/2,3,0}^{2,2}(\bar{G}_k\bar{\beta}_k, -2\bar{\Lambda}_k) \\
& - 48\pi\bar{G}_k\bar{\beta}_k h_2 h_4 \tilde{\Psi}_{D/2,2,0}^{2,2}(\bar{G}_k\bar{\beta}_k, -2\bar{\Lambda}_k) \\
& - (32\pi\bar{G}_k\bar{\beta}_k)^2 h_1 h_3^2 \tilde{\Psi}_{D/2,2,0}^{0,3}(\bar{G}_k\bar{\beta}_k, -2\bar{\Lambda}_k) \\
& - 64\pi\bar{G}_k\bar{\beta}_k h_1 h_3 h_4 \tilde{\Psi}_{D/2,1,0}^{0,3}(\bar{G}_k\bar{\beta}_k, -2\bar{\Lambda}_k) - h_1 h_4^2 \tilde{\Psi}_{D/2,0,0}^{0,3}(\bar{G}_k\bar{\beta}_k, -2\bar{\Lambda}_k) \\
& + (32\pi\bar{G}_k\bar{\beta}_k)^3 h_3^2 \tilde{\Psi}_{D/2,4,0}^{1,3}(\bar{G}_k\bar{\beta}_k, -2\bar{\Lambda}_k) \\
& + 4(32\pi\bar{G}_k\bar{\beta}_k)^2 h_3 h_4 \tilde{\Psi}_{D/2,3,0}^{1,3}(\bar{G}_k\bar{\beta}_k, -2\bar{\Lambda}_k) \\
& + 96\pi\bar{G}_k\bar{\beta}_k h_4^2 \tilde{\Psi}_{D/2,2,0}^{1,3}(\bar{G}_k\bar{\beta}_k, -2\bar{\Lambda}_k) \\
& + 2(32\pi\bar{G}_k\bar{\beta}_k)^3 h_2 h_3 \tilde{\Psi}_{D/2,5,0}^{2,3}(\bar{G}_k\bar{\beta}_k, -2\bar{\Lambda}_k) \\
& + 3(32\pi\bar{G}_k\bar{\beta}_k)^2 h_2 h_4 \tilde{\Psi}_{D/2,4,0}^{2,3}(\bar{G}_k\bar{\beta}_k, -2\bar{\Lambda}_k) \\
& + (32\pi\bar{G}_k\bar{\beta}_k)^3 h_2^2 \tilde{\Psi}_{D/2,6,0}^{3,3}(\bar{G}_k\bar{\beta}_k, -2\bar{\Lambda}_k) \\
& \left. + \left(-\frac{11R^{(0)'(0)}}{2(1-2\bar{\Lambda}_k)} + \frac{192\pi\bar{G}_k\bar{\beta}_k+11R^{(0)'(0)}}{2(1-2\bar{\Lambda}_k)^2} \right) \delta_{D,2} \right]
\end{aligned}$$

$$\begin{aligned}
& + \left(-\frac{1}{4(144\pi\bar{G}_k\bar{\beta}_k-(1-2\bar{\Lambda}_k))} + \frac{1}{4(1-2\bar{\Lambda}_k)} \right. \\
& \left. + \frac{1}{2(96\pi\bar{G}_k\bar{\beta}_k-(1-2\bar{\Lambda}_k))} - \frac{24\pi\bar{G}_k\bar{\beta}_k}{(1-2\bar{\Lambda}_k)(96\pi\bar{G}_k\bar{\beta}_k-(1-2\bar{\Lambda}_k))} \right) \delta_{D,4} \Big], \quad (D.8)
\end{aligned}$$

$$\begin{aligned}
C_3 = & -\frac{1}{2(4\pi)^{\frac{D}{2}}} \Big[32\pi\bar{G}_k\bar{\beta}_k h_{15} \tilde{\Psi}_{D/2-2,0,1}^{0,1}(\bar{G}_k\bar{\beta}_k, -2\bar{\Lambda}_k) - 32\pi\bar{G}_k\bar{\beta}_k h_{17} \tilde{\Phi}_{D/2-1}^1(-2\bar{\Lambda}_k) \\
& + \frac{16\pi\bar{G}_k\bar{\beta}_k}{3} h_3 \tilde{\Psi}_{D/2-1,0,0}^{0,1}(\bar{G}_k\bar{\beta}_k, -2\bar{\Lambda}_k) + \frac{16\pi\bar{G}_k\bar{\beta}_k}{3} h_2 \tilde{\Psi}_{D/2-1,0,1}^{1,1}(\bar{G}_k\bar{\beta}_k, -2\bar{\Lambda}_k) \\
& - \frac{(32\pi\bar{G}_k\bar{\beta}_k)^2}{6} h_2 \tilde{\Psi}_{D/2-1,2,1}^{1,2}(\bar{G}_k\bar{\beta}_k, -2\bar{\Lambda}_k) - \frac{(32\pi\bar{G}_k\bar{\beta}_k)^2}{6} h_3 \tilde{\Psi}_{D/2-1,1,1}^{0,2}(\bar{G}_k\bar{\beta}_k, -2\bar{\Lambda}_k) \\
& - \frac{16\pi\bar{G}_k\bar{\beta}_k}{3} h_4 \tilde{\Psi}_{D/2-1,0,1}^{0,2}(\bar{G}_k\bar{\beta}_k, -2\bar{\Lambda}_k) - (32\pi\bar{G}_k\bar{\beta}_k)^2 h_{11} \tilde{\Psi}_{D/2,1,0}^{2,0}(\bar{G}_k\bar{\beta}_k, -2\bar{\Lambda}_k) \\
& + 16\pi\bar{G}_k\bar{\beta}_k h_{11} h_{21} \tilde{\Phi}_{D/2}^2(-2\bar{\Lambda}_k) - (32\pi\bar{G}_k\bar{\beta}_k)^2 h_5 \tilde{\Psi}_{D/2,0,1}^{1,1}(\bar{G}_k\bar{\beta}_k, -2\bar{\Lambda}_k) \\
& - \frac{2(32\pi\bar{G}_k\bar{\beta}_k)^2}{d^2} \tilde{\Psi}_{D/2,1,0}^{1,1}(\bar{G}_k\bar{\beta}_k, -2\bar{\Lambda}_k) + 32\pi\bar{G}_k\bar{\beta}_k h_2 h_3 \tilde{\Psi}_{D/2,0,0}^{1,1}(\bar{G}_k\bar{\beta}_k, -2\bar{\Lambda}_k) \\
& + \frac{(32\pi\bar{G}_k\bar{\beta}_k)^3}{2} h_2 \tilde{\Psi}_{D/2,2,1}^{1,2}(\bar{G}_k\bar{\beta}_k, -2\bar{\Lambda}_k) - 2(32\pi\bar{G}_k\bar{\beta}_k)^2 h_2 h_3 \tilde{\Psi}_{D/2,1,1}^{1,2}(\bar{G}_k\bar{\beta}_k, -2\bar{\Lambda}_k) \\
& - 48\pi\bar{G}_k\bar{\beta}_k h_2 h_4 \tilde{\Psi}_{D/2,0,1}^{1,2}(\bar{G}_k\bar{\beta}_k, -2\bar{\Lambda}_k) - (32\pi\bar{G}_k\bar{\beta}_k)^2 h_2 h_3 \tilde{\Psi}_{D/2,2,0}^{1,2}(\bar{G}_k\bar{\beta}_k, -2\bar{\Lambda}_k) \\
& - (32\pi\bar{G}_k\bar{\beta}_k)^2 h_6 \tilde{\Psi}_{D/2,0,1}^{0,2}(\bar{G}_k\bar{\beta}_k, -2\bar{\Lambda}_k) - (32\pi\bar{G}_k\bar{\beta}_k)^2 h_3^2 \tilde{\Psi}_{D/2,1,0}^{0,2}(\bar{G}_k\bar{\beta}_k, -2\bar{\Lambda}_k) \\
& - 32\pi\bar{G}_k\bar{\beta}_k h_3 h_4 \tilde{\Psi}_{D/2,0,0}^{0,2}(\bar{G}_k\bar{\beta}_k, -2\bar{\Lambda}_k) - (32\pi\bar{G}_k\bar{\beta}_k)^2 h_2^2 \tilde{\Psi}_{D/2,2,1}^{2,2}(\bar{G}_k\bar{\beta}_k, -2\bar{\Lambda}_k) \\
& + (32\pi\bar{G}_k\bar{\beta}_k)^3 h_3^2 \tilde{\Psi}_{D/2,2,1}^{0,3}(\bar{G}_k\bar{\beta}_k, -2\bar{\Lambda}_k) \\
& + 2(32\pi\bar{G}_k\bar{\beta}_k)^2 h_3 h_4 \tilde{\Psi}_{D/2,1,1}^{0,3}(\bar{G}_k\bar{\beta}_k, -2\bar{\Lambda}_k) + 32\pi\bar{G}_k\bar{\beta}_k h_4^2 \tilde{\Psi}_{D/2,0,1}^{0,3}(\bar{G}_k\bar{\beta}_k, -2\bar{\Lambda}_k) \\
& + 2(32\pi\bar{G}_k\bar{\beta}_k)^3 h_2 h_3 \tilde{\Psi}_{D/2,3,1}^{1,3}(\bar{G}_k\bar{\beta}_k, -2\bar{\Lambda}_k) \\
& + 2(32\pi\bar{G}_k\bar{\beta}_k)^2 h_2 h_4 \tilde{\Psi}_{D/2,2,1}^{1,3}(\bar{G}_k\bar{\beta}_k, -2\bar{\Lambda}_k) \\
& + (32\pi\bar{G}_k\bar{\beta}_k)^3 h_2^2 \tilde{\Psi}_{D/2,4,1}^{2,3}(\bar{G}_k\bar{\beta}_k, -2\bar{\Lambda}_k) \\
& \left. - \frac{96\pi\bar{G}_k\bar{\beta}_k}{(1-2\bar{\Lambda}_k)} \delta_{D,2} + \left(\frac{36\pi\bar{G}_k\bar{\beta}_k}{144\pi\bar{G}_k\bar{\beta}_k-(1-2\bar{\Lambda}_k)} - \frac{24\pi\bar{G}_k\bar{\beta}_k}{96\pi\bar{G}_k\bar{\beta}_k-(1-2\bar{\Lambda}_k)} \right) \delta_{D,4} \right]. \quad (D.9)
\end{aligned}$$

All these coefficient functions $A_1, A_2, A_3, B_1, B_2, B_3, C_1, C_2$ and C_3 depend on the D -dependent prefactors $h_i, i = 1, \dots, 47$ reading

$$\begin{aligned}
h_1 &= \frac{D-2}{D-1}, \quad h_2 = \frac{D-4}{D}, \quad h_3 = \frac{D^2-8D+4}{2D(D-1)}, \quad h_4 = -\frac{(D-2)(D-4)}{D(D-1)}, \quad h_5 = \frac{D^2-4D-2}{2D^2}, \\
h_6 &= \frac{(D-4)^2}{2D(D-1)}, \quad h_7 = \frac{5D^4-48D^3+148D^2-112D+16}{4D^2(D-1)^2}, \quad h_8 = \frac{D^2+D-4}{2}, \\
h_9 &= \frac{(D+3)(D+2)(D^2-5D+2)}{12D(D-1)}, \quad h_{10} = -\frac{D^2-6}{3D}, \quad h_{11} = \frac{(D+1)(D-2)}{2}, \\
h_{12} &= -\frac{D^4-2D^3-5D^2+16D-14}{2D(D-1)}, \quad h_{13} = -\frac{2(D+1)}{D}, \\
h_{14} &= \frac{5D^6-7D^5-139D^4-545D^3-898D^2+504D-360}{720D^2(D-1)^2}, \quad h_{15} = \frac{5D^2-7D+6}{360D(D-1)},
\end{aligned}$$

$$\begin{aligned}
h_{16} &= \frac{5D^4-7D^3-54D^2-180D+180}{180D^2(D-1)}, & h_{17} &= \frac{(D+2)(D+1)(D-5)}{12(D-1)}, \\
h_{18} &= \frac{(D+2)(D^5-5D^4-5D^3+43D^2-68D+18)}{12D^2(D-1)^2}, & h_{19} &= \frac{5D^2-28D+20}{2D(D-1)}, \\
h_{20} &= \frac{(D+3)(D-2)}{3D^2}, & h_{21} &= 2\frac{D^2-3D+4}{D(D-1)}, & h_{22} &= \frac{(D-3)(D^3-D^2-4D+8)}{4D(D-1)}, \\
h_{23} &= \frac{D^6-5D^5+3D^4+31D^3-86D^2+98D-50}{2D^2(D-1)^2}, & h_{24} &= -2\frac{D+3}{D^2}, \\
h_{25} &= \frac{3D^4-12D^3+9D^2+24D-40}{4D(D-1)}, & h_{26} &= \frac{D^2-6D+2}{D(D-1)}, \\
h_{27} &= \frac{15D^4-178D^3+628D^2-632D+176}{4D^2(D-1)^2}, & h_{28} &= -\frac{9(D^2-6D+4)}{2D(D-1)}, \\
h_{29} &= \frac{5D^4-52D^3+168D^2-128D+16}{4D^2(D-1)^2}, & h_{30} &= \frac{3D^2-16D+12}{2D(D-1)}, \\
h_{31} &= \frac{5D^6-27D^5-71D^4-405D^3-342D^2-960D+360}{720D^2(D-1)^2}, \\
h_{32} &= -\frac{D^6-3D^5-7D^4+5D^3+26D^2-82D+12}{12D^2(D-1)^2}, \\
h_{33} &= \frac{D^6-5D^5+7D^4-13D^3+42D^2-42D+2}{2D^2(D-1)^2}, \\
h_{34} &= \frac{5D^6-7D^5-119D^4-593D^3-846D^2+480D-360}{360D^2(D-1)^2}, \\
h_{35} &= -\frac{D^6-3D^5-11D^4+9D^3+54D^2-134D+36}{3D^2(D-1)^2}, \\
h_{36} &= 3\frac{D^6-5D^5+7D^4-9D^3+46D^2-62D+14}{D^2(D-1)^2}, & h_{37} &= \frac{(D+2)(D^3-6D^2+3D-6)}{3D(D-1)}, \\
h_{38} &= -2\frac{D^4-2D^3+3D^2-4D-2}{D(D-1)}, & h_{39} &= \frac{5D^2-7D+6}{45D(D-2)}, \\
h_{40} &= \frac{30D^5-115D^4-362D^3+721D^2+182D+264}{90D(D-1)(D-2)}, \\
h_{41} &= -2\frac{3D^6-17D^5+25D^4+39D^3-166D^2+224D-96}{3D^2(D-1)(D-2)}, & h_{42} &= 4\frac{(D-1)(D-4)^2}{D(D-2)}, \\
h_{43} &= -\frac{(D+2)(D^3-6D^2+3D-6)}{3D(D-1)(D-2)}, & h_{44} &= 2\frac{D^4-2D^3+3D^2-4D-2}{D(D-1)(D-2)}, \\
h_{45} &= \frac{D^4-3D^3+32D-32}{D^2}, & h_{46} &= -\frac{D^4-13D^2-24D+12}{6D(D-1)}, & h_{47} &= \frac{D^4-2D^3-D^2-4D+2}{D(D-1)}.
\end{aligned} \tag{D.10}$$

The Arnowitt-Deser-Misner Decomposition

In this appendix we explain the relation between the metric formulation of gravity and the foliated version of it, known as the Arnowitt-Deser-Misner (ADM) decomposition [187]. The former is based on a D -dimensional manifold \mathcal{M} and the corresponding spacetime metric $\tilde{g}_{\mu\nu}$. At this point we do not specify the signature, it might be Euclidean $(+, +, \dots)$ or Lorentzian $(-, +, +, \dots)$. To distinguish these two cases we introduce the signature parameter $\varepsilon = \text{sig } \tilde{g}_{\mu\nu} = \pm 1$.

The foundation of the ADM decomposition is a foliation of \mathcal{M} , which is constructed as follows. We start by defining a time function $\tau(x)$, which assigns a time τ to every spacetime point x . This can be used to divide the spacetime manifold \mathcal{M} into a stack of spatial slices $\Sigma_{\tau_i} = \{x : \tau(x) = \tau_i\}$. The hypersurfaces Σ_{τ_i} have the spatial dimension $d = D - 1$ and are equipped with a normal vector n^μ . If we assume the vector field $\partial_\mu \tau$ to be timelike for Lorentzian signature we can define the normal vector n^μ to be future directed by demanding $n^\mu \partial_\mu \tau > 0$. The normalisation reads $\tilde{g}_{\mu\nu} n^\mu n^\nu = \varepsilon$. The relation between these two vector fields is given by $n_\mu = \varepsilon \tilde{N} \partial_\mu \tau$, where we introduced the lapse function \tilde{N} for normalisation.

Besides the normal vector n^μ we introduce a vector field t^μ satisfying $t^\mu \partial_\mu \tau = 1$. Furthermore, in addition to the spacetime coordinates x^μ we introduce coordinates y^i on the spatial slices. Note that we are using letters from the middle of the Greek alphabet μ, ν, \dots for spacetime indices and letters from the middle of the Roman alphabet i, j, \dots for spatial indices. Using integral curves γ along the vector field t^μ we can relate the coordinate systems on neighbouring slices by choosing y^i to be constant along such a curve. To translate the coordinate system x^μ into the system (τ, y^i) one has to use the Jacobian

$$t^\mu = \left. \frac{\partial x^\mu}{\partial \tau} \right|_{y^i}, \quad e_i^\mu = \left. \frac{\partial x^\mu}{\partial y^i} \right|_\tau. \quad (\text{E.1})$$

The new objects e_i^μ span the tangent space of the spatial slices and are thus per-

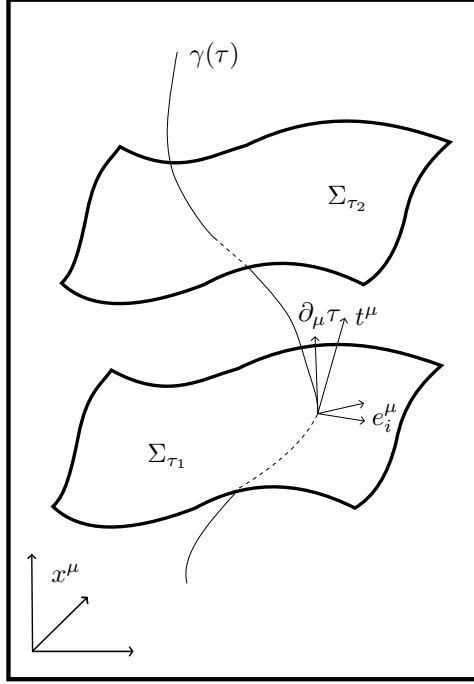


Figure E.1: The foliation of spacetime into spatial slices Σ_{τ_i} . Depicted are the integral curve γ along the vector field t^μ , the basis e_i^μ on the spatial slice and the vector field $\partial_\mu \tau$ perpendicular to the hypersurface.

perpendicular to the normal vector of the hypersurfaces $n_\mu e_i^\mu = 0$. The vector t^μ on the other hand is neither tangential nor perpendicular to the spatial slices, but tangential to the curve γ . Thus it can be decomposed into components as

$$t^\mu = \tilde{N}n^\mu + \tilde{N}^i e_i^\mu. \quad (\text{E.2})$$

The lapse function \tilde{N} is the length of t^μ in time direction and the shift vector \tilde{N}^i is the projection of t^μ onto the spatial slice. A sketch of this decomposition with the various introduced objects can be found in Figure E.1.

Finally we can rewrite the infinitesimal squared line element ds^2 in terms of the new quantities. To see this we start with the replacement within the coordinate one-form. From (E.1) we get

$$dx^\mu = t^\mu d\tau + e_i^\mu dy^i = \tilde{N}n^\mu d\tau + \left(dy^i + \tilde{N}^i d\tau\right) e_i^\mu. \quad (\text{E.3})$$

Squaring this one-form with the spacetime metric $\tilde{g}_{\mu\nu}$, we encounter the projection of this metric to the spatial slice $\tilde{\sigma}_{ij} = \tilde{g}_{\mu\nu} e_i^\mu e_j^\nu$. Using this, the line element reads

$$ds^2 = \tilde{g}_{\mu\nu} dx^\mu dx^\nu = \varepsilon \tilde{N}^2 d\tau^2 + \tilde{\sigma}_{ij} \left(dy^i + \tilde{N}^i d\tau \right) \left(dy^j + \tilde{N}^j d\tau \right). \quad (\text{E.4})$$

To give this final result of this appendix in a more readable way we write the relation between the spacetime metric $\tilde{g}_{\mu\nu}$ and the new fields \tilde{N} , \tilde{N}^i , $\tilde{\sigma}_{ij}$ in matrix notation.

$$\tilde{g}_{\mu\nu} = \begin{pmatrix} \varepsilon \tilde{N}^2 + \tilde{N}_i \tilde{N}^i & \tilde{N}_j \\ \tilde{N}_i & \tilde{\sigma}_{ij} \end{pmatrix}, \quad \tilde{g}^{\mu\nu} = \begin{pmatrix} \frac{1}{\varepsilon \tilde{N}^2} & -\frac{\tilde{N}^j}{\varepsilon \tilde{N}^2} \\ -\frac{\tilde{N}^i}{\varepsilon \tilde{N}^2} & \tilde{\sigma}^{ij} + \frac{\tilde{N}^i \tilde{N}^j}{\varepsilon \tilde{N}^2} \end{pmatrix}. \quad (\text{E.5})$$

Here the contraction of spatial indices is understood to be with respect to the spatial metric $\tilde{\sigma}_{ij}$.

The Right Hand Side of the Foliated Flow Equation

F.1 The Second Variations of the Anisotropic Gravitational Action

In this appendix we evaluate the second variation of the anisotropic gravitational action (10.1) of Section 10.1. To organise the evaluation of the variation we split the truncation (10.1) into four parts. Therefore we have to vary the following terms

$$\begin{aligned}
 I_1 &= \int d\tau d^d x \sqrt{\sigma} K_{ij} [\sigma^{ik} \sigma^{jl}] K_{kl}, & I_2 &= \int d\tau d^d x \sqrt{\sigma} K_{ij} [\sigma^{ij} \sigma^{kl}] K_{kl}, \\
 I_3 &= \int d\tau d^d x \sqrt{\sigma}, & I_4 &= \int d\tau d^d x \sqrt{\sigma} R.
 \end{aligned} \tag{F.1}$$

Here σ denotes the determinant of the spatial metric and, R is the corresponding spatial scalar curvature and K_{ij} is the extrinsic curvature given in (10.3). We evaluate the second variation of the four terms I_1, \dots, I_4 and, for convenience, decompose the fluctuation metric $h_{ij} = \langle \hat{\sigma}_{ij} \rangle$ into a traceless and trace part according to

$$h_{ij} = h_{ij}^T + \frac{1}{d} \bar{\sigma}_{ij} h, \quad \bar{\sigma}^{ij} h_{ij}^T = 0. \tag{F.2}$$

Implementing the gauge fixing leads to vanishing shift vector and a lapse function equal to one. Thus the result of the variation reads

$$\begin{aligned}
 \delta^2 I_1 &= \int_D \left[-\frac{1}{2} h^{Tij} \partial_\tau^2 h_{ij}^T - \frac{1}{2d} h \partial_\tau^2 h + (\partial_\tau \ln \chi) \left(\frac{d-4}{4d} h \partial_\tau h - \frac{d+4}{4} h^{Tij} \partial_\tau h_{ij}^T \right) \right. \\
 &\quad \left. + (\partial_\tau \ln \chi)^2 \left(\frac{d^2 - 2d - 16}{16d} h^2 - \frac{d-4}{8} h^{Tij} h_{ij}^T \right) \right],
 \end{aligned}$$

$$\begin{aligned}
\delta^2 I_2 &= \int_D \left[-\frac{1}{2} h \partial_\tau^2 h + (\partial_\tau \ln \chi) \left(\frac{d-4}{4} h \partial_\tau h - d h^{\text{T}ij} \partial_\tau h_{ij}^{\text{T}} \right) \right. \\
&\quad \left. + (\partial_\tau \ln \chi)^2 \left(\frac{d^2-2d-16}{16} h^2 - \frac{d^2}{8} h^{\text{T}ij} h_{ij}^{\text{T}} \right) \right], \\
\delta^2 I_3 &= \int_D \left[-\frac{1}{2} h^{\text{T}ij} h_{ij}^{\text{T}} + \frac{d-2}{4d} h^2 \right], \\
\delta^2 I_4 &= \int_D \left[h \left(\frac{(d-2)(d-1)}{2d^2} \Delta + \frac{(d-2)(d-4)}{4d^2} \bar{R} \right) h - \frac{1}{2} h_{ij}^{\text{T}} \left(\Delta + \frac{d^2-3d+4}{d(d-1)} \bar{R} \right) h^{\text{T}ij} \right. \\
&\quad \left. + \frac{d-2}{d} h \bar{\nabla}_i \bar{\nabla}_j h^{\text{T}ij} - h^{\text{T}ik} \bar{\nabla}_k \bar{\nabla}_l h^{\text{T}lj} \bar{\sigma}_{ij} \right]. \tag{F.3}
\end{aligned}$$

Here we abbreviated $\int_D = \int d\tau d^d x \sqrt{\bar{\sigma}}$ and $\bar{\nabla}$ denotes the covariant derivative with respect to $\bar{\sigma}_{ij}$. Furthermore $\Delta = -\bar{\sigma}^{ij} \bar{\nabla}_i \bar{\nabla}_j$ is the corresponding Laplace operator. Obviously there is still an off-diagonal term in $\delta^2 I_4$ which makes our life harder when we want to evaluate the inverse of $\Gamma_k^{(2)} + \mathcal{R}_k$. Thus we decompose the metric a bit further and will use the TT decomposition, also known as the York decomposition [175].

$$h_{ij}^{\text{T}} = h_{ij}^{\text{TT}} + \bar{\nabla}_i \xi_j + \bar{\nabla}_j \xi_i + \bar{\nabla}_i \bar{\nabla}_j \varsigma + \frac{1}{d} \bar{\sigma}_{ij} \Delta \varsigma. \tag{F.4}$$

The new fields satisfy $\bar{\sigma}^{ij} h_{ij}^{\text{TT}} = 0$, $\bar{\nabla}^i h_{ij}^{\text{TT}} = 0$ and $\bar{\nabla}^i \xi_i = 0$. Inserting this decomposition into the second variations is a lengthy exercise and it helps to use the following intermediate results

$$\begin{aligned}
\int_D h^{\text{T}ij} h_{ij}^{\text{T}} &= \int_D \left\{ h^{\text{TT}ij} h_{ij}^{\text{TT}} + 2\xi^i \left[\Delta - \frac{1}{d} \bar{R} \right] \xi_i + \frac{d-1}{d} \varsigma \left[\Delta^2 - \frac{1}{d-1} \bar{R} \Delta \right] \varsigma \right\}, \\
\int_D h^{\text{T}ij} \Delta h_{ij}^{\text{T}} &= \int_D \left\{ h^{\text{TT}ij} \Delta h_{ij}^{\text{TT}} + 2\xi_i \left[\Delta - \frac{1}{d} \bar{R} \right] \left[\Delta - \frac{d+1}{d(d-1)} \bar{R} \right] \xi^i \right. \\
&\quad \left. + \frac{d-1}{d} \varsigma \left[\Delta^2 - \frac{1}{d-1} \bar{R} \Delta \right] \left[\Delta - \frac{2}{d-1} \bar{R} \right] \varsigma \right\}, \\
\int_D h^{\text{T}ik} \bar{\nabla}_k \bar{\nabla}^l h_{li}^{\text{T}} &= - \int_D \left\{ \xi^i \left[\Delta - \frac{1}{d} \bar{R} \right] \left[\Delta - \frac{1}{d} \bar{R} \right] \xi_i \right. \\
&\quad \left. + \frac{(d-1)^2}{d^2} \varsigma \left[\Delta^2 - \frac{1}{d-1} \bar{R} \Delta \right] \left[\Delta - \frac{1}{d-1} \bar{R} \right] \varsigma \right\}, \\
\int_D h \bar{\nabla}^i \bar{\nabla}^j h_{ij}^{\text{T}} &= \int_D \frac{d-1}{d} h \left[\Delta^2 - \frac{1}{d-1} \bar{R} \Delta \right] \varsigma. \tag{F.5}
\end{aligned}$$

At this point it becomes apparent that it is useful to redefine the fields ξ^i and ς according to

$$\varsigma \mapsto \sqrt{\Delta} \sqrt{\Delta - \frac{1}{(d-1)} \bar{R}} \varsigma, \quad \xi^j \mapsto \sqrt{\Delta - \frac{1}{d} \bar{R}} \xi^j. \tag{F.6}$$

Note that at this point we already did two field redefinitions. We started with the York decomposition $h_{ij} \rightarrow (h_{ij}^{\text{TT}}, \xi_i, \varsigma, h)$ which was followed by (F.6). Both cause

a change of integration variables in the path integral and thus produce Jacobians. However, it was shown in [150] that the Jacobians corresponding to these two field redefinitions cancel each other for the spherical background (10.5). Now we can combine the field redefinition (F.6) and the intermediate formula (F.5) and insert this into the second variations (F.3). To shorten the notation we introduce

$$C_{2\Gamma} = \frac{d^2 - 3d + 4}{d(d-1)}, \quad C_0 = \frac{(d-2)(d-1)}{d^2} \quad (\text{F.7})$$

to finally find the second variations of the monomials I_1, \dots, I_4 to become

$$\begin{aligned} \delta^2 I_1 &= -\frac{1}{2} \int_D \left\{ h^{ij\text{TT}} \partial_\tau^2 h_{ij}^{\text{TT}} + \frac{d-1}{d} \varsigma \partial_\tau^2 \varsigma + 2\xi^j \partial_\tau^2 \xi_j + \frac{1}{d} h \partial_\tau^2 h \right. \\ &\quad + (\partial_\tau \ln \chi) \left[\frac{d+4}{2} h^{\text{TT}ij} \partial_\tau h_{ij}^{\text{TT}} - \frac{d-4}{2d} h \partial_\tau h + (d+4) \xi^i \partial_\tau \xi_i \right. \\ &\quad \left. \left. + \frac{(d+4)(d-1)}{2d} \varsigma \partial_\tau \varsigma \right] \right. \\ &\quad \left. + (\partial_\tau \ln \chi)^2 \left[\frac{d-4}{4} h^{\text{TT}ij} h_{ij}^{\text{TT}} - \frac{d^2-2d-16}{8d} h^2 + \frac{d+1}{2} \xi^i \xi_i \right. \right. \\ &\quad \left. \left. + \frac{(d+8)(d-1)}{4d} \varsigma \varsigma \right] \right\}, \\ \delta^2 I_2 &= -\frac{1}{2} \int_D \left\{ h \partial_\tau^2 h \right. \\ &\quad + (\partial_\tau \ln \chi) \left[2dh^{\text{TT}ij} \partial_\tau h_{ij}^{\text{TT}} - \frac{d-4}{2} h \partial_\tau h + 4d \xi^i \partial_\tau \xi_i \right. \\ &\quad \left. \left. + 2(d-1) \varsigma \partial_\tau \varsigma \right] \right. \\ &\quad \left. + (\partial_\tau \ln \chi)^2 \left[\frac{d^2}{4} h^{\text{TT}ij} h_{ij}^{\text{TT}} - \frac{d^2-2d-16}{8} h^2 + \frac{d^2+4d}{2} \xi^i \xi_i \right. \right. \\ &\quad \left. \left. + \frac{(d+8)(d-1)}{4} \varsigma \varsigma \right] \right\}, \\ \delta^2 I_3 &= \int_D \left\{ -\frac{1}{2} h^{ij\text{TT}} h_{ij}^{\text{TT}} - \frac{d-1}{2d} \varsigma^2 - \xi^j \xi_j + \frac{d-2}{4d} h^2 \right\}, \\ \delta^2 I_4 &= \int_D \left\{ \frac{1}{2} C_0 h \left[\Delta + \frac{d-4}{2(d-1)} \bar{R} \right] h - \frac{1}{2} h_{ij}^{\text{TT}} \left[\Delta + C_{2\Gamma} \bar{R} \right] h^{ij\text{TT}} - \frac{d-2}{d} \bar{R} \xi_i \xi^i \right. \\ &\quad \left. + \frac{1}{2} C_0 \varsigma \left[\Delta - \bar{R} \right] \varsigma + C_0 h \left[\Delta^2 - \frac{1}{d-1} \bar{R} \Delta \right]^{1/2} \varsigma \right\}. \quad (\text{F.8}) \end{aligned}$$

Here we used that the spatial Laplacian is time independent and thus commutes with ∂_τ . It is convenient to organise the terms quadratic in the fluctuations ac-

ording to the components. Abbreviating $\partial_\tau \ln \chi = \gamma$ we find

$$\delta^2 \Gamma_{\text{TT}}^{\text{grav}} = \frac{\sqrt{\varepsilon}}{16\pi G_k} \int d^D x \sqrt{\sigma} \frac{1}{2} h_{ij}^{\text{TT}} \left[\Delta + C_{2\text{T}} \bar{R} - 2\Lambda_k - \frac{1}{\varepsilon} \partial_\tau^2 \right. \\ \left. + \gamma \frac{4d\lambda_k - d - 4}{2\varepsilon} \partial_\tau + \gamma^2 \frac{d^2 \lambda_k + 4 - d}{4\varepsilon} \right] h^{\text{TT}ij}, \quad (\text{F.9})$$

$$\delta^2 \Gamma_{\xi\xi}^{\text{grav}} = \frac{\sqrt{\varepsilon}}{16\pi G_k} \int d^D x \sqrt{\sigma} \xi_i \left[\frac{d-2}{d} \bar{R} - 2\Lambda_k - \frac{1}{\varepsilon} \partial_\tau^2 \right. \\ \left. + \gamma \frac{4d\lambda_k - d - 4}{2\varepsilon} \partial_\tau + \gamma^2 \frac{(d^2 + 4d)\lambda_k - d - 1}{4\varepsilon} \right] \xi^i, \quad (\text{F.10})$$

$$\delta^2 \Gamma_{\zeta\zeta}^{\text{grav}} = \frac{\sqrt{\varepsilon}}{16\pi G_k} \int d^D x \sqrt{\sigma} \frac{1}{2} \zeta \left[-C_0(\Delta - \bar{R}) - \frac{2(d-1)}{d} \Lambda_k - \frac{d-1}{d\varepsilon} \partial_\tau^2 \right. \\ \left. + \gamma \frac{(d-1)(4d\lambda_k - d - 4)}{2d\varepsilon} \partial_\tau + \gamma^2 \frac{(d-1)(d+8)(d\lambda_k - 1)}{4d\varepsilon} \right] \zeta, \quad (\text{F.11})$$

$$\delta^2 \Gamma_{hh}^{\text{grav}} = \frac{\sqrt{\varepsilon}}{16\pi G_k} \int d^D x \sqrt{\sigma} \frac{1}{2} h \left[-C_0 \Delta - \frac{(d-2)(d-4)}{2d^2} \bar{R} + \frac{d-2}{d} \Lambda_k + \frac{d\lambda_k - 1}{d\varepsilon} \partial_\tau^2 \right. \\ \left. - \gamma \frac{(d-4)(d\lambda_k - 1)}{2d\varepsilon} \partial_\tau - \gamma^2 \frac{(d^2 - 2d - 16)(d\lambda_k - 1)}{8d\varepsilon} \right] h, \quad (\text{F.12})$$

$$\delta^2 \Gamma_{h\zeta}^{\text{grav}} = -\frac{\sqrt{\varepsilon}}{16\pi G_k} \int d^D x \sqrt{\sigma} C_0 h \left[\Delta^2 - \frac{1}{d-1} \bar{R} \Delta \right]^{1/2} \zeta. \quad (\text{F.13})$$

This final result of our second variation is not diagonal yet in the fields. However, we find a block diagonal form where each block can be inverted on its own. The off-diagonal terms in the scalar sector can be handled separately and the inversion as well as the evaluation of the trace is done in Appendix F.2.

F.2 The Scalar Trace

In this appendix we evaluate the scalar trace appearing in Section 10.2. The starting point is (10.20) which reads

$$\mathcal{T}_{\text{scalar}} = \frac{1}{2} \text{Tr}_D \left[\frac{\Gamma_{\zeta\zeta}^{(2)} \partial_t \mathcal{R}_k^{hh} + \Gamma_{hh}^{(2)} \partial_t \mathcal{R}_k^{\zeta\zeta} - 2\Gamma_{h\zeta}^{(2)} \partial_t \mathcal{R}_k^{h\zeta}}{\Gamma_{hh}^{(2)} \Gamma_{\zeta\zeta}^{(2)} - \Gamma_{h\zeta}^{(2)} \Gamma_{\zeta h}^{(2)}} \right] \quad (\text{F.14})$$

with the second variations given in (10.9) - (10.11) and the regulators given in (10.16). The index D at the trace shows that it includes a D -dimensional momentum integral.

Note that the field ζ is constrained as discussed in Appendix C.2 and thus has a different expansion in eigenmodes than the field ϕ . Explicitly the lowest two eigenmodes of ζ do not contribute and thus we should be careful with mixed terms as we are considering them here. However these effects have been investigated in detail in [119]. There the authors show that all effects are proportional to $\delta_{d,2}$ and $\delta_{d,4}$. As we are interested in $d = 3$, these subtleties do not affect our computation and will not be considered any further.

Finally we are not interested in the complete trace, but only in constant terms, terms proportional to the background scalar curvature \bar{R} and terms proportional to $\gamma^2 = (\partial_\tau \ln \chi)^2$. Thus we use an expansion for \bar{R} and γ and omit all higher-order terms.¹ Therefore we start to investigate the denominator in (F.14) which is a function of both parameters

$$\frac{\sqrt{\varepsilon}}{16\pi G_k} f(\bar{R}, \gamma) = \Gamma_{hh}^{(2)} \Gamma_{\zeta\zeta}^{(2)} - \Gamma_{h\zeta}^{(2)} \Gamma_{\zeta h}^{(2)}. \quad (\text{F.15})$$

In order to expand the expression under the trace we have to calculate $f(0,0)$, $\partial_{\bar{R}} f(0,0)$, $\partial_\gamma f(0,0)$ and $\partial_\gamma^2 f(0,0)$. These can be evaluated to

$$\begin{aligned} f(0,0) &= f_{00}^1 P_k + f_{00}^2, & \partial_{\bar{R}} f(0,0) &= f_{10}^1 P_k + f_{10}^2, \\ \partial_\gamma f(0,0) &= f_{01}^1 P_k + f_{01}^2, & \partial_\gamma^2 f(0,0) &= f_{02}^1 P_k + f_{02}^2 \end{aligned} \quad (\text{F.16})$$

with the prefactors f_{pq}^r given in terms of the spatial dimension d and the dimensionless quantities

$$\bar{\Lambda}_k = \frac{\Lambda_k}{k^2}, \quad m = \frac{2\pi}{\beta k}, \quad \bar{G}_k = G_k k^{d-1}, \quad \lambda_k. \quad (\text{F.17})$$

Explicitly the prefactors read

$$\begin{aligned} f_{00}^1 &= C_0 \left(k^2 \bar{\Lambda}_k - \frac{1 - \lambda_k}{\varepsilon} m^2 n^2 k^2 \right), \\ f_{00}^2 &= C_0 \left(k^2 \bar{\Lambda}_k - \frac{1 - \lambda_k}{\varepsilon} m^2 n^2 k^2 \right) w_0 k^2, \\ f_{10}^1 &= -\frac{d-2}{2d} C_0, \\ f_{10}^2 &= \frac{2(d-3)}{d} C_0 \bar{\Lambda}_k k^2 - \frac{d-6+2d\lambda_k}{2d\varepsilon} C_0 m^2 n^2 k^2, \end{aligned}$$

¹Note that here \bar{R} and γ are merely bookkeeping devices and no dynamical objects.

$$\begin{aligned}
f_{01}^1 &= iC_0 \frac{-3d\lambda_k + d + 2}{2\varepsilon} mnk, \\
f_{01}^2 &= -i \frac{2(d-1)(d\lambda_k - 1)(d\lambda_k - 2)}{d^2} m^3 n^3 k^3 \\
&\quad + i \frac{(d-1)((6d^2 - 16d)\lambda_k - d^2 - 4d + 16)}{2d^2\varepsilon} \bar{\Lambda}_k k^3 mn, \\
f_{02}^1 &= -C_0 \frac{(d+16)(d\lambda_k - 1)}{4\varepsilon}, \\
f_{02}^2 &= \frac{(d-1)(d^2 + 2d - 16)(d\lambda_k - 1)}{d^2\varepsilon} \bar{\Lambda}_k k^2 \\
&\quad + \frac{(d-1)(d\lambda_k - 1)(6d(d-8)\lambda_k - 3d^2 + 4d + 64)}{4d^2} m^2 n^2 k^2. \tag{F.18}
\end{aligned}$$

Here we introduced w_0 in the second line as

$$w_0 = \frac{1}{\bar{\Lambda}_k - \frac{1-\lambda_k}{\varepsilon} m^2 n^2} \left(-2\bar{\Lambda}_k^2 + \frac{d-4+2d\lambda_k}{(d-2)\varepsilon} \bar{\Lambda}_k m^2 n^2 - \frac{(d\lambda_k-1)}{(d-2)} m^4 n^4 \right). \tag{F.19}$$

This can be used to perform the expansion in \bar{R} and γ

$$\begin{aligned}
\frac{1}{a + b\bar{R}} &= \frac{1}{a} - \frac{b\bar{R}}{a^2} + O(\bar{R}^2), \\
\frac{1}{a + b\gamma + c\gamma^2} &= \frac{1}{\gamma} - \frac{b\gamma}{a^2} + \frac{b^2 - ac}{a^3} \gamma^2 + O(\gamma^3). \tag{F.20}
\end{aligned}$$

Furthermore we need

$$\frac{1}{(a + b\gamma + c\gamma^2)^2} = \frac{1}{a^2} + O(\gamma). \tag{F.21}$$

To evaluate these expansions systematically we decompose $\mathcal{T}_{\text{scalar}}$, for convenience, according to

$$\mathcal{T}_{\text{scalar}} = \mathcal{T}_{\text{scalar}}^{\text{I}} + \mathcal{T}_{\text{scalar}}^{\text{II}} + \mathcal{T}_{\text{scalar}}^{\text{III}}. \tag{F.22}$$

These three parts can be expanded separately in \bar{R} and γ to give

$$\begin{aligned}
\mathcal{T}_{\text{scalar}}^{\text{I}} &= \frac{1}{2} \text{Tr}_D \left[\frac{\Gamma_{\zeta\zeta}^{(2)} \partial_t \mathcal{R}_k^{hh}}{\Gamma_{hh}^{(2)} \Gamma_{\zeta\zeta}^{(2)} - \Gamma_{h\zeta}^{(2)} \Gamma_{\zeta h}^{(2)}} \right] \\
&= -\frac{C_0}{2} \sqrt{\varepsilon} \sum_n \text{Tr}_d \left\{ \frac{\partial_t (\beta Z_{Nk} R_k)}{\beta Z_{Nk}} \left[\frac{-C_0 P_k + b_1}{f(0,0)} + \bar{R} \left(\frac{b_2}{f(0,0)} - \frac{-C_0 P_k + b_1}{f(0,0)^2} \partial_{\bar{R}} f(0,0) \right) \right] \right. \\
&\quad \left. + \gamma^2 \left(\frac{2b_4}{f(0,0)} - \frac{b_3}{f(0,0)^2} \partial_\gamma f(0,0) + \frac{-C_0 P_k + b_1}{2} \left(-\frac{\partial_\gamma^2 f(0,0)}{f(0,0)^2} + 2\frac{(\partial_\gamma f(0,0))^2}{f(0,0)^3} \right) \right) \right\},
\end{aligned}$$

$$\begin{aligned}
\mathcal{T}_{\text{scalar}}^{\text{II}} &= \frac{1}{2} \text{Tr}_D \left[\frac{\Gamma_{hh}^{(2)} \partial_t \mathcal{R}_k^{\zeta\zeta}}{\Gamma_{hh}^{(2)} \Gamma_{\zeta\zeta}^{(2)} - \Gamma_{h\zeta}^{(2)} \Gamma_{\zeta h}^{(2)}} \right] \\
&= -\frac{C_0}{2} \sqrt{\varepsilon} \sum_n \text{Tr}_d \left\{ \frac{\partial_t (\beta Z_{Nk} R_k)}{\beta Z_{Nk}} \left[\frac{-C_0 P_k + b_5}{f(0,0)} + \bar{R} \left(\frac{b_6}{f(0,0)} - \frac{-C_0 P_k + b_5}{f(0,0)^2} \partial_{\bar{R}} f(0,0) \right) \right. \right. \\
&\quad \left. \left. + \gamma^2 \left(\frac{2b_8}{f(0,0)} - \frac{b_7}{f(0,0)^2} \partial_\gamma f(0,0) + \frac{-C_0 P_k + b_5}{2} \left(-\frac{\partial_\gamma^2 f(0,0)}{f(0,0)^2} + 2 \frac{(\partial_\gamma f(0,0))^2}{f(0,0)^3} \right) \right) \right] \right\}, \\
\mathcal{T}_{\text{scalar}}^{\text{III}} &= \frac{1}{2} \text{Tr}_D \left[\frac{-2\Gamma_{h\zeta}^{(2)} \partial_t \mathcal{R}_k^{h\zeta}}{\Gamma_{hh}^{(2)} \Gamma_{\zeta\zeta}^{(2)} - \Gamma_{h\zeta}^{(2)} \Gamma_{\zeta h}^{(2)}} \right] \\
&= -C_0^2 \sqrt{\varepsilon} \sum_n \text{Tr}_d \left\{ \frac{\partial_t (\beta Z_{Nk} R_k)}{\beta Z_{Nk}} \left[\frac{P_k}{f(0,0)} - \bar{R} \left(\frac{(2(d-1))^{-1}}{f(0,0)} + \frac{P_k \partial_{\bar{R}} f(0,0)}{f(0,0)^2} \right) \right. \right. \\
&\quad \left. \left. + \gamma^2 \left(-\frac{P_k \partial_\gamma^2 f(0,0)}{f(0,0)^2} + 2 \frac{P_k (\partial_\gamma f(0,0))^2}{f(0,0)^3} \right) \right] \right\}. \tag{F.23}
\end{aligned}$$

Here we omitted irrelevant terms and introduced for better readability the abbreviations

$$\begin{aligned}
b_1 &= -\frac{2(d-1)}{d} \bar{\Lambda}_k k^2 + \frac{d-1}{d\varepsilon} m^2 n^2 k^2, & b_5 &= \frac{d-2}{d} \bar{\Lambda}_k k^2 - \frac{d\lambda_k - 1}{d\varepsilon} m^2 n^2 k^2, \\
b_2 &= C_0, & b_6 &= -\frac{(d-2)(d-4)}{2d^2}, \\
b_3 &= i \frac{(d-1)(4d\lambda_k - d - 4)}{2d\varepsilon} mnk, & b_7 &= -i \frac{(d-4)(d\lambda_k - 1)}{2d\varepsilon} mnk, \\
b_4 &= \frac{(d-1)(d+8)(d\lambda_k - 1)}{4d\varepsilon}, & b_8 &= -\frac{(d\lambda_k - 1)(d^2 - 2d - 16)}{8d\varepsilon}. \tag{F.24}
\end{aligned}$$

These should not be confused with the abbreviations introduced in the main text. We used the same symbols here, since a confusion is very unlikely.

Now all traces appearing in (F.23) are of the form discussed in Appendix C. Thus we can evaluate the traces and combine the result for $\mathcal{T}_{\text{scalar}}^{\text{I}}$, $\mathcal{T}_{\text{scalar}}^{\text{II}}$ and $\mathcal{T}_{\text{scalar}}^{\text{III}}$. The result is very lengthy and thus again we introduce abbreviations, labeled with a_k , $k = 1, \dots, 14$, to improve the readability. The result, after evaluating the trace, reads

$$\begin{aligned}
\mathcal{T}_{\text{scalar}} &= -\frac{2\sqrt{\varepsilon}}{(4\pi)^{d/2}} \sum_n \int d^d x \sqrt{\sigma} k^d \left[a_1 q_{d/2}^{1,0} \right. \\
&\quad \left. + \frac{\bar{R}}{k^2} \left(\frac{a_1}{6} q_{d/2-1}^{1,0} + a_2 X q_{d/2}^{1,0} + (a_3 + a_4 m^2 n^2) X q_{d/2}^{2,0} + a_5 X q_{d/2}^{2,-1} \right) \right]
\end{aligned}$$

$$\begin{aligned}
& + \frac{\gamma^2}{k^2} \left(a_6 X q_{d/2}^{1,0} + (a_7 + a_8 m^2 n^2 + a_9 X m^2 n^2 + a_{10} X m^4 n^4) X q_{d/2}^{2,0} \right. \\
& \quad + (a_{11} + a_{12} X m^2 n^2) X q_{d/2}^{2,-1} + (a_{13} + a_{14} m^2 n^2 + a_{15} m^4 n^4) X^2 m^2 n^2 q_{d/2}^{3,0} \\
& \quad \left. + (a_{16} + a_{17} m^2 n^2) X^2 m^2 n^2 q_{d/2}^{3,-1} + a_{18} X^2 m^2 n^2 q_{d/2}^{3,-2} \right). \quad (\text{F.25})
\end{aligned}$$

Here the q functions are defined as $q_n^{p,q}(w) = \Phi_n^{p,q}(w) - \frac{1}{2} \eta_N \tilde{\Phi}_n^{p,q}(w)$ and understood to be evaluated at w_0 , given in (F.19). The anomalous dimension reads $\eta_N = -\partial_t \ln(\beta Z_{Nk})$, the threshold functions $\Phi, \tilde{\Phi}$ can be found in Appendix C.4 and the prefactors read

$$\begin{aligned}
X &= \left(\bar{\Lambda}_k - \frac{1-\lambda_k}{\varepsilon} m^2 n^2 \right)^{-1}, \\
a_1 &= -\frac{1}{2}, \quad a_2 = \frac{d-2}{4d}, \quad a_3 = \frac{d-3}{d} \bar{\Lambda}_k, \quad a_4 = -\frac{d-6+2d\lambda_k}{4d\varepsilon}, \quad a_5 = -\frac{d-2}{4d}, \\
a_6 &= \frac{(d+16)(d\lambda_k-1)}{16\varepsilon}, \quad a_7 = \frac{(d^2+2d-16)(d\lambda_k-1)\bar{\Lambda}_k}{4\varepsilon(d-2)}, \\
a_8 &= \frac{(d\lambda_k-1)(6d(d-8)\lambda_k-3d^2+4d+64)}{16(d-2)}, \quad a_9 = \frac{(3d\lambda_k-d-2)((6d-16)d\lambda_k-d^2-4d+16)\bar{\Lambda}_k}{8(d-2)}, \\
a_{10} &= -\frac{(d\lambda_k-1)(d\lambda_k-2)(3d\lambda_k-d-2)}{2\varepsilon(d-2)}, \quad a_{11} = -\frac{(d+16)(d\lambda_k-1)}{16\varepsilon}, \quad a_{12} = -\frac{(3d\lambda_k-d-2)^2}{8}, \\
a_{13} &= \frac{((6d^2-16d)\lambda_k-d^2-4d+16)^2 \bar{\Lambda}_k^2}{8(d-2)^2}, \quad a_{14} = -\frac{((6d^2-16d)\lambda_k-d^2-4d+16)\bar{\Lambda}_k(d\lambda_k-1)(d\lambda_k-2)}{\varepsilon(d-2)^2}, \\
a_{15} &= \frac{2(d\lambda_k-1)^2(d\lambda_k-2)^2}{(d-2)^2}, \quad a_{16} = -\frac{(3d\lambda_k-d-2)((6d^2-16d)\lambda_k-d^2-4d+16)\bar{\Lambda}_k}{4(d-2)}, \\
a_{17} &= \frac{(3d\lambda_k-d-2)(d\lambda_k-1)(d\lambda_k-2)}{(d-2)\varepsilon}, \quad a_{18} = \frac{(3d\lambda_k-d-2)^2}{8}. \quad (\text{F.26})
\end{aligned}$$

The scalar trace (F.25) constitutes the final result of this appendix. Added to the TT trace in Section 10.2 it gives the right hand side of the foliated Wetterich equation (9.11).

F.3 Summing the Matsubara Modes

This appendix treats the sums over Matsubara modes which are left after performing the operator traces in Section 10.2. Due to simplicity we start with the TT sector, before turning to the Matsubara sums in the scalar sector. The sums appearing in (10.30) are of the form $\sum_n (m^2 n^2)^r q_l^{p,q}(w_{2T})$ where

$$w_{2T} = -2\bar{\Lambda}_k + \varepsilon^{-1} m^2 n^2. \quad (\text{F.27})$$

The q functions have been defined in Section 10.2 and read

$$q_l^{p,q}(w) = \Phi_l^{p,q}(w) - \frac{1}{2} \eta_N \tilde{\Phi}_l^{p,q}(w), \quad \eta_N = -\partial_t \ln(\beta Z_{Nk}). \quad (\text{F.28})$$

The threshold functions are given in Appendix C and we specify to the simple result (C.32) reached for the optimised cutoff. Therefore all sums are of the form $\sum_n n^{2r} (1 + w_{2T})^{-p}$ with w_{2T} given in (F.27). The infinite sums can be performed by utilising the master formulas

$$\sum_{n=-\infty}^{\infty} \frac{1}{n^2 + x^2} = \frac{\pi}{x \tanh(\pi x)}, \quad \sum_{n=-\infty}^{\infty} \frac{1}{n^2 - x^2} = -\frac{\pi}{x \tan(\pi x)}. \quad (\text{F.29})$$

To shorten the notation we introduce the following summed threshold functions for $r \leq p - 1$

$$\Upsilon_l^{p,r} = \sum_{n=-\infty}^{\infty} (m^2 n^2)^r \Phi_l^{p,q}(w_{2T}), \quad \tilde{\Upsilon}_l^{p,r} = \sum_{n=-\infty}^{\infty} (m^2 n^2)^r \tilde{\Phi}_l^{p,q}(w_{2T}). \quad (\text{F.30})$$

There are only few combinations of p and r appearing in (10.30), which are $(p, r) = (1, 0), (2, 0), (3, 1)$. The summation of $\Upsilon_l^{1,0}$ is fairly simple since it is a direct implementation of the master formula (F.29). The evaluation gives

$$\Upsilon_l^{1,0} = \frac{1}{\Gamma(l+1)} \frac{\pi}{m} \sqrt{\frac{\varepsilon}{1-2\bar{\Lambda}_k}} \frac{1}{\tanh\left(\frac{\pi}{m} \sqrt{\varepsilon(1-2\bar{\Lambda}_k)}\right)}. \quad (\text{F.31})$$

The next summed threshold functions, $\Upsilon_l^{p,0}, p > 1$, can be deduced iteratively from the first one by considering $\Upsilon_l^{p+1,0} = \frac{1}{2^p} \partial_{\bar{\Lambda}_k} \Upsilon_l^{p,0}$. This leads to

$$\Upsilon_l^{2,0} = \frac{1}{\Gamma(l+1)} \frac{\sqrt{\varepsilon} \pi}{2m(1-2\bar{\Lambda}_k)} \left(\frac{(\sqrt{1-2\bar{\Lambda}_k})^{-1}}{\tanh\left(\frac{\pi}{m} \sqrt{\varepsilon(1-2\bar{\Lambda}_k)}\right)} + \frac{\sqrt{\varepsilon} \pi}{m \sinh\left(\frac{\pi}{m} \sqrt{\varepsilon(1-2\bar{\Lambda}_k)}\right)^2} \right). \quad (\text{F.32})$$

Terms with higher values for r can be found recursively via $\Upsilon_l^{p+1,r+1} = -\frac{\varepsilon}{2^p m} (m^2)^{r+1} \partial_m (\Upsilon_l^{p,r} / (m^2)^r)$. This iteration gives us the last missing summed threshold function, which reads

$$\Upsilon_l^{3,1} = \frac{1}{\Gamma(l+1)} \frac{\pi}{16m^3} \left(\frac{\varepsilon}{1-2\bar{\Lambda}_k} \right)^{\frac{3}{2}} \left(\frac{2m^2}{\tanh\left(\frac{\pi}{m} \sqrt{\varepsilon(1-2\bar{\Lambda}_k)}\right)} + \frac{2\pi m \sqrt{\varepsilon} \sqrt{1-2\bar{\Lambda}_k}}{\sinh\left(\frac{\pi}{m} \sqrt{\varepsilon(1-2\bar{\Lambda}_k)}\right)^2} - \frac{4\pi^2 \varepsilon (1-2\bar{\Lambda}_k)}{\tanh\left(\frac{\pi}{m} \sqrt{\varepsilon(1-2\bar{\Lambda}_k)}\right) \sinh\left(\frac{\pi}{m} \sqrt{\varepsilon(1-2\bar{\Lambda}_k)}\right)^2} \right). \quad (\text{F.33})$$

The threshold functions denoted with a tilde are related to the ones above by $\tilde{\Upsilon}_l^{p,r} = \frac{\Gamma(l+1)}{\Gamma(l+2)} \Upsilon_l^{p,r}$. Finally, for convenience, we introduce the summed version of the q functions which we denote by

$$T_l^{p,r} = \Upsilon_l^{p,r} - \frac{1}{2} \eta_N \tilde{\Upsilon}_l^{p,r}. \quad (\text{F.34})$$

Similar considerations have to be done for the scalar part. However this is more involved since w_0 is a polynomial of second order in n^2 and thus the master formula (F.29) can not be applied directly. To boil the appearing terms down to the form (F.29) we use the partial fraction decomposition. Therefore we write

$$\begin{aligned} 1 + w_0 &= \frac{\kappa_1 \bar{\Lambda}_k - 2\kappa_2 \bar{\Lambda}_k^2 + \left(\frac{d-4+2d\lambda_k}{(d-2)\varepsilon} \kappa_3 \bar{\Lambda}_k - \kappa_1 \frac{1-\lambda_k}{\varepsilon} \right) m^2 n^2 + \kappa_4 \frac{(1-d\lambda_k)}{(d-2)} m^4 n^4}{\kappa_5 \bar{\Lambda}_k - \frac{1-\lambda_k}{\varepsilon} m^2 n^2} \Bigg|_{\kappa_1=\dots=\kappa_5=1} \\ &= \frac{\kappa_4 \frac{1-d\lambda_k}{d-2} m^4 (n^2 - w_+) (n^2 - w_-)}{\kappa_5 \bar{\Lambda}_k - \frac{1-\lambda_k}{\varepsilon} m^2 n^2} \Bigg|_{\kappa_1=\dots=\kappa_5=1} \end{aligned} \quad (\text{F.35})$$

where we introduced five auxiliary parameters $\kappa_1, \dots, \kappa_5$. The zeros w_{\pm} are given as

$$\begin{aligned} w_{\pm} &= -\frac{d-2}{2(1-d\lambda_k)m^2\kappa_4} \left(\frac{d-4+2d\lambda_k}{(d-2)\varepsilon} \kappa_3 \bar{\Lambda}_k - \kappa_1 \frac{1-\lambda_k}{\varepsilon} \right) \\ &\pm \sqrt{\frac{(d-2)^2}{4(1-d\lambda_k)^2 m^4 \kappa_4^2} \left(\frac{d-4+2d\lambda_k}{(d-2)\varepsilon} \kappa_3 \bar{\Lambda}_k - \frac{\kappa_1(1-\lambda_k)}{\varepsilon} \right)^2 - \frac{(d-2)\bar{\Lambda}_k(\kappa_1-2\kappa_2\bar{\Lambda}_k)}{(1-d\lambda_k)m^4\kappa_4}} \end{aligned} \quad (\text{F.36})$$

and can be used to evaluate the partial fraction decomposition of $(1+w_0)^{-1}$. The result reads

$$\begin{aligned} \frac{1}{1+w_0} &= \frac{d-2}{(1-d\lambda_k)m^4\kappa_4} \left[\frac{\frac{1}{w_+-w_-} \left(\frac{1-\lambda_k}{\varepsilon} m^2 n^2 - \kappa_5 \bar{\Lambda}_k \right)}{n^2 - w_-} \right. \\ &\quad \left. - \frac{\frac{1}{w_+-w_-} \left(\frac{1-\lambda_k}{\varepsilon} m^2 n^2 - \kappa_5 \bar{\Lambda}_k \right)}{n^2 - w_+} \right] \end{aligned} \quad (\text{F.37})$$

which finally contains two terms of the form of the master formula. For the rest we can follow the lines of the TT part. The end of Appendix F.2, or (10.33), shows that terms of the following form appear on the right hand side of the flow equation

$$\begin{aligned} \Psi_{l,s}^{p,r} &= \sum_{n=-\infty}^{\infty} \frac{(m^2 n^2)^r}{\left(\bar{\Lambda}_k - \frac{1-\lambda_k}{\varepsilon} m^2 n^2 \right)^s} \Phi_l^{p,q}(w_0), \\ \tilde{\Psi}_{l,s}^{p,r} &= \sum_{n=-\infty}^{\infty} \frac{(m^2 n^2)^r}{\left(\bar{\Lambda}_k - \frac{1-\lambda_k}{\varepsilon} m^2 n^2 \right)^s} \tilde{\Phi}_l^{p,q}(w_0). \end{aligned} \quad (\text{F.38})$$

Starting with the easiest one, we can use the partial fraction decomposition (F.37) to sum the threshold function $\Phi_l^{1,0}(w_0)$. The summed threshold function, with all auxiliary parameters set to one, reads

$$\Psi_{l,0}^{1,0} = \frac{1}{\Gamma(1+l)} \frac{d-2}{1-d\lambda_k} \frac{\pi}{m^4(w_+-w_-)} \left[\frac{\bar{\Lambda}_k - \frac{1-\lambda_k}{\varepsilon} m^2 w_-}{\sqrt{w_-} \tan(\pi\sqrt{w_-})} - \frac{\bar{\Lambda}_k - \frac{1-\lambda_k}{\varepsilon} m^2 w_+}{\sqrt{w_+} \tan(\pi\sqrt{w_+})} \right]. \quad (\text{F.39})$$

However, we need further summations, which are more complicated. Investigating the result at the end of Appendix F.2 we find that the following combinations are needed: $(p, r, s) = (1, 0, 1), (2, 0, 1), (2, 1, 1), (2, 1, 2), (2, 2, 2), (3, 1, 2), (3, 2, 2), (3, 3, 2)$. To find all these terms we start with $\Psi_{l,1}^{1,0}$. This can be found by taking one derivative with respect to the parameter κ_5 . Afterwards we set it to one, since we will not need it again. We use $\frac{1}{\Lambda_k} \partial_{\kappa_5} \Psi_{l,0}^{1,0} = \Psi_{l,1}^{1,0}$ to find

$$\Psi_{l,1}^{1,0} = \frac{1}{\Gamma(1+l)} \frac{d-2}{1-d\lambda_k} \frac{\pi}{m^4(w_+-w_-)} \left[\frac{1}{\sqrt{w_-} \tan(\pi\sqrt{w_-})} - \frac{1}{\sqrt{w_+} \tan(\pi\sqrt{w_+})} \right]. \quad (\text{F.40})$$

For all further terms we can use the following rules, which use the other auxiliary parameters $\kappa_1, \dots, \kappa_4$

$$\begin{aligned} \Psi_{l,s}^{p+1,r} &= -\frac{1}{p} \partial_{\kappa_1} \Psi_{l,s}^{p,r}, & \Psi_{l,s+1}^{p+1,r+1} &= -\frac{1}{p} \frac{(d-2)\varepsilon}{(d-4+2d\lambda_k)\Lambda_k} \partial_{\kappa_3} \Psi_{l,s}^{p,r}, \\ \Psi_{l,s+1}^{p+1,r} &= \frac{1}{2p\bar{\Lambda}_k^2} \partial_{\kappa_2} \Psi_{l,s}^{p,r}, & \Psi_{l,s+1}^{p+1,r+2} &= -\frac{1}{p} \frac{d-2}{1-d\lambda_k} \partial_{\kappa_4} \Psi_{l,s}^{p,r}. \end{aligned} \quad (\text{F.41})$$

Applying these rules we determine

$$\begin{aligned} \Psi_{l,1}^{2,0} &= -\frac{1}{\Gamma(1+l)} \frac{\pi(d-2)^2}{2m^8\varepsilon(1-d\lambda_k)^2(w_+-w_-)^3} \\ &\left[\frac{m^2w_-(\lambda_k-1)(3w_++w_+)+\varepsilon\bar{\Lambda}_k(5w_--w_+)}{w_-^{3/2} \tan(\pi\sqrt{w_-})} - \frac{m^2w_+(\lambda_k-1)(3w_++w_-)+\varepsilon\bar{\Lambda}_k(5w_+-w_-)}{w_+^{3/2} \tan(\pi\sqrt{w_+})} \right. \\ &\left. + \frac{\sqrt{w_-}\pi(w_--w_+)(m^2w_-(\lambda_k-1)+\varepsilon\bar{\Lambda}_k)}{w_-^{3/2} \sin(\pi\sqrt{w_-})^2} + \frac{\sqrt{w_+}\pi(w_--w_+)(m^2w_+(\lambda_k-1)+\varepsilon\bar{\Lambda}_k)}{w_+^{3/2} \sin(\pi\sqrt{w_+})^2} \right], \end{aligned} \quad (\text{F.42})$$

$$\begin{aligned} \Psi_{l,1}^{2,1} &= \frac{1}{\Gamma(1+l)} \frac{\pi(d-2)^2}{2m^6\varepsilon(1-d\lambda_k)^2(w_--w_+)^3} \\ &\left[\frac{m^2w_-(3w_++w_-)(\lambda_k-1)+\varepsilon(3w_++w_+)\bar{\Lambda}_k}{\sqrt{w_-} \tan(\pi\sqrt{w_-})} - \frac{m^2w_+(w_++3w_-)(\lambda_k-1)+\varepsilon(3w_++w_-)\bar{\Lambda}_k}{\sqrt{w_+} \tan(\pi\sqrt{w_+})} \right. \\ &\left. + \frac{\pi(w_--w_+)(m^2w_-(\lambda_k-1)+\varepsilon\bar{\Lambda}_k)}{\sin(\pi\sqrt{w_-})^2} + \frac{\pi(w_--w_+)(m^2w_+(\lambda_k-1)+\varepsilon\bar{\Lambda}_k)}{\sin(\pi\sqrt{w_+})^2} \right], \end{aligned} \quad (\text{F.43})$$

$$\begin{aligned} \Psi_{l,2}^{2,1} &= \frac{1}{\Gamma(1+l)} \frac{\pi(d-2)^2}{2m^6(1-d\lambda_k)^2(w_--w_+)^3} \\ &\left[\frac{3w_++w_+}{\sqrt{w_-} \tan(\pi\sqrt{w_-})} - \frac{w_++3w_+}{\sqrt{w_+} \tan(\pi\sqrt{w_+})} - \frac{\pi(w_+-w_-)}{\sin(\pi\sqrt{w_-})^2 \sin(\pi\sqrt{w_+})^2} \right. \\ &\left. + \frac{\pi(w_+-w_-)(\cos(\pi\sqrt{w_-})^2 - \sin(\pi\sqrt{w_-})^2)}{2 \sin(\pi\sqrt{w_-})^2 \sin(\pi\sqrt{w_+})^2} + \frac{\pi(w_+-w_-)(\cos(\pi\sqrt{w_+})^2 - \sin(\pi\sqrt{w_+})^2)}{2 \sin(\pi\sqrt{w_-})^2 \sin(\pi\sqrt{w_+})^2} \right], \end{aligned} \quad (\text{F.44})$$

$$\Psi_{l,2}^{2,2} = \frac{1}{\Gamma(1+l)} \frac{\pi(d-2)^2}{2m^4(1-d\lambda_k)^2(w_- - w_+)^3} \left[\frac{\sqrt{w_-}(w_- + 3w_+)}{\tan(\pi\sqrt{w_-})} - \frac{\sqrt{w_+}(3w_- + w_+)}{\tan(\pi\sqrt{w_+})} + \pi(w_- - w_+) \left(\frac{w_-}{\sin(\pi\sqrt{w_-})^2} + \frac{w_+}{\sin(\pi\sqrt{w_+})^2} \right) \right], \quad (\text{F.45})$$

$$\begin{aligned} \Psi_{l,2}^{3,0} = & \frac{1}{\Gamma(1+l)} \frac{\pi(d-2)^3}{8m^{12}\varepsilon(1-d\lambda_k)^3(w_- - w_+)^5} \\ & \left[\frac{m^2 w_+ (\lambda_k - 1) (-w_-^2 + 14w_- w_+ + 35w_+^2) + 3\varepsilon \bar{\Lambda}_k (w_-^2 - 6w_- w_+ + 21w_+^2)}{w_+^{5/2} \tan(\pi\sqrt{w_+})} \right. \\ & - \frac{m^2 w_- (\lambda_k - 1) (35w_-^2 + 14w_- w_+ - w_+^2) + 3\varepsilon \bar{\Lambda}_k (21w_-^2 - 6w_- w_+ + w_+^2)}{w_-^{5/2} \tan(\pi\sqrt{w_-})} \\ & + \frac{2\pi^2 (w_- - w_+)^2 (m^2 w_+ (\lambda_k - 1) + \varepsilon \bar{\Lambda}_k)}{w_+^{3/2} \tan(\pi\sqrt{w_+}) \sin(\pi\sqrt{w_+})^2} - \frac{2\pi^2 (w_- - w_+)^2 (m^2 w_- (\lambda_k - 1) + \varepsilon \bar{\Lambda}_k)}{w_-^{3/2} \tan(\pi\sqrt{w_-}) \sin(\pi\sqrt{w_-})^2} \\ & + \frac{\pi (w_+ - w_-) (m^2 w_+ (w_- + 11w_+) (\lambda_k - 1) - 3\varepsilon \bar{\Lambda}_k (w_- - 5w_+))}{w_+^2 \sin(\pi\sqrt{w_+})^2} \\ & \left. + \frac{\pi (w_+ - w_-) (m^2 w_- (11w_- + w_+) (\lambda_k - 1) + 3\varepsilon \bar{\Lambda}_k (5w_- - w_+))}{w_-^2 \sin(\pi\sqrt{w_-})^2} \right], \quad (\text{F.46}) \end{aligned}$$

$$\begin{aligned} \Psi_{l,2}^{3,1} = & - \frac{1}{\Gamma(1+l)} \frac{\pi(d-2)^3}{8m^{10}\varepsilon(1-d\lambda_k)^3(w_- - w_+)^5} \\ & \left[- \frac{3m^2 w_+ (\lambda_k - 1) (w_-^2 + 10w_- w_+ + 5w_+^2) - \varepsilon \bar{\Lambda}_k (w_-^2 - 14w_- w_+ - 35w_+^2)}{w_+^{3/2} \tan(\pi\sqrt{w_+})} \right. \\ & + \frac{3m^2 w_- (\lambda_k - 1) (5w_-^2 + 10w_- w_+ + w_+^2) + \varepsilon \bar{\Lambda}_k (35w_-^2 + 14w_- w_+ - w_+^2)}{w_-^{3/2} \tan(\pi\sqrt{w_-})} \\ & - \frac{2\pi^2 (w_- - w_+)^2 (m^2 w_+ (\lambda_k - 1) + \varepsilon \bar{\Lambda}_k)}{\sqrt{w_+} \tan(\pi\sqrt{w_+}) \sin(\pi\sqrt{w_+})^2} + \frac{2\pi^2 (w_- - w_+)^2 (m^2 w_- (\lambda_k - 1) + \varepsilon \bar{\Lambda}_k)}{\sqrt{w_-} \tan(\pi\sqrt{w_-}) \sin(\pi\sqrt{w_-})^2} \\ & + \frac{\pi (w_- - w_+) (m^2 w_+ (5w_- + 7w_+) (\lambda_k - 1) + \varepsilon \bar{\Lambda}_k (w_- + 11w_+))}{w_+ \sin(\pi\sqrt{w_+})^2} \\ & \left. + \frac{\pi (w_- - w_+) (m^2 w_- (7w_- + 5w_+) (\lambda_k - 1) + \varepsilon \bar{\Lambda}_k (11w_- + w_+))}{w_- \sin(\pi\sqrt{w_-})^2} \right], \quad (\text{F.47}) \end{aligned}$$

$$\begin{aligned} \Psi_{l,2}^{3,2} = & - \frac{1}{\Gamma(1+l)} \frac{\pi(d-2)^3}{8m^8\varepsilon(1-d\lambda_k)^3(w_- - w_+)^5} \\ & \left[(m^2 w_- (\lambda_k - 1) + \varepsilon \bar{\Lambda}_k) \left(- \frac{12\sqrt{w_+}(w_- + w_+)}{\tan(\pi\sqrt{w_+})} + \frac{3(w_-^2 + 6w_- w_+ + w_+^2)}{\sqrt{w_-} \tan(\pi\sqrt{w_-})} \right) \right. \\ & + \frac{2\pi^2 w_- (w_- - w_+)^2}{\sqrt{w_-} \tan(\pi\sqrt{w_-}) \sin(\pi\sqrt{w_-})^2} + \pi(w_- - w_+) \left(\frac{3w_- + 5w_+}{\sin(\pi\sqrt{w_-})^2} + \frac{4w_+}{\sin(\pi\sqrt{w_+})^2} \right) \\ & - (m^2 w_+ (\lambda_k - 1) + \varepsilon \bar{\Lambda}_k) \left(- \frac{12\sqrt{w_-}(w_- + w_+)}{\tan(\pi\sqrt{w_-})} + \frac{3(w_-^2 + 6w_- w_+ + w_+^2)}{\sqrt{w_+} \tan(\pi\sqrt{w_+})} \right) \\ & \left. + \frac{2\pi^2 w_+ (w_- - w_+)^2}{\sqrt{w_+} \tan(\pi\sqrt{w_+}) \sin(\pi\sqrt{w_+})^2} - \pi(w_- - w_+) \left(\frac{5w_- + 3w_+}{\sin(\pi\sqrt{w_+})^2} + \frac{4w_-}{\sin(\pi\sqrt{w_-})^2} \right) \right], \quad (\text{F.48}) \end{aligned}$$

$$\begin{aligned}
\Psi_{l,2}^{3,3} = & -\frac{1}{\Gamma(1+l)} \frac{\pi(d-2)^3}{8m^6\varepsilon(1-d\lambda_k)^3(w_- - w_+)^5} \\
& \left[\frac{\sqrt{w_-}(-m^2w_-(w_-^2 - 14w_-w_+ - 35w_+^2)(\lambda_k - 1) + 3\varepsilon\Lambda_k(w_-^2 + 10w_-w_+ + 5w_+^2))}{\tan(\pi\sqrt{w_-})} \right. \\
& + \frac{\sqrt{w_+}(m^2w_+(w_+^2 - 14w_-w_+ - 35w_-^2)(\lambda_k - 1) - 3\varepsilon\Lambda_k(w_+^2 + 10w_-w_+ + 5w_-^2))}{\tan(\pi\sqrt{w_+})} \\
& - \frac{2\pi^2w_+^{3/2}(w_- - w_+)^2(m^2w_+(\lambda_k - 1) + \varepsilon\Lambda_k)}{\tan(\pi\sqrt{w_+})\sin(\pi\sqrt{w_+})^2} + \frac{2\pi^2w_-^{3/2}(w_- - w_+)^2(m^2w_-(\lambda_k - 1) + \varepsilon\Lambda_k)}{\tan(\pi\sqrt{w_-})\sin(\pi\sqrt{w_-})^2} \\
& + \pi(w_- - w_+) \left(\frac{w_-(-m^2w_-(w_- - 13w_+)(\lambda_k - 1) + 3\varepsilon\Lambda_k(w_- + 3w_+))}{\sin(\pi\sqrt{w_-})^2} \right. \\
& \left. \left. + \frac{w_+(m^2w_+(13w_- - w_+)(\lambda_k - 1) + 3\varepsilon\Lambda_k(3w_- + w_+))}{\sin(\pi\sqrt{w_+})^2} \right) \right]. \tag{F.49}
\end{aligned}$$

Similar to the transverse traceless sector we note that $\tilde{\Psi}_{l,s}^{p,r} = \frac{\Gamma(l+1)}{\Gamma(l+2)}\Psi_{l,s}^{p,r}$. Furthermore, for convenience, we introduce the summed version of the q functions which we denote by

$$S_{l,s}^{p,r} = \Psi_{l,s}^{p,r} - \frac{1}{2}\eta_N\tilde{\Psi}_{l,s}^{p,r}. \tag{F.50}$$

In Section 10.2 the flow equations are given in terms of (F.34) and (F.50). This is a very compact notation and makes the beta functions readable.

Bibliography

- [1] Pippard B. Brown, L. and A. Pais. *"Twentieth Century Physics"*. CRC Press, 2010.
- [2] G. Aad et al. Observation of a new particle in the search for the Standard Model Higgs boson with the ATLAS detector at the LHC. *Phys.Lett.*, B716:1–29, 2012, arXiv:1207.7214.
- [3] S. Chatrchyan et al. Observation of a new boson at a mass of 125 GeV with the CMS experiment at the LHC. *Phys.Lett.*, B716:30–61, 2012, arXiv:1207.7235.
- [4] G. 't Hooft and M.J.G. Veltman. One loop divergencies in the theory of gravitation. *Annales Poincare Phys.Theor.*, A20:69–94, 1974.
- [5] M. H. Goroff and A. Sagnotti. The Ultraviolet Behavior of Einstein Gravity. *Nucl.Phys.*, B266:709, 1986.
- [6] A.E.M. van de Ven. Two loop quantum gravity. *Nucl.Phys.*, B378:309–366, 1992.
- [7] J. F. Donoghue. Introduction to the effective field theory description of gravity. 1995, arXiv:9512024.
- [8] C.P. Burgess. Quantum gravity in everyday life: General relativity as an effective field theory. *Living Rev.Rel.*, 7:5, 2004, arXiv:0311082.
- [9] J. F. Donoghue. The effective field theory treatment of quantum gravity. *AIP Conf.Proc.*, 1483:73–94, 2012, arXiv:1209.3511.
- [10] J. M. Gracia-Bondia. Notes on 'quantum gravity' and non-commutative geometry. *Lect.Notes Phys.*, 807:3–58, 2010, arXiv:1005.1174.
- [11] J. Polchinski. *"String Theory"*, volume 1. Cambridge University Press, 1998.

-
- [12] J. Polchinski. *"String Theory"*, volume 2. Cambridge University Press, 1998.
- [13] A. Ashtekar. Introduction to loop quantum gravity and cosmology. *Lect. Notes Phys.*, 863:31–56, 2013.
- [14] S. Weinberg. Ultraviolet Divergences in Quantum Theories of Gravitation. *General Relativity: An Einstein centenary survey*, Eds. Hawking, S.W., Israel, W; Cambridge University Press, pages 790–831, 1979.
- [15] P. Horava. Membranes at Quantum Criticality. *JHEP*, 0903:020, 2009, arXiv:0812.4287.
- [16] P. Horava. Quantum Gravity at a Lifshitz Point. *Phys.Rev.*, D79:084008, 2009, arXiv:0901.3775.
- [17] T. Regge. General Relativity without Coordinates. *Nuovo Cim.*, 19:558–571, 1961.
- [18] J. Ambjorn, J. Jurkiewicz, and R. Loll. A Nonperturbative Lorentzian path integral for gravity. *Phys.Rev.Lett.*, 85:924–927, 2000, arXiv:0002050.
- [19] J. Ambjorn, J. Jurkiewicz, and R. Loll. Nonperturbative 3-D Lorentzian quantum gravity. *Phys.Rev.*, D64:044011, 2001, arXiv:0011276.
- [20] J. Ambjorn, J. Jurkiewicz, and R. Loll. Dynamically triangulating Lorentzian quantum gravity. *Nucl.Phys.*, B610:347–382, 2001, arXiv:0105267.
- [21] R. Loll. Discrete approaches to quantum gravity in four-dimensions. *Living Rev.Rel.*, 1:13, 1998, arXiv:9805049.
- [22] J. Ambjorn, A. Goerlich, J. Jurkiewicz, and R. Loll. Nonperturbative Quantum Gravity. *Phys.Rept.*, 519:127–210, 2012, arXiv:1203.3591.
- [23] J. Laiho and D. Coumbe. Evidence for Asymptotic Safety from Lattice Quantum Gravity. *Phys.Rev.Lett.*, 107:161301, 2011, arXiv:1104.5505.
- [24] J. Laiho and D. Coumbe. Asymptotic safety and lattice quantum gravity. *PoS*, LATTICE2011:005, 2011.
- [25] D. Coumbe and J. Laiho. Exploring the Phase Diagram of Lattice Quantum Gravity. *PoS*, LATTICE2011:334, 2011, arXiv:1201.2864.
- [26] J. Berges, N. Tetradis, and C. Wetterich. Nonperturbative renormalization flow in quantum field theory and statistical physics. *Phys.Rept.*, 363:223–386, 2002, arXiv:0005122.

-
- [27] J. Polonyi. Lectures on the functional renormalization group method. *Central Eur.J.Phys.*, 1:1–71, 2003, arXiv:0110026.
- [28] B. Delamotte. An Introduction to the nonperturbative renormalization group. *Lect.Notes Phys.*, 852:49–132, 2012, arXiv:0702365.
- [29] O. Lauscher and M. Reuter. Fractal spacetime structure in asymptotically safe gravity. *JHEP*, 0510:050, 2005, arXiv:0508202.
- [30] M. Reuter and F. Saueressig. Fractal space-times under the microscope: A Renormalization Group view on Monte Carlo data. *JHEP*, 1112:012, 2011, arXiv:1110.5224.
- [31] S. Rechenberger and F. Saueressig. The R^2 phase-diagram of QEG and its spectral dimension. *Phys.Rev.*, D86:024018, 2012, arXiv:1206.0657.
- [32] J. Ambjorn, J. Jurkiewicz, and R. Loll. Spectral dimension of the universe. *Phys.Rev.Lett.*, 95:171301, 2005, arXiv:0505113.
- [33] J. Ambjorn, J. Jurkiewicz, and R. Loll. Reconstructing the universe. *Phys.Rev.*, D72:064014, 2005, arXiv:0505154.
- [34] D. Benedetti and J. Henson. Spectral geometry as a probe of quantum spacetime. *Phys.Rev.*, D80:124036, 2009, arXiv:0911.0401.
- [35] P. Horava. Spectral Dimension of the Universe in Quantum Gravity at a Lifshitz Point. *Phys.Rev.Lett.*, 102:161301, 2009, arXiv:0902.3657.
- [36] L. Modesto. Fractal Structure of Loop Quantum Gravity. *Class.Quant.Grav.*, 26:242002, 2009, arXiv:0812.2214.
- [37] F. Caravelli and L. Modesto. Fractal Dimension in 3d Spin-Foams. 2009, arXiv:0905.2170.
- [38] E. Magliaro, C. Perini, and L. Modesto. Fractal Space-Time from Spin-Foams. 2009, arXiv:0911.0437.
- [39] L. Modesto and P. Nicolini. Spectral dimension of a quantum universe. *Phys.Rev.*, D81:104040, 2010, arXiv:0912.0220.
- [40] D. Benedetti. Fractal properties of quantum spacetime. *Phys.Rev.Lett.*, 102:111303, 2009, arXiv:0811.1396.
- [41] G. Giasemidis, J. F. Wheeler, and S. Zohren. Dynamical dimensional reduction in toy models of 4D causal quantum gravity. *Phys.Rev.*, D86:081503, 2012, arXiv:1202.2710.

-
- [42] G. Giasemidis, J. F. Wheeler, and S. Zohren. Multigraph models for causal quantum gravity and scale dependent spectral dimension. *J.Phys.*, A45:355001, 2012, arXiv:1202.6322.
- [43] S. Carlip. Spontaneous Dimensional Reduction in Short-Distance Quantum Gravity? 2009, arXiv:0909.3329.
- [44] S. Carlip. The Small Scale Structure of Spacetime. pages 69–84, 2009, arXiv:1009.1136.
- [45] T. P. Sotiriou, M. Visser, and S. Weinfurtner. From dispersion relations to spectral dimension - and back again. *Phys.Rev.*, D84:104018, 2011, arXiv:1105.6098.
- [46] T. P. Sotiriou, M. Visser, and S. Weinfurtner. Spectral dimension as a probe of the ultraviolet continuum regime of causal dynamical triangulations. *Phys.Rev.Lett.*, 107:131303, 2011, arXiv:1105.5646.
- [47] G. Calcagni. Geometry and field theory in multi-fractional spacetime. *JHEP*, 1201:065, 2012, arXiv:1107.5041.
- [48] G. Calcagni. Diffusion in multi-fractional spacetimes. *Phys.Rev.*, E87:012123, 2013, arXiv:1205.5046.
- [49] A. Bonanno and M. Reuter. Renormalization group improved black hole space-times. *Phys.Rev.*, D62:043008, 2000, arXiv:0002196.
- [50] Y. Cai and D. A. Easson. Black holes in an asymptotically safe gravity theory with higher derivatives. *JCAP*, 1009:002, 2010, arXiv:1007.1317.
- [51] M. Reuter and E. Tuiran. Quantum Gravity Effects in the Kerr Spacetime. *Phys.Rev.*, D83:044041, 2011, arXiv:1009.3528.
- [52] A. Bonanno and M. Reuter. Spacetime structure of an evaporating black hole in quantum gravity. *Phys.Rev.*, D73:083005, 2006, arXiv:0602159.
- [53] R. Casadio, S. D.H. Hsu, and B. Mirza. Asymptotic Safety, Singularities, and Gravitational Collapse. *Phys.Lett.*, B695:317–319, 2011, arXiv:1008.2768.
- [54] K. Falls, D. F. Litim, and A. Raghuraman. Black Holes and Asymptotically Safe Gravity. *Int.J.Mod.Phys.*, A27:1250019, 2012, arXiv:1002.0260.
- [55] K. Falls and D. F. Litim. Black hole thermodynamics under the microscope. 2012, arXiv:1212.1821.

-
- [56] M. Reuter and H. Weyer. Running Newton constant, improved gravitational actions, and galaxy rotation curves. *Phys.Rev.*, D70:124028, 2004, arXiv:0410117.
- [57] M. Reuter and H. Weyer. On the Possibility of Quantum Gravity Effects at Astrophysical Scales. *Int.J.Mod.Phys.*, D15:2011–2028, 2006, arXiv:0702051.
- [58] B. Koch. Renormalization group and black hole production in large extra dimensions. *Phys.Lett.*, B663:334–337, 2008, arXiv:0707.4644.
- [59] T. Burschil and B. Koch. Renormalization group improved black hole space-time in large extra dimensions. *Zh.Eksp.Teor.Fiz.*, 92:219–225, 2010, arXiv:0912.4517.
- [60] J. Hewett and T. Rizzo. Collider Signals of Gravitational Fixed Points. *JHEP*, 0712:009, 2007, arXiv:0707.3182.
- [61] D. F. Litim and T. Plehn. Signatures of gravitational fixed points at the LHC. *Phys.Rev.Lett.*, 100:131301, 2008, arXiv:0707.3983.
- [62] E. Gerwick, D. Litim, and T. Plehn. Asymptotic safety and Kaluza-Klein gravitons at the LHC. *Phys.Rev.*, D83:084048, 2011, arXiv:1101.5548.
- [63] B. Dobrich and A. Eichhorn. Can we see quantum gravity? Photons in the asymptotic-safety scenario. *JHEP*, 1206:156, 2012, arXiv:1203.6366.
- [64] A. Bonanno and M. Reuter. Cosmology with selfadjusting vacuum energy density from a renormalization group fixed point. *Phys.Lett.*, B527:9–17, 2002, arXiv:0106468.
- [65] A. Bonanno and M. Reuter. Cosmology of the Planck era from a renormalization group for quantum gravity. *Phys.Rev.*, D65:043508, 2002, arXiv:0106133.
- [66] A. Bonanno and M. Reuter. Cosmological perturbations in renormalization group derived cosmologies. *Int.J.Mod.Phys.*, D13:107–122, 2004, arXiv:0210472.
- [67] E. Bentivegna, A. Bonanno, and M. Reuter. Confronting the IR fixed point cosmology with high redshift supernova data. *JCAP*, 0401:001, 2004, arXiv:0303150.
- [68] M. Reuter and H. Weyer. Renormalization group improved gravitational actions: A Brans-Dicke approach. *Phys.Rev.*, D69:104022, 2004, arXiv:0311196.
- [69] A. Bonanno and M. Reuter. Entropy signature of the running cosmological constant. *JCAP*, 0708:024, 2007, arXiv:0706.0174.

-
- [70] B.F.L. Ward. Planck Scale Cosmology in Resummed Quantum Gravity. *Mod.Phys.Lett.*, A23:3299–3305, 2008, arXiv:0808.3124.
- [71] S. Weinberg. Asymptotically Safe Inflation. *Phys.Rev.*, D81:083535, 2010, arXiv:0911.3165.
- [72] S.-H. H. Tye and J. Xu. Comment on Asymptotically Safe Inflation. *Phys.Rev.*, D82:127302, 2010, arXiv:1008.4787.
- [73] A. Contillo. Evolution of cosmological perturbations in an RG-driven inflationary scenario. *Phys.Rev.*, D83:085016, 2011, arXiv:1011.4618.
- [74] A. Bonanno, A. Contillo, and R. Percacci. Inflationary solutions in asymptotically safe $f(R)$ theories. *Class.Quant.Grav.*, 28:145026, 2011, arXiv:1006.0192.
- [75] M. Hindmarsh and I. D. Saltas. $f(R)$ Gravity from the renormalisation group. *Phys.Rev.*, D86:064029, 2012, arXiv:1203.3957.
- [76] Y. Cai and D. A. Easson. Asymptotically safe gravity as a scalar-tensor theory and its cosmological implications. *Phys.Rev.*, D84:103502, 2011, arXiv:1107.5815.
- [77] A. Contillo, M. Hindmarsh, and C. Rahmede. Renormalisation group improvement of scalar field inflation. *Phys.Rev.*, D85:043501, 2012, arXiv:1108.0422.
- [78] M. Hindmarsh, D. Litim, and C. Rahmede. Asymptotically Safe Cosmology. *JCAP*, 1107:019, 2011, arXiv:1101.5401.
- [79] C. Rahmede. The asymptotic safety scenario and scalar field inflation. 2013, arXiv:1301.5495.
- [80] Y. Cai, Y. Chang, P. Chen, D. A. Easson, and Taotao Qiu. Higgs Modulated Reheating of RG improved Inflation in light of the Planck data. 2013, arXiv:1304.6938.
- [81] A. Bonanno. An effective action for asymptotically safe gravity. *Phys.Rev.*, D85:081503, 2012, arXiv:1203.1962.
- [82] M. E. Peskin and D. V. Schroeder. *An Introduction to Quantum Field Theory*. Perseus Books, 1995.
- [83] C. Wetterich. Exact evolution equation for the effective potential. *Phys.Lett.*, B301:90–94, 1993.
- [84] D. F. Litim. Optimization of the exact renormalization group. *Phys.Lett.*, B486:92–99, 2000, arXiv:0005245.

-
- [85] D. F. Litim. Optimized renormalization group flows. *Phys.Rev.*, D64:105007, 2001, arXiv:0103195.
- [86] J. M. Pawłowski. Aspects of the functional renormalisation group. *Annals Phys.*, 322:2831–2915, 2007, arXiv:0512261.
- [87] M. Reuter and C. Wetterich. Average action for the Higgs model with Abelian gauge symmetry. *Nucl.Phys.*, B391:147–175, 1993.
- [88] M. Reuter and C. Wetterich. Running gauge coupling in three-dimensions and the electroweak phase transition. *Nucl.Phys.*, B408:91–132, 1993.
- [89] M. Reuter and C. Wetterich. Effective average action for gauge theories and exact evolution equations. *Nucl.Phys.*, B417:181–214, 1994.
- [90] M. Reuter and C. Wetterich. Exact evolution equation for scalar electrodynamics. *Nucl.Phys.*, B427:291–324, 1994.
- [91] H. Gies. Introduction to the functional RG and applications to gauge theories. *Lect.Notes Phys.*, 852:287–348, 2012, arXiv:0611146.
- [92] S. Weinberg. *Critical Phenomena for Field Theorists*. 1976.
- [93] K. G. Wilson and M. E. Fisher. Critical exponents in 3.99 dimensions. *Phys.Rev.Lett.*, 28:240–243, 1972.
- [94] B. Rosenstein, B. J. Warr, and S. H. Park. The Four Fermi Theory Is Renormalizable in (2+1)-Dimensions. *Phys.Rev.Lett.*, 62:1433–1436, 1989.
- [95] K. Gawedzki and A. Kupiainen. Renormalizing the Nonrenormalizable. *Phys.Rev.Lett.*, 55:363–365, 1985.
- [96] C. de Calan, P.A. Faria da Veiga, J. Magnen, and R. Seneor. Constructing the three-dimensional Gross-Neveu model with a large number of flavor components. *Phys.Rev.Lett.*, 66:3233–3236, 1991.
- [97] H. Gies, J. Jaeckel, and C. Wetterich. Towards a renormalizable standard model without fundamental Higgs scalar. *Phys.Rev.*, D69:105008, 2004, arXiv:0312034.
- [98] H. Gies and M. M. Scherer. Asymptotic safety of simple Yukawa systems. *Eur.Phys.J.*, C66:387–402, 2010, arXiv:0901.2459.
- [99] H. Gies, S. Rechenberger, and M. M. Scherer. Towards an Asymptotic-Safety Scenario for Chiral Yukawa Systems. *Eur.Phys.J.*, C66:403–418, 2010, arXiv:0907.0327.

-
- [100] M. M. Scherer, H. Gies, and S. Rechenberger. An Asymptotic-safety mechanism for chiral Yukawa systems. *Acta Phys.Polon.Supp.*, 2:541, 2009, arXiv:0910.0395.
- [101] H. Gies, S. Rechenberger, M. M. Scherer, and L. Zambelli. An asymptotic safety scenario for gauged chiral Higgs-Yukawa models. 2013, arXiv:1306.6508.
- [102] O. Zanusso, L. Zambelli, G.P. Vacca, and R. Percacci. Gravitational corrections to Yukawa systems. *Phys.Lett.*, B689:90–94, 2010, arXiv:0904.0938.
- [103] A. Codello and R. Percacci. Fixed Points of Nonlinear Sigma Models in $d \geq 2$. *Phys.Lett.*, B672:280–283, 2009, arXiv:0810.0715.
- [104] R. Percacci and O. Zanusso. One loop beta functions and fixed points in Higher Derivative Sigma Models. *Phys.Rev.*, D81:065012, 2010, arXiv:0910.0851.
- [105] M. Fabbrichesi, R. Percacci, A. Tonero, and O. Zanusso. Asymptotic safety and the gauged $SU(N)$ nonlinear σ -model. *Phys.Rev.*, D83:025016, 2011, arXiv:1010.0912.
- [106] F. Bazzocchi, M. Fabbrichesi, R. Percacci, A. Tonero, and L. Vecchi. Fermions and Goldstone bosons in an asymptotically safe model. *Phys.Lett.*, B705:388–392, 2011, arXiv:1105.1968.
- [107] R. Percacci and L. Rachwal. On classicalization in nonlinear sigma models. *Phys.Lett.*, B711:184–189, 2012, arXiv:1202.1101.
- [108] R. Flore, A. Wipf, and O. Zanusso. Functional renormalization group of the non-linear sigma model and the $O(N)$ universality class. 2012, arXiv:1207.4499.
- [109] H. Gies. Renormalizability of gauge theories in extra dimensions. *Phys.Rev.*, D68:085015, 2003, arXiv:0305208.
- [110] M. Shaposhnikov and C. Wetterich. Asymptotic safety of gravity and the Higgs boson mass. *Phys.Lett.*, B683:196–200, 2010, arXiv:0912.0208.
- [111] F. Bezrukov, M. Y. Kalmykov, B. A. Kniehl, and M. Shaposhnikov. Higgs Boson Mass and New Physics. *JHEP*, 1210:140, 2012, arXiv:1205.2893.
- [112] C. Wetterich. Where to look for solving the gauge hierarchy problem? *Phys.Lett.*, B718:573–576, 2012, arXiv:1112.2910.

-
- [113] D. Benedetti, P. F. Machado, and F. Saueressig. Four-derivative interactions in asymptotically safe gravity. 2009, arXiv:0909.3265.
- [114] M. Reuter. Nonperturbative evolution equation for quantum gravity. *Phys.Rev.*, D57:971–985, 1998, arXiv:9605030.
- [115] A. Codello and R. Percacci. Fixed points of higher derivative gravity. *Phys.Rev.Lett.*, 97:221301, 2006, arXiv:0607128.
- [116] D. Benedetti, P. F. Machado, and F. Saueressig. Taming perturbative divergences in asymptotically safe gravity. *Nucl.Phys.*, B824:168–191, 2010, arXiv:0902.4630.
- [117] O. Lauscher and M. Reuter. Is quantum Einstein gravity nonperturbatively renormalizable? *Class.Quant.Grav.*, 19:483–492, 2002, arXiv:0110021.
- [118] O. Lauscher and M. Reuter. Towards nonperturbative renormalizability of quantum Einstein gravity. *Int.J.Mod.Phys.*, A17:993–1002, 2002, arXiv:0112089.
- [119] O. Lauscher and M. Reuter. Flow equation of quantum Einstein gravity in a higher derivative truncation. *Phys.Rev.*, D66:025026, 2002, arXiv:0205062.
- [120] A. Codello, R. Percacci, and C. Rahmede. Ultraviolet properties of f(R)-gravity. *Int.J.Mod.Phys.*, A23:143–150, 2008, arXiv:0705.1769.
- [121] A. Codello, R. Percacci, and C. Rahmede. Investigating the Ultraviolet Properties of Gravity with a Wilsonian Renormalization Group Equation. *Annals Phys.*, 324:414–469, 2009, arXiv:0805.2909.
- [122] K. Falls, D.F. Litim, K. Nikolakopoulos, and C. Rahmede. A bootstrap towards asymptotic safety. 2013, arXiv:1301.4191.
- [123] P. F. Machado and F. Saueressig. On the renormalization group flow of f(R)-gravity. *Phys.Rev.*, D77:124045, 2008, arXiv:0712.0445.
- [124] D. Benedetti and F. Caravelli. The Local potential approximation in quantum gravity. *JHEP*, 1206:017, 2012, arXiv:1204.3541.
- [125] M. Demmel, F. Saueressig, and O. Zanusso. Fixed-Functionals of three-dimensional Quantum Einstein Gravity. *JHEP*, 1211:131, 2012, arXiv:1208.2038.
- [126] M. Demmel, F. Saueressig, and O. Zanusso. Fixed Functionals in Asymptotically Safe Gravity. 2013, arXiv:1302.1312.

-
- [127] D. Benedetti, K. Groh, P. F. Machado, and F. Saueressig. The Universal RG Machine. *JHEP*, 1106:079, 2011, arXiv:1012.3081.
- [128] K. Groh, F. Saueressig, and O. Zanusso. Off-diagonal heat-kernel expansion and its application to fields with differential constraints. 2011, arXiv:1112.4856.
- [129] A. Codello and O. Zanusso. On the non-local heat kernel expansion. *J.Math.Phys.*, 54:013513, 2013, arXiv:1203.2034.
- [130] K. Groh, S. Rechenberger, F. Saueressig, and O. Zanusso. Higher Derivative Gravity from the Universal Renormalization Group Machine. *PoS, EPS-HEP2011:124*, 2011, arXiv:1111.1743.
- [131] D. Becker and M. Reuter. Running boundary actions, Asymptotic Safety, and black hole thermodynamics. *JHEP*, 1207:172, 2012, arXiv:1205.3583.
- [132] D. Becker and M. Reuter. Asymptotic Safety and Black Hole Thermodynamics. 2012, arXiv:1212.4274.
- [133] K. Groh and F. Saueressig. Ghost wave-function renormalization in Asymptotically Safe Quantum Gravity. *J.Phys.*, A43:365403, 2010, arXiv:1001.5032.
- [134] A. Eichhorn, H. Gies, and M. M. Scherer. Asymptotically free scalar curvature-ghost coupling in Quantum Einstein Gravity. *Phys.Rev.*, D80:104003, 2009, arXiv:0907.1828.
- [135] A. Eichhorn and H. Gies. Ghost anomalous dimension in asymptotically safe quantum gravity. *Phys.Rev.*, D81:104010, 2010, arXiv:1001.5033.
- [136] R. Percacci and D. Perini. Constraints on matter from asymptotic safety. *Phys.Rev.*, D67:081503, 2003, arXiv:0207033.
- [137] R. Percacci and D. Perini. Asymptotic safety of gravity coupled to matter. *Phys.Rev.*, D68:044018, 2003, arXiv:0304222.
- [138] G. Narain and R. Percacci. Renormalization Group Flow in Scalar-Tensor Theories. I. *Class.Quant.Grav.*, 27:075001, 2010, arXiv:0911.0386.
- [139] G. Narain and C. Rahmede. Renormalization Group Flow in Scalar-Tensor Theories. II. *Class.Quant.Grav.*, 27:075002, 2010, arXiv:0911.0394.
- [140] P. Dona and R. Percacci. Functional renormalization with fermions and tetrads. 2012, arXiv:1209.3649.
- [141] A. Eichhorn and H. Gies. Light fermions in quantum gravity. *New J.Phys.*, 13:125012, 2011, arXiv:1104.5366.

-
- [142] A. Eichhorn. Quantum-gravity-induced matter self-interactions in the asymptotic-safety scenario. *Phys.Rev.*, D86:105021, 2012, arXiv:1204.0965.
- [143] G.P. Vacca and O. Zanusso. Asymptotic Safety in Einstein Gravity and Scalar-Fermion Matter. *Phys.Rev.Lett.*, 105:231601, 2010, arXiv:1009.1735.
- [144] A. Codello. Large N Quantum Gravity. *New J.Phys.*, 14:015009, 2012, arXiv:1108.1908.
- [145] J. Daum, U. Harst, and M. Reuter. Running Gauge Coupling in Asymptotically Safe Quantum Gravity. *JHEP*, 1001:084, 2010, arXiv:0910.4938.
- [146] S. Folkerts, D. F. Litim, and J. M. Pawłowski. Asymptotic freedom of Yang-Mills theory with gravity. *Phys.Lett.*, B709:234–241, 2012, arXiv:1101.5552.
- [147] U. Harst and M. Reuter. QED coupled to QEG. *JHEP*, 1105:119, 2011, arXiv:1101.6007.
- [148] M. Reuter and F. Saueressig. Renormalization group flow of quantum gravity in the Einstein-Hilbert truncation. *Phys.Rev.*, D65:065016, 2002, arXiv:0110054.
- [149] M. Reuter and H. Weyer. Quantum gravity at astrophysical distances? *JCAP*, 0412:001, 2004, arXiv:0410119.
- [150] O. Lauscher and M. Reuter. Ultraviolet fixed point and generalized flow equation of quantum gravity. *Phys.Rev.*, D65:025013, 2002, arXiv:0108040.
- [151] D. F. Litim and J. M. Pawłowski. Flow equations for Yang-Mills theories in general axial gauges. *Phys.Lett.*, B435:181–188, 1998, arXiv:9802064.
- [152] E. Manrique and M. Reuter. Bimetric Truncations for Quantum Einstein Gravity and Asymptotic Safety. *Annals Phys.*, 325:785–815, 2010, arXiv:0907.2617.
- [153] E. Manrique, M. Reuter, and F. Saueressig. Matter Induced Bimetric Actions for Gravity. *Annals Phys.*, 326:440–462, 2011, arXiv:1003.5129.
- [154] E. Manrique, M. Reuter, and F. Saueressig. Bimetric Renormalization Group Flows in Quantum Einstein Gravity. *Annals Phys.*, 326:463–485, 2011, arXiv:1006.0099.
- [155] D. Benedetti. On the number of relevant operators in asymptotically safe gravity. 2013, arXiv:1301.4422.
- [156] D. Litim and A. Satz. Limit cycles and quantum gravity. 2012, arXiv:1205.4218.

-
- [157] I. Donkin and J. M. Pawłowski. The phase diagram of quantum gravity from diffeomorphism-invariant RG-flows. 2012, arXiv:1203.4207.
- [158] S. Nagy, J. Krizsan, and K. Sailer. Infrared fixed point in quantum Einstein gravity. *JHEP*, 1207:102, 2012, arXiv:1203.6564.
- [159] N. Christiansen, D. F. Litim, J. M. Pawłowski, and A. Rodigast. Fixed points and infrared completion of quantum gravity. 2012, arXiv:1209.4038.
- [160] A. Codello. Scaling Solutions in Continuous Dimension. *J.Phys.*, A45:465006, 2012, arXiv:1204.3877.
- [161] U. Harst and M. Reuter. The 'Tetrad only' theory space: Nonperturbative renormalization flow and Asymptotic Safety. *JHEP*, 1205:005, 2012, arXiv:1203.2158.
- [162] D. ben Avraham and S. Havlin. *Diffusion and Reactions in Fractals and Disordered Systems*. Cambridge University Press, 2000.
- [163] B. Mandelbrot. How long is the coast of britain? statistical self-similarity and fractional dimension. *Science*, 156(3775):636–638, May 1967.
- [164] L. F. Richardson. The problem of contiguity : an appendix of statistics of deadly quarrels. In *General systems yearbook*, volume 6, pages 139+. Statistic of Deadly Quarrels, 1961.
- [165] B. S. DeWitt. Dynamical theory of groups and fields. 1965.
- [166] R.T. Seeley. Complex powers of an elliptic operator. *Proc.Symp.Pure Math.*, 10:288–307, 1967.
- [167] E. Manrique, S. Rechenberger, and F. Saueressig. Asymptotically Safe Lorentzian Gravity. *Phys.Rev.Lett.*, 106:251302, 2011, arXiv:1102.5012.
- [168] S. Rechenberger and F. Saueressig. A functional renormalization group equation for foliated spacetimes. *JHEP*, 1303:010, 2013, arXiv:1212.5114.
- [169] A. Contillo, S. Rechenberger, and F. Saueressig. Renormalization group flows of Hořava-Lifshitz gravity at low energies. 2013.
- [170] R. M. Wald. *General Relativity*. University of Chicago Press, 1984.
- [171] A. Dasgupta and R. Loll. A Proper time cure for the conformal sickness in quantum gravity. *Nucl.Phys.*, B606:357–379, 2001, arXiv:0103186.
- [172] C. Teitelboim. Quantum Mechanics of the Gravitational Field. *Phys.Rev.*, D25:3159, 1982.

-
- [173] C. Teitelboim. The Proper Time Gauge in Quantum Theory of Gravitation. *Phys.Rev.*, D28:297, 1983.
- [174] P. Horava and C. M. Melby-Thompson. General Covariance in Quantum Gravity at a Lifshitz Point. *Phys.Rev.*, D82:064027, 2010, arXiv:1007.2410.
- [175] Jr. York, J. W. Conformally invariant orthogonal decomposition of symmetric tensors on Riemannian manifolds and the initial value problem of general relativity. *J.Math.Phys.*, 14:456–464, 1973.
- [176] S. Floerchinger. Analytic Continuation of Functional Renormalization Group Equations. *JHEP*, 1205:021, 2012, arXiv:1112.4374.
- [177] D. F. Litim. Wilsonian flow equation and thermal field theory. 1998, arXiv:9811272.
- [178] D. F. Litim and J. M. Pawłowski. Non-perturbative thermal flows and resummations. *JHEP*, 0611:026, 2006, arXiv:0609122.
- [179] P. Fischer and D. F. Litim. Fixed points of quantum gravity in extra dimensions. *Phys.Lett.*, B638:497–502, 2006, arXiv:0602203.
- [180] A. De Felice and S. Tsujikawa. $f(R)$ theories. *Living Rev.Rel.*, 13:3, 2010, arXiv:1002.4928.
- [181] C. P.L. Berry and J. R. Gair. Linearized $f(R)$ Gravity: Gravitational Radiation and Solar System Tests. *Phys.Rev.*, D83:104022, 2011, arXiv:1104.0819.
- [182] L.D. Faddeev and V.N. Popov. Feynman Diagrams for the Yang-Mills Field. *Phys.Lett.*, B25:29–30, 1967.
- [183] L.F. Abbott. Introduction to the Background Field Method. *Acta Phys.Polon.*, B13:33, 1982.
- [184] M. Niedermaier and M. Reuter. The Asymptotic Safety Scenario in Quantum Gravity. *Living Rev.Rel.*, 9:5, 2006.
- [185] M. A. Rubin and C. R. Ordonez. Eigenvalues and Degeneracies for n-Dimensional Tensor Spherical Harmonics. 1983.
- [186] M. A. Rubin and C. R. Ordonez. Symmetric Tensor Eigen Spectrum of the Laplacian on n Spheres. *J.Math.Phys.*, 26:65, 1985.
- [187] R. L. Arnowitt, S. Deser, and C. W. Misner. Dynamical Structure and Definition of Energy in General Relativity. *Phys.Rev.*, 116:1322–1330, 1959.
- [188] D. Adams. *"So Long, and Thanks for All the Fish"*. Del Rey, 1999.

Acknowledgement

At the end I would like to take the opportunity to spread my gratitude among the various people, who contributed directly or indirectly to this thesis.

First and foremost my special thanks goes to Frank Saueressig for giving me the opportunity to join his group as a PhD student. I would like to thank for his continuous support and abundance of patience with me. It is mainly his credit that this thesis came into being with the current quality and quantity.

Secondly I would like to thank Renate Loll for the possibility to submit this thesis to the Radboud University. Her comments on the manuscript shall be acknowledged as well.

Furthermore, special thanks goes to Martin Reuter. I benefitted much from his seemingly all-embracing knowledge. Moreover I have to thank him for many interesting and funny anecdotes during several lunches and dinners.

In addition I would like to thank all my collaborators for working with me and explaining me a huge amount of things I should have known before. In alphabetic order these are Jacqueline A. Bonnet, Adriano Contillo, Holger Gies, Kai Groh, Elisa Manrique, Jan M. Pawlowski, Michael M. Scherer, Luca Zambelli and Omar Zanusso.

Among them, I would like to single out my office mates Kai Groh and Adriano Contillo. I enjoyed many interesting discussions with them, where the topics ranged far beyond physics.

Special thanks go as well to Daniel Becker, Maximilian Demmel, Andreas Nink and Gregor Schollmeyer for carefully proofreading parts of this thesis. Their comments and suggestions improved this text considerably.

Another thanks go to Ulrich Harst for all the discussions during the train travels between Mainz and Frankfurt making them enjoyable.

I would like to thank the whole group including Alessandro Codello for the enjoyable atmosphere in the offices and the mensa. Especially I would like to thank for the various group events, which often contained conversations about physics. As my time in this great group ends I am tempted to cite Douglas Adams [188] and say "So long, and thanks for all the fish".

Last but not least I would like to acknowledge the financial support by the Deutsche Forschungsgemeinschaft (DFG), who supported my Ph.D. position within the Emmy-Noether program (Grant SA/1975 1-1).

Curriculum Vitae

Stefan Rechenberger was born on the 1st of September 1983 in Dresden, Germany Democratic Republic. His secondary education ended at the Gymnasium Senftenberg in 2003 with the receipt of the general qualification for university entrance. After nine months of military service he started his undergraduate studies in mathematics and physics at the Friedrich-Schiller-Universität Jena. He graduated in 2010 with a diploma thesis on "Asymptotic Safety of Yukawa Systems" under the supervision of Prof. Dr. Holger Gies. Subsequent he joined the group of Frank Saueressig at the Johannes Gutenberg-Universität Mainz which went to the Radboud Universiteit Nijmegen in spring 2013. Under his supervision he did his doctoral research about asymptotically safe quantum gravity. The result of this work is subsumed in the present thesis.

